SSC-EOI0011

SSCL-SR-1166

5-25-90

Expression Of Interest

A CALORIMETER-BASED HIGH-RATE DETECTOR FOR THE SSC

S. Dye, G. Jones, C. Oh, S. Klein, J.P. Miller, D. Perlman,
B.L. Roberts, M.A. Rahman, J. Stone, L. Sulak**, F. Wittel, and W. Worstell
Boston University

C. Lane
Drexel University

D. Winn
Fairfield University

J. Hofteizer
LeCroy Research Corp.

G. Alverson, W. Faissler, M. Glaubman, A. Grimes, I. Leedom,
J. Moromisato, E. Pothier, S. Reucroft**, E. Saletan and E. von Goeler
Northeastern University

W.L. Dunn, F. O'Foghlundha, S.K. Myers, I.D. Simpkins and A.M. Yacout
Quantum Research

T. Kamon and R. Webb**
Texas A&M University

with Engineering Proposals and Endorsements from Industrial Affiliates

Bicron
C. Hurlbut*

The Charles Stark Draper Laboratory
F. Ayer*

Hamamatsu Corp.
J. Murray*

Oak Ridge National Laboratory Detector Center
J.W. Stapleton and A. Gabriel*

Optectron
P. Jacquet*

RCA/General Electric
R.J. McIntyre*

Teledyne Brown Engineering
J.K. Woosley*

Thinking Machines Corp.
J. Mucci*

Union Carbide Industrial Gases Inc.
S. L. Saupp*

The TEXAS Collaboration
(Totally hermetic EXperiment At the Supercollider)

May 25, 1990

*Contact person
**Co-spokesman

Abstract

The conceptual design for an SSC detector that focuses on calorimetry is presented. The physics goals include searches for elementary scalars of low mass ($M_H < 2M_W$) and high mass ($M_H > 600\,\mathrm{GeV}$), for heavy supersymmetric matter, for compositeness and for strong vector-boson interactions. Examples of the relevant signatures are $H \to \gamma\gamma$; $H \to Z\,Z^*$; $H \to l\nu q\bar{q}$, $ll\nu\nu$, $llq\bar{q}$; $\tilde{g}\tilde{g} \to E_T^{miss} + > 2\,\mathrm{jets}$; and a jet excess at high p_T. These goals may be achieved with high precision, fast, compensated, and truly hermetic calorimetry, optimized for electrons, photons, jets, and missing energy. All the goals require operation at high luminosity. The additional concerns of γ-γ and jet-jet separation, as well as survival in a high radiation environment, are solved by an unusually large inner radius of the detector. The detector concept consists of the following few and well defined components:

- a scintillating fiber tracking system incorporating an imaging pre-radiator,
- a projective, finely segmented, thick scintillator calorimeter, and
- a muon TRD trigger and spectrometer.

The design allows for total hermeticity to $\eta = 5.5$. The trigger response to electrons, muons, jets and missing energy is well-matched to the SSC crossing time. High speed, fine segmentation and a large inner radius imply that early operation at a luminosity of $10^{34}\,\mathrm{cm}^{-2}\mathrm{s}^{-1}$ should be possible. This allows one to address the small cross-sections and branching ratios associated with the subset of our goals that are complementary to those of the large multi-purpose detectors. Basing this design on existing technology ensures timely construction at a reasonable cost. The physics capability and justification for this approach, as well as the details of an initial design, are presented.

Table of Contents

Introduction	1
Physics Goals	3
Detector Conceptual Design	6
Anticipated Detector Performance and Physics Reach	23
Milestones to Define Detailed Design	28
Request for Funds	33
Preliminary Cost Estimate	36
TEXAS Management Scheme	38
Conclusions	39
Acknowledgements	39
References	41
Figure Captions	43
Preliminary Mechanical Engineering Design by Draper Laboratory	A1
Engineering Program on Muon TRD Spectrometer	A8
Proposals for Engineering Design and Systems Integration	
Bicron Corp.	P1
The Charles Stark Draper Laboratory Inc.	P6
Hamamatsu Corp.	P9
LeCroy Corp.	P12
Oak Ridge National Laboratory	P15
Optectron	P16
Quantum Research Services	P18
RCA/General Electric	P19
Teledyne Brown Engineering	P21
Thinking Machines Corp.	P23
Union Carbide Industrial Gases Inc.	P24

Introduction

We propose a simple and hermetic SSC detector that optimizes fast calorimetry for electrons and the measurement of jets and missing energy. Figures [1-8] show the detector conceptual design. A fiber calorimeter is complemented by a central scintillating fiber tracker pre-radiator and an outer muon spectrometer. The muon system uses TRD and dE/dx for fast triggering and momentum analysis. The three components and their few subsystems are assembled in a geometry that provides easy access and repair. The detector incorporates proven technology, or techniques currently at the prototype stage, to assure on-time construction at a predictable and limited cost.

The signatures for anticipated new physics at the SSC have been well documented and provide a basis for optimizing the design of a focussed detector. Higgs searches require lepton and jet reconstruction over the widest possible rapidity range. Signatures for supersymmetry demand excellent missing transverse energy sensitivity, and therefore truly hermetic calorimetry. Technicolor and substructure searches require fine calorimeter segmentation and compensation for good dijet invariant mass resolution. Some of the distinctive goals of the TEXAS detector, such as the search at high luminosity for an intermediate mass Higgs in the $\gamma\gamma$ and ZZ^* channels, or a heavy Higgs at the extreme of the SSC reach, pose specific problems. We address them by letting the inner radius R of the calorimeter be large (2 meters). The $\gamma\gamma$ and jet-jet separation increase as R, while the radiation dose diminishes as R^{-2}. The calorimeter proper is preceded only by a beryllium pipe and a low-Z fiber tracker. At high luminosity and with a good jet-jet mass-resolution, we can search for rare but clean signatures of supersymmetry. We can also measure high p_T jets with the precision required to search at high mass for technicolor and substructure.

The precision of calorimetry increases with energy E as $1/\sqrt{E}$ + a constant. A calorimeter with no dead space for services or structural elements can yield high resolution in the TeV regime for electrons, missing E_T and jets, provided sources of systematic error are properly minimized. A very fast detector has obvious advantages in triggering and pile-up rejection, particularly at a luminosity $\mathcal{L} = 10^{34}$ cm^{-2}s^{-1}.

For the measurement of muon energies we propose the use of transition radiation techniques sensitive to $\gamma \equiv E_\mu/m$ (an unsaturated observable at SSC energies). Transition radiation devices offer a unique alternative with broad η acceptance at a fraction of the cost of a magnetic device. There is indeed a compromise in resolution, but this is compensated by the superior resolution for electrons and the presumption of $e - \mu$ universality.

Preceding the calorimeter is a tracker and imaging pre-radiator. The pre-radiator consists of alternate superlayers (z, u, v) of scintillating fibers and lead sheets. The tracker includes three scintillating fiber superlayers. Fiber readout will be either by pixellated Silicon Intensified Target tubes or by avalanche photodiode arrays. Both are being investigated. The tracker/pre-radiator system occupies a cylindrical region between radii of 1 m and 2 m. The innermost cylindrical volume is not instrumented, leaving space for a high resolution vertex detector which could be added later if the physics so dictates.

We propose to use cast lead eutectic scintillator fiber calorimetry. It is electronically fast, simple and easily manufactured. It has excellent energy resolution, can be arbitrarily segmented, and is naturally projective and hermetic. It is structurally designed to avoid inactive boundaries and supports. The specific optimization and tower structure we propose provides radiation hardness, homogeneity, hermeticity, electron/hadron compensation and easy *in-situ* access and calibration. The towers are monolithic, projective, self-supporting and modular. The imaging pre-radiator gives superior position resolution on e and γ and excellent e/hadron separation. Spatial segmentation in η and ϕ is 0.025 in the electromagnetic and 0.05 in the hadronic compartment. Calorimetric coverage is continuous to $\eta = 5.5$. We use recirculable, radiation-hard liquid scintillator and tungsten absorber in the forward region for $\eta \geq 3$. Here, capillary tubes replace fibers allowing us to extend the fiber manufacturing technique to a liquid scintillator. The tungsten absorption length (one half that of lead) prevents shower size from dominating the segmentation. The energy resolutions ($6.5\%/\sqrt{E}$ and $30\%/\sqrt{E}$ for electromagnetic and hadronic components) are saturated by energy-independent terms which reach 0.5% for electrons and 1% for hadrons at high energy. With the pre-radiator, the electron/hadron separation is better than 5×10^{-4}.

The TRD muon-momentum analysis borrows its detailed implementation from that of large-area muon detector of similar size (MACRO). Liquid scintillator slabs would provide prompt signals with good timing resolution for associating streamer tube tracks in (ϕ, θ) and TRD hits with calorimeter hits in a 2 μs trigger pipeline. The TRD spectrometer gives better than 10% resolution at 200 GeV (as seen in Fig. 9), providing a level-1 high-p_T trigger. The TRD spectrometer information can then be used in conjunction with the scintillating fiber calorimeter to give a high-level missing E_T trigger.

In optimizing calorimetry (and avoiding cracks, solenoid support structures, etc.) we have eliminated a central magnetic field, thereby giving up the measurement of charge for $|\eta| < 1.5$. A narrow non-projective readout path at $\eta = 0$ remains. The entire detector is in two self-supporting mirror-image halves. The overall performance, simplicity and economy of the TEXAS detector, with only *three* basic components, outweighs, in our opinion, the limited benefits of measuring lepton charges (generally a two-fold suppression of background). Furthermore, our non-magnetic design preserves the narrow spatial structure of jets at the SSC, providing good jet triggering and reconstruction efficiency.

With the basic choices on the detector design and technology already made, we concentrate on the specific technical issues concerning a timely and final design. The experiment can accommodate the large luminosities required to search for a variety of rare fundamental processes. This detector is a natural complement to the larger multipurpose experiments, both technologically and from the point of view of the physics goals.

Physics Goals

The search for new physics signals at the highest possible mass scale (1 TeV and above) and for the evasive "light" Higgs necessitates the highest possible luminosity, $\mathcal{L} = 10^{34}\,\mathrm{cm}^{-2}\mathrm{s}^{-1}$, and justifies a specialized detector optimizing the calorimetry. The signatures for new physics at the SSC have been well-documented by many authors[1-10] and are only briefly outlined here.

The most mysterious features of the standard model are the origin of particle masses, and the properties of the postulated Higgs particle. Its mass is unpredictable, but the natural scale lies between the weak scale ($M_H \sim \mathcal{O}(M_Z)$ or the eventual lower limit from LEP-II), and the "unitarity-limit"; the energy at which the interactions between intermediate vector bosons become strong ($M_H \sim 1\,\mathrm{TeV}$). Full coverage of this domain ought to be a major goal for the SSC. The TEXAS detector is designed to excel in the evasive high and low ends of the anticipated mass domain. The design choices necessary for this capability are also useful for many other important physics goals.

Heavy Scalars

Consider a heavy Higgs ($M_H > 600\,\mathrm{GeV}$), with its low rate of production. To detect it, one must use the channels $H \to ZZ \to$ jet jet ll and $H \to WW \to$ jet jet $l\nu$, since they have branching ratios some 22 and 160 times that of the decays of the ZZ pair into charged leptons. An energy resolution better than $35\% / \sqrt{E} + 1\%$ is necessary for jet-jet reconstruction of the W's, as shown in Fig. 10. The backgrounds to these modes can be reduced by tagging the scattered-quark jets that accompany the process of Higgs production by IVB fusion,[11] as can be seen in Fig. 11. The figure shows that the rapidity required to tag the spectator jets must reach $\eta \sim 5$.

The same technique of background reduction by jet-tagging helps in the channel $H \to ZZ \to ll\nu\nu$,[12] which has 6 times the rate of the four-charged-lepton mode. This is shown in Fig. 12, in terms of p_T^{back}, the total scalar p_T in the half plane opposite to the Z-direction.[13] The figure also shows that random calorimetric gaps of 2% of 4π, or coverage to $\eta \leq 5$ severely degrade the signal. The signal over background for M_H=800 GeV is 24/7 events for an integrated luminosity of $10^4\,\mathrm{pb}^{-1}$, a mere one tenth of an SSC year at $\mathcal{L} = 10^{34}\,\mathrm{cm}^{-2}\mathrm{s}^{-1}$. (Cuts E_T^{miss} >120 GeV, $\eta < 5$ and $p_T > 20$ GeV for the tagging jets have been applied in estimating these event rates[9]). In Fig. 13, one can see how fast the signal decreases as M_H climbs the range from 400 to 800 MeV. Clearly, it is crucial to operate at the highest possible luminosity to investigate the upper end of the anticipated Higgs-mass domain.

In the $H \to WW \to$ jet jet $l\nu$ channel the principal difficulty is the $t\bar{t} \to b\bar{b}W^+W^-$ background. With an assumed calorimetry resolution and segmentation worse than the TEXAS goals and lepton isolation plus other cuts,[14] the background is found to be drastically reduced leading to a signal-to-noise ratio of 200/100 events for $M_H = 1\,\mathrm{TeV}$, $m_t = 150\,\mathrm{GeV}$ and an integrated luminosity of $10^{40}\,\mathrm{cm}^{-2}$.

None of the above channels is accessible without calorimetry excelling in energy resolution and dynamic range, in angular resolution, and in rapidity coverage. These characteristics are needed both to minimize the QCD background and to avoid false missing E_T signals.

Intermediate-Mass Scalars

We focus next on Higgs detection in the $M_H < 2\,M_W$ regime, and in particular on the notoriously difficult $H \to \gamma\gamma$ mode. Detection of a signal in this channel is made possible by a large inner-radius calorimeter design, with good energy resolution, inherent $\gamma\gamma$ separation, and large-luminosity reach. In Fig. 14 one can see how meager the signal/background is for M_H=150 GeV with one year of running at $\mathcal{L} = 10^{33}\,\mathrm{cm}^{-2}\mathrm{s}^{-1}$ and an excellent [extraordinary] mass resolution of 1.9 [0.8] GeV/c^2. The TEXAS mass resolution of 1.3 GeV/c^2, and operation at 10 times the quoted luminosity, appear to make this decay accessible.

The $H \to Z\,Z^*$ channel followed by $Z \to ee, \mu\mu$ decays is rate-limited, but copious enough[15] at $\mathcal{L} = 10^{33}\,\mathrm{cm}^{-2}\mathrm{s}^{-1}$ to find the Higgs in the range 130 GeV$< M_H < 2M_Z$. An intermediate-mass Higgs is a very narrow resonance, so that with excellent electron energy resolution, the same range can be covered in the all-e channel, with a luminosity of $10^{34}\,\mathrm{cm}^{-2}\mathrm{s}^{-1}$.

Supersymmetry

Consensus has it that supersymmetry is one of the most attractive extensions of the standard model, and its "minimal, low-energy" version a likely target for discovery at SSC energies. The crucial signature is missing transverse energy,[16] E_T^{miss}. At the modest energies of the LHC,[17] Fig. 15 shows that the signals protrude over the background only by a factor of two, for all explorable values of the gluino or squark masses. A linear response and a gapless calorimetric coverage are obvious requirements. The same message[13] is conveyed at SSC energies by Fig. 16 in terms of p_T^{out}, the missing momentum transverse to the plane of the beam and the highest p_T jet. The figure is for $m_{\tilde{g}} = 750$ GeV, a hadron-calorimeter resolution of $70\%/\sqrt{E}$ (two times less precise than our goal), $(\phi \times \theta)$ segmentation of (0.05×0.05), and coverage to $\eta = 6$. The signal is not rate-limited, but would rapidly become so[17] with a modest increase in $m_{\tilde{g}}$. As $m_{\tilde{g}}$ is decreased the problem is no longer the counting rate, but the hermeticity of the device. A crude estimate[13] indicates that a 5 cm crack at $\eta = 3$ more than trebles the inescapable neutrino background. Supersymmetry is an ideal advocate of a precise and hermetic calorimeter that can operate at high luminosity.

Technicolor

An obvious goal for SSC experimentation is to determine whether or not intermediate vector bosons (IVBs) interact strongly at subprocess energies of order 1 TeV. This will happen if $M_H > 1$ TeV, or if the breakdown of electroweak symmetry has a dynamical origin. Technicolor is an explicit example of a consistent theory of dynamical symmetry breaking and strongly interacting IVBs. In the simplest technicolor model, the only technihadrons accessible at the SSC are likely to be the spin-one technirhos, $\rho_T^{\pm}$ and ρ_T^0. The ρ_T mass is estimated to be 2 $\sqrt{(3/N_T)}$ TeV, where $N_T > 2$ is the number of technicolors. The discovery modes are $\rho_T^{\pm} \to Z\,W^{\pm}$ and $\rho_T^0 \to W^+\,W^-$. We show the expected number[18] of events in the WZ channel in Fig. 17 as a function of M_{WZ}, with $|\eta_{W,Z}| < 1.5$, and one year of running at $\mathcal{L} = 10^{33}\,\mathrm{cm}^{-2}\mathrm{s}^{-1}$. The dotted-dashed line is the standard-model result,

and the expectations for $N_T = 2, 4, 6$ are also shown. The estimated number of events in the range $M(\rho_T) \pm \Gamma(\rho_T)$ is total (background) = 400 (220), 1400 (200), 3100 (180), for $N_T = 2, 4, 6$, respectively. For specific IVB-decay channels, these numbers must be reduced by the corresponding branching ratios, *e.g.*, $W \to l\nu$ (11%) and $Z \to ee$ (3%). Once more, high luminosity and the capability to reconstruct high p_T IVBs from jets are both called for.

Substructure

History teaches us that a new level of substructure is found every time that we are satisfied with a complete list of "elementary" entities. At the SSC, substructure down to distances $d = \Lambda^{-1}$, $\Lambda \sim 20$ TeV is explorable. Quite generally, the new physics would first manifest itself[19] as new "Fermi" (four-fermion) interactions that modify the high p_T jet or lepton yields, relative to QCD expectations updated by HERA results. The example in Fig. 18 shows the predicted deviations at $\eta = 0$, for one year of running at $\mathcal{L} = 10^{33}\,\mathrm{cm}^{-2}\mathrm{s}^{-1}$, Λ =10 and 20 TeV, and with $\delta = \pm 1$ the sign of the $(\bar{q}q\bar{q}q)$ contact interaction. An obvious requirement is a linear calorimetric response over a large dynamic range. To estimate a total number of events, multiply $\Delta p_T\, d\sigma/dp_T d\eta|_{\eta=0}$ by ~ 6, the extent of the flat rapidity range. The reach in Λ is clearly related to the ability to operate at high luminosity: depending on the details of the new physics, $\mathcal{L} = 10^{34}\,\mathrm{cm}^{-2}\mathrm{s}^{-1}$ may be needed to unveil a quark substructure characterized by a scale as high as $\Lambda \sim 20$ TeV.

Conclusions

The search for elementary scalars in a broad mass domain requires good sensitivity in the measurement of multiple charged leptons, missing transverse energy, jet energy, and single photons. Supersymmetric particle searches need a detector emphasizing missing E_T and multiple jet reconstruction ($n_{jet} > 2$). The search for technicolor necessitates good W and Z identification in leptonic and hadronic decay modes. The search for quark and lepton substructure calls for accurate jet E_T-measurement, highly segmented jet calorimetry, and linearity over a broad energy range. In addition, searches for a new neutral gauge boson, Z', involve high resolution di-lepton or di-jet mass reconstruction. A search for a new W' in the channel $W' \to e\nu$ requires good measurement of electron, jet and missing energies.

All of the above "new-physics" signatures of high-mass and/or low-rate have large fractions of their modes in channels which would most naturally use calorimetry for detection, triggering and background reduction. We have thus designed a specialized detector, focussed on signatures that demand excellent calorimetry. We push it to the highest attainable energy resolution, segmentation, rate capability and hermeticity. We make no compromises to accomodate other detector components. In searching for new physics, our detector capitalizes on the measurement of electron, photon and jet energies, and on an angular resolution comparable to the inherent size and opening angles of the two types of showers. These calorimetric features are complemented by fast muon triggering and a fast missing-E_T measurement.

We have seen, in a variety of physics examples, that excellence in electron and hadron calorimetry, as well as the ability to run at high luminosity, are essential goals for an SSC detector.

Detector Conceptual Design

The conceptual design of the TEXAS detector gives priority to the calorimeter, since optimal calorimeter performance is essential for our physics goals. In our opinion the SSC will be better served by several detectors, each of which is optimized for specific physics goals rather than by compromising their individual performance in an attempt to do everything. TEXAS is optimized for high efficiency, high luminosity operation with maximum mass reach, with an emphasis on electron identification and energy measurement. With our physics goals guiding our detector decisions, we have achieved a high degree of specificity in our conceptual design. Those options which we retain are implementation options which will not fundamentally alter the system design, e.g. photomultipliers vs. vacuum photodiodes for scintillating calorimeter readout, rather than scintillating calorimetry vs. liquid argon calorimetry. Whenever possible, we rely upon conceptually simple and proven techniques which will yield a detector that is relatively inexpensive and easy to construct.

The first fundamental design decision has been to eliminate magnetic fields. By designing a completely non-magnetic detector, we have freed the calorimetric systems from the constraints that a central or muon detection magnetic field and associated coils place on:

- calorimeter hermeticity and uniformity;
- the inner and outer radius, rapidity coverage, segmentation, density and geometry of the calorimeter;
- jet spatial and energy resolution (magnetic spreading of low-momentum or showering particles);
- the operational characteristics of readout devices (PMTs) and calibration systems; and
- the readout complexity and triggering capability of the tracking system.

A second fundamental design decision has been to require that the detector and all its subsystems be operational and survivable at luminosity of 10^{34} $cm^{-2}sec^{-1}$. For the calorimeter, this requires signal integration times be on the order of the bunch-crossing time, along with a large inner radius and a high degree of segmentation. SSC calorimeters must operate at 3 orders of magnitude more luminosity and at an order of magnitude more energy and event complexity than existing large 4π calorimeters. This has driven us to select scintillator as our active element and scintillating fibers as our preferred implementation. For the tracking and pre-radiator system also, we need the speed of scintillator and the flexibility of fibers. For the muon system, we require triggering speed and adequate resolution both to reconstruct intermediate vector bosons from their muonic decays and to measure missing energy. We do not, however, allow the muon system to impact negatively upon the calorimeter performance, and we focus upon electrons rather than muons in our high-luminosity operation.

Calorimeter

The physics goals of the TEXAS detector require fast, high-resolution calorimetry with an emphasis on electron identification and precision measurement of electrons, photons, jets and missing energy. Detector response speed is particularly important for lepton isolation cuts, especially when exploiting the full physics reach of the SSC at luminosity of 10^{34} cm^{-2}sec^{-1}. We thus have chosen scintillator as the active element of our calorimeter system. Electron identification in the presence of a formidable QCD jet background requires fine lateral segmentation, longitudinal segmentation with preradiator and electromagnetic calorimeter compartments, and fast concerted operation with tracking and pre-radiator imaging. Operation at luminosity of 10^{34} cm^{-2}s^{-1} also incurs very substantial radiation damage, in particular in the forward regions. We address this with our large inner radius and with the use of radiation-hard plastic scintillator throughout the central detector, and with the use of liquid scintillator in the forward regions.

We aim to achieve rapidity coverage to $|\eta| = 5.5$ in a smooth manner, preserving detector hermeticity and providing a fast signal for missing transverse energy. For the hadronic calorimeter, plastic scintillating fibers provide a fast, compensated and high-resolution device. The large inner radius of the calorimeter allows for flexibility and easy installation of the fiber tracker, imaging pre-radiator, and electromagnetic calorimeter sections, while preserving possibilities for upgrading the central region with vertex chambers or other future technology. The TEXAS calorimeter is easily scaled in size and in segmentation without major design changes or disruption of system integration. Its final parameters will be determined by physics potential studies over the next year, and will accommodate a range of costs and capabilities.

Electromagnetic Calorimeter:

Separate electromagnetic and hadronic calorimeters can give important information for electron identification while decoupling the calorimeter design for each type of shower. This allows for different segmentation and mechanical support for the two sections, facilitates triggering, and provides for different transitions at tower boundaries as appropriate for the different shower sizes. For a scintillating fiber calorimeter, narrow electromagnetic showers sample many fewer fibers than do hadronic showers, with consequently greater demands upon uniformity of response between fibers and across module boundaries. The choice of fiber diameter and other properties involve trade-offs between calorimeter cost and performance which benefit from a separate optimization for the electromagnetic and hadronic sections. Radiation damage is also much greater near the electromagnetic shower maximum, while the effect of fiber attenuation length upon energy resolution (from longitudinal shower fluctuations) is much less.

Requiring lateral and longitudinal shower containment gives a fast signal for electron identification. We are also encouraged by recent results from the SPACAL collaboration which have demonstrated an e/π separation from a single longitudinal scintillating fiber

calorimeter alone of better than 10^{-3}, using pulse shapes. Fast constant fraction discriminators and simple analog circuitry are used to produce a "Full Width One Fifth Max" fast discriminator giving a direct e/π signal.[20]

Our current design calls for a scintillating fiber electromagnetic calorimeter with the fibers spliced at a mass-coupling connector to clear optical fibers for readout as indicated in Fig. 19. We are developing a prototype of this device within the context of the SSCintCal SSC subsystem. We couple 1 mm scintillating fibers with the EM calorimeter to bundles of clear fibers with less than the 1 mm diameter for readout through non-projective cracks in the hadronic calorimeter. The diameter mismatch decreases the fiber-to-fiber variation in coupling efficiency while minimizing the size of the gaps between hadronic calorimeter towers. The possibility of distributing readout fibers through the body of the downstream hadron calorimeter tower is also under study. Outside the hadron calorimeter, each EM fiber bundle will pass through an optical mixer (to minimize the effect of PMT efficiency variation across the photocathode) for readout by a single photomultiplier. Electromagnetic calorimeter modules will have their axes several degrees offset from pointing, in a pinwheel arrangement, to avoid "channelling" of electrons along individual fibers. The use of a thick pre-radiator to spread showers before entering the calorimeter may eliminate the need for such an angular offset, but this will require further study.

The calorimeter's potential for high energy resolution, scaling like $1/\sqrt{E}$, depends at low energy upon minimizing sampling fluctuations and at high energy upon minimizing systematic errors from nonuniformity or nonlinearity. The SPACAL collaboration has built and tested an electromagnetic calorimeter prototype with energy resolution of $13\%/\sqrt{E} + 0.5\%$[21] with the first term determined by sampling fluctuations. The sampling fraction (20% fibers by volume) for this calorimeter was determined by the requirement of "compensation" or an equal response for electromagnetic and hadronic showers, as discussed in more detail in the next section. The JETSET collaboration has built and tested an electromagnetic calorimeter prototype which has been optimized for energy resolution (50% fibers by volume) and achieved $6.5\%/\sqrt{E}$[22] .

For our conceptual design we anticipate a higher packing fraction within the electromagnetic section than would be allowed in a completely compensating device to emphasize our priority of measuring electrons and gammas, in particular for reconstructing light Higgs decays. The performance of a calorimeter which is compensating only within its hadronic region, with separate readout of its electromagnetic region, is poorly understood at present. We are performing simulations and constructing modules to test this arrangement within the SSCintCal subsystem effort. The choice of absorber/scintillator packing fraction and the tradeoff between resolution at lower energies and degradation of compensation will clearly require detailed study in advance of the proposal.

An attractive method of calorimeter construction would be to cast fibers within low-melting point eutectic lead alloy, as has been done at Boston University. Small electromagnetic calorimeters which have been constructed by this method are shown in Fig. 20, and have been measured to provide $16\%/\sqrt{E}$ resolution with a compensating packing fraction. Casting can minimize construction costs by eliminating the need for machining of tower

surfaces. A keystoned structure of such modules has been found by finite-element analysis to be self-supporting and to withstand creep, even for hadronic modules formed entirely of this material. A separate electromagnetic calorimeter, being much less massive, would bear a much smaller mechanical load and could be bound together with aluminum hoops like a barrel. The mechanical load of the EM calorimeter could then be transferred to the hadronic calorimeter, supported as described in the next section. Alternative methods using grooved or punched lead as pioneered by SPACAL are also amenable to automation, and will compete with the casting process described above in the comparison of prototypes for low-cost construction.

We are also considering techniques which would combine the electromagnetic and hadronic calorimeter sections into monolithic towers. To preserve compensation, the ratio of fiber to lead must be constant, and several possible variations of having parallel fibers of varying lengths in the keystone towers are presented in the SSCintCal Subsystem proposal. One advantage of this design is some natural longitudinal segmentation. A disadvantage is the spatial non-uniformity introduced across towers. Another way to preserve compensation in a tapered tower would be with stepped-diameter fibers which are oriented and stepped longitudinally along the tapered tower from front to back. For a 2-2.5 m radius calorimeter, the diameter growth of the fiber needed to preserve compensation is about a factor of 2.5 from the front to the back. This design is attractive because: a) the fibers can be calibrated more easily from end to end without the introduction of cracks, b) it may be simpler to construct than two-section devices, c) it introduces no dead areas from structural supports or coupling regions, and d) it is inherently more uniform across castings. Such a device might be combined with the method of e/π separation from pulse shape as explored by the SPACAL collaboration. Stepped fibers would require an automated splicing machine to create splices with uniform efficiency at the few percent level. This is simplified by the light being launched into successively larger and larger fiber segments. Another option under investigation is the use of "dichromatic" fibers for longitudinal segmentation, with red EM front ends spliced to green hadronic back ends and the output light split and filtered.

The relative merits of monolithic and two-section calorimeters will be carefully explored in subsystem work leading up to a detector proposal. The possibility of embedding radiation-hard quartz-window PMTs within the boundary between separate electromagnetic and hadronic scintillating fiber sections also bears study as it would eliminate any need for non-projective hadronic calorimeter cracks. A separate electromagnetic section would provide the possibility of an extremely high-resolution electromagnetic calorimeter. For example, one could construct the electromagnetic calorimeter entirely from BaF_2 crystals. Readout might be performed by filtering out the BaF_2 slow component and measuring the fast component with UV-sensitive PMTs.

Three important issues which must be addressed in establishing the viability of scintillating fiber calorimetry for the SSC are radiation damage, energy calibration, and the linearity and dynamic range of readout devices. There has been substantial recent progress in the development of radiation-hard plastic scintillating fibers with existing materials showing slight damage after exposure to several MegaRad doses. Effects of dose rate and dose conditions (particularly the surrounding atmosphere), annealing behavior, and varying fluor

and substrate chemistry upon fiber light yield and attenuation are under vigorous study by SSCintCal collaborators and other groups. We anticipate that these efforts will yield fibers with at least an order of magnitude more radiation resistance within the next year or two. The large inner radius of the TEXAS calorimeter helps decrease the radiation dose rate, and just using currently available plastic scintillator we would expect minimal difficulty to at least $|\eta| = 2$ at luminosity of 10^{33} (i.e. 1 MRad/yr). This estimate is subject to some uncertainty with regard to dose rate dependence and annealing behavior, but it is conservative in its assessment of both effects. Note that the radiation dose in the hadron calorimeter is an order of magnitude below that in the electromagnetic calorimeter. In the forward regions, where the radiation levels are highest, we expect to use liquid scintillator instead of plastic scintillating fibers as described below. A separate electromagnetic calorimeter (which receives the most intense and localized dose) could if necessary be replaced while leaving the hadronic calorimeter intact, since it would constitute only a small part of the total calorimeter cost.

Calibration of a scintillating fiber calorimeter can be carried out through a combination of laser light injection, fixed and moveable radioactive sources, compact accelerator radiation sources, and physics signals such as $Z \rightarrow e^+e^-$ (2 Hz rate at 10^{33} luminosity). Optical laser or low noise arc-lamp optical calibration of scintillator systems have achieved better than 0.5% long-term stability in large systems. Light injection on a quartz fiber into scintillator tests the entire system response, exciting the scintillator secondary fluors to emit the correct scintillator spectral distribution and time response. Light could be injected both from the inner and outer part of the calorimeter to separate scintillator and photodetector effects. Careful timing and spectral filtering can help resolve damage along a fiber. Radioactive sources, connected to flexible wire which could be moved along "sheaths" within the calorimeter, could be used for absolute energy measurement, to test detector response uniformity and to provide cross-calibration between detector modules. An interesting option is the use of compact accelerators for calibration, providing either gamma rays (10-20 MeV radionuclide line sources and 25 MeV high flux bremmstrahlung spectra) or neutrons (dd, dt, pBe etc. at 0.5-14 MeV) for absolute calibration and calibration in depth. Finally, the implementation of a low-threshold, two-electron calibration trigger is under careful study for the use of $Z \rightarrow e^+e^-$ events to help calibrate EM calorimetry. Minimum-bias and even cosmic-ray events may also have some usefulness in cross-calibrating detector channels and monitoring detector stability.

Another technical difficulty with scintillation systems is finding pulse-mode photodetectors capable of linear conversion of light to electrons over 4-5 orders of magnitude (say 50 MeV to 5 TeV) with a reasonable gain (at least $10^3 - 10^4$). Most existing photomultipliers begin to show substantial non-linearities over a dynamic range of a few 10^3, along with rate and recent pulse history-dependent gain shifts. The use of two PMTs per channel could help solve this problem by effectively extending the dynamic range. One alternative would exploit recent progress in developing diode-anode photoelectron target tubes. In these device, photoelectrons are accelerated to high voltage so that they create ionization pairs in a simple solid-state diode 1 cm^2 target. The diode might be Si, GaAs, diamond film, or might be replaced by an ion-chamber integrated circuit. The developers of this technology include Burle, D.E.P., Phillips and Hamamatsu. Vacuum photomultiplier devices are very radiation

hard when equipped with quartz windows, so that these IC-multipliers should survive as well.

Hadronic Calorimeter:

The key reasons to choose scintillating fiber technology for the hadron calorimeter are its speed, ease of lateral segmentation, potential for $35\%/\sqrt{E} + 1\%$ energy resolution in a compensated device, hermeticity and uniformity out to large values of rapidity, and negligible readout noise with external active devices. In our conceptual design, photomultiplier readout is distributed about the outer surface of the device, with no active devices within the body of the calorimeter. Drawings of the device and an engineering conceptual design for its mechanical support are given in Appendix A, provided by Draper Laboratory. Projective towers of scintillating fibers and lead alloy are combined into two hermetically sealed halves ($-2.5 < \eta < 0$, $0 < \eta < 2.5$) which are smoothly integrated with forward liquid scintillator-based calorimetry. Readout is through photomultipliers distributed on the outer surface of the hadronic calorimeter. A narrow gap at $\eta = 0$ allows for readout of the tracking and imaging preradiator systems, while electromagnetic calorimeter towers are read out through non-projective cracks between hadronic calorimeter towers.

The strictest requirements for integration speed of hadronic calorimetry come from the need for lepton isolation cuts to reduce backgrounds from c and b quarks. At 10^{34} luminosity, we expect $\approx$ 16 minimum bias interactions per bunch crossing. Fig. 21 shows a 1% probability of generating $E_t > 5\,\mathrm{GeV}$ within a cone $\Delta R = 0.4$ for 10 piled-up minimum bias events. Pileup of soft interactions as a background to hard interactions is often manageable because the event topologies and P_t spectra of the particles are very different. The pileup of a rare event plus one or more fairly common events requires careful study, but is clearly much less of a problem for a faster device. Pileup also degrades the jet energy resolution. Studies have shown that the dijet mass resolution of a 1 TeV object decaying into 2 jets degrades by factors of 2 or more for 10 minimum bias events piled up, for jet cone half-opening angles greater than 45 degrees.[23]

Scintillation techniques are the best presently available for high speed calorimetry, even in the face of longer times for shower development. Scintillators can have an integral pulse risetime (to 90% of the full pulse integral) of less than 5 ns. The full energy of a shower can be measured to 1% within 10 ns after the shower is fully absorbed. Fig. 22 shows the phototube pulses from a test of the SPACAL scintillating fiber calorimeter prototypes with 150 GeV pions, demonstrating a 4 ns risetime and a 30 ns integration time. This prototype device did not however fully contain hadron showers, so that the time required by a scintillating fiber calorimeter to collect all the neutron signal required for a completely compensating device awaits future measurement. It is nonetheless evident from these preliminary measurements that it will not greatly exceed 30 ns. In addition, lepton isolation cuts do not require precision hadronic measurement and thus can probably be performed with a 16 ns integration over one bunch crossing.

Calorimetry performance improves with larger radius and increased transverse segmentation, as illustrated in Fig. 23. For the TEXAS calorimeter, our conceptual design has an

inner radius of 2 meters and segmentation to $0.05\eta \times 0.05\phi$ in the hadronic and $0.025\eta \times 0.025\phi$ in the electromagnetic regions. This implies 40,000 hadronic towers and 160,000 electromagnetic channels. Both jet energy resolution and dijet mass resolution benefit as we increase these parameters. A 2-meter radius calorimeter ($R/\Lambda = 10$) could reconstruct a 500 GeV W dijet mass with a σ of 3-4 GeV when segmented to 0.03×0.03, compared to 6-8 GeV when segmented to 0.05×0.05 at 1-meter radius. One of our design goals will be to optimize the calorimeter price and performance as a function of the segmentation and radius. The electromagnetic segmentation must also be strongly coupled with the pre-radiator segmentation and performance. With a scintillating fiber calorimeter, segmentation can be modified just by bundling output fibers in different ways, so that an upgrade could be achieved by merely increasing the number of readout channels.

While optimal segmentation requires further detailed study, it is clear that high R/Λ and high segmentation are necessary for extracting the jet-jet and multijet signals of new physics and IVB decays from standard model QCD (particularly top quark) backgrounds. A high degree of transverse segmentation allows:

- better resolution of individual particle energies for electron isolation cuts,
- better jet-cone angle fitting,
- better centroid fitting to unfold or identify overlapping jet cones, and
- lower singles rate in individual towers for unfolding of overlapping minimum bias events and better tagging of multiple events in the same beam crossing.

Finally, fine transverse segmentation with longitudinal separation into electromagnetic and hadronic compartments provides redundant information for electron identification, since shower width and length are highly correlated.

Compensated calorimetry, with an equal response to electrons and to hadrons, is essential for high-resolution jet energy measurements over an extended dynamic range. Compensation in a lead/plastic scintillator system is predicted in Monte Carlo studies and has been demonstrated with prototypes in test beams. Because of the importance of low-energy neutrons and recoil protons to the compensation signal, precise compensation is impossible in a non-hydrogenous calorimeter. Lack of compensation gives rise to a constant energy resolution term degrading calorimeter performance at high energy, since the fraction of jet energy going into electromagnetic particles varies between jets at the same energy. Good jet energy resolution is essential for reconstruction of the hadronic decays of intermediate vector bosons in the presence of vicious QCD jet backgrounds. Compensation and calorimeter linearity are also important in reconstructing a compositeness signal from high P_T jet cross section as a function of p_T. Light attenuation in scintillating fiber calorimeters can also degrade calorimeter linearity and energy resolution (through longitudinal shower fluctuations). This effect can be minimized with long fiber attenuation lengths, such as may be obtained at longer wavelengths.

Physics needs for missing E_t triggering and measurement require a uniform and hermetic calorimeter, extending to large values of rapidity. Cracks or dead regions can give both a loss of resolution and a shift in the overall energy scale. Such energy shifts, inefficiencies, and dead regions can fake a missing E_t signal. TEXAS uses projective calorimeter towers to minimize cracks and nonuniformities, with the effects of residual readout cracks and thin support structures under careful study. Large rapidity range coverage is also necessary in order to keep backgrounds to missing E_t signatures below the irreducible neutrino limit. Fig. 24 shows the cross-section vs. p_T missing for beam holes from $\eta = 3$ to $\eta = 6$. Comparison with the missing p_T signal from neutrinos indicates the need for rapidity coverage to at least $\eta = 5.5$. In the very forward regions ($\eta = 3$ to $\eta = 5.5$) transverse energy flow measurements are performed by liquid scintillator-based calorimetry as described in the next section.

The TEXAS calorimeter uses projective geometry throughout, with the front faces of the calorimeter as normal as possible to the particle directions, to avoid feedthrough to adjacent towers and to minimize albedo. The thickness of the calorimeter is dictated by containment: more is better. For precision calorimetry, we require 99% containment. This implies a minimum of 11 absorption lengths at 90° growing to 14 interaction lengths below 30°. Together with the large inner radius, this forces the muon system to be very large indeed, which has contributed to our choice of a somewhat novel TRD muon system. Our choice of large calorimeter thickness also lowers punchthrough into this muon system.

The primary readout requirements for the TEXAS calorimeter are speed (digitization at the crossing rate) and dynamic range (10 MeV – 10 TeV). Presently available photomultipliers have no problem with the former requirement, but the latter is something of a challenge. Similarly, an ADC which can accomplish an effective 20-bit dynamic range with 16 ns digitization is a challenge. The physics requirement for this extended dynamic range needs more study, as does the possibility of separating fast and high-resolution digitizing functions.

Several ADC options are possible and are being investigated by LeCroy Research. We forsee at least three possible schemes:

(1) Multiple flash encoders with a digital decoder. This is a brute-force approach using today's technology. The required dynamic range would be obtained using 3 10-bit flash ADC's offset in gain by 3 bits each. Such an approach is uneconomical at this time but may be feasible in the future.

(2) $\Sigma - \Delta$ ADC's, as used currently in telecommunications. These devices obtain high resolution from relatively simple ADC's using sampling rates well above the signal frequencies and digital filtering. They are quite attractive because the data stream is inherently serial (single-bit) and could easily be transmitted on a single (digital) optical fiber to off-detector electronics. However, much R&D is required to develop a device which operates at the required speed.

(3) A "floating-point" ADC being developed at FNAL by G.W. Foster, C. Newman-Holmes and others is likely to meet our requirements. Its specifications include the following: (a) a 60 MHz digitization rate, (b) a floating-point result with 9-bit accuracy and 19-bit dynamic range, and (c) a low cost of $60/channel. The ADC/digital trigger is shown

in Fig. 25. The ADC requires development of an analog ASIC (Application-Specific Integrated Circuit) as in Fig. 26, which uses fast current switching and binary-weighted capacitors to digitize a 4-bit exponent. A normalized analog mantissa is digitized with a conventional FADC to 8-bit precision. The conceptual design for the TEXAS calorimeter trigger is discussed in a later section.

Forward Calorimeter:

The forward calorimeter regions, from $\eta = 3$ to $\eta = 5.5$ suffer the most intense radiation dose, have the largest rapidity range coverage per unit area (and per unit of shower size cross-sectional area), and have the least demands for high-resolution energy measurement. These regions all form a small part of the total calorimeter volume, and thus of the total cost. It is therefore appropriate to consider a separate radiation-hard technology for these areas. We retain our physics motivation of fast calorimetry for fast trigger decisions and for pileup rejection, leading us to the choice of replaceable liquid scintillator. This plug might be constructed of heavimet or tungsten, to contain shower feedthrough to adjacent cells and across the beampipe. Such a device would have an absorption length much smaller than a lead device with similar geometry. Fig. 27 shows a schematic novel liquid approach by our Texas A&M collaborators. It features non-projective channels for the liquid scintillator lined with radiation-hard total internal reflection films for light trapping. Fig. 28 shows photographs of a liquid scintillator electromagnetic calorimeter test module constructed with capillary tubes cast within a low melting-point eutectic lead alloy. The cast block is encased in a stainless-steel filling tank with acrylic windows for testing, and was filled with liquid scintillator under vacuum. The light yields have been shown to be equal to plastic fiber calorimeters with the same geometry.

The forward calorimeter is smoothly joined to the electromagnetic and hadronic calorimeters at $\eta = 3$. Simulations have shown that a 5 cm crack at 3 m from the interaction at $\eta = 3$ (the typical "corner" in calorimeter designs) increases the irreducible missing p_T ($\eta = 6$ hole + neutrino) background by a factor of 5-10 for missing E_t out of 500 GeV. We are aware of the consequences of our closed geometry for neutron albedo and for "splash-over" of shower particles from one side of the beampipe to the other, and both effects are under study. If necessary, the endplug calorimeters could be moved forward along the beampipe to mitigate these effects. Fig. 29 shows the consequence of limiting calorimeter rapidity, from which we can see that the beamhole beyond $|\eta| < 5.5$ adds little to the irreducible neutrino missing p_T background. For our conceptual design, we retain our "closed egg" geometry to emphasize our commitment to hermetic containment and missing E_t measurement.

Tracker and Imaging Pre-Radiator

The innermost section of the TEXAS detector consists of a scintillating fiber tracker and imaging pre-radiator system. Fig. 6 gives a conceptual diagram of the device. The tracker is composed of 3 *zuvzuv* plastic scintillating fiber (PSF) superlayers. At $\eta = 0$, the first

superlayer is at a radius of 1.0m, the second at 1.4m and the third at 1.8m. At the outer radius of the tracker there are 9 *zuv* PSF layers separated by thin ($\approx 2\,\mathrm{mm}$) lead sheets so that the early part of the shower development can be measured and tracked accurately. The tracker therefore merges into the first part of the calorimeter to form an imaging pre-radiator.

Signals from the tracking system are extracted along a narrow non-projective readout path in the calorimeter at $\eta = 0$. The tracking detector, and per force the whole detector, will be constructed in two mirror sections. Signals are read out either optically, in which case scintillating fibers will be spliced to optical fibers and the electro-optical devices will be outside the calorimeter and in a relatively low radiation region, or electrically, in which case the electro-optical devices will be on the inside of the calorimeter.

It should be emphasized that the requirements placed on a tracking system inside a non-magnetic detector are much less stringent than those for a tracker in a magnetic field. In the case of a magnetic tracker, the need for an accurate determination of the abscissa of a curving track requires the best possible resolution. In a non-magnetic detector it is sufficient to identify straight tracks. We are presently assuming that 1mm diameter fibers are adequate for this system. With the above stated dimensions, the tracker section has $\approx 2 \times 150{,}000$ channels and the pre-radiator has $\approx 2 \times 300{,}000$ channels.

The imaging pre-radiator is approximately 2.5 L_{rad} thick and provides fine grained transverse and longitudinal electromagnetic shower sampling in 9 super-layers. The transverse resolution is determined by the size of the fibers used. Neighboring layers will be offset by half a fiber spacing. The longitudinal sampling must be sufficient to separate electrons from hadrons to better than 1% and deep enough to allow, for approximately 95% of cases, both photons from a π^0 to have converted. The exact pre-radiator lead and fiber thicknesses will be determined during subsystem R&D work and will be chosen so as to preserve the compensation of the entire calorimeter; in any case, a $\approx$100 GeV electron loses only $\approx$0.1-0.3% of its energy in the first 3 L_{rad}. Fig. 30 illustrates the rejection power and electron efficiency that has been achieved by a pre-radiator in conjunction with a prototype scintillating fiber calorimeter by the SPACAL group.[21] The fine longitudinal segmentation together with the fine transverse segmentation provides a detailed picture of shower development and therefore of shower measurement. Furthermore, the initial development of the shower in the pre-radiator will lessen the effect of channeling in the fiber calorimeter, especially with thicker pre-radiators.

There are three major challenges associated with a PSF tracker/pre-radiator system, all of which are being actively researched via our sub-system R&D (for example[24] and our industrial affiliates:

- the first involves the ability of the PSF to have a good light yield after significant doses of radiation;
- the second involves the PSF readout;
- the third involves the support structure.

The question of the radiation hardness of the scintillating fibers becomes even more important when the SSC runs at the highest luminosity. The technology of scintillating

fibers is rapidly advancing at this time. In particular radiation resistance and light yields of fibers have both greatly improved in the past few years as the chemistry of plastic scintillators and their optical properties have been better understood. One of our industrial affiliates is Bicron and another is Optectron of France (see Appendix II) and we intend to cooperate closely with both of these in the development of suitable fibers. We also have good ties with Kyowa Gas of Japan who also manufacture high quality PSF.

The different possible readout elements have also seen much progress in recent years. However, suitable devices for operating in the exacting environment of the SSC have yet to be demonstrated. There are several very promising techniques but at this stage the complex decision based on the criteria of cost, simplicity of use and radiation resistance, among others, cannot yet be made. The list of possible readout solutions includes: a) the Avalanche Photo-diode being developed by one of our industrial affiliates, RCA/GE (see Appendix II) as a PSF readout device in a multidiode array format, b) the Rockwell SSPM (solid state photomultiplier) presently being investigated in another subsystem R&D program,[25] c) the Teledyne-Brown SDL (solid state diode laser), and d) the Burle SIT (Silicon Intensified Tube) which uses a pixel detector as photoelectron target in a standard image intensifier geometry.

For the support structure we are planning to work closely with ORNL as industrial affiliate (see Appendix II) in the development of lightweight carbon-fiber/epoxy support cylinders. Most of the details of this R&D work are described elsewhere[24] . Since it would be advantageous for the shape of the pre-radiator to match as closely as possible the inner calorimeter surface and the tracker super layers to match the pre-radiator, we shall investigate in some detail the feasibility of variable radius support cylinders. Fig. 6 illustrates the shape of the tracker pre-radiator.

The primary motivation for a pre-radiator detector is to provide good identification of electrons and photons, and to help measure their positions, energies and angles with high precision, while rejecting pions and fake electron signals. Electron identification in calorimeters is based on differences in em-hadron shower development. The lateral, longitudinal and time development of the showers differ for electrons and hadrons; with methods based on these differences, rejections of $10^2 - 10^3$ can be achieved. However, different calorimeter signals are highly correlated since the major source of misidentification comes from electromagnetic fluctuations in the hadron signal. A pre-radiator that samples early shower development will provide uncorrelated information. Furthermore, when an electron is accompanied by a hadron, calorimetric methods fail, restricting electron identification to isolated tracks only. An imaging pre-radiator does not suffer from these limitations as it can separate electrons from other particles at distances as small as a few mm, enabling some electron identification inside jets.

The imaging pre-radiator can be considered as a highly longitudinally and transversely segmented lead-PSF calorimeter, with the fibers transverse to the particle directions. It is a natural intermediary or link between a tracker and the electromagnetic front-end of a compensated calorimeter. Recently the UA2 experiment at CERN has demonstrated that an imaging pre-radiator can greatly enhance the quality of data in a non-magnetic tracking

detector.[26] An imaging pre-radiator provides redundant and detailed structural information which is important for untangling complex jet events and which is normally unavailable with presently conceived trackers and calorimeters together.

We are also considering the necessity of having a straw-tube TRD system (inside the tracker) to complete the electron identification. Such a system, which is applicable only for low energy electrons ($< 100\,\mathrm{GeV}$) would compliment our good electron identification supplied by the pre-radiator and our ability to do so close to and even inside jets. Besides this, it provides redundant information for the tracking system which would simplify the task of understanding complex events. Whether or not we propose such a complementary system will depend on the results of experience with tracker/pre-radiator systems and sub-system R&D.

So, to summarise, at the SSC a tracker/pre-radiator is essential for:

- tagging photons and electrons with high efficiency and electron/hadron rejection of at least 10^2 even in complex events where isolation cuts cannot be applied,
- measuring the starting point of an electromagnetic shower with high spatial accuracy (1 mm or better),
- identifying fake electrons formed by the overlap of a charged hadron with a photon. This is especially important in a non-magnetic detector where an E/p cut cannot be made,
- separating direct single photons from π^o's on an event-by-event basis. The photons from a 100 GeV π^o separate by at most 2.6 mm/m; in TEXAS they have a separation of ≈ 5 mm at the calorimeter inner surface.
- unambiguously assigning electromagnetic showers with a bunch crossing.

The tracker/pre-radiator is an effective component of a precision calorimeter system, providing redundant and essential information for electron/photon physics. It uses a proven technique with very good potential to work at the speed needed for SSC experiments. The smooth transition between a pure scintillating fiber tracker and the full calorimeter is a unique and powerful concept.

Muon Spectrometer

Muon detection and measurement are essential for confirming the universality of lepton decay channels of the Higgs, for a missing energy calculation in the fast trigger and for new physics signatures in general. Normally the electron channels observed with the exceptional calorimetric resolution will always have equivalent muon channels. Because muon identification has such a large confidence level, confirmation of electron modes in the muon channel is essential. The muon energy range of interest is from 60-600 GeV (gamma of $\approx$600 - 6,000) for most heavy mass physics, a very modest dynamic range, as shown, for example, by the acceptance curves for 400 and 800 GeV Higgs in Fig. 31 . Essentially 90% of all muons from the Higgs are found between 100 GeV and 600 GeV for M_H between 400-800 GeV.

At the SSC, practically all muons below 60 GeV are from c and b decay. Their rate ($\sim 10^4$ Hz for $p_T < 10$ GeV, see Fig. 32) exiting the calorimeter is a serious problem for large muon systems with long drift times and high spatial resolution. Furthermore, charge discrimination is useful, but not overwhelmingly so (see Fig. 33) for the Higgs signal. Above 400 GeV masses, only a factor of 2-3 reduction in the diboson mass background is achieved by knowing the sign of the charge of a particle (before any lepton discrimination cuts). Most magnetic systems only cover a limited range ($|\eta| < 1.5$, $p < 200$ GeV). Muon energy resolutions of 10–20% can find the Higgs for M_H >400 GeV (Fig. 9.). Even in the "marginal" case of the 20% muon energy resolution, the Higgs signal is $\approx 2-3$ standard deviations above background with no other cuts for $M_H = 400$ GeV. For the very heavy Higgs with a 200 GeV top quark, the 4 lepton mass bump is so wide that the modest resolution that we achieve for the muons will suffice (see Fig. 13).

An optimized calorimeter design should be unconstrained by typical magnetic solutions for muon energy measurement– solid iron toroids are heavy, expensive and create large radiative losses. Air-core magnets are expensive and cumbersome; furthermore, the chamber areas are large relative to the required precision of 100μ or better.

In contrast to the sagitta which decreases with energy, the TRD yield increases with gamma. With sufficient radiator a TRD provides a natural way to measure momentum at high gamma. The TRD yield at saturation achieved in recent systems is about 25-30 X-rays above a 4 KeV threshold per meter of detector thickness. Fig. 34 shows typical TRD yields as a function of gamma. The detector sets are typically ≈ 9 cm radiator, either polyethylene foam or embossed polypropylene films, to 1 cm of Xe-proportional gas detector. Recently foams with very uniform cell and wall sizes have been used, achieving 85% of the ideal TRD yield[27] . The maximum quasi-linear response range for a TRD is 20:1, corresponding typically to γs of 500 to 10,000. This fortuitously corresponds to muon momenta from 50-1,000 GeV.

Further, a dE/dx measurement in the relativistic rise region is sensitive over a muon energy range of $\sim 10-100$ GeV, as shown for a typical TRD X-ray detector in Fig. 35

The motivations to use TRD and dE/dx to measure the muon momenta are the following:

a) Low cost for a large system - The large calorimeter with a large outer radius forces us to be conscious of the costs of a muon system. TRD and dE/dx do not require ultra-high mechanical precision, and therefore have a much reduced cost per area of chamber. Furthermore 10's of ktonnes of iron or a large superconducting magnet yoke is not necessary. The cost per m^2 of the MACRO prototype, which should achieve 30% momentum resolution is only \$100/m^2.

b) Trigger and speed - TRDs can generate a rapid muon energy trigger by thresholds alone - unlike precision wire systems. Coupled with position, a first level p_T trigger is formed. Also a rapid missing transverse energy calculation can be made.

c) Modularity and access - the lightweight foam radiator and chamber modules are easily assembled inside a lightweight spaceframe which moves easily for calorimeter access.

d) Negligible radiative muon losses - energy fluctuations are small compared with iron toroids.

e) Insensitivity to muons with energies less than $\sim$ 50 GeV. The TRD threshold can be set to ignore the low energy muon "background".

The MACRO experiment is currently making plans to install large ($2 \times 2.6 \times 6$ m^3) TRD modules to measure muons deep underground of the same energy as at the SSC. The total MACRO system will be a similar size to TEXAS. The MACRO expenditures can be scaled to give a cost of about \$1,000/m^2 at the SSC.

We have scaled the MACRO experience to the SSC. We consider a 60 layer polyfoam and Xe+CF_4 150 ns X-ray drift tube system with a total thickness of 6 m, as contrasted with a 2.6m Ar system. Limited streamer tubes provide tracking and liquid scintillator counters trigger. The system construction cost is \$30-\$60 million. Figures [3, 4] show details of the TRD system as implemented for the SSC experiment. The resolution can be optimized to the gamma range of physics interest as shown in Fig. 36 . The optimization procedure requires choosing the proper foam wall thickness and bubble size and the proper X-ray chamber thicknesses. Fig. 37 shows initial calculated resolutions as scaled from the D0 collaboration at FNAL. The TRD system provides a resolution of better than 30% at 50 GeV, 6% at 200 GeV, +50% and -20% at 600 GeV. A dE/dx measurement for low momenta could provide a $\approx$ 30% resolution from 10–100 GeV.

The muon TRD-dE/dx provides a modest cost solution to the muon detection problem with a large calorimeter. The resolution is sufficient for the high mass physics goals. Furthermore, it allows the generation of a high momentum trigger in the first stage of event readout. It is inherently transparent to low energy muons which are uninteresting for many high mass physics signals.

The TEXAS trigger

Our conceptual design for the TEXAS trigger will have three levels: a fast analog trigger (approx 200 nsec decision time), a pipelined digital second level trigger (approx 10 μsec decision time 700 ns including propagation delay), and a processor-based third level trigger. The third level trigger will be implemented by an on-line processor farm, after readout of the entire event. The fast analog trigger is necessary to reduce the amount of data that must be stored while waiting for the second level trigger to complete. It has inputs from the calorimeter (for electrons and jets) and the muon scintillator.

The calorimeter triggers are based on supertowers (4×4 arrays of towers). To ensure complete coverage, the supertowers are overlapping such that the point where 4 super towers meet is the center of another supertower. The overlap is used to reduce losses from jets and electrons in the cracks between towers. To find jets, the energy in a supertower is summed. This energy is then compared to a number of (programmable) thresholds, for example, 50

GeV, 100 GeV and 200 GeV. A count is made over the entire detector to determine the number of jets above each of these thresholds. This can be done with simple analog busses: each supertower above a given threshold injects a current pulse into the appropriate bus. Equalizing the timing will require delay cables in various places on the bus structure. An early conversion of signals from electronic to optical (with fiber optic buses) may be necessary to avoid synchronous noise problems.

The electron trigger is similar. The electron energy is found by summing the electromagnetic energy in the central four towers only. If enough energy goes into the hadronic section behind it, the electron will be vetoed. It may also be vetoed if there is enough electromagnetic energy in the outer 12 towers.

The fast muon trigger is found by requiring a time coincidence in the liquid scintillator boxes. All of the trigger signals are brought together at $\eta = 0$. A programmable logic unit makes the decision, allowing for triggers such as: 2 electrons above 50 GeV, 1 jet above 100 GeV and at least 1 muon. Because of potential problems with synchronous noise, we may need optical couplings to obtain signals for total E and E_T. This first level trigger should appear in about 700 nsec. It can be used to trigger zero suppression and data storage where needed. It is anticipated that the first level trigger rate would be less than 100 kHz.

The second level trigger uses digital hardware. It has somewhat more sophisticated electron, jet, and muon identification. In addition, the total energy and missing energy are calculated. The most likely candidate is a digital pipeline on the calorimeter. Electronics at calorimeter tower (or supertower) will yield the total energy, E_T, jet energy (assuming that a jet hit the tower) and electron energy (if the energy deposition matches that of an electron). This information is passed down the detector in a pipeline, which advances one step each beam crossing. At each stage, the pipeline contains the total energy summed so far and a list of the highest energy electrons and jets encountered up to that stage. At each step, a tower adds its energy to the running energy sum and compares its jet and electron energy to the lists. High energy candidates are added to the list, replacing lower energy events.

The pipelines run parallel to the beampipe, originating at high η, and flowing toward η=0. At the detector waist, the energy is weighted by $\cos\theta$ and $\sin\theta$ and summed to find the missing energy. The jet lists are combined to produce a final list. The electron significance is refined by integrating tracking and preshower information. Muon triggers include information from scintillator timing and tracking by using lookup table pattern recognition and TRD data. This data is presented to a programmable logic unit to make a second level trigger. The second level trigger rate should be of the order 100 Hz.

A second level trigger initiates data read-out. Each tower stores an event "history" in a memory equal in depth to the trigger pipeline. Triggered events are read out either through a dedicated digital port (dead-time-less) or through the trigger pipeline (incurring some dead-time).

Because of the simplicity of the TEXAS tracking, and the matching of calorimeter towers to hadronic jet sizes, the event size is much smaller than with multipurpose SSC detectors. The anticipated data size is less than 200 kBytes, comparable with the CDF event size. At 100 Hz, the data flow rate is 20 MB/sec, also comparable to CDF.

During readout, the data is loaded into the memory of one of a farm of processors which handle both the third level trigger and on-line reconstruction. Dual ported memory is used; the data is dumped on one bus and the memory is then switched to the processor. Because of the small event size and the simplicity of the tracking, the CPU requirements are minimal by SSC standards. CDF planned on 400 mips of CPU power; 2000 mips seems adequate for TEXAS. This is easily satisfied by 50 RISC CPU's, each with 40 mips of processing power.

This CPU farm will filter the events and write out at a maximum event rate of a few Hz, probably supplemented by exhaustive histogramming of data from rejected events. This data rate could be handled by a single 6250 bpi tape drive, while a number of more modern technologies could be used to reduce the required effort in handling the gigabyte/hour produced.

Computation for TEXAS

The computing power needed to design,[28–32] control and analyse the different phases of an SSC experiment dwarfs all of our previous efforts.

So far, there has been only limited activity in the use of *supercomputers* for high energy physics. Almost all of it has been associated with the "vector processor" type of supercomputer.[33] In this approach computations are performed simultaneously on collections of data arranged into a vector array, rather than operating on each individual data element one at a time in sequence ("scalar processing"). This vector-parallel technique is the basis of traditional supercomputers, particularly those of Cray Research Inc. Powerful as these machines are, they are most efficient for those problems which can be cast into the vector format. There is a great deal of debate as to whether the typical problems of high energy physics are well suited to this approach. Another approach to supercomputing has only recently become commercially available: "massively parallel processors". In its simplest form the idea is to have many processors all available to work on a problem simultaneously. An arrangement where these processors are the nodes of a matrix lends itself quite naturally to many problems in theoretical physics, a good example is the computation required for Lattice Gauge Theories. Their application to high energy physics has only recently been begun.

Our collaboration is fortunate to have access to a 32,000 processor supercomputer at Boston University, the CM-2 "Connection Machine". It also has a resident "SSC Experiments Computation Group" lead by Richard Brower and Robert Wilson. This group, supported by an SSC sub-systems R&D award, is investigating the application of fine-grained parallelism to high enery physics problems and it is currently focusing on two aspects of interest to us. The first is an implementation of the widely used electromagnetic shower simulation code, EGS4. The group has agreed to use the TEXAS scintillating fiber calorimeter geometry as one of the first realistic production runs of the new code. This capability should allow us to run much more detailed simulations of our calorimeter designs than would be possible on less powerful machines.

The second project, pattern recognition in tracking and calorimetry at the SSC and possibly also triggering, has even greater potential for the analysis of experiments. These very CPU-intensive tasks are inherently parallel and should find a natural solution on a CM-style architecture. With assistance from computer scientists at the university and at Thinking Machines Corporation, the CM group is exploring a range of algorithms that are in current use. For example, a parallel implementation of the Hough transformation, a common technique for identifying straight tracks, as in a non-magnetic detector, is already operational.

Our goal is to support the efforts of the Connection Machine group whilst at the same time making use of the more traditional computing facilities available to us.

Anticipated Detector Performance and Physics Reach

In our discussion below we have characterized the TEXAS detector in the following manner:

Tracking System and Imaging Preradiator:

- Spatial Resolution = $< 1\,\mathrm{mm}$
- Speed = $< 15\,\mathrm{ns}$
- Coverage = $|\eta| < 3$
- e/π rejection = 30
- γ/e rejection = 100
- γ/π^0 rejection = 10
- Electron efficiency = 0.99

Electromagnetic Calorimeter:

- Resolution = $7\%/\sqrt{E} + 0.5\%$
- Speed = $< 15\,\mathrm{ns}$
- Coverage = $|\eta| < 3$
- Segmentation = $0.03\eta \times 0.03\phi$
- e/π rejection = 300
- Electron efficiency = 0.95

Hadronic Calorimeter:

- Resolution = $30\%/\sqrt{E} + 1\%$
- Speed = $20\,\mathrm{ns}$
- Coverage = $|\eta| < 3$
- Segmentation = $0.05\eta \times 0.05\phi$
- e/h = 1.0 ± 0.05

Forward Calorimeter:

- Resolution = $30\%/\sqrt{E} + 2\%$
- Speed = $20\,\mathrm{ns}$
- Coverage = $|\eta| < 5.5$

Muon Spectrometer:

- Resolution = 15% for $p > 0.1\,\mathrm{TeV/c}$, $\approx 0.15\%/p^2$ for $0.05 < p < 0.1$
- Speed = $100\,\mathrm{ns}$
- Coverage = $|\eta| < 3$

Higgs Physics

The physics of electroweak symmetry breaking is fundamental to the SSC. The TEXAS detector particularly targets intermediate-mass ($M_Z/2 < M_H < 2M_Z$) and very high mass Higgs bosons ($M_H > 600\,\mathrm{GeV}$). The standard Higgs boson provides a useful benchmark for detector performance and it should be confirmed or eliminated from $100 < M_H < 1000\,\mathrm{GeV}$ at the SSC. For the intermediate mass case, where one must rely upon rare decays to obtain a clean signal, TEXAS excels in electromagnetic energy resolution, electron efficiency, electron identification, γ/e and γ/π^0 discrimination, and high-rate capability for increased statistics and hence better single-to-noise. In the very high mass range, TEXAS uses its high-rate capability to extend the physics reach of gold-plated 4-lepton channels, combined with the use of more difficult (but better statistics) intermediate vector boson decays to neutrinos or jets.

Standard model Higgs production rates (as a function of the top quark mass) and intermediate-mass decay rates are illustrated in fig. 38 .[34] A Higgs lighter than 90 GeV is accessible at LEP II, while recent CDF results indicate that $m_t > M_Z$ so that $H \to t\bar{t}$ decays are disallowed for $M_H < 2M_Z$. Backgrounds for $H \to b\bar{b}$ and $H \to \tau\bar{\tau}$ swamp the signal, both for H and $(W + H)$ production.[9] We therefore consider the decays $H \to \gamma\gamma$, $H \to ZZ^*$, and $H \to WW^*$, where the asterisk indicates virtual particle production.

Higgs $\to \gamma\gamma$

The rare decay $H \to \gamma\gamma$ has branching ratio $\sim 10^{-3}$, yielding around 500 events per SSC year and more with increasing top mass.[35] This channel is useful for $110\mathrm{GeV} < M_H < 2M_Z$, with the lower limit dependent upon luminosity and detector resolution. The signature is a pair of isolated high-p_T photons, with no missing p_T and minimal hadronic activity. Irreducible continuum background arises from the QCD direct production of photon pairs via $q\bar{q} \to \gamma\gamma$ and $gg \to \gamma\gamma$. In addition, QCD jet-jet events where both jets fluctuate to mimic photons must be rejected at the 10^8 level, and jet-γ events must be rejected at the 10^4 level. Detection of the Higgs to $\gamma\gamma$ decay in the presence of these backgrounds thus provides a useful benchmark for the capabilities of the electromagnetic calorimeter and imaging preradiator.

Excellent electromagnetic energy resolution is necessary to distinguish the $H \to \gamma\gamma$ signal from the $q\bar{q} \to \gamma\gamma$ background. (see fig. 14.) The fine EM calorimeter segmentation of the TEXAS detector should permit triggering on isolated photons with transverse energy of > 10 GeV for $|\eta_\gamma| < 5$. As stated earlier, the TEXAS electromagnetic resolution is in between the two cases shown in fig. 14; in addition, one year of operation at $\mathcal{L} = 10^{34}\mathrm{cm}^{-2}\mathrm{s}^{-1}$ will triple the statistical significance of the signal. In addition to having high luminosity and good energy resolution for extracting a 2γ signal, the detector must preserve this sample through high photon efficiency while rejecting QCD jet-jet and $Z^0 \to e^+e^-$ backgrounds. The principle background comes from jets where a leading π^0 converts most of the jet energy into an electromagnetic shower. In a Monte Carlo study[36] using parameters similar to that of the TEXAS calorimeter (but with segmentation of $\Delta\eta = \Delta\phi = 0.1$), one QCD jet in 10^3 faked an isolated photon. Half of these fake photons may be rejected as having $E_T < 20\,\mathrm{GeV}$, and we expect to further improve background rejection with our greater segmentation and with

our imaging preradiator. The preradiator distinguishes energetic neutral pions from direct photons, by resolving separate electromagnetic showers from $\pi^o \rightarrow \gamma\gamma$. Photon conversions in the tracker are not a problem with $< 0.10 L_R$ for $|\eta_\gamma| < 3$. Tracking efficiency of 99% is sufficient to reduce $2 \times 10^7 Z \rightarrow e^+e^-$ decays per SSC year to a negligible background.

Higgs $\rightarrow ZZ^*, WW^*$

For 130 GeV $< M_H < 2M_Z$, the Higgs can be sought as a narrow resonance in the channel $H \rightarrow ZZ^* \rightarrow eeee$. The production cross section for Higgs by gg fusion is about 100 pb in this mass range (for $m_t \approx 90$ GeV), falling slightly for increasing top quark mass.[37] This gives an event rate of ≈ 60 events/SSC year for $M_H = 160$ GeV, $m_t = 90$ GeV, $M_{Z^*} > 25$ GeV. The cut on the invariant mass of the reconstructed Z^* is needed to remove the background from $q\bar{q} \rightarrow Z\gamma^*$. Further background arises from $gg \rightarrow Ztt$ or Zbb, with several times the signal strength at the Higgs peak.[38] Requiring isolation cuts on the electrons and further reducing the event statistics. This channel therefore necessitates high electron efficiency at high luminosity to obtain a statistically significant sample. In addition, the energy resolution of the EM calorimeter should be better than $\sigma_E/E = 1\% + 15\%/\sqrt{E}$.

If an intermediate mass standard Higgs exists, measurements in both the $\gamma\gamma$ and ZZ^* channels would give important information about the physics of the Higgs sector through the relative couplings to gauge bosons. Another channel which might be experimentally accessible is $H \rightarrow WW^* \rightarrow \nu e \nu e$. Although a Higgs mass peak cannot be directly reconstructed, there may be a Jacobian peak above the background from continuum W W pairs.[39] This channel requires cuts on missing transverse momentum (> 20 GeV), the transverse momentum of the electrons ($p_T(e) > 20$ GeV), and the angle in the transverse plane between the electrons ($\Delta\phi > 160°$). This last cut is to reduce the background from $Z \rightarrow \tau\bar{\tau}$. Backgrounds from heavy-quark pair production followed by semileptonic decays need further study, as does the background from $t \rightarrow Wb$ decays for a heavy top. The channel $H \rightarrow WW^* \rightarrow \nu e \nu e$ requires further study with a detailed detector simulation, but the high-luminosity capability, electron efficiency, and hermiticity (as discussed below) of the TEXAS detector ought to permit this measurement.

$H \rightarrow ZZ \rightarrow llll$

The Higgs to 4 electron signature is gold-plated. The background arises not only from continuum Z-Z production, but also from $Z +$ jets, dominated by $gg \rightarrow Zt\bar{t}$ and $t\bar{t}$ decays where the $t\bar{t}$ decays produce leptons. These backgrounds are removed by a combination of lepton isolation cuts (to remove leptons from light quark jets), rapidity cuts, transverse momentum cuts on the leptons, lack of missing E_T, and reconstructed Z invariant mass. We have included these cuts in a Monte Carlo simulation of the TEXAS detector, with the results shown in Fig. 39 for $m_t = 120 GeV$ and M_H=300, 400, 600, and 800 GeV. As expected, the signal is well-resolved from the background, so that we are only statistics-limited at high energy. For $M_H > 600$ GeV, electron efficiency and the ability to operate at high luminosity determine the physics reach of the apparatus in this channel. Further detailed studies of the detector performance at high luminosity will be needed to establish the upper M_H limit in this channel, but our preliminary results show good sensitivity to $M_H > 800$ GeV after one year at $\mathcal{L} = 10^{34} \mathrm{cm}^{-2}\mathrm{s}^{-1}$.

By including the channel $H \rightarrow ee\mu\mu$, we triple our statistics over that available from $H \rightarrow eeee$ alone. The TEXAS muon spectrometer has a somewhat different response from a more conventional muon magnetic spectrometer or toroid, as discussed earlier in the Conceptual Design section. We have included this response function in our Monte Carlo study of the TEXAS detector sensitivity to this channel. The results are shown in Fig. 40 , again for $m_t = 120GeV$ and M_H=300, 400, 600, and 800 GeV. The momentum resolution function for the TEXAS muon spectrometer is below 10% for much of the relevant momentum range. As with the 4-electron channel described above, a firm upper limit on the physics reach of the apparatus requires more work clarifying lepton efficiency and background sensitivity as a function of machine luminosity. Again as for the 4-electrons, however, by designing for fast and simple detector operation we anticipate reaching beyond $M_H > 800\,\mathrm{GeV}$ in high-luminosity SSC operation.

The TEXAS detector has limited capability for measuring the $H \rightarrow ZZ \rightarrow \mu\mu\mu\mu$ channel, as shown in Fig. 41. This is because one of the four muons frequently has momentum of $< 50\,\mathrm{GeV/c}$, where the TEXAS muon spectrometer has poor resolution. This channel only contributes 1/2 the statistics of the $H \rightarrow ee\mu\mu$ channel, so we may neglect it. In this way, TEXAS is complementary to large multiple-purpose detectors with magnetic muon systems, magnetic tracking, and slower calorimeters. While they choose $H \rightarrow 4\mu$ and abandon $H \rightarrow 4e$ at high luminosity, we do the opposite.

$H \rightarrow ZZ \rightarrow ll\nu\nu$

Another way to extend the reach in M_H is to use the channel $H \rightarrow ZZ \rightarrow ee\nu\nu$. This gives us a factor of 6 increase in statistics over the 4-electron mode, but at the cost of an invariant mass constraint on the Z which decays to neutrinos. Background arises from the ZZ continuum and from the WZ continuum with $W \rightarrow l\nu$, if the lepton is undetected. The most important source of background, however, is from $Z + jet$ where much of the jet energy fails to be detected. This background is removed through a transverse momentum cut on the Z, and on the quantity ${p_t}^{back} = \Sigma_i|{p_t}^i|$, with the sum running over all particles in the transverse half-plane opposite the Z. A distribution of the latter quantity for signal and background is shown in Fig. 13. The resolution on ${p_t}^{back}$ degrades rapidly if one loses detector hermeticity through cracks, or through poor rapidity coverage. A detailed study of this channel for the TEXAS detector is not yet complete, but the detector simplicity and large rapidity range naturally yield a very hermetic device.

There may be a further capability to extract this signal from the Z jet background by using spectator quark jet information. These jets are produced at large rapidity ($3 < |\eta| < 5$) and typically have p_t of order M_W.[40] The forward calorimeter for the TEXAS detector is designed to perform high-resolution compensated hadron calorimetry at high rapidity, using radiation-hard liquid scintillator within an absorber with very short interaction length. The totally hermetic geometry is designed to preserve ${p_t}^{back}$ resolution to $|\eta| = 5$, although definitive proof of its efficacy awaits further detailed Monte Carlo work.

$H \rightarrow ZZ \rightarrow lljetjet$

If they can be resolved from backgrounds, the mixed hadronic-leptonic decays of the ZZ channel provide 20 times the statistics of the 4-lepton mode. Background arises from QCD

processes giving Z plus jets, where the jets combine to form the invariant mass of the Z within detector resolution.[41] Hadronic energy resolution and the spectator jet triggering that we discussed earlier are clearly critical in limiting this background. The TEXAS calorimeter provides hermetic containment and precision hadronic calorimetry to high rapidity. The hadronic segmentation may easily be augmented to improve the hadronic resolution of our scintillating fiber calorimeter; the optimization of this hadronic segmentation awaits detailed study of signal and background in this and similar channels.

Another method which has been studied to increase the signal-to-noise in this channel is to cut on the charged multiplicity of the events. Jets from Z's from the decay of Higgs bosons have much lower charged multiplicity on average than do jets from the QCD backgrounds.[42] With the TEXAS detector, the scintillating fiber tracking system/imaging pre-radiator system is designed to measure charged multiplicity fast enough to resolve multiple interactions within a beam crossing by the reconstruction of distinct interaction vertices.

$H \rightarrow WW \rightarrow l\nu jetjet$

The mixed hadronic-leptonic decays of the WW system have larger statistics and may be more amenable to background suppression than the analogous ZZ decays described above.[43] A recent study has analyzed backgrounds including $q\bar{q} \rightarrow WW \rightarrow l\nu jetjet$ for a heavy top quark.[44] A set of cuts that includes lepton isolation and high transverse momentum for the lepton and jets gave 200 signal events on a 100-event background for $M_H = 1$TeV and m_t=175 GeV. Spectator jet tagging and charged multiplicity measurements are similarly effective in removing backgrounds in this channel. Measurement of longitudinal WW and ZZ production at very high energies is fundamental to understanding the dynamics of electroweak symmetry breaking. For a non-resonant Higgs sector, this relatively high-statistics channel may be essential.

Beyond the Standard Model

We have previously examined several signatures of physics beyond the Standard Model in our discussion of Physics Goals. Generally, the same virtues of speed, high electromagnetic and hadronic resolution, large rapidity coverage, total hermiticity from seamless construction, large inner radius, and simplicity of design reap benefits in these physics pursuits as well. Supersymmetry places an emphasis on linearity and the measurement of missing p_T, as does detection of $H \rightarrow ZZ \rightarrow ee\nu\nu$. The search for new gauge vector bosons emphasizes electron efficiency and jet resolution, in order to extend the physics reach to the highest possible masses. A detector design for $H \rightarrow ZZ \rightarrow eeee$ and $H \rightarrow eejetjet$ capability will naturally excel in these measurements. Evidence for technicolor interactions could be obtained by measuring W W and W Z scattering at extremely high energy, as discussed under $H \rightarrow WW \rightarrow e\nu jetjet$ and $H \rightarrow ZZ \rightarrow eejetjet$ earlier. Sensitivity to quark substructure is a consequence of a linear and well-compensated calorimeter, which will also be necessary for reconstructing W and Z masses from high p_T jets. In each case our strategy of fast operation gives us access to rare events by exploiting high luminosity, and our strategy of uncompromised calorimetry gives us access to difficult decay modes through high resolution and good hermeticity.

Milestones to Define Detailed Design

We propose a highly focussed 12-18 month program to produce: a) an accurate estimate of the cost and time to build the TEXAS detector; b) a full assessment of the physics potential; c) high level of confidence in the technology; d) a complete proposal.

This process is essential for a project which may require about $180 million ± 20% to complete. We have budgeted about 4% of $180 million to proceed with this one-year plan, about 33% of the average yearly cost over an 8-year construction cycle. We would intend this development funding to proceed past the deadline for proposals, up until the decision on the proposals is made by the PAC, in order to keep the group working at full speed through an approval.

We have identified several areas where the technological and cost confidence should be improved and have budgeted considerable funding. These are: a) radiation hard scintillating fibers; b) low cost high pulse linearity pmts; c) pixel detectors at a few $/pixel; d) muon TRD performance.

In order to make this short-term plan a reality, we have also budgeted funds for temporary engineering and technical help and the managerial and secondary help needed to launch this plan. Many of these personnel will be hired immediately through Draper Labs working at the Universities, through specialty technical help agencies or by the TEXAS staff. Physicists will be relieved as much as possible from administrative duties and paper work by this plan.

TEXAS Simulation Milestones:

Calorimeter Response Simulation Milestones (June, 1991)

These studies of generic scintillating fiber tower geometries are designed to investigate various configurations of the basic spaghetti concept in order to find one or two arrangemem-nts to build in hardware in the tapered tower geometry required of a 4 π detector. These studies will examine the various questions outlined previously in the section on calorimeter concept. By January, 1991 all alternatives will have been investigated and answers found from the computer studies. These will address:

- compensation, energy resolution and linearity determination for alternate longitudinal fiber arrangements and fiber diameters;
- longitudinal segmentation studies;
- non-compensated em section studies;
- transverse segmentation and uniformity studies across towers;
- radiation dose studies inside towers;
- energy deposition time studies;
- single particle e/ π separation;
- projective angle energy resolution.

Physics Simulation Milestones (Sept, 1991)

Once the detector fiber geometries are specified from the outcome of the fiber geometry studies (input from A above, and from hardware design studies), the basic physics benchmarks to optimize the overall calorimeter schematic system design can be fully studied, although these studies will begin in parallel with A above on a more idealized tower.

- Dielectron mass resolution for Z^0 as a function of p_t, with backgrounds
- Dijet mass resolution for W as a function of p_t, with backgrounds
- $H \rightarrow \gamma\gamma$ mass resolution with continuum background
- Higgs mass resolution to ZZ to eevv
- Higgs mass resolution to ZZ to jetjetee

These calorimetric benchmarks will be run while varying the basic schematic detector system parameters, to be then integrated with the tracker and pre-radiator responses. (calorimeter radii, calorimeter segmentation, y coverage, etc.)

Full Detector Simulation (1992-3)

A complete and realistic simulation can occur after a more detailed engineering design is in place, specifying where potential readout equipment, structural materials etc. will be positioned as nearly as possible to the final experimetal design.

Calorimeter Milestones

A major advantage of our approach to arriving at an SSC proposal is that we have already chosen the basic configuration and technology of the calorimeter. Since the only technologies that we are considering are the technical variations of a scintillating fiber calorimeter system designed to operate in the SSC environment, we can concentrate on its design optimization by specifying some physics signal and background benchmarks, and by studying them with the variation of both the basic calorimeter parameters and the implementation technology details.

At the end of the EOI/EDIA cycle the collaboration will be in a position to present to the PAC the physics benefits of our detector design as a function of cost and complexity for a baseline design and reasonable extensions.

Mechanical and Electrical Design Engineering Milestones

- Calorimeter Structural/System Engineering (Jan-March, 1991) This includes the basic details and information needed to demonstrate the structural integrity of both cast-in-place and grooved projective lead-fiber calorimeter options, that they can be assembled, and the initial cost scaling estimates for the following variations: radius at 90° from 2m to 3m; maximum y coverage of plastic fiber calorimeter from y=4 to y=2; depth from 11 to 16 interaction lengths; variation in length and inner contour along the beam from +/- 10 m to +/-25 m; variation in transverse segmentation from 0.02-0.05; longitudinal segmentation from 1-4 pieces.

At the end of this process, a realistic price should emerge for the basic material and structural assembly, except for the cost of the fiber itself. There will be some cost uncertainty due to the exact technique for fiber insertion into the lead matrix not having been determined (a basic automated grooved lead technique would be assumed as a baseline estimate).

- Calorimeter Readout Engineering Estimate (March, 1991) As mentioned previously, the readout of the proposed scintillater based calorimeter requires the development of a number of new readout designs. The engineering requirements include: PMT specifications; HV system; PMT calibration; front end electronics; mechanical support system.

Calorimeter Prototype and Hardware Engineering Test Milestones

The successful implementation of the detector concept requires the development of several new materials for detector construction as well as the detectors themselves. Our group will be working closely with our industrial affiliates to assist in the timely development of the following items: radiation hard scintillation fibers, Bicron; PMT prototypes from Hamamatsu, Phillips, Burle, DEP and EMI for a high linearity PMT with a cost between $50-150 each in 50K lots. In parallel with these development projects, our group will also be actively engaged in a vigorous prototype construction program aimed at investigating the problems associated with constructing both cast and laminated lead scintillating fiber calorimeters and the industrialization of the fabrication of the modules. These studies should be well under way by the end of 1991.

Note that the physics prototypes for extensive test beam studies follow at least one engineering prototype. Some milestones will probably be soft staged (3 month periods) to accomodate minor feedback modifications. Time is allotted for iteration cycles after the most critical first milestones.

Calorimeter System Design Integration Milestones

By the 4th quarter of 1993, a calorimeter design concept should be complete, having considered installation, repair, systems integration factors and 2 physics testing iteration cycles, ready for final prototype prints, construction and test during 1994.

By mid-1994, complete electro-optic/electronic readout systems should be ready for manufacture.

A partially-automated tower factory should be able to come on-line in mid-1995 capable of manufacturing (after a 6 month ramp-up) 10 towers per hour over 2 shifts at 250 days/year. It would probably have compact accelerators (25 MeV electrons, 14 MeV neutrons typical) for energy calibration tests and an optical test facility to ensure quality of delivered towers by mid 1997 or early 1998.

Tracker/Pre-radiator Milestones

As has been pointed out earlier, there are only three major study areas involving the tracker/pre-radiator system. These involve:

- the development of plastic scintillating fibers sufficiently radiation hard to function for ten years without appreciable deterioration in the demanding environment of the SSC with a luminosity of $10^{34}cm^{-2}s^{-1}$;
- the identification of suitable electro-optical readout devices and their interface with the fibers. This will also include studies of scintillating fiber/optical fiber splicing techniques;
- the investigation of carbon fiber/epoxy support structures for the scintillating fiber superlayers.

The first area will be investigated in cooperation with both Bicron and Optectron and also as part of an SSC subsystem study[24] . The second area will be investigated with RCA, Teledyne Brown, Burle Industries, etc. The third will be studied in collaboration with ORNL.

By the time that we write the full TEXAS proposal, we intend to have already chosen the appropriate radiation hard scintillating fibers and to have built a prototype carbon fiber support structure. We will have tested several readout options, but anticipate that a final readout decision will not yet have been made.

The following milestones should keep us on schedule:

- **By November 1990** Choose fiber samples for radiation tests. Identify plausible readout options. Choose appropriate readout devices for radiation tests. Identify needed radiation tests. Identify support structure prototype needs.
- **By March 1991** Radiation tests completed. Identify any necessary second-round radiation tests. First tests of readout devices complete (eg. sensitivity, linearity, stability, etc). First tests of fiber splicing tests complete. First readout interface options under study.
- **By July 1991** Based on the radiation test results, splicing tests and other fiber mechanical properties, preliminary final choice of plastic scintillating fiber made. First round readout device feasibility tests completed. Identify second round tests. Prototype carbon fiber support structure built and tests identified.

Muon Spectrometer Milestones

The muon TRD system is attractive because of its: a) low mass compared with iron toroids (≈ 8 kg/m^3 vs 8,000 kg/m^3) allowing access and construction around our very large calorimeter; b) potential for lower cost; c) high speed triggering, with sufficient resolution and speed to find the heavy Higgs and to calculate a fast missing transverse energy trigger.

The milestones for the first 1-2 years, must be such as to give a high degree of confidence in these assessments. The beam tests will use existing or planned TRD's for studies in muon beams to provide design data. Participants from outside the TEXAS collaboration will be funded for help with these tests.

As pointed out earlier, there are seven major areas of study involving the development and optimization of the muon spectrometer. These include the following:

- Carrying out a detailed Monte Carlo and design study to investigate the effects of the choice of radiator materials, radiator geometry, chamber configuration, electronics implementation, background rates and physics signatures on the physics performance of this spectrometer(Sept. 1991);
- Carrying out TRD hardware and data studies using existing TRD systems from MACRO and/or other available chambers in order to develop a prototype design for TEXAS(Jan. 1992);
- Development of TRD electronics including preamp and ADC systems(Sept. 1991);
- Design of the TRD mechanical support structure and system integration into the TEXAS detector(Nov. 1991);
- Design of the Xe gas delivery and recycling system(Nov. 1991);
- Development of a Muon tracker and trigger system(Nov. 1991);
- Design of a backup solid iron toroid muon spectrometer for comparision(Dec. 1991).

We propose a highly focussed 12-18 month program to produce: a) an accurate estimate of the cost and time to build the TEXAS detector, b) a full assessment of the physics potential, c) high level of confidence in the technology, and d) a complete proposal.

This process is essential for a project which may require about $150 million 1 20% to complete. We have budgeted about 5% of $150 million to proceed with this one year plan, about 40an 8 year construction cycle. We would intend this development funding to proceed past the deadline for proposals, up until the decision on the proposals is made by the PAC, in order to keep the group working at full speed through an approval.

We have identified several areas where the technological and cost confidence should be improved, and have budgeted considerable funding. These are: a) rad hard scintillating fibers, b) low cost high pulse linearity pmt, c) pixel detectors at a few $/pixel, d) Muon TRD performance.

In order to make this one year plan a reality, we have also budgeted funds for temporary engineering and technical help, and the managerial and secondary help needed to do this one year plan quickly. Many of these personnel will be hired immediately through Draper Labs working at the Universities, through specialty technical helop agencies, or by the TEXAS staff. Physicists will be relieved as much as possible from administrative duties and paper work by this plan.

I - TEXAS Concept

(1) Monte Carlo: Texas A&M, B.U., Northeastern

- 1 1-year temp. systems programmer @ $150K ea.
- 4 1-year temp. computer techs/shift ops @ $80k ea.
- 3 physicist 1 year leave-of-absence/visitors @ $100K ea.
- 6 work stations (Apollo or equiv.) @ $25K ea.
- computer time, $150K

(2) System Integration (EDIA/WBS): Draper Labs

- Main Contractor: Draper Labs, $1,000K
- System Integration Subcontracts, $250K

(3) TEXAS Group Operations: Draper, B.U.

- TEXAS scientific sec. @ $90K
- TEXAS communications/reports exec. sec. @ $60K
- TEXAS business and contracts officer @ $90K
- TEXAS travel/group meetings/communications @ $140K
- TEXAS manager of temporary technical personnel @ $100K

SUB-TOTAL: $2,600K

II - Fiber Tracker/Preradiator

(1) Physics Performance/Design Input: Northeastern

- Monte Carlo - 1/2 1-year temp. computer tech @ $40k ea.
- 1 Physicist Leave-of-Absence/visitor @ $100K ea.

(2) Mech. Engineering/Costing: Northeastern, Oak Ridge, Draper

- Composite barrels and mechanical alignment: Oak Ridge, $400K
- 1-year temp. mech engineers @ $150K
- 1 CAD workstation @ $60K

(3) Fiber Tracker/Preradiator Fiber Tests: Bicron, Northeastern, B.U.

- Fiber materials: Bicron, $100K
- Fiber splicing: $100K, t.b.d.
- 1-year temp.Tech/junior engineer @ $80K
- Equipment: $30K

(4) Electro-Optics: Northeastern, Fairfield, RCA, Hamamatsu (others to be determined)

- A.P.D. development: RCA, $300K (N.U.)
- Vacuum Photocathode Pixel Detector: Hamamatsu, or t.b.d, $300K (F.U.)
- Test hardware: $50K

SUBTOTAL: $1,700K

III Calorimeter

(1) Radiation-Hard Fibers: Bicron, $300K

(2) Cast Pb Matrix prototype: Bicron, B.U.

- 1 temp. techs @ $80K ea.
- 1 temp. mech eng. @ $125K ea.
- 1 temp. machinist @ $100K ea.
- equipment: $100K
- M&S, consumables: $100K

(3) Grooved/Holed Pb Matrix prototype: t.b.d.

- $500K (new collaborators/SCCINTCAL collab)

(4) Forward Liquid Calorimeter Prototypes: TAMU, Fairfield, BU

- 1 temp.tech @ $80K
- 1 temp. mech. eng. @ $125K ea.
- equipment: $50K
- M&S, consumables: $100K

(4) Calorimeter Electronics: BU, LeCroy

- HV and calib, ADC: LeCroy, $250K
- Trigger: 1 temp. EE @ $125K

(5) Photodetector Development: Hamamatsu, B.U., Fairfield, t.b.d.

- 4-5 decade linear low cost pmt: Hamamatsu, $250K
  : other contract, $250K

(6) Calorimeter Cell Manufacturing Engineering: Bicron, Draper - $100K

SUBTOTAL: $2,650K

IV Muon System:

(1) Monte Carlo: N.U. + t.b.d.	$50K
(2) Experimental Test Collaboration:	$400K
(3) Trigger counters: Drexel,	$50K
(4) Mech. Design: NU,	$100K
(5) Gas: Union Carbide	$150K
(6) Foam: t.b.d.	$100K
(7) TRD electronics: LeCroy:	$150K
SUBTOTAL:	$1,000K
TOTAL:	$7,950K

PRELIMINARY COST ESTIMATE

The central tracker design and cost was made by S. Reucroft and members of the SSC Subsystem R&D task for which he is spokesman. The pre-radiator costing was the work of P. Cushman (Yale) and R. Rusack (Rockefeller).

The fiber calorimeter is also the subject of an SSC subsystem task (SSCINTCAL). The costing stems from experience in construction of electromagnetic detectors for the new muon g-2 experiment at Brookhaven. These estimates were compared with actual costs of a large experiment by D. Hertzog (Illinios). He extrapolated the "Jetset" experience at LEAR to obtain similar costs for the TEXAS fiber calorimeter. The calibration system cost was contributed by V. Barnes (Purdue). Anticipated fiber costs are due to C. Hurlbut (Bicron). R. Webb extrapolated his experince with prototype liquid scintillator modules to estimate the cost of the forward tungsten endcap. Initial costing for the mechanical support structure was done by L. Wilk and J. Paradiso and their team at Draper Laboratory, extrapolating their experience in designing the L3 superstructure at CERN. The calorimeter electronics costs were derived from the experience at CDF of G.W. Foster (FNAL) and E. Hazen for the SSCINTCAL subsystem project. LeCroy Research Systems also provided numbers for the preliminary costing of the electronics.

The muon spectrometer is an extrapolation of MACRO technology and manufacturing experience. B. Barish (CIT) suggested design changes for the TEXAS application and costed the large liquid scintillator trigger counters. E. Iarocci (Frascati) made cost estimates for the fast limited streamer tube trackers and electronics. Cost estimates for the Xenon gas and purification system were provided by A.J. Westendorf (Union Carbide) and S. Saupp (Linde).

TEXAS Detector
PRELIMINARY COST ESTIMATE

Central Tracker/Preradiator

		($M)
Mechanics		
1mm fibers 900K @ $15	3 layers (Tracker)	14
	9 layers (Pre-Radiator)	3
Construction + leadsheet		1
Electronics		
Channels 300K @ $20 (Tracker)		6
Channels 600K @ $20 (Pre-Radiator)		12
Cables		1
		$37

Calorimeter Mechanics

200K Calorimeter channels

1mm Scintillating fiber @ $200/km, 150,000km	30
Lead @ ($2k/T × 5kT)	10
Bonding, weaving	3
Construction and labor	6
Photo multipliers and lightguides (200K @ $100)	20
Calibration system	1
Forward Calorimeter	8
	$78

Calorimeter Electronics

200K Electronics channels

Analog "exponent" digitizer 20 bit @ $10	2
100MHz FADC 8 bit @ $25/chip Sony	5
Trigger gate array @ $25	5
PC Boards, cables, connectors @ $15	3
High voltage @ $50/multiplexed 8PMs + Bases @ $15	4
	$19

Muon Trigger Counters

900 Liquid scintillator boxes

PVC Boxes + mirrors	2
Liquid scintillator	1
Labor	2
Photomultipliers + bases (3600 channels)	1
Electronics trigger and ADC + HV	1
	$7

Muon Tracking

56K Limited streamer tubes + 56K strips

8-tube chambers (7K)	2
Transverse strips, gas system, HV	1
Digital readout electronics, 100K channels	1
	$4

Muon TRD's Mechanics

Foam and extruded tubes (300K channels)	5
Xenon	6
Gas System	1
Assembly	1
	$13

Muon TRD Electronics

30K Multiplexed Channels

Preamps @ $10 and shapers @ $20/pc board components	1
FADC's @ $80/pc board and components	2
Labor	2
	$5

Data Acquisition

Trigger (level 2 & 3)	3
50 RISC Processors (40 MIPS each)	1
	$4

All Mechanical Support Structures

Design, engineering, and analysis	2
Calorimeter support piers	1
Bridges	1
Moving structure	1
Muon C-Tanks	4
Muon End Cap Tanks	2
	$11

Project Cost	$178
Contingency @ 10%	18
Total Project Cost	$196

TEXAS Management Scheme

The TEXAS detector is relatively simple. It has only three hardware subsystems, and it is anticipated that the eventual TEXAS collaboration will be small by SSC standards. Consequently, a straightforward management scheme is envisioned.

Until the formal proposal is approved by the SSC laboratory, overall coordination of the collaboration is in the hands of three project spokespersons: Reucroft (Northeastern U.), Sulak (Boston U.), and Webb (Texas A & M). They are responsible for formal communication with the SSC laboratory. Two standing committees manage the technical and financial operations of the project. The technical committee is empowered to make all decisions necessary to ensure a fully operational detector at SSC turn-on. The financial committee is responsible for developing the budget and for fiscal oversight of the project. A project director nominated by the spokespersons and approved by vote of the collaboration membership coordinates technical operations and serves as chief financial administrator. A contract manager appointed by the director manages the day-to-day fiscal operations of the project.

Meetings of the collaboration, where all members with or without Ph. D. have one vote, take place three or four times a year. Collaboration meetings are chaired by one of the project spokespersons on a rotating basis. The meetings represent an open forum where progress will be reviewed. Members of the technical committee, including its chairman, are elected and new collaboration members are accepted in the course of these proceedings. Decisions are by majority vote.

The financial committee is chaired by one of the project spokespersons. Its members include the principal investigator from each collaborating institution, the chairman of the technical committee, and the project director. The principal investigators have the authority to make financial commitments on behalf of their home institutions and are responsible for administrating their individual budgets. The financial committee presents recommendations at collaboration meetings for approval by the membership.

The technical committee consists of seven members elected by the collaboration and a chairman who is one of the spokespersons. Five members are responsible for the specific detector subsystems: tracker/pre-radiator, calorimeter, muon spectrometer, on-line software, and off-line software. A consulting engineer and the project director complete this group.

Both committees meet immediately prior to collaboration meetings and at any other appropriate times called by the respective chairmen. Both groups establish *ad hoc* subcommittees and working groups as deemed necessary.

A request to join the collaboration should be made in writing, stating the number of collaborators involved and their areas of expertise. The request will be considered at the following collaboration meeting, to which the applicant may be invited. A decision will be made by majority vote.

The structure of the collaboration after approval, including the election procedure for spokespersons, will be determined by the entire collaboration at that time.

Conclusion

We propose an SSC detector concept with precision calorimetry as the guiding aspect of the design. Its performance is not compromised by the constraints imposed by a magnetic spectrometer. TEXAS offers the possibility of operation at high luminosity and has precise calorimetry, both essential for full coverage of the natural range of Higgs masses. The features demanded by the physics: speed, energy resolution, segmentation, full rapidity coverage, uniformity, stability and hermeticity make this specialized detector concept attractive, and complementary to other designs. The conceptual simplicity of our three-basic-component detector facilitates construction, access and design. This specialized and cost-effective detector will be sensitive to most of the new physics anticipated at the SSC, and can be ready at start-up time.

Acknowledgements

The choice of the physics focus for this specialized detector was strongly influenced by J. Rohlf (Boston) and by our theoretical colleagues. In particular, we thank S. Chivukula, K. Lane (Boston), A. De Rújula and J. Ellis (CERN), S. Glashow (Harvard), H. Goldberg and P. Nath (Northeastern) for many informative discussions. This document could not have been produced without the encouragement of De Rújula.

We acknowledge the effort of a great many people in developing the detector concept. The central tracker design was conceived in collaboration with J.S. Whitaker (Boston). The pre-radiator work (with P. Cushman, Yale and R. Rusack, Rockefeller), the scintillating fiber tracking and a tracking electron TRD option (of Whitaker) are each the subjects of SSC Subsystem R & D work. An initial design incorporating a straw tracking option for a central detector benefited from development at Boston by S. Ahlen, J. Beatty, E. Booth, A. Marin, J. Rohlf and B. Zhou.

The fiber calorimeter is also part of an SSC Subsystem R & D task (SSCINTCAL). The construction of the electromagnetic section was modeled after that of the detectors for the new Brookhaven muon g-2 experiment. The rad-hard liquid scintillator portion of the calorimeter (for $\eta > 3$) has been designed in collaboration with T. Bowcock and S. White (Texas A & M). The calibration concept has been developed with contributions from V. Barnes (Purdue). D. Hertzog (Illinois) extrapolated the "jetset" at LEAR experience to obtain cost estimates for the scintillating fiber hadronic calorimeter.

K. Johnson (Florida State) was responsible for demonstrating the high radiation tolerance of new scintillating fibers. C. Hurlbut of Bicron Corp contributed to understanding the radiation hard aspects of the fiber calorimetry and the costing of the calorimeter. A. David

and N. Diaczonko (Texas A&M) and D. Higby (Boston) have built the liquid scintillator prototypes. Design of the mechanical support structures was done at Boston by R. Bruni, T. Coan, S. Glass, and D. Higby. Initial costing for these structures was done by L. Wilk and J. Paradiso and their team at Draper Laboratories. E. Hazen (Boston) developed the electronics, triggering and data acquisition concepts. One option for the conceptual design of the calorimeter electronics is that of G. W. Foster (Fermilab) and Hazen for the SSCINTCAL Subsystem R&D Project. We thank W. Le Croy of LeCroy Research Systems for his critique of and help with the preliminary of costing the electronics.

The muon spectrometer is an extrapolation of MACRO technology and manufacturing experience. B. Barish (Caltech) suggested design changes for the SSC and helped cost the large liquid scintillator trigger counters. E. Iarocci (Frascati) made cost estimates for the fast limited streamer tube trackers and their electronics. An option for the end cap chambers using knife edges was designed by R. Battiston (Perugia).

P. Spinelli (Bari) kindly provided extensive information, test beam studies, and simulations from the prototype studies for the MACRO muon TRD. Independently, J.R. Hubbard and M. Pansant (Saclay) extrapolated their D0 experience with $6m^2$ of electron TRD's to this SSC application and provided design ideas and optimizations. V. Chernyatin, B. Dolgoshein (Moscow Physical Engineering Institute) and A. Schmeleva (Lebedev Institute, Moscow) have also optimized the design parameters for a muon TRD system which can achieve the physics goals. A. Vorobyov and V. Schegelsky of the Nuclear Physics Institute, Leningrad have offered their enormous practical experience from building three generations of TR devices. M. Sheaff (Wisconsin) has shared her insight obtained from building the world's first 4m deep transition radiation detector. Preliminary cost estimates for the xenon gas and purification system were provided by A.J. Westendorf of Union Carbide as well as S. Saupp and T. Schulte of Linde.

The capability of providing $10^{34}/cm^2$-s luminosity at a dedicated interaction region was pursued by S. Geer(Harvard) and T. Bowcock(Texas A&M).

REFERENCES

1. **E. Eichten et al.,** *Rev. Mod. Phys.* **56, 579(1984).**
2. *Proceedings of the 1984 Snowmass Workshop on the Design and Utilization of the Superconducting Super Collider* , **edited by R. Donaldson and J.G. Morfin.**
3. *Proceedings of the 1986 Snowmass Workshop on "Physics of the Superconducting Super Collider"*, **edited by R. Donaldson and J. Marx.**
4. *Proceedings of the 1987 Berkeley Workshop on "Experiments, Detectors and Experimental Areas for the Supercollider"* , **edited by R. Donaldson and M. Gilchriese.**
5. *Proceedings of the 1988 Snowmass Workshop on "High Energy Physics in the 1990s".*
6. *Proceedings of the ECFA-CERN Workshop on the LHC, Lausanne,* March 1984, *CERN 84-10.*
7. *Proceedings of the Workshop on Physics at Future Colliders* , CERN 87-07, La Thuile (1987).
8. *Feasibility of Experiments at High Luminosity at the Large Hadron Collider* , edited by J. Mulvey, CERN 88-2 (1988).
9. J. Gunion *et al. The Higgs-Hunters Guide* , UCD 89-4 (1989).
10. P. Jenni, *Aspects of Jets and Calorimetry at Future Hadron Colliders* , Barcelona, Sept. 1989, and *CERN-EP/89-148,* Nov. 1989.
11. R. Cahn *et al., Phys. Rev.* **D35**, 1626(1987)
12. V. Barger, T. Han and R.J.N. Phillips, *Phys. Rev.* **D37** 2005(1988).
13. F.E. Paige and E.M. Wang, *Hermeticity Requirements at the SSC*, BNL preprint, July 1989.
14. R. Kauffman and C.P. Yuan, Argonne preprint *ANL-HEP-PR-90-13,* March 1990.
15. J.F. Gunion, G.L. Kane and J. Wudka, Nucl. Phys. **B299** 231(1988).
16. Barnett, *et al.*, in Ref. 5.
17. R. Batley in Ref. 5.
18. S. Chivukula in *"TeV Physics"*, edited by G. Domokos and S. Kovesi-Domokos, World Scientific (1988).
19. E. Eichten, K. Lane, and J. Preskill, *Phys. Rev. Lett.* **50**, 811(1983).
20. Private communications from R. DeSalvo and M. Livan, to appear in print summer 1990.
21. H. Paar,*"Status of Scintillating Fiber Calorimetry" in Proceedings of Barcelona ECFA Meeting*, Sept. 1989.
22. D. Hertzog,*"Scintillating Fiber Calorimetry" in Proceedings of Tallahassee Workshop on Radiation Damage to Scintillator*, edited by K. Johnson (1990)
23. T. Akesson,*Proceedings of the ECFA Workshop on the LHC* , CERN 84-10 (1984).
24. A Hybrid Central Tracking Chamber for the SSC, A. Goshaw and S. Reucroft et al., SSC Subsystem proposal (1989)
25. M. Atac *et al., Proposal to Develop a High-Rate Tracking Detector Subsystem for the SSC using Scintillating Fibers,* SSC Subdivision proposal (1989)
26. UA2 Collaboration, J. Alitti et al., CERN EP/90-20 (1990).
27. B. Dolgoshein, private communication
28. R.J. Wilson, "Computing Needs for the Superconducting Super Collider", (unpublished), presented to the Computing Working Group, 1988 Summer Study on High Energy Physics in the 1990s, sponsored by the American Physical Society in Snowmass, CO, 1988
29. Experiments, Detectors and Experimental Areas for the Supercollider, Berkeley, CA, 1987; R. Donaldson and M. Gilchriese, editors
30. Appel et al, "Offline Computing and Networking", Workshop on Triggering, Data Acquisition and Computing for High Energy/High Luminosity Hadron-Hadron Colliders, FERMILAB, IL, November 1985; B. Cox, R. Fenner, P. Hale, editors

31. A. Firestone et al, "Computing Requirements at the SSC", Proceedings of the 1984 Summer Study on the Design and Utilization of the SSC (SNOWMASS '84), Snowmass, CO, 1984; R. Donaldson and J. Morfin, editors.

32. R. Diebold, "Computing Needs of the SSC", IEEE 1984 Nuclear Science Symposium

33. SCRI School on Vector Computing in Experimental High Energy Physics, Tallahassee, FL, 1988

34. I. Hinchliffe, "Physics at Large Transverse Momenta",*Proceedings of the 1987 Berkeley Workshop on "Experiments, Detectors and Experimental Areas for the Supercollider"* , edited by R. Donaldson and M. Gilchriese, p. 8.

35. D.Atwood et. al., "Intermediate Mass Higgs Boson(s)",*Proceedings of the 1987 Berkeley Workshop on "Experiments, Detectors and Experimental Areas for the Supercollider"* , edited by R. Donaldson and M. Gilchriese, p. 8.

36. C. Barter *et al* in[s] .

37. J.Gunion, G. Kane, and J. Wudka, *Nuc. Phys.* **B299** (1988) p.243-247

38. E. Wang and G. Hanson, *Proceedings of the 1988 Snowmass Workshop on "High Energy Physics in the 1990s"* , edited by S. Jensen, p. 111

39. E. Glover, J. Ohnemus, and S. Willenbrock, *Phys. Rev.* **D37** (1988) 3193.

40. R.N. Cahn et. al.

41. R. Kleiss and W. Stirling, *Phys. Lett.* **200B** , (1986) 826.

42. J. Gunion *et. al.* , preprint UCD-88-38 (1988)

43. G. Kane and C.-P. Yuan, *Phys. Rev.* **D 40**, 2244 (1989)

44. R. Kauffman and C.-P. Yuan, preprint ANL-HEP-PR-90-13 (1990)

FIGURE CAPTIONS

1. The TEXAS SSC Detector within its Experimental Hall
2. Cross-Sectional View of One-Half the TEXAS SSC Detector
3. Axial View of the TEXAS SSC Detector
4. Detailed Axial View of the TEXAS Muon Spectrometer
5. Cross-Sectional Side View of one-quarter of the TEXAS Scintillating Fiber Calorimeter
6. Scintillating Fiber Tracker and Imaging Preradiator for the TEXAS Detector
7. Plan View of the TEXAS Detector in Open Mode for Assembly and Maintenance
8. Axial View of the TEXAS Detector in Open Mode for Assembly and Maintenance
9. TRD Muon Spectrometer Resolution as a Function of Momentum.
10. Reconstructed dijet mass from a 600 GeV Higgs decay at two calorimeter energy resolutions: $35\%/\sqrt{E}+2\%$ (dashed) and $50\%/\sqrt{E}+5\%$ (solid) histograms. Ideal curve is also shown. UA2 Montecarlo results from D. Froidevaux in Ref. 7.
11. Potential of triggering on two high-η jets in heavy Higgs searches[11] . The decay chain is $H \to WW \to$ jet jet $l\nu$. (a) is the rapidity distribution of the jet-jet pair, (b) is that of the two tagging jets. The need for coverage to $|\eta| > 5$ is apparent.
12. (a) Distribution of p_T^{back} (defined in the text) for a detector hermetic to $|\eta| = 5$, with perfect efficiency and resolution. (b) Same as (a) with $15\%[40\%]/\sqrt{E}$ electromagnetic [hadronic] calorimeter resolution, and segmentation $(\phi \times \eta) = (0.05 \times 0.05)$. (c) Same as (b) with 2% random dead calorimetric cells. From R.N. Cahn et al. in Ref. 4.
13. Signal of $H \to ZZ \to llll$, and the standard model background (from $q\bar{q}$ annihilation), to be increased by ~ 1.7 to include the gg channel. PYTHIA results for the ZZ invariant mass distribution (from Ref. 6) for a standard SSC year at $\mathcal{L} = 10^{33}\,\mathrm{cm}^{-2}\mathrm{s}^{-1}$. Coverage is only to $|\eta_z| = 1.5$, efficiency and resolution for e's and μ's are assumed to be ideal.
14. Results of C. Barter *et al.*in Ref. 5 on the signal and background in one year of running at $\mathcal{L} = 10^{33}\,\mathrm{cm}^{-2}\mathrm{s}^{-1}$ for an $M_H = 150$ GeV Higgs in the $\gamma\gamma$ channel. Cuts are applied at $|\eta| < 3$, $E_T > 10$ GeV and $|\cos\theta^*| < 0.8$ on both γ's, with θ^* the photon scattering angle in the c.m.s. frame. (a) is for a mass resolution of 1.9 GeV, (b) for 0.8 GeV.
15. Distribution of true missing transverse energy for (a) squark and (b) gluino pair production (solid curves and histograms), for several values of $\tilde{q}$ and $\tilde{g}$ masses. The dots are standard-model backgrounds, with $m_t = 40\,\mathrm{GeV}$. Results for $m_t = 200\,\mathrm{GeV}$ differ appreciably[17] only for $E_T^{miss} < 0.5$ TeV.
16. Distribution of events in p_T^{out} (as defined in the text), for $m_{\tilde{g}} = 750$ GeV. The filled dots show the signal and the background is the sum of the other symbols. A variety of cuts[13] have been applied to enhance the signal/noise ratio.
17. Signal and background for charged technirho production and decay[18] showing the event distribution as a function of M_{WZ}. The dotted-dashed line is the standard model background. Dashed, dotted and full lines are for $N_T = 6, 4, 2$, respectively.
18. Substructure effects on the p_T distribution of events at $\eta = 0$. Solid line is the standard background, $\delta = \pm 1$ is the sign of the extra four-q contact interaction, Λ is the substructure scale (private communication of Marcello Campari).
19. Longitudinally Segmented Scintillating Fiber Calorimeter.
20. Electromagnetic Calorimeter Modules Constructed from Scintillating Fibers Cast within a Eutectic Lead Alloy Matrix. (a) Fibers before Casting. (b) 9 Cast Calorimeter Blocks.
21. Background E_t from Piled-up Minimum Bias Interactions in a Highly Segmented Calorimeter.
22. Phototube Pulses from the SPACAL Calorimeter.

23. Effect of Calorimeter Radius on Dijet Mass Resolution.

24. Cross Section for p_T as a Function of Rapidity Coverage.

25. ADC and Second Level Trigger for One Calorimeter Tower.

26. Floating-Point ADC Prescaler Application-Specific Integrated Circuit (ASIC).

27. TEXAS Liquid Scintillator Forward Calorimeter Design.

28. Photo of Liquid Scintillator Electromagnetic Module.

29. Missing p_T as a Function of Rapidity Coverage.

30. The Measured e/π Rejection Power and Electron Efficiency of a SPACAL Test Calorimeter with Preradiator

31. Lepton acceptance vs. energy of the most energetic lepton for 400 and 800 GeV/c^2 $H \rightarrow 4\ell$. (From Ref. 5

32. Rate of muons from b and c decay exiting the calorimeter vs. p_T taken from Ref. 4.

33. Di-boson mass at levels three levels of charge discrimination. Curve b shows continuum ZZ mass with no neutrals. Curve c shows background suppression of a factor of four if lepton charge is known, as expected from combinatorics.(Taken from E. Wang et al. in Ref. 5)

34. Typical TRD yields as a function of γ from[45]

35. dE/dx for a typical TRD x-ray chamber as a function of γ from[46]

36. The calculated energy resolution for five alternative TRD systems for TEXAS (from P. Spinelli)

37. Momentum resolution for TEXAS TRD System calculated by J.R. Hubbard and M. Pansart.

38. Production and Decay of Intermediate Mass Higgs Bosons[47]

39. $SignalandBackgroundforH \rightarrow eeee$ in TEXAS

40. $SignalandBackgroundforH \rightarrow ee\mu\mu$ in TEXAS

41. TEXAS Resolution for $H \rightarrow ZZ \rightarrow \mu\mu\mu\mu$

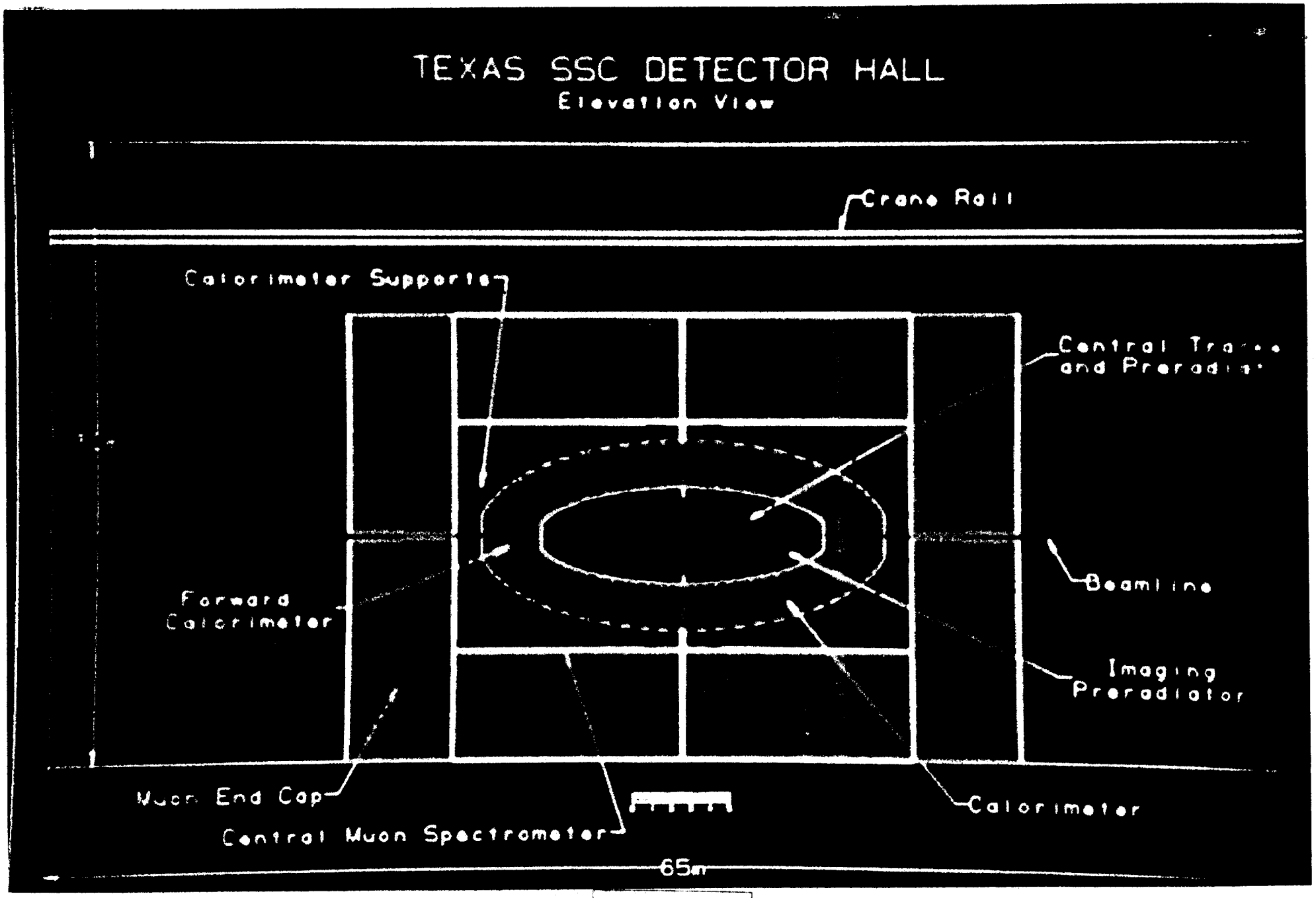
TEXAS SSC DETECTOR HALL
Elevation View
Crane Rail
Calorimeter Supports
Central Tracks
and Preradiator
Beamline
Forward
Calorimeter
Imaging
Preradiator
Muon End Cap
Calorimeter
Central Muon Spectrometer
65m

Figure 1

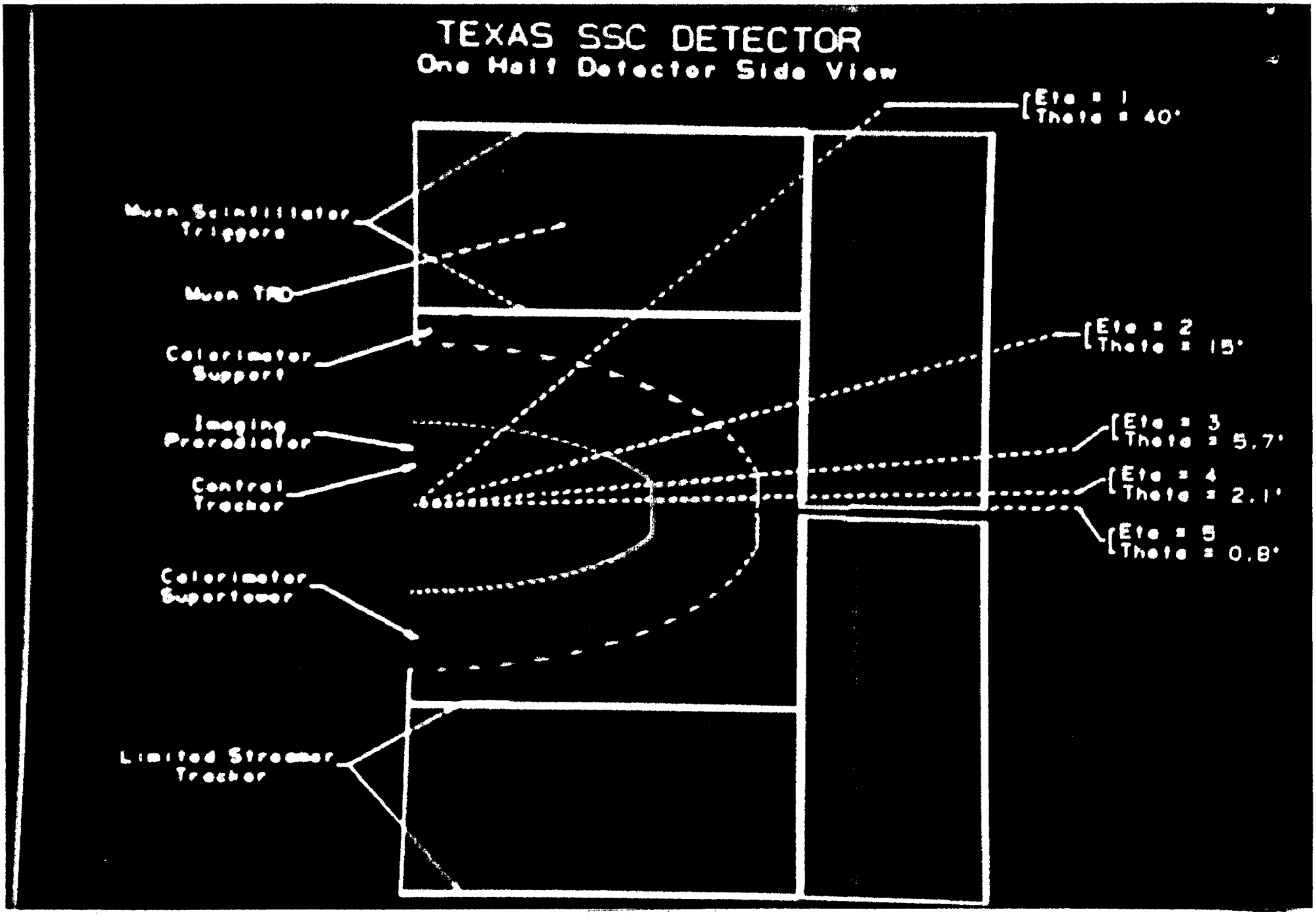
TEXAS SSC DETECTOR
One Half Detector Side View
Muon Scintillator Triggers
Muon TRD
Calorimeter Support
Imaging Preradiator
Central Tracker
Calorimeter Supertower
Limited Streamer Tracker
Eta = 1
Theta = 40°
Eta = 2
Theta = 15°
Eta = 3
Theta = 5.7°
Eta = 4
Theta = 2.1°
Eta = 5
Theta = 0.8°

Figure 2

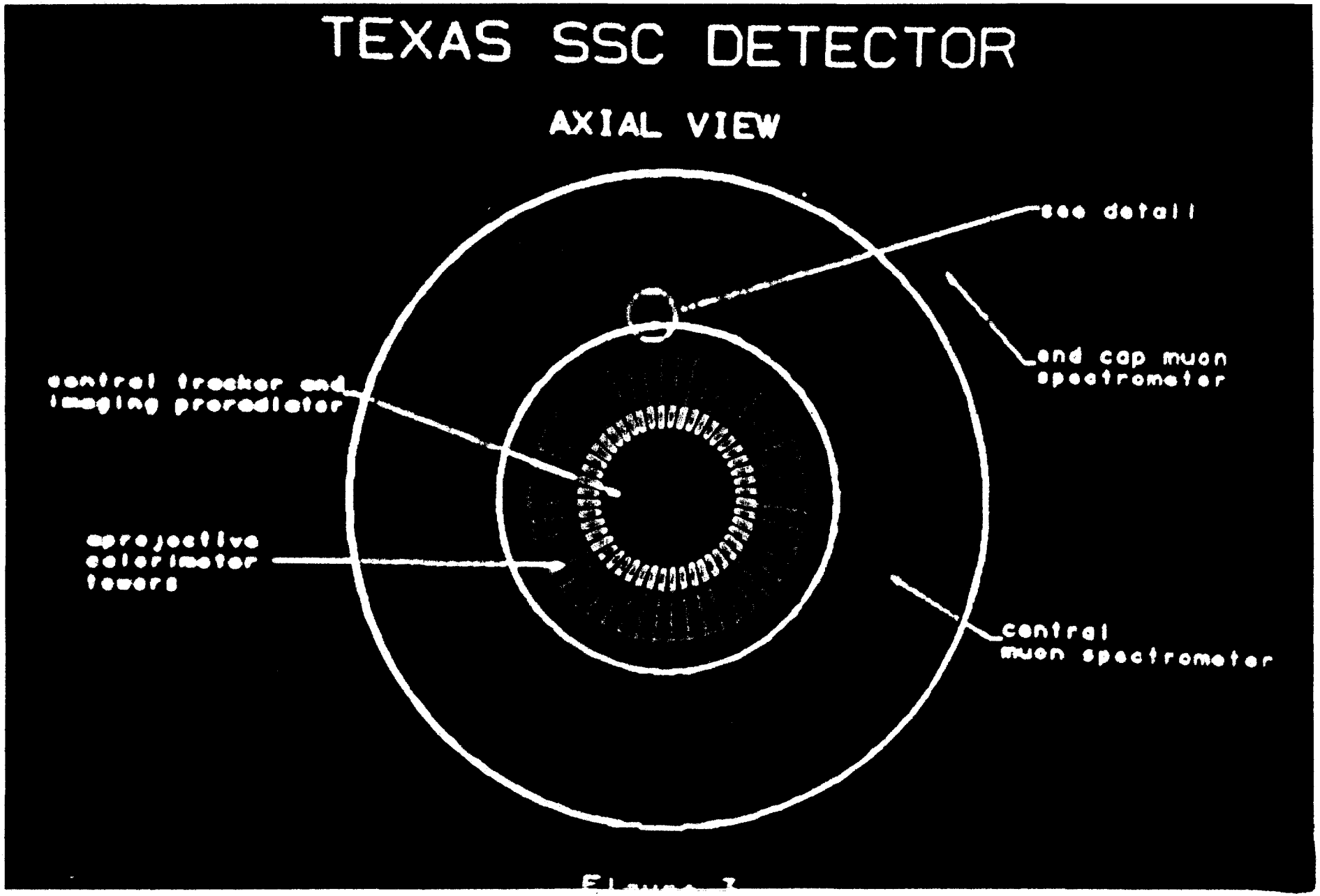
TEXAS SSC DETECTOR
AXIAL VIEW
see detail
end cap muon spectrometer
central tracker and imaging preradiator
aerojective calorimeter towers
central muon spectrometer

Figure 3

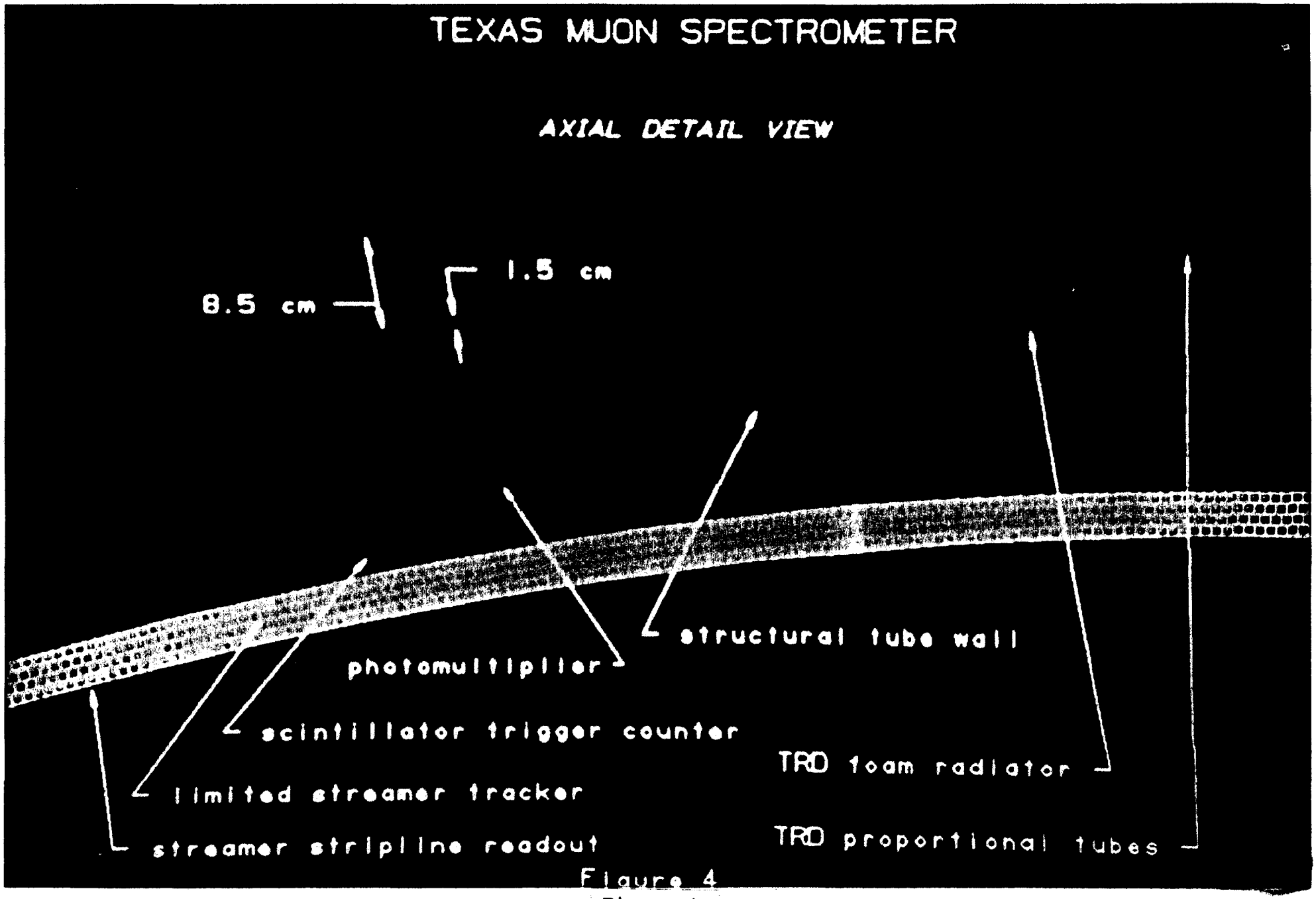
TEXAS MUON SPECTROMETER
AXIAL DETAIL VIEW
8.5 cm
1.5 cm
structural tube wall
photomultiplier
scintillator trigger counter
TRD foam radiator
limited streamer tracker
TRD proportional tubes
streamer stripline readout
Figure 4

Figure 4

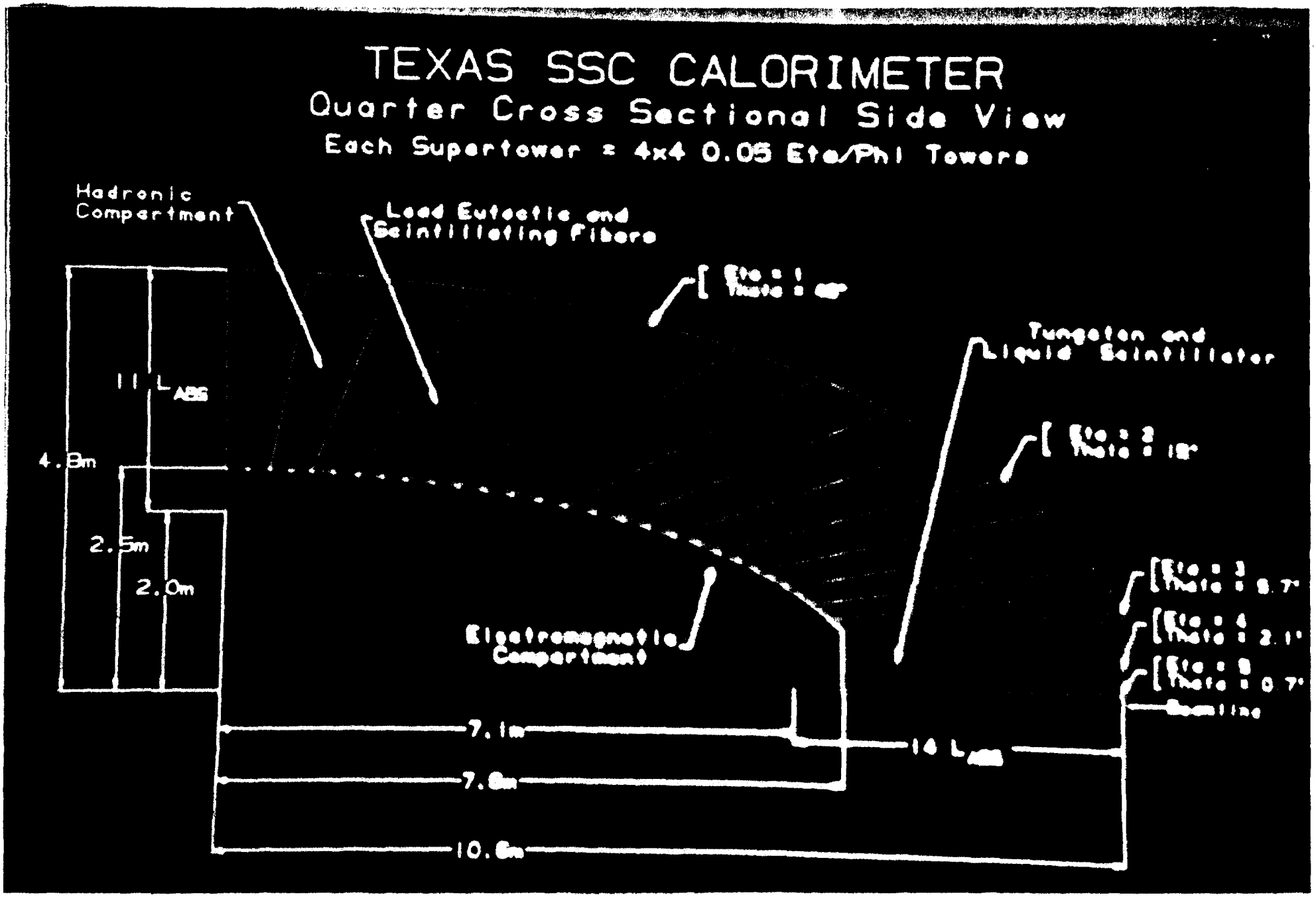
TEXAS SSC CALORIMETER
Quarter Cross Sectional Side View
Each Supertower = 4x4 0.05 Eta/Phi Towers
Hadronic Compartment
Lead Eutectic and Scintillating Fibers
Tungsten and Liquid Scintillator
11 L ABS
4.8m
2.5m
2.0m
Electromagnetic Compartment
7.1m
7.8m
10.8m
14 L ABS

Figure 5

TEXAS SSC DETECTOR

1/4 Central Tracker and Preradiator

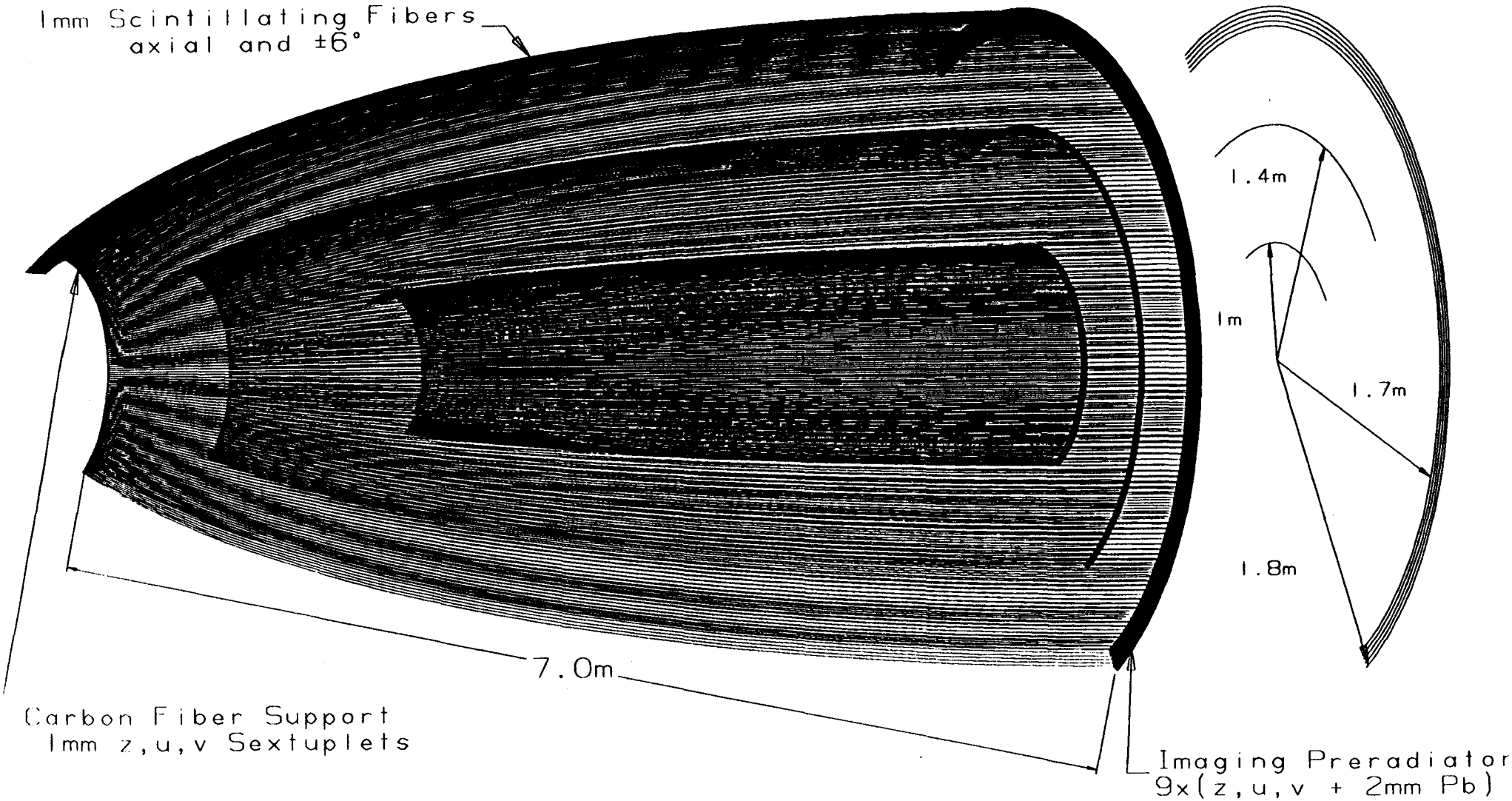

Figure 6

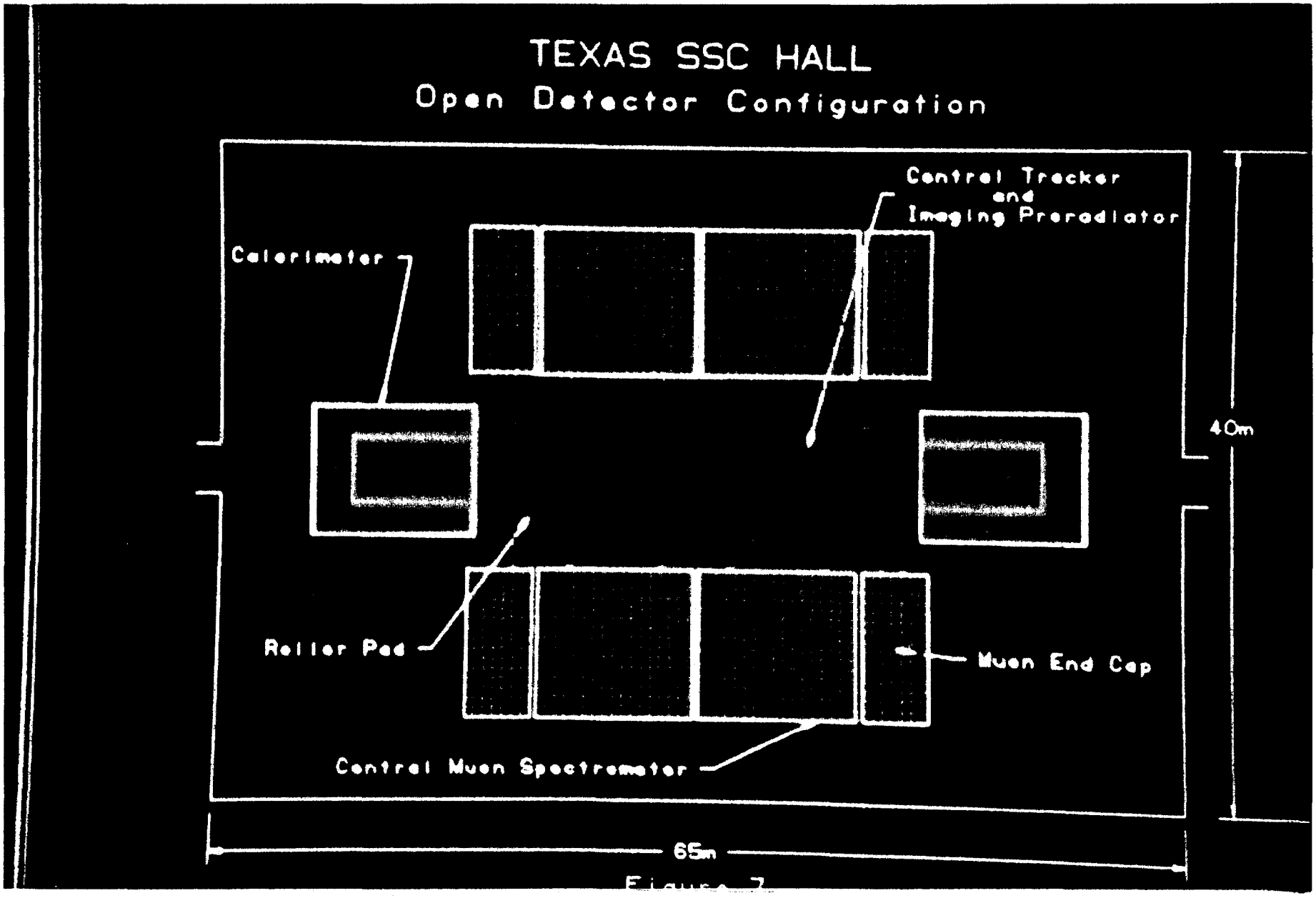
TEXAS SSC HALL
Open Detector Configuration
Central Tracker
and
Imaging Preradiator
Calorimeter
40m
Roller Pad
Muon End Cap
Central Muon Spectrometer
65m

Figure 7

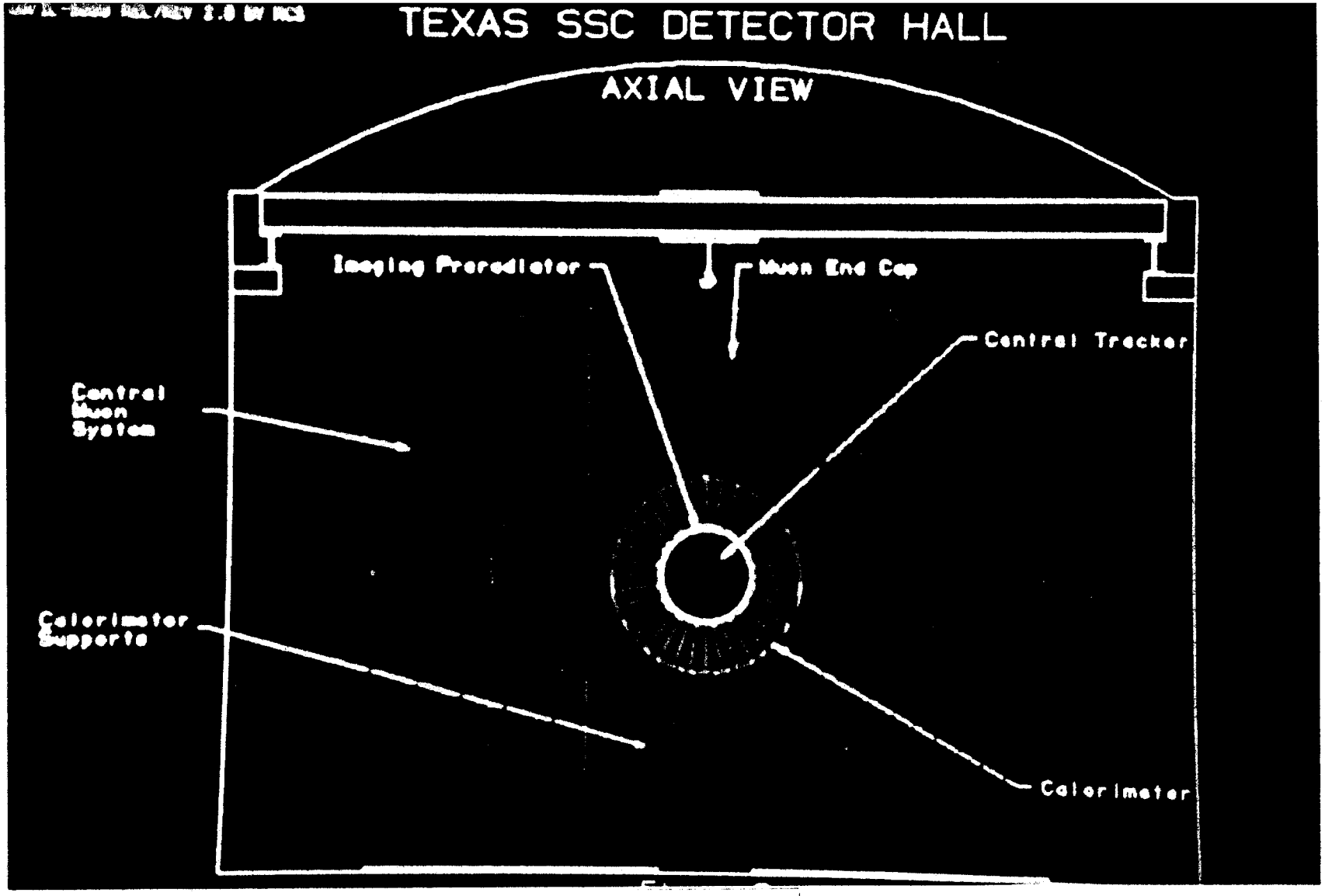
TEXAS SSC DETECTOR HALL
AXIAL VIEW
Imaging Preradiator
Muon End Cap
Central Tracker
Central Muon System
Calorimeter Supports
Calorimeter

Figure 8

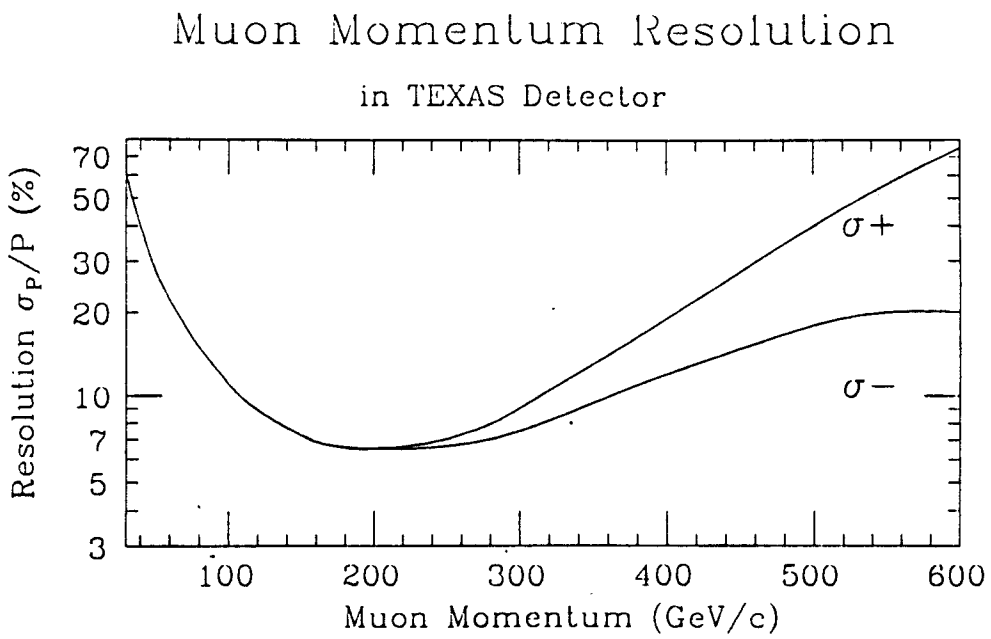

Figure 9

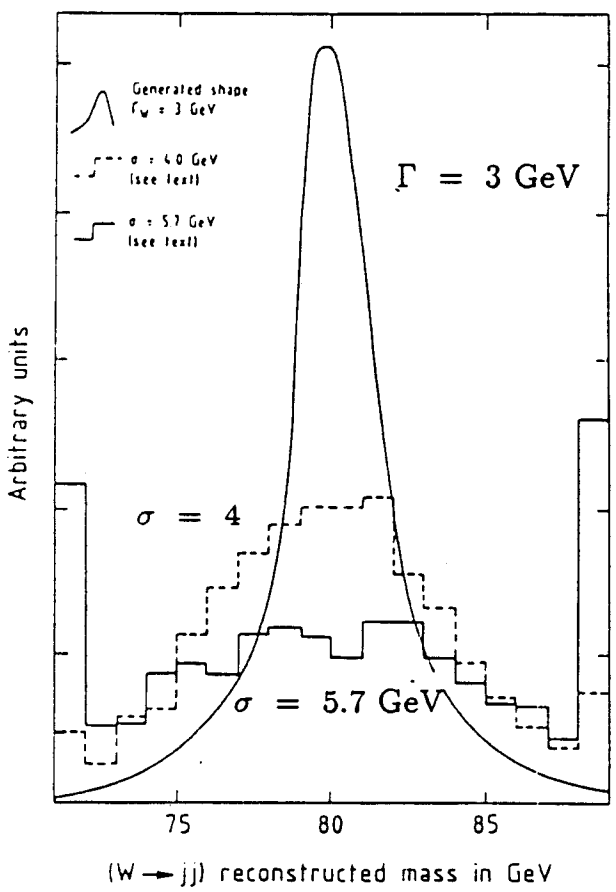

Figure 10

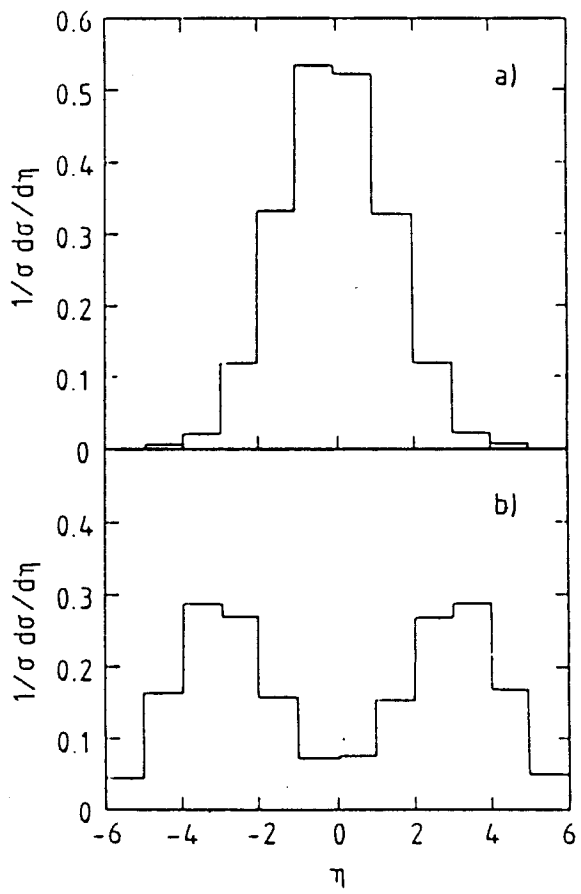

Figure 11

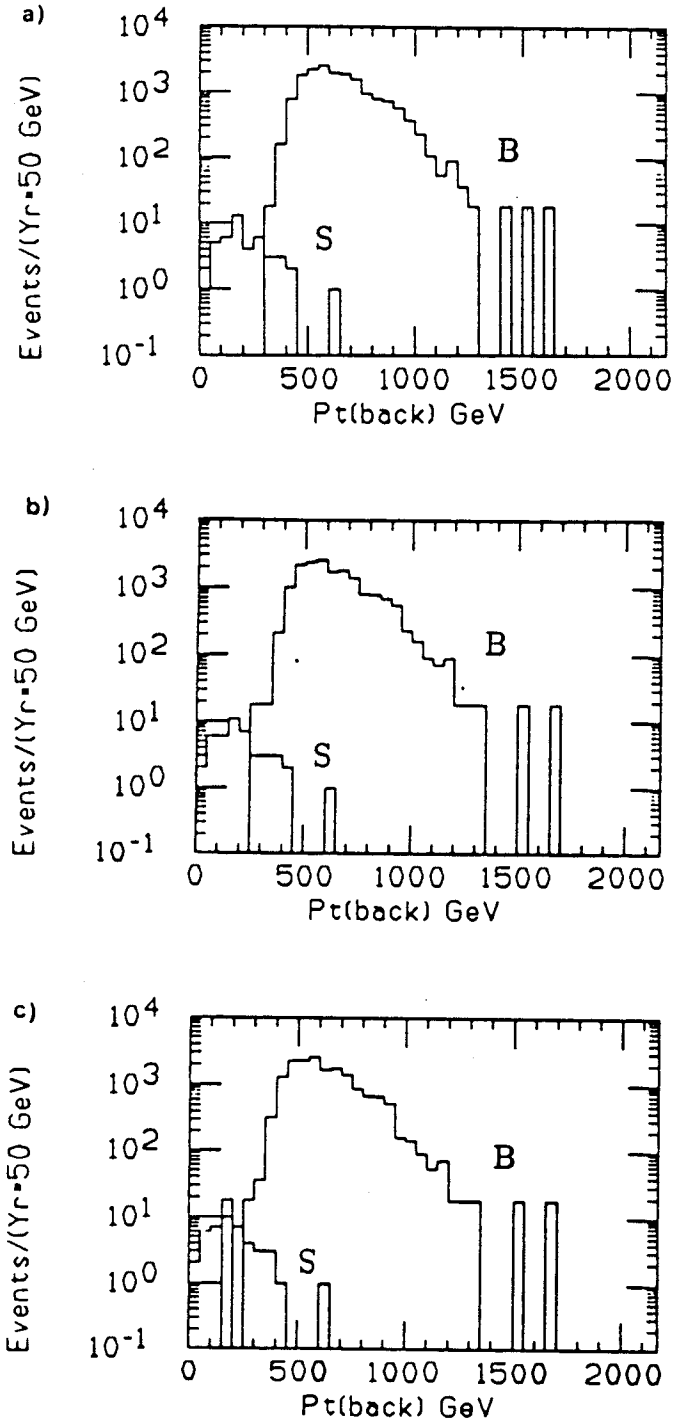

Figure 12

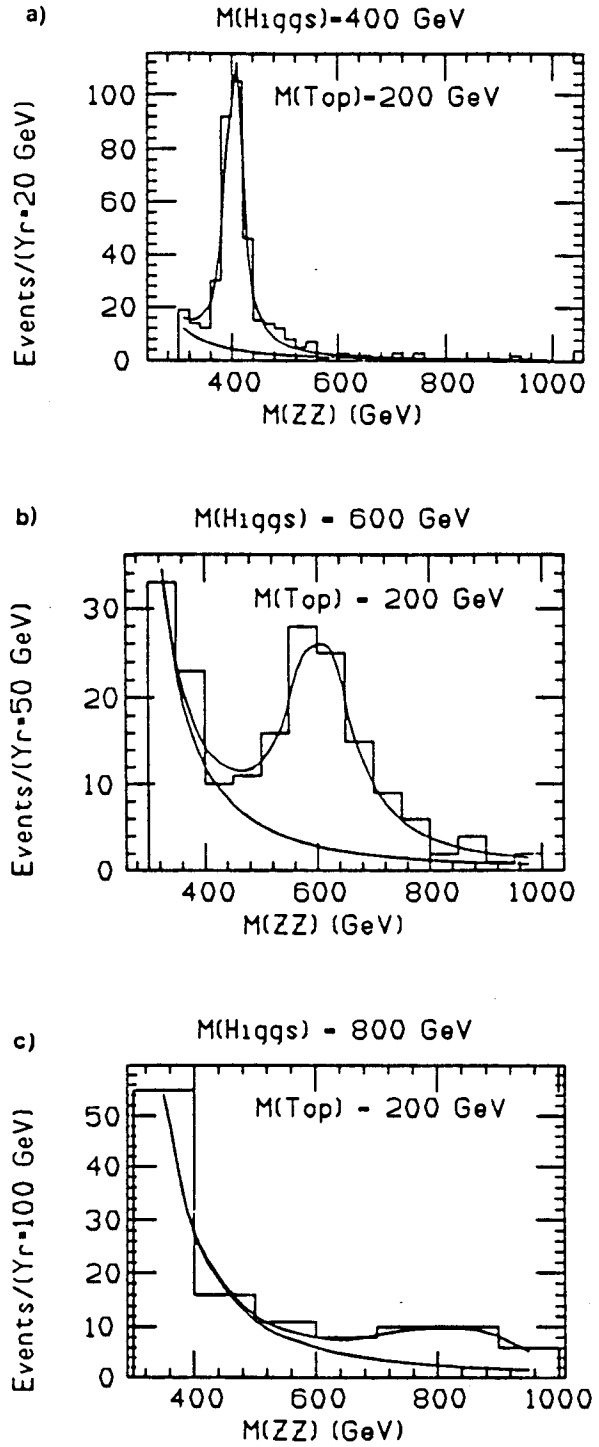

Figure 13

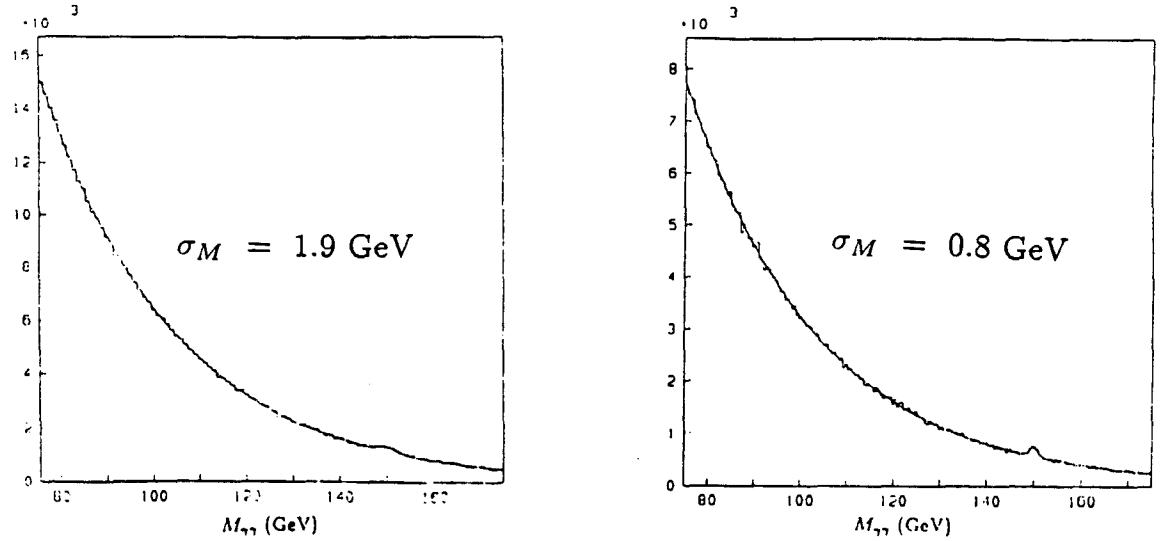

Figure 14

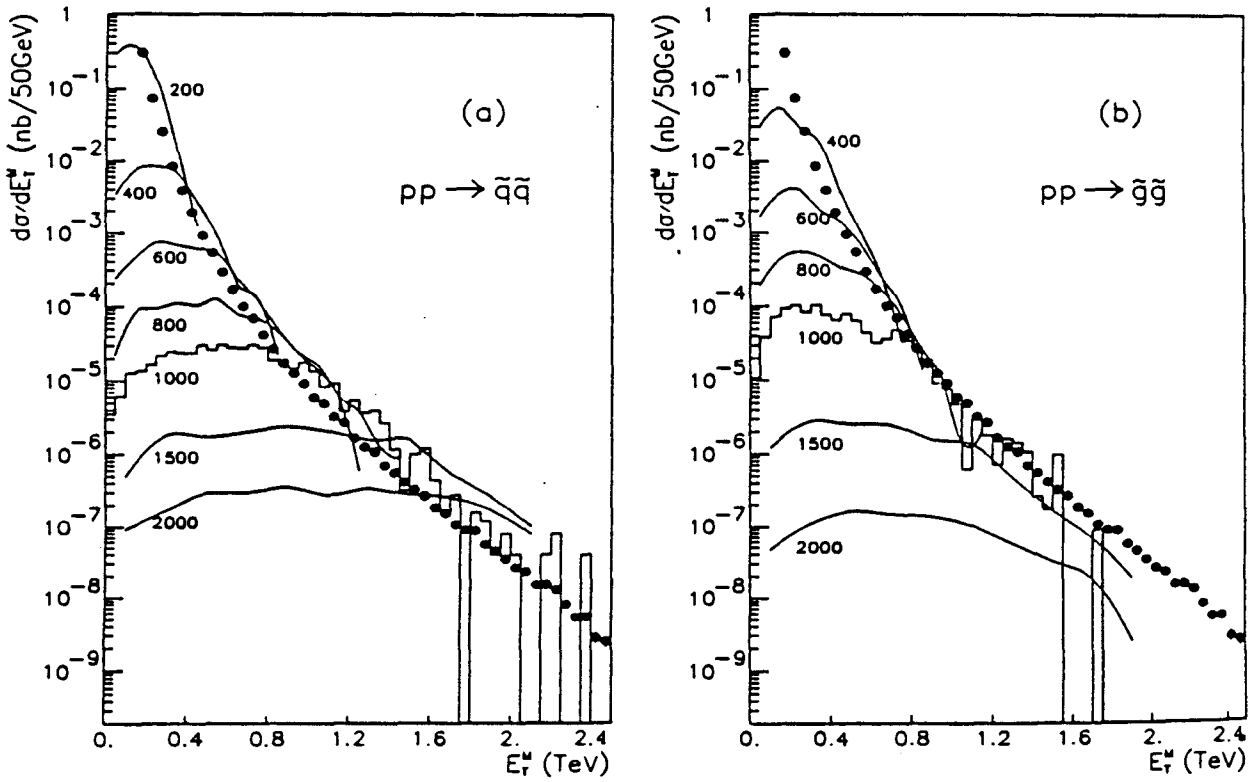

Figure 15

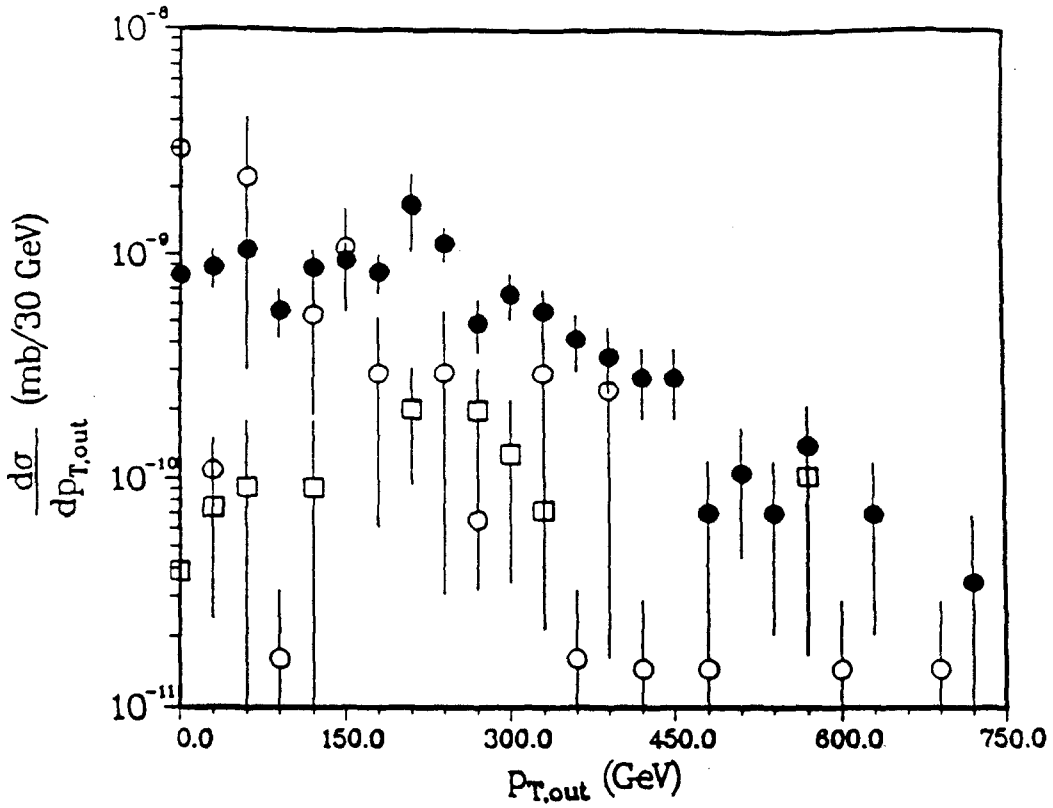

Figure 16

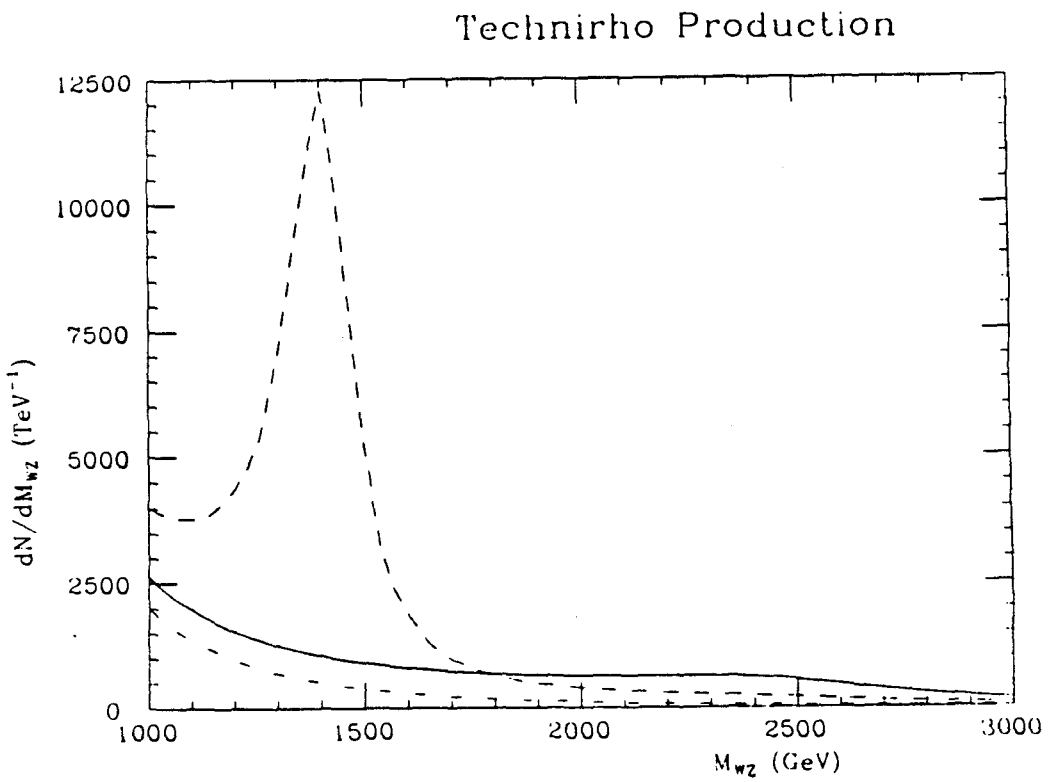

Figure 17

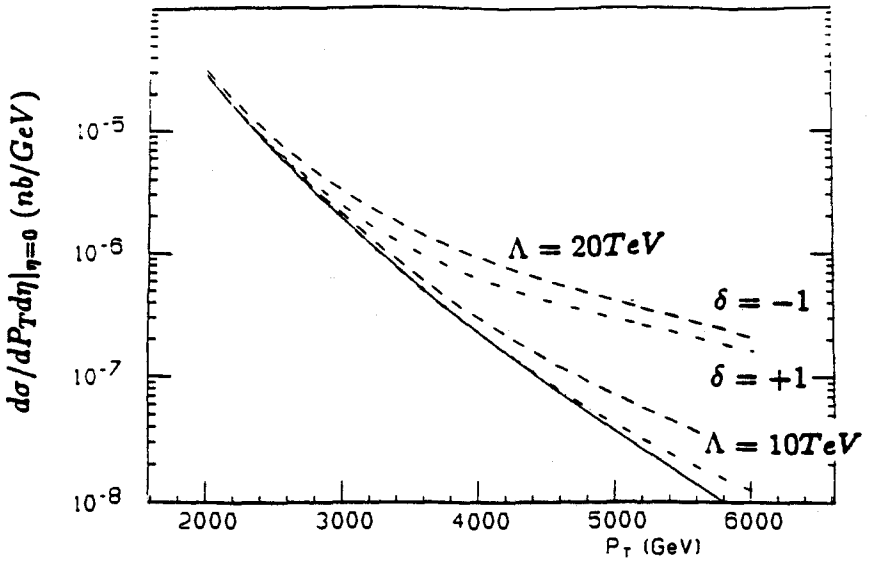

Figure 18

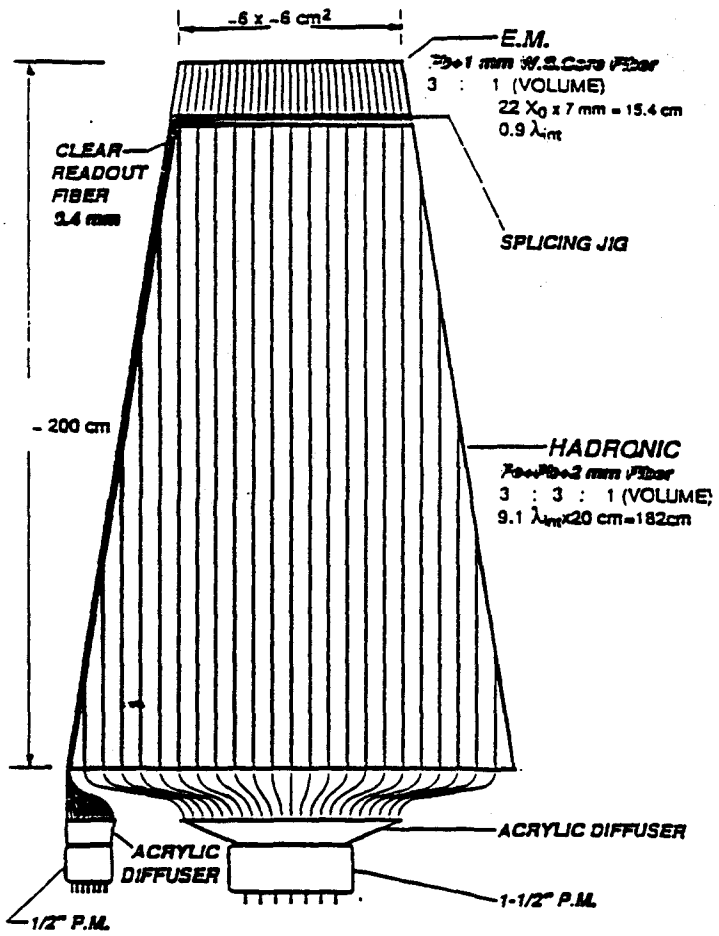

Figure 19

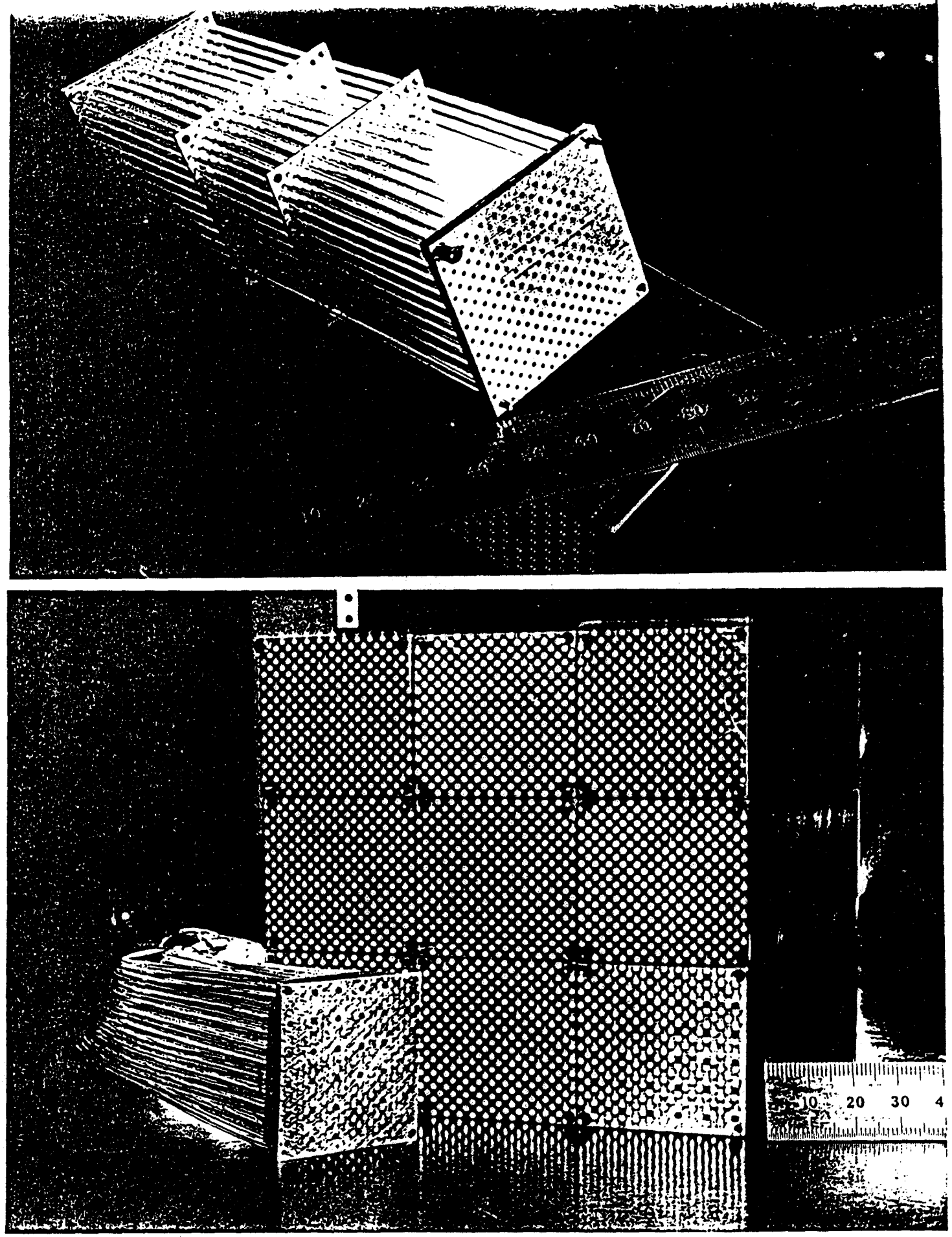

Figure 20

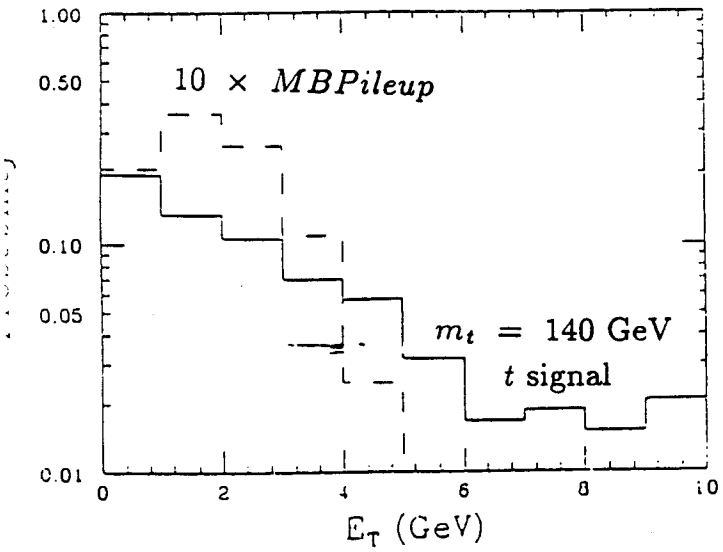

Figure 21

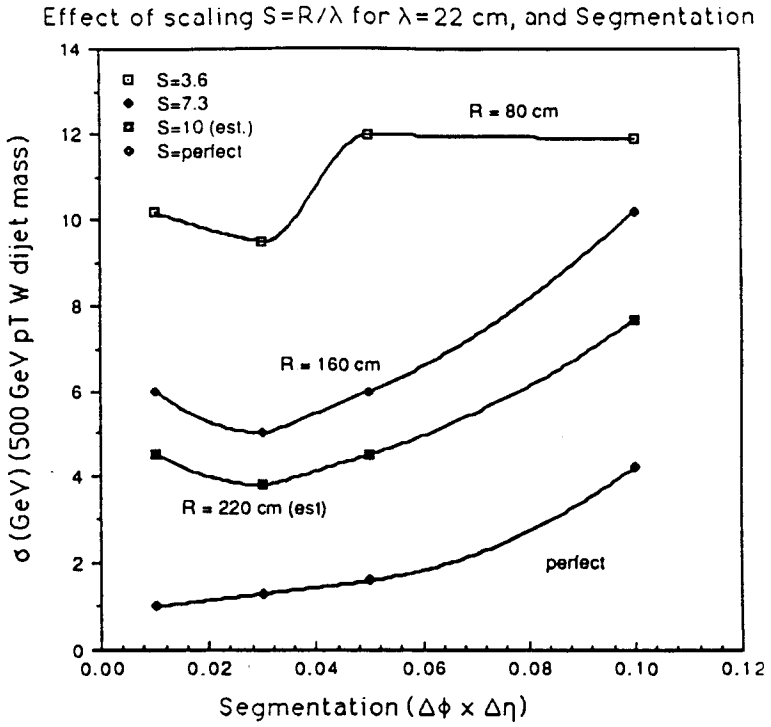

Figure 23

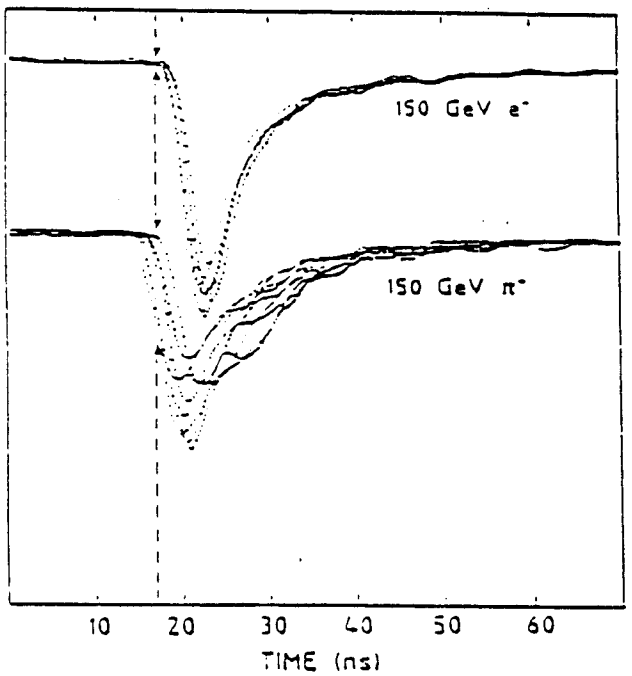

Figure 22

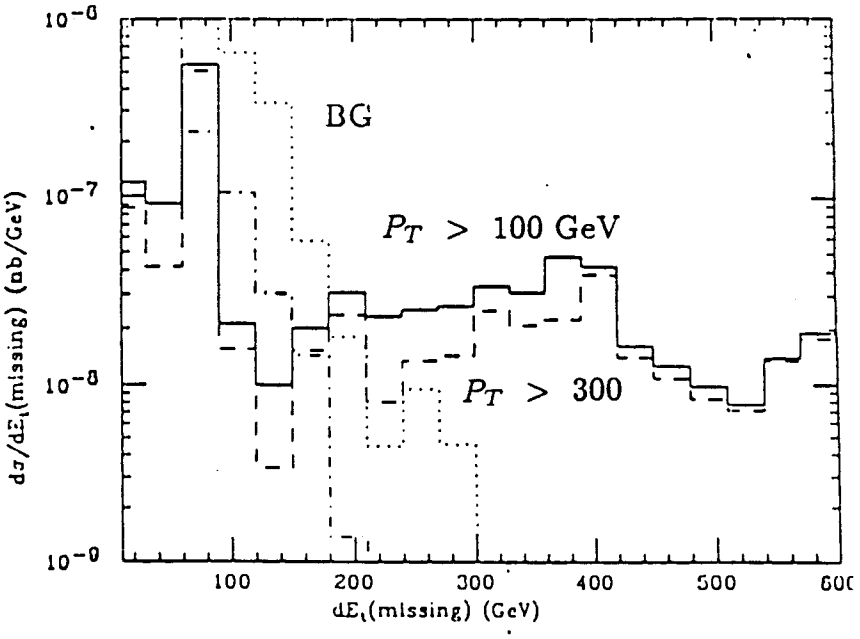

Figure 24

ADC + (2nd level) Trigger for 1 Calorimeter Tower

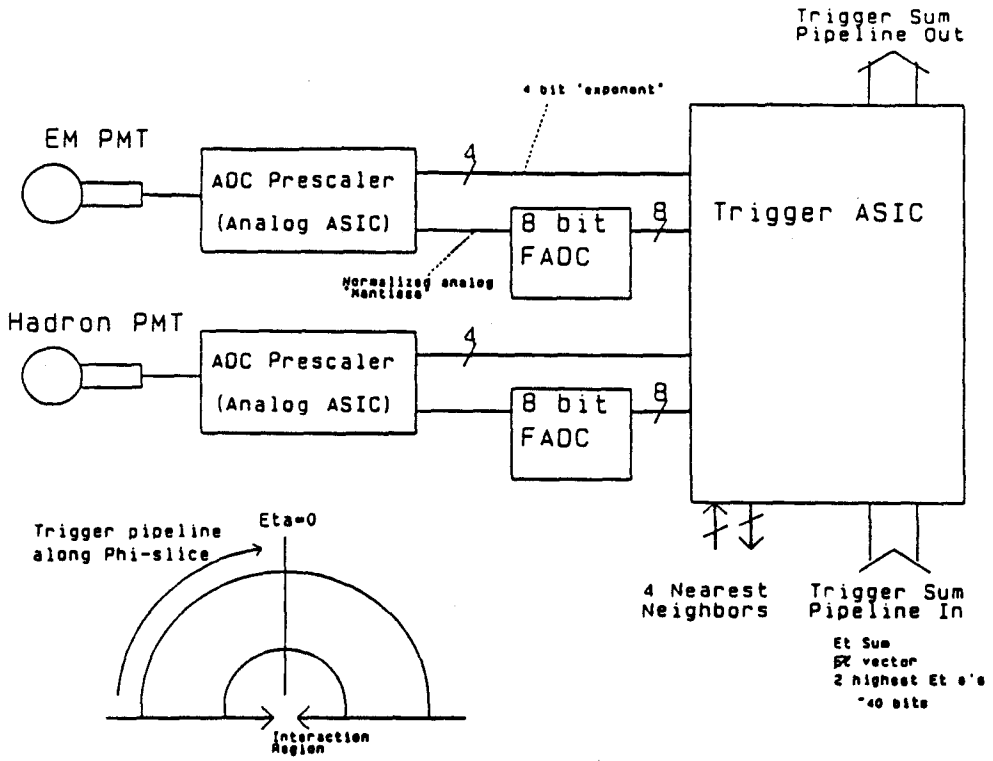

Figure 25

ADC Prescaler (analog ASIC)

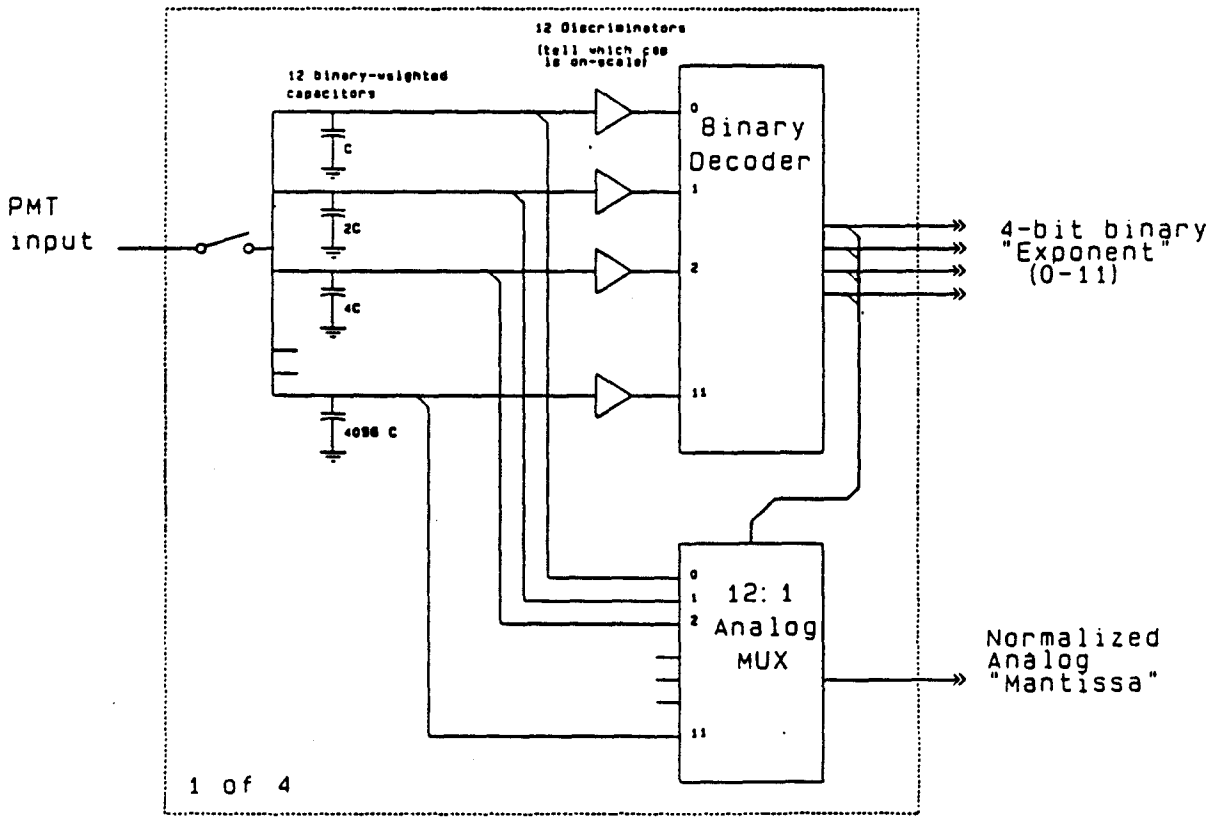

Figure 26

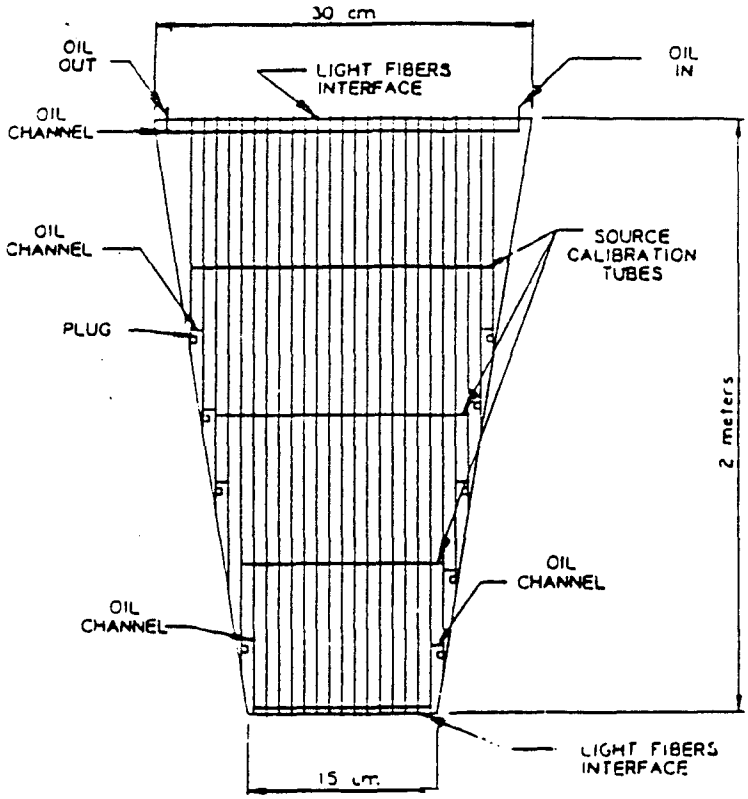

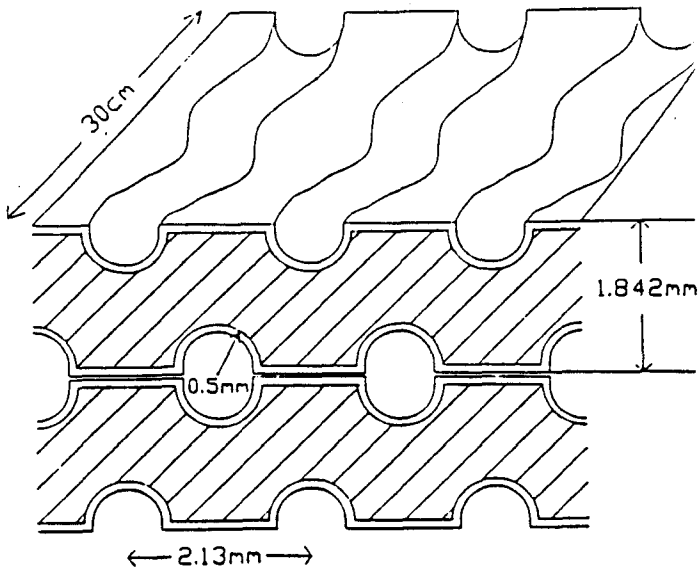

Figure 27

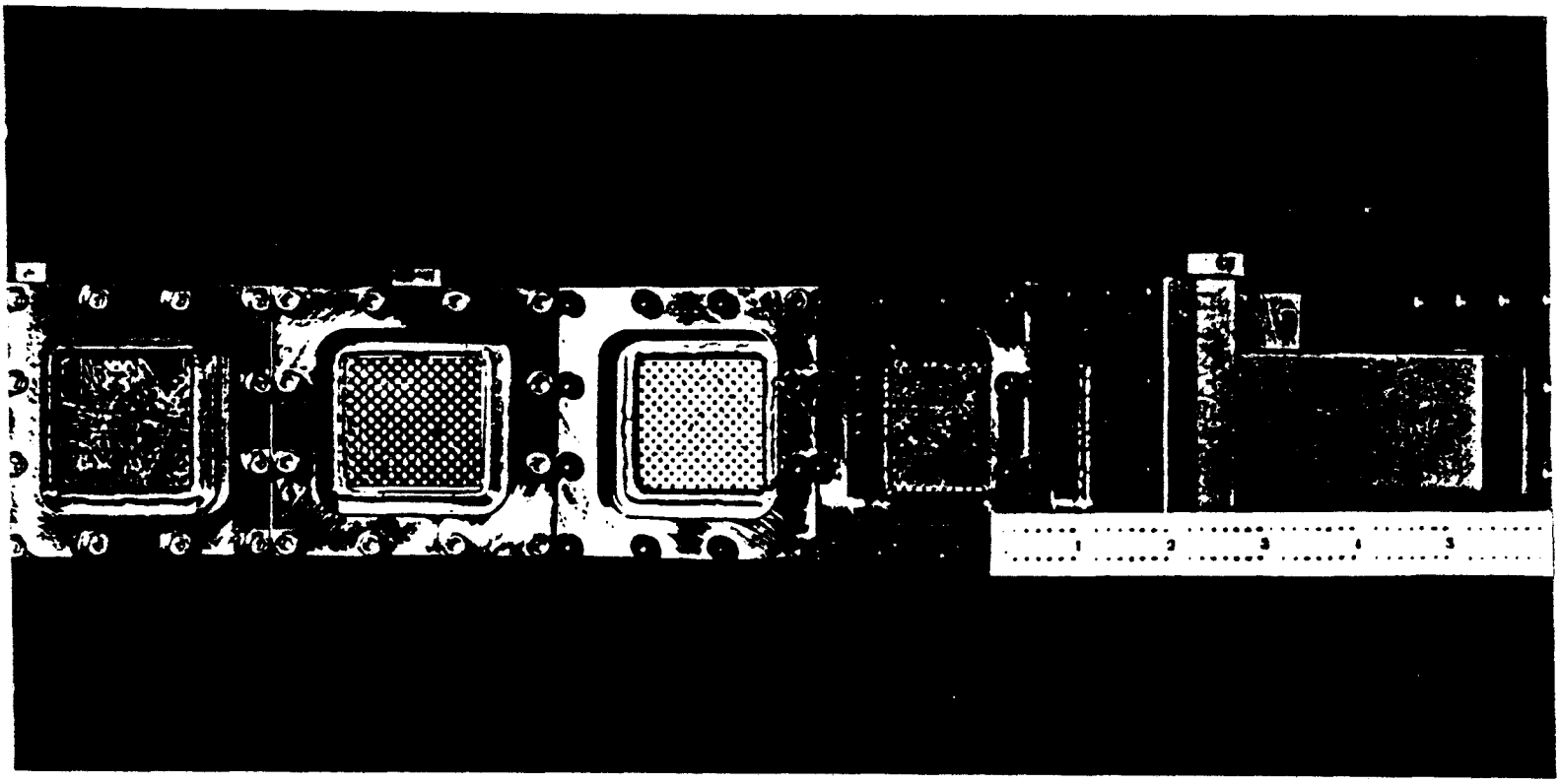

Figure 28

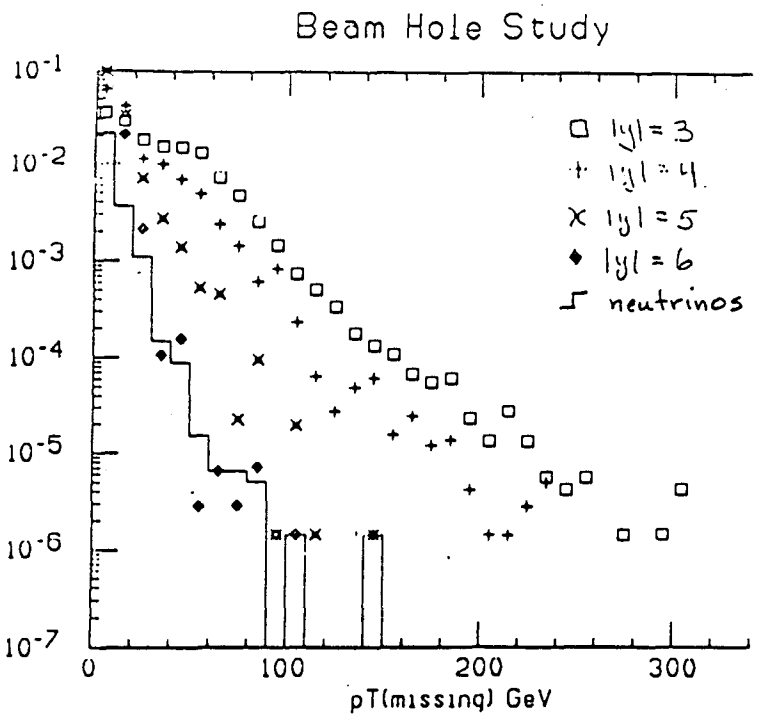

Figure 29

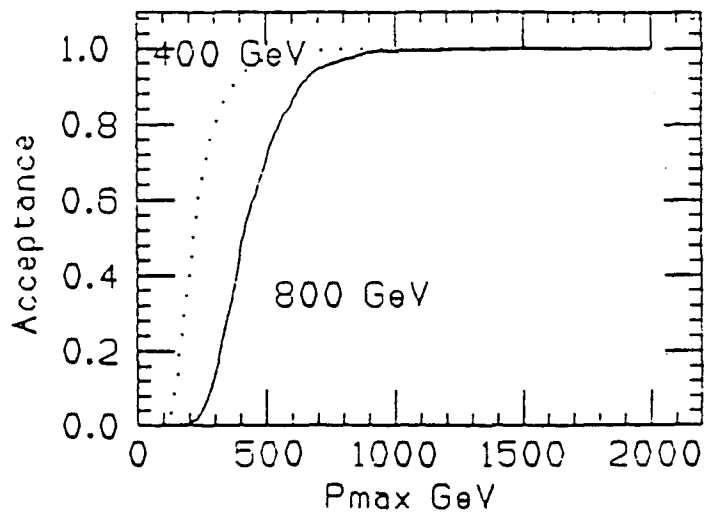

Figure 30

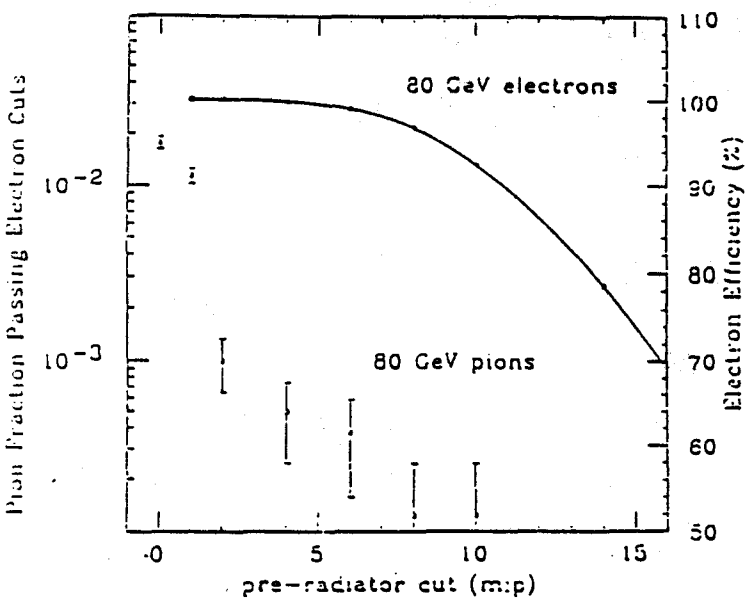

Figure 31

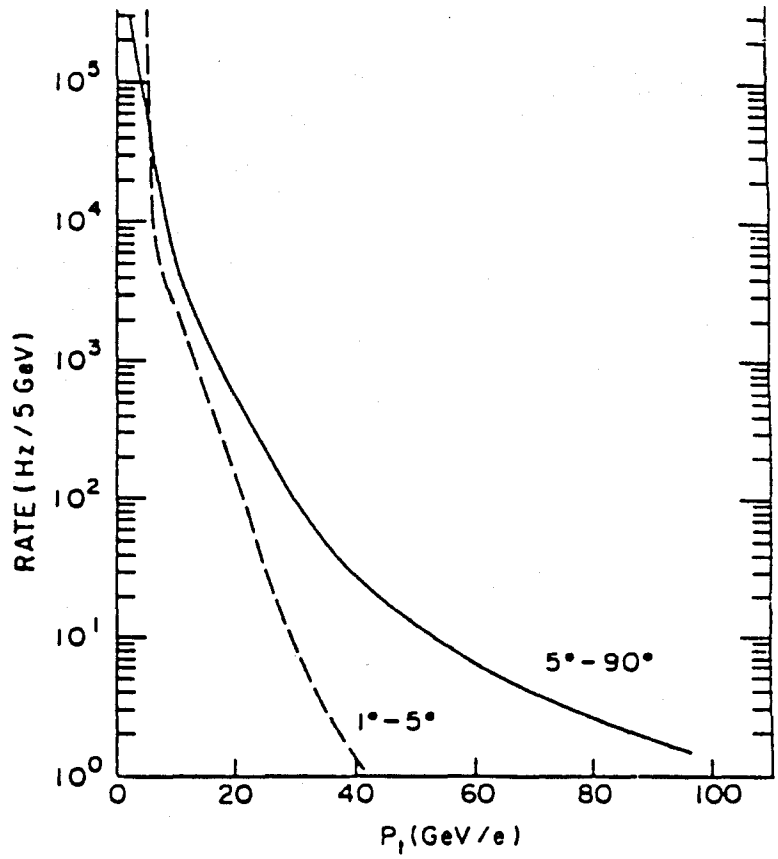

Figure 32

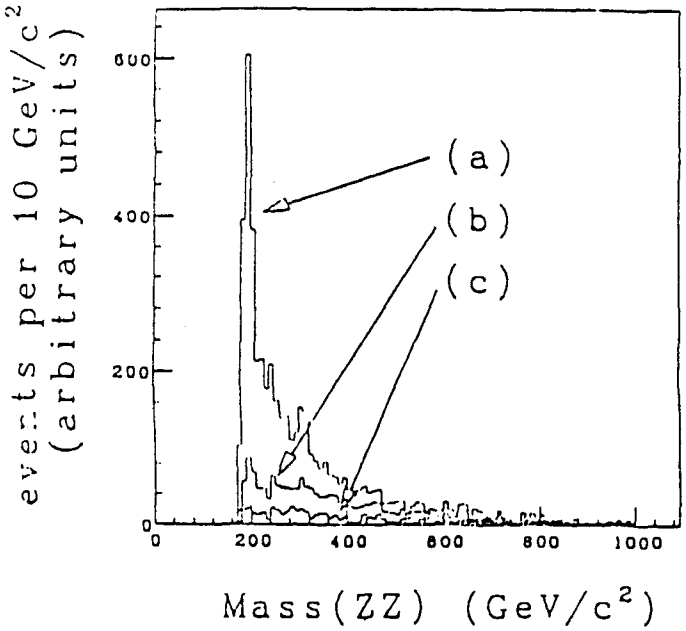

Figure 33

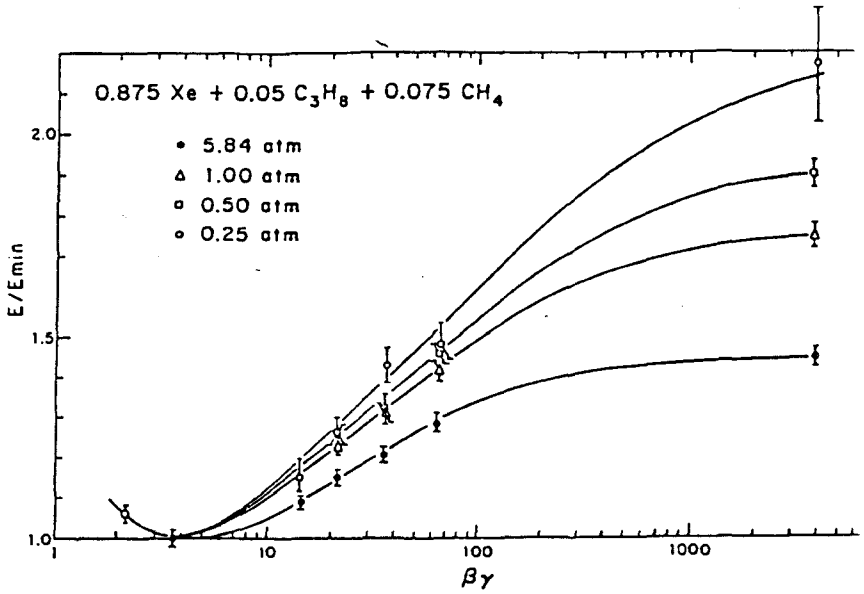

Figure 35

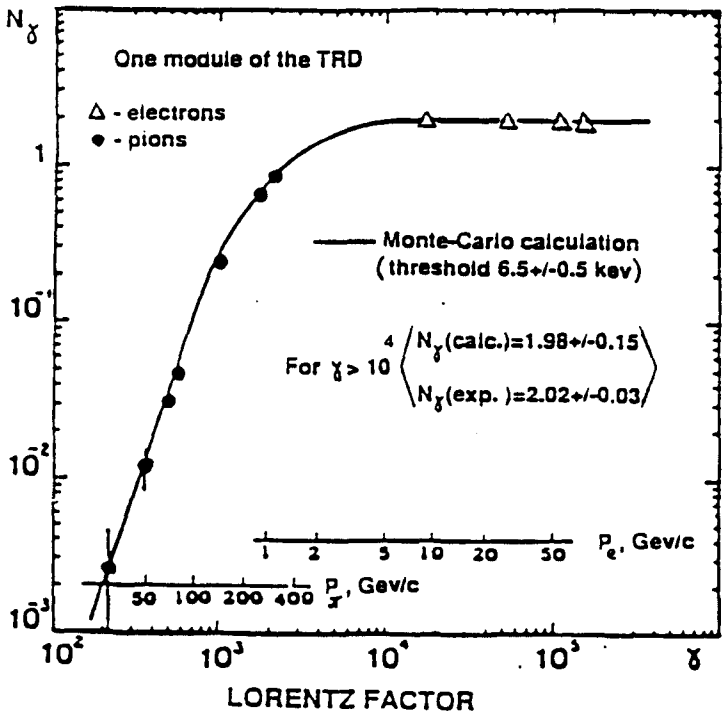

Figure 34

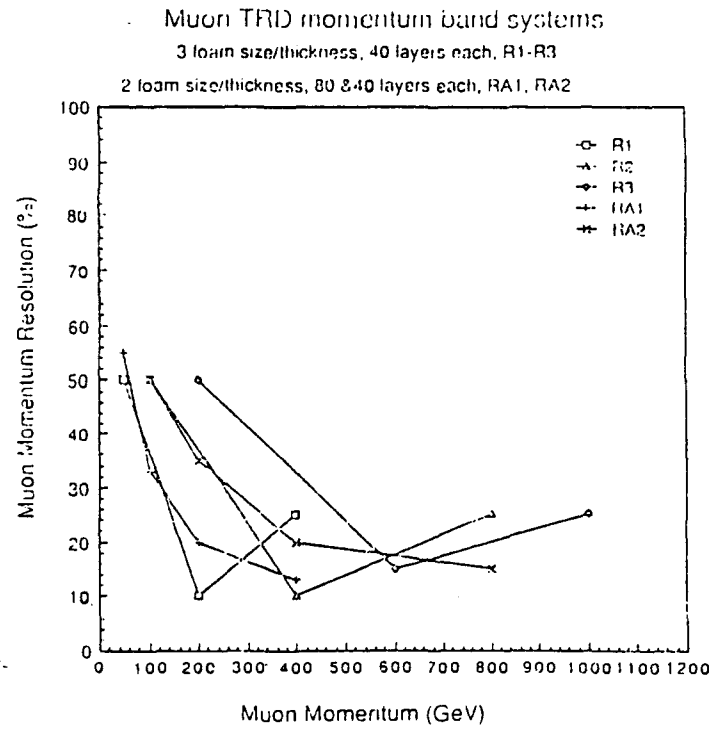

Figure 36

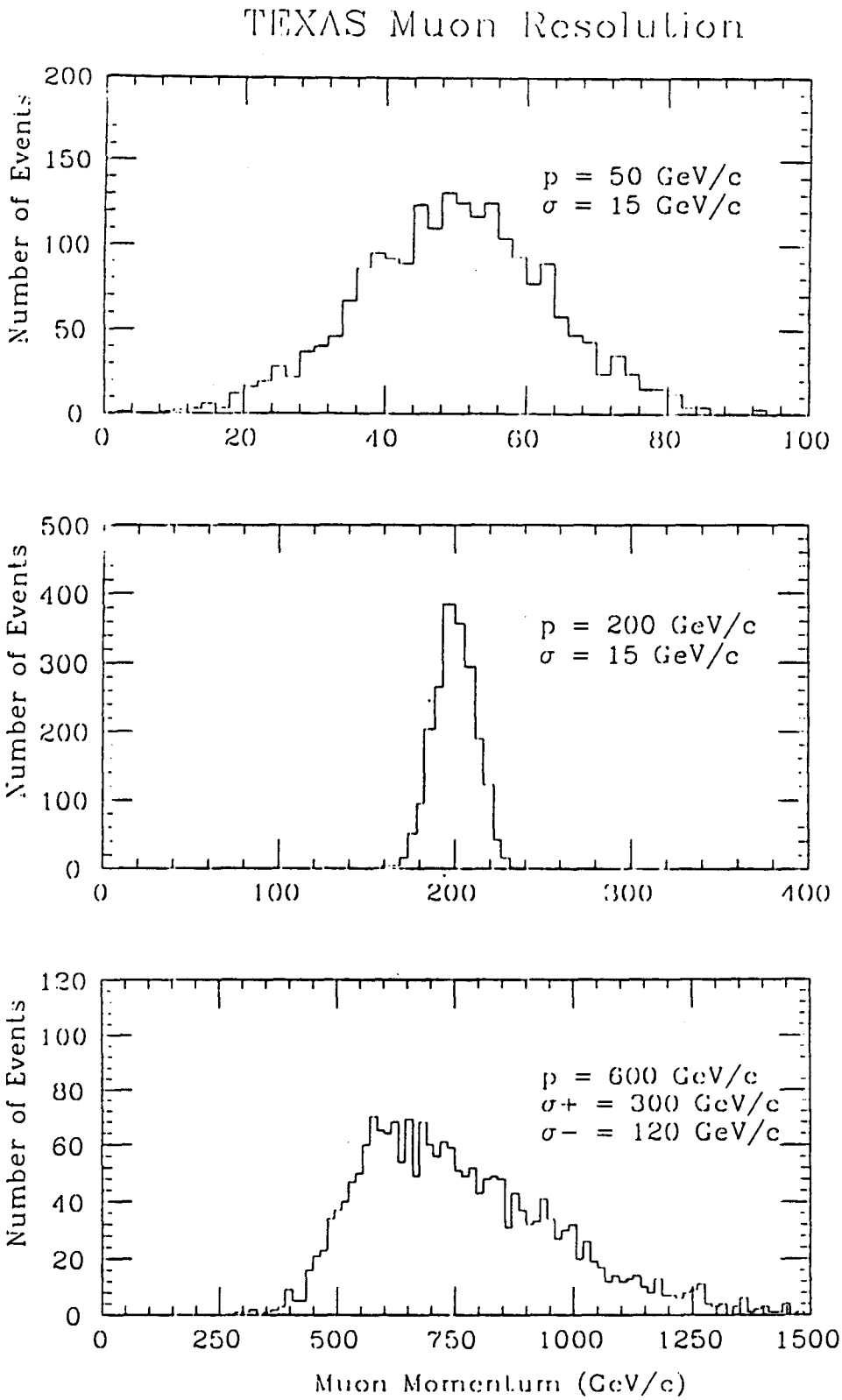
TEXAS Muon Resolution
Number of Events
p = 50 GeV/c
σ = 15 GeV/c
p = 200 GeV/c
σ = 15 GeV/c
p = 600 GeV/c
σ+ = 300 GeV/c
σ− = 120 GeV/c
Muon Momentum (GeV/c)

Figure 37

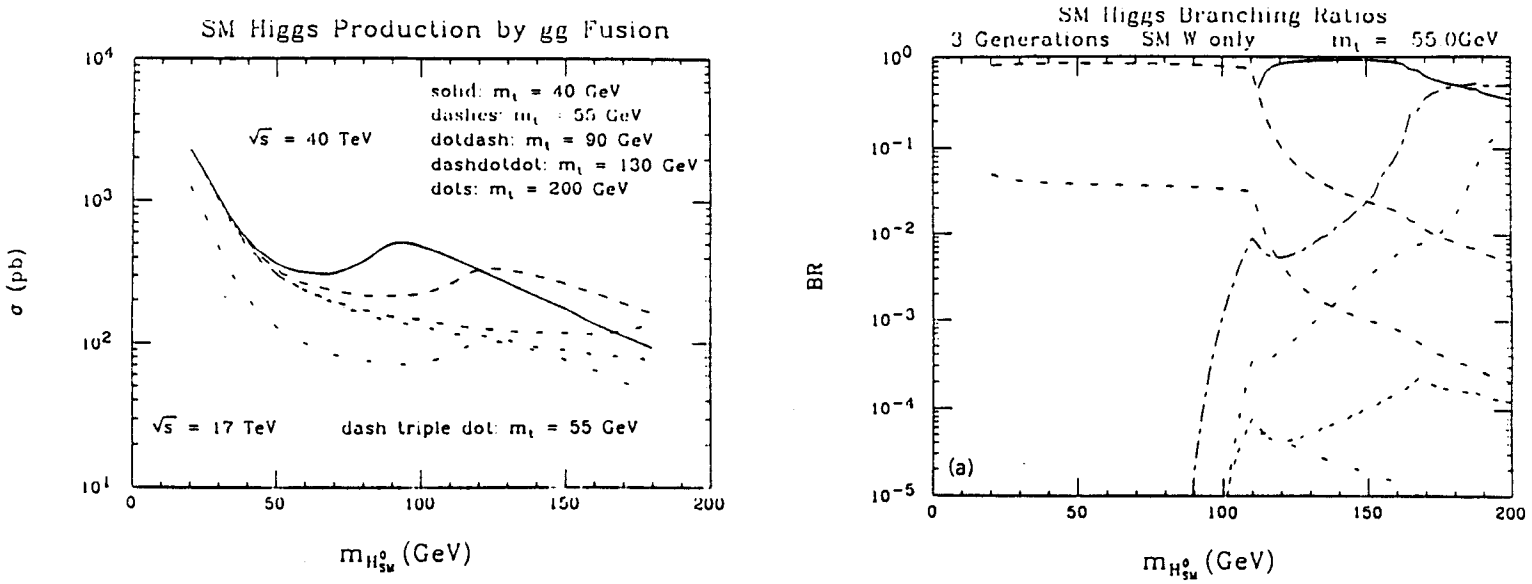

Figure 38

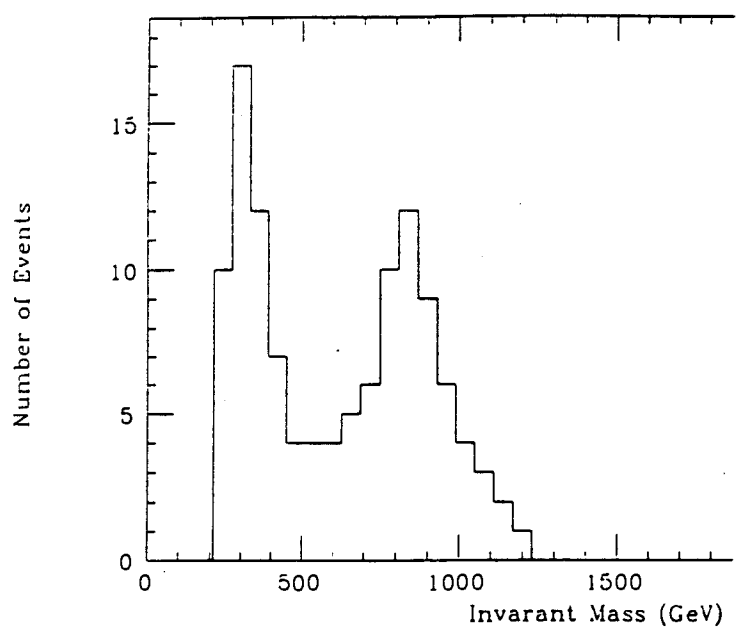

Figure 39

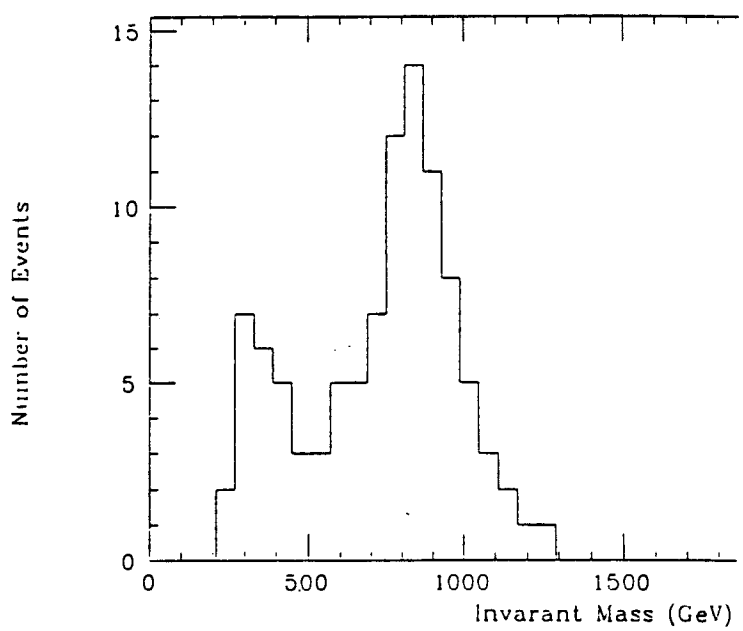

Figure 40

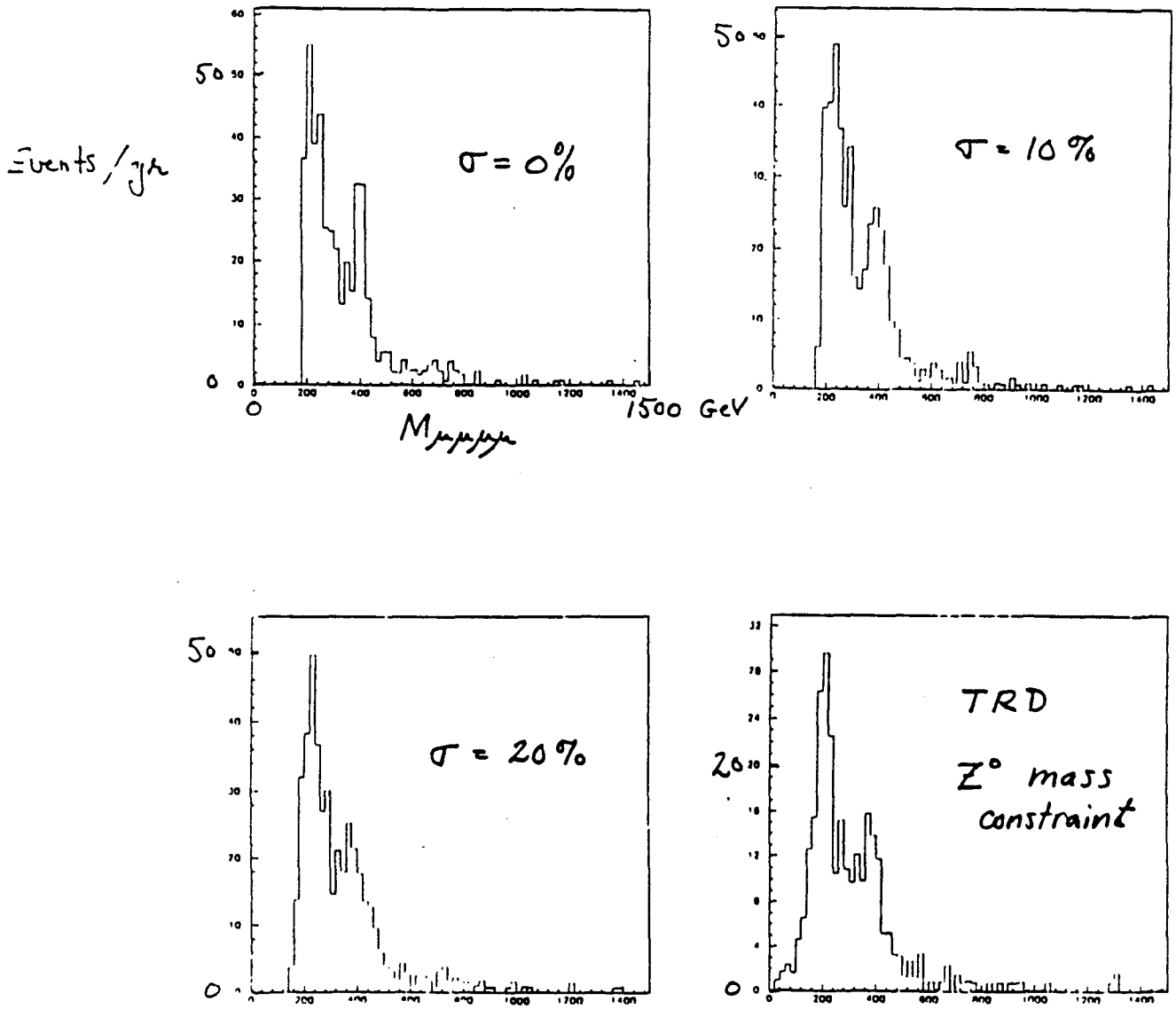

Figure 41

SCINTILLATOR CALORIMETER SUPPORT STRUCTURAL DESIGN AND EVALUATION

1. Introduction & Approach

The objective of this study performed by the Charles Stark Draper Laboratory in Cambridge, MA (May 1990) is to assess the feasibility of a structural system to support the scintillator calorimeter of the Superconducting Supercollider (SSC) as proposed by a Texas collaboration. To address this feasibility study we have designed, modeled, analyzed and evaluated a preliminary structural system capable of maintaining various elements of the calorimeter within required tolerances when exposed to operational environments.

The outcome of this evaluation provides a first-cut design for the calorimeter structural support with dimensions of shell, shapes of rings, reinforcements and frame members. Special attention is given to many dimensional constraints imposed by the physics of the experiment as well the assembly procedures of the calorimeter since they are expected to have a significant impact on structural support design decisions.

The analysis of a finite element model was used to identify the deformations of the structure under the enormous mass of the supertowers, establish stress levels throughout the support structure and provide force and moment components necessary for the evaluation of structural stability.

The proposed structural support system was evaluated to show that it can carry the 2200 tons of supertowers (half the calorimeter) with acceptable deformations and tolerable stress levels. In addition overall and local stability checks exhibit generous factors of safety. It should be emphasized that this is only a first cut design for the overall support system and many localized problems need to be addressed that could ultimately alter this design.

The total weight of the structure for one half of the calorimeter is ~150 tons of steel so that the entire calorimeter support will require approximately 300 tons of steel.

2. Design Concept Considerations

The choice of a structural support system for the calorimeter is subordinated to many design parameters associated with various phases and modes of construction, supertower erection sequences and available space dictated by detector physics requirements. These parameters are expected to play a major role in the design approach and impact design decisions.

The assembly of the structural system and the supertowers is recognized as the most critical issue because it affects not only delicate construction procedures with tight tolerances but has a primordial influence on the final design concept. Section 3 addresses these issues and suggests possible erection procedures. Alignment and tolerance problems are discussed within the context of the erection suggested. While different assembly techniques will create many intermediate structural configurations that need to be investigated, the present study focuses on the evaluation of the <u>final</u> structural system. Note that this system can be adapted to the demands of many construction techniques and modified to reflect special conditions and splices associated with a particular erection mode.

The primary function of the structure is to support the very heavy and dense mass of the supertowers contained between two ellipsoids (6436 Kips for half the calorimeter). Since the structure must offer a continuous surface to the supertowers' bases for support, a ring stiffened ellipsoidal shell was selected as a logical solution. The shell behaves as a very deep beam and its overall depth (9.4 m diameter maximum at the center) offers significant stiffness capable of delivering reaction loads to end support frames approximately 10 m apart. Note that the center line of the calorimeter is 10 m above ground thus placing special demands on the tall end frames design to insure adequate stability.

In order to secure overall stability of the ellipsoidal shell sitting on the 2 end frames a longitudinal central wall was designed that provides the necessary bracing. This 10.17 m long wall framing into the end frames offers additional vertical support to the ellipsoidal shell. The amount of gravity load picked up by this wall is a function of relative stiffness between the shell itself and the wall. Note that it is not desirable to carry a significant portion of the ellipsoidal shell mass by the central wall, because it could distort the calorimeter circularity. Further analysis iterations are expected to lead to an ideal "balanced" situation.

The design of these frames must respect many physics driven dimensional constraints and yet provide the necessary stiffness to insure acceptable deformations, stress levels and stability. The following limitations have been placed on the width of each frame:

Center Frame	25 cm
End Frame	25 cm
Longitudinal Frame	20 cm (10 cm preferably)

One must realize also that the shell plate is pierced by a large number of holes on a defined grid to accommodate the passage of the tower fibers thus reducing the plate carrying capacity and imposing restrictions on structural reinforcements size and locations. It is important to limit the structures complexity in order to minimize possible interference with the arrangements of a vast electronics network.

3. Calorimeter Assembly Procedure

Each half of the calorimeter consists of an assembly of 7,680 pyramidal towers. One hundred and twenty-eight towers are arranged in a group to form the shape of a hollow truncated cone. Sixty of these hollow cones nest to form a stack that completes the calorimeter half.

The towers are cast in sheet metal sheaths for strength, protection, and most importantly, for joining the towers together at the small end of the formed cone. Threaded steel inserts are cast into the large end of the towers to fix that end to the tower support structure.

Two methods of assembly of the calorimeter have been explored, the "Modular Ring Method" and the "Shell-Sector Method". In the "modular ring" method of calorimeter assembly, each cone (made up of 128 towers) is attached to a separate steel supporting ring. The 60 rings are then bolted, surface-to-surface, to form the nested stack of cones which completes the calorimeter and structural assembly (see Figures 1, 2 and 3).

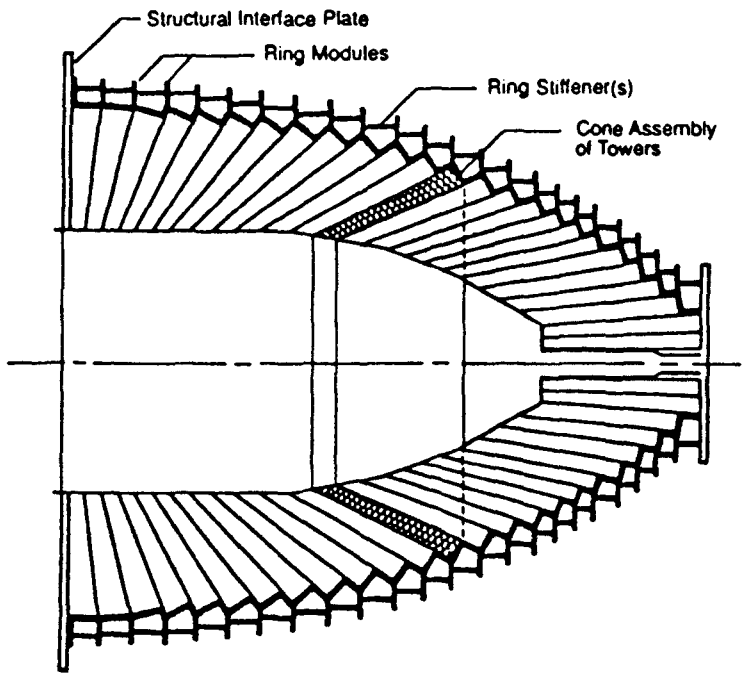

Figure 1. Modular ring calorimeter enclosure.

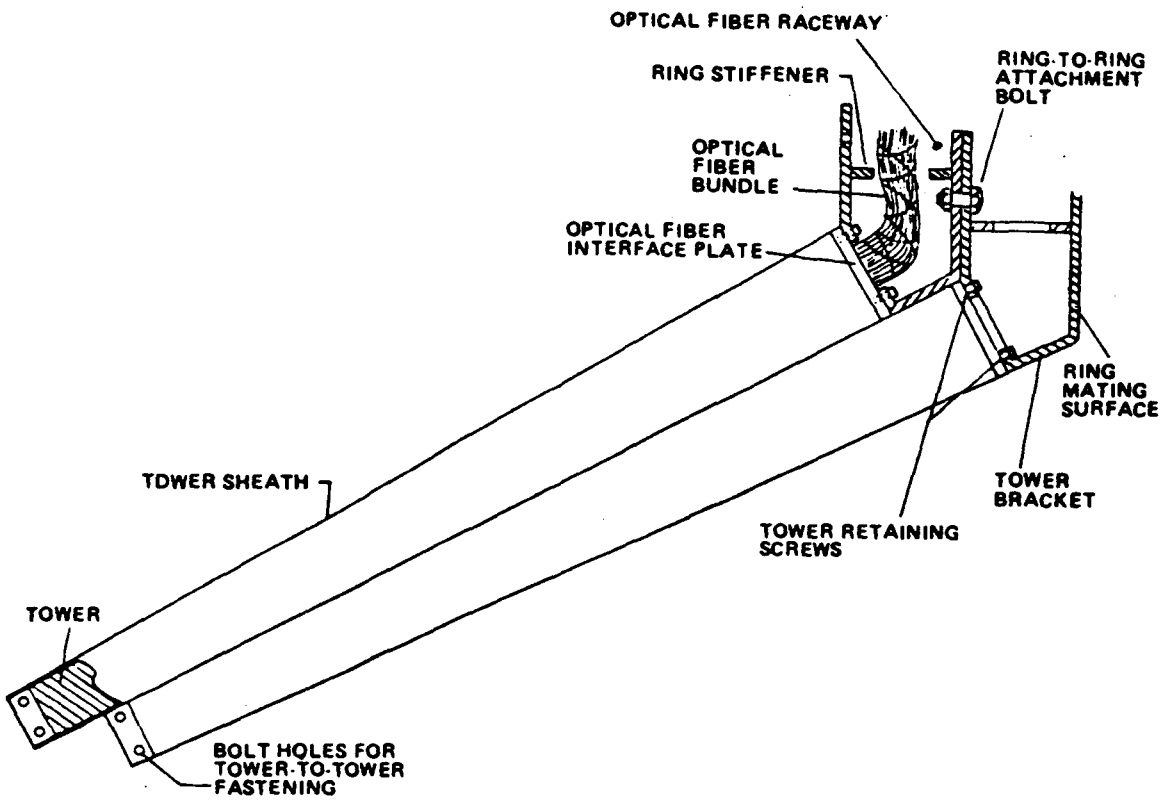

Figure 2. Two ring modules and tower attachment detail.

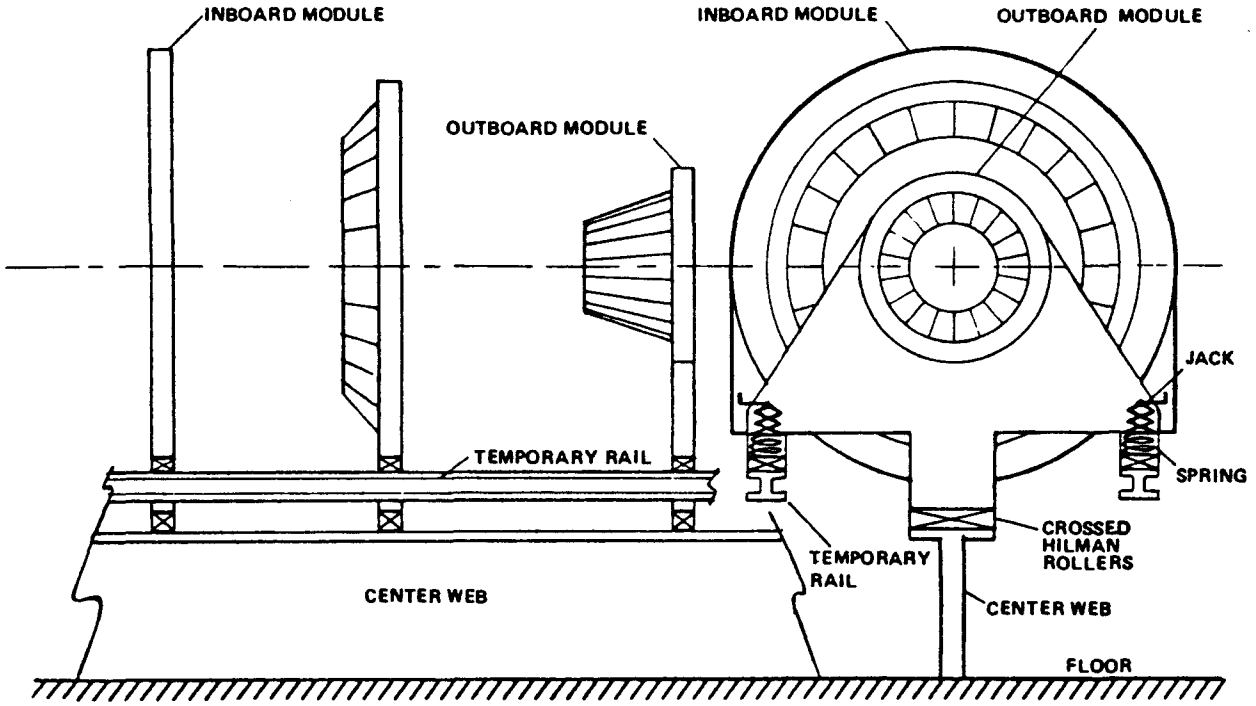

Figure 3. Rail layout.

The modular ring method of assembly is outlined as follows:

(1) The first modular ring to be assembled is the largest diameter ring (and cone). This module is located at the inboard end of the calorimeter half; the end where the two halves of the calorimeter come together.

(2) With the first ring horizontal, the towers are installed to form the cone. After alignment of the towers, their inner ends are fastened together to make the cone rigid.

(3) The ring is lowered into the hall and bolted, axis horizontal, to the end support frames.

(4) The next ring in the stack, the second ring, is assembled, aligned, lowered into the hall and bolted to the first ring. Temporary rails help support the second and subsequent rings until calorimeter assembly is finished.

(5) Successive ring modules are added using the same assembly sequence until the calorimeter is complete. When the forward calorimeter towers are added and the outboard end support frames are attached, the temporary rails for ring support are removed.

The second concept explored for assembling the calorimeter is the "Shell & Sector Method". This method involves fabricating a reinforced shell structure that holds the lower 50% (3,840 towers) of the 7,680 towers that make up one half of the calorimeter. The upper 50% of the towers are held in place by 180° structural sectors, or half rings similar to the full rings used in the modular ring method of assembly.

Both the "modular ring" and "shell & sector" techniques appear to be viable methods of assembly. Further study may reveal other, more attractive, options.

4. Structural Support Design Description

The structural support for the calorimeter includes two identical halves (mirror images) that must be capable of moving away from each other to gain access to the inside tracker and the calorimeter interior space. Figure 4 shows the two separate structures models in an open position. Design, modelling and evaluation are therefore presented here for one independent half portion of the calorimeter.

The main structural system is a ring stiffened ellipsoidal shell with radii a = 10.7 m and b = c = 4.7 m. The shell truncated 10.17 m from the center offers an opening of 3.14 m diameter for the calorimeter end plug. The 2 cm thick shell is reinforced by 10 outside rings disposed 1.00 meter on center. A larger ring is provided at the center of the shell as well as the end face. The center ring is a tube intentionally stiff (36 X 36 X 4 cm) because it is anticipated to provide support for half of the center tracker as a cantilever. Eight reinforcements (same properties as the rings) run the length the ellipsoid 45° apart, around the circumference. Longitudinal reinforcements are added also every 22.5° for the first 4 m of the shell near the center where additional stiffness is required.

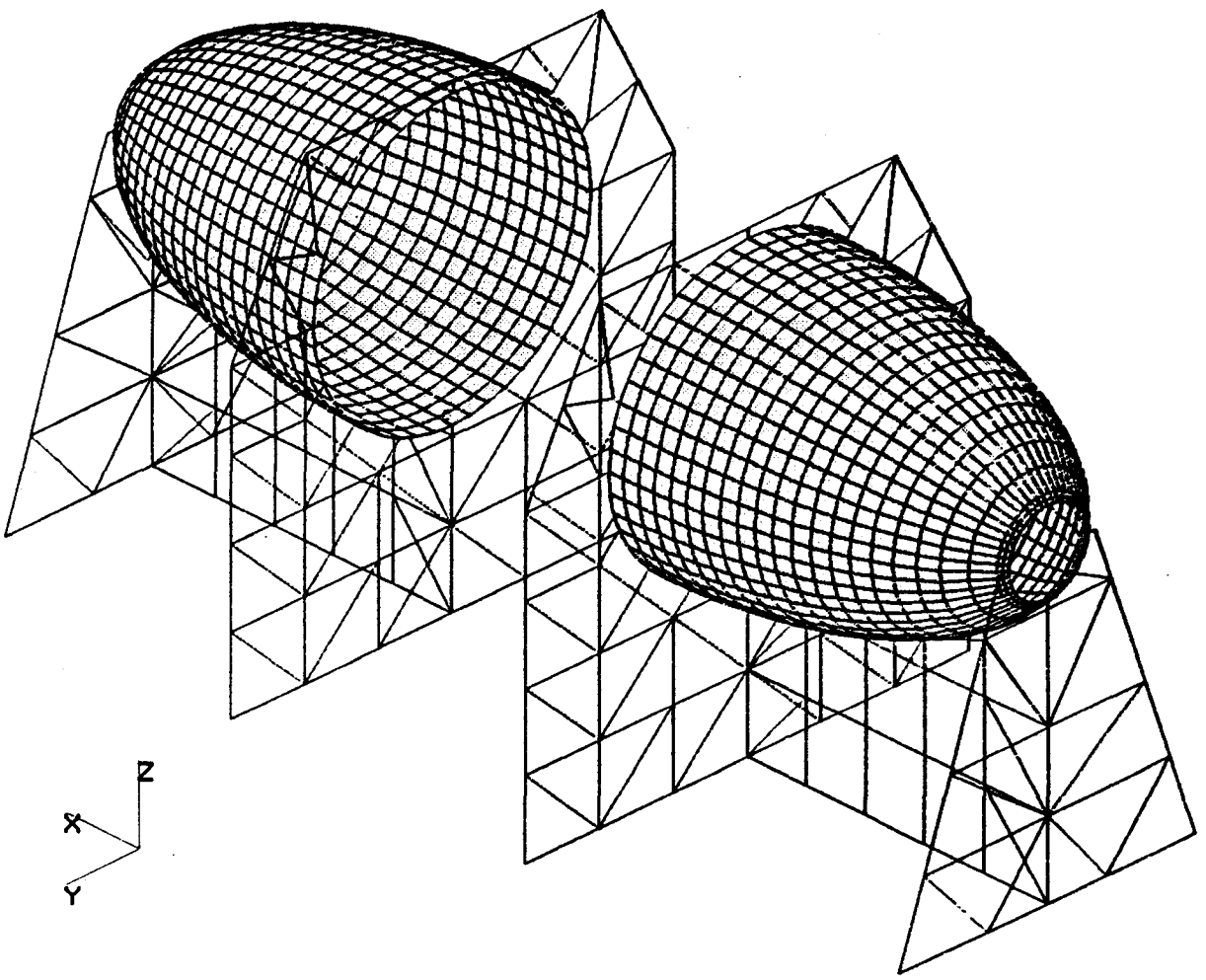

Figure 4: Calorimeter Halves in Open Position Finite Element Model Discretization

The ellipsoidal shell acts as beam with reactions picked up by two vertical end frames. The center frame has a width of 25 cm and uses rectangular tubes (25 X 40 X 4 for vertical members) disposed in a truss like configuration for better material efficiency. This frame is designed and configured to help preserve shell circularity in an area of very large reaction loads. The end frame of trapezoidal shape and 25 cm wide supports a lesser reaction load but this advantage is somewhat lost because of the 10 m unsupported length of its members. Out of plane stability of the frame main members require relatively large stiffness properties to insure acceptable slenderness.

A longitudinal frame, provided under the shell, connects the two end frames thus insuring longitudinal overall stability. The width of this frame must be minimized at all cost since the radiation along the vertical center plane of the calorimeter is more intense and cannot trade extremely valuable space for the structural support. The vertical frame includes 4 interior posts (20 X 40 X 3 tube) with width limited to 20 cm. A revised design will increase the number of posts to 8 while reducing their width to 10 cm. Table 1 summarized the shape and dimension of the main elements of the structural support system.

The material proposed for the shell and the frames is a high strength steel of Fy = 50 ksi (yield stress).

Table 1 Structural Components Description

Element	Configuration & Dimension	
Shell	Plate 2 cm thick	
Circular Rings & Longitudinal Reinforcements	T Section:	22 cm X 1.5 cm web 16 cm X 2 cm flange
Center Ring	Tubes:	36 X 36 X 4
End Ring		30 X 30 X 2
Center Frame	Tubes:	25 X 40 X 4 Vertical 25 X 25 X 3 Diagonal & Horizontal
End Frame	Tubes:	25 X 40 X 3 Vertical & Diagonal 25 X 25 X 3 Horizontal & Diagonal
Longitudinal Frame	Tubes:	20 X 40 X 3 Vertical 20 X 20 X 2 Horizontal & Diagonal

5. Finite Element Model and Analysis Results

By invoking symmetry about a vertical plane the finite-element model of only half the structure can be considered. Figure 4 is a view of the model where relative dimensions and elements can be identified. The finite-element model of half of the structural support contains: 528 shell elements and 618 beams for a total of 4326 DoF's.

The mass of the supertowers was assumed to be distributed uniformly along the circumference at each station of the shell axis. The loading is computed from the volume enclosed between two ellipsoids at each station x and assigned as body loading to the shell.

The structural steel mass is computed automatically by the program and assigned to the appropriate nodes.

Our first design exhibited large deformations and required modifications. With (a) additional shell stiffening near the center of the calorimeter, (b) a significant increase in the edge ring and (c) broadening of the center wall, the deformations of the structure now remain very small with a maximum of 3 mm. Figure 5 shows views of the undeformed and deformed (grossly exaggerated) structural system for comparison. Most of the deformations occur in the highly stressed supporting frames while the shell itself remains very close to its original configuration but undergoes rigid body motions. The maximum distortion of 3 mm is expected to increase somewhat when many construction details, joints and interference constraints will be taken into consideration and will affect flexibility.

The 2 cm thick shell is stressed both circumferentially (hoop stresses) and longitudinally as it acts as a deep beam in bending. The stress reported in the color coded plot of Figure 5 refer to a stress state expressed by von Mises criterion. The maximum stresses recorded must be increased to allow for loss of material due to holes in the shell plate (factor of 1.25) and stress concentration estimated at 2. Under these conditions shell stresses associated with the overall support structure remain under 5 Ksi. (Note that $6.894\ 10^6\ N/M^2 = 1$ ksi). It should be emphasized that local bending stresses will be significant (estimated at 12 ksi) in comparison but they will depend on the attachment mode of the supertowers to the plate.

The supporting frames are the most stressed elements of the structural system and since the frame members are mostly in compression their allowable stresses must decrease to insure stability. Actual load have been compared to the critical allowable load as defined by the AISC Steel Code. Conservative assumptions have been used for the stability check although no allowance was made for bending which is however small. Generous factors of safety between 1.5 and 4.0 have been identified above and beyond the one already included in the critical allowable load. Results show that the end frame could be stiffened in order to even out the deflections along the center line of the calorimeter. It is evident that many iterations also could optimize the design and use material more efficiently.

The breakdown of the tonnage of structural steel required for the support system of one half calorimeter is as follows:

Shell Plate	40.0	Tons
Shell Reinforcements	31.8	
Frames	87	
Total	158.8	Tons

With another iteration the weight of the center frame is expected to decrease without affecting deformations and stresses appreciably. In summary the structures of the support system of the entire calorimeter will require approximately 300 tons of steel.

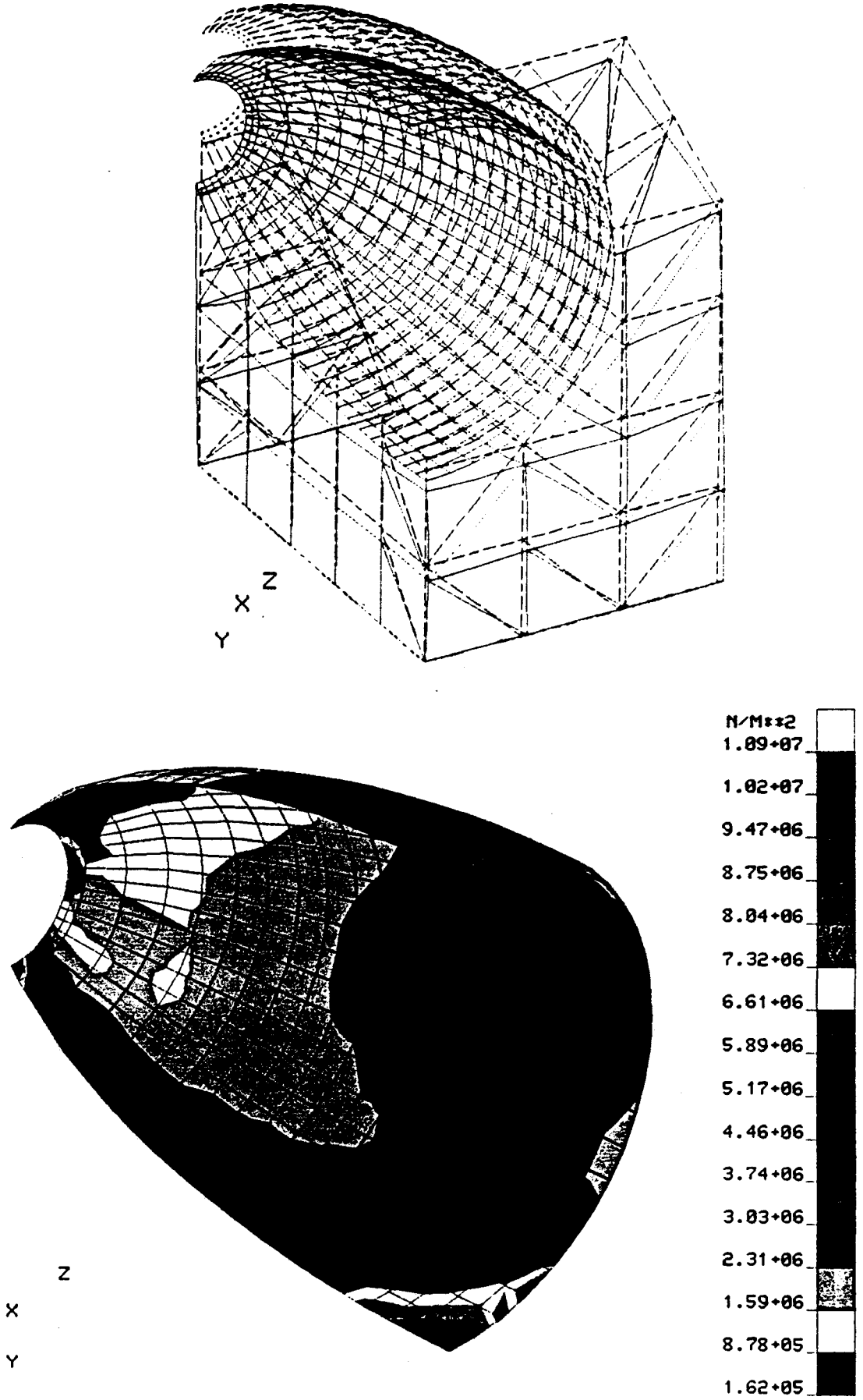

Figure 5: Finite-element Deformations and Shell Stresses (gravity load)

Muon TRD Spectrometer

Engineering Program

B. Dolgoshein (Moscow Physics Engineering Institute), C. Lane, S. Reucroft, M. Sheaff (Wisconsin), A. Schmeleva (Lebedev University), L. Sulak, E. von Goeler*, A. Vorobyov (Leningrad University), and D. Winn

Apparatus: E769, FNAL, Beam line TRD with π, μ, in 250 GeV positive beam (Sheaff)
E761 FNAL, experiment with momentum analyzed π, μ, e (Vorobyov)

At least three of the anticipated proposals for first round SSC detectors include Transition Radiation Detectors (TRD's). The TR technique has matured considerably over the past decade; however, there are still some questions that need to be answered in a systematic way if TRD's are to be most effectively used in the SSC environment. Some of these questions can be answered using existing detectors now operating in beamlines at Fermilab and at CERN. Others will require R and D efforts of a rather modest scope for which technical support and a small amount of equipment are needed.

The anticipated use of large volume TRD's filled with gas mixtures composed predominantly of Xenon (and therefore expensive) presupposes the ability to build a recirculating gas system which is stable in time. The table and figure indicate requirements of a suitable gas recirculation system. Industrial support is expected to be necessary for its development.

Relatively compact TRD's (total depth ≈30-50cm) built for the innermost region of SSC detectors offer the attractive possibility of efficient electron identification with large pion rejection for pion momenta below 100 Gev/c. (Monte-Carlo calculations indicate a rejection factor ~ 100 for a typical 25 module system). Such devices provide the ability to identify both isolated electrons and electrons in jets.

Unique to the TEXAS detector, we propose to develop the TRD technique to determine muon momenta in the region appropriate for the SSC (60 GeV $< p <$ 600 GeV). This momentum range is larger than that covered by the usual excitation curve of a convential, simple TRD system. We shall attempt to optimize the construction of the TRD prototypes we study in order to extend this dynamic range. We shall study not only the yield of X-ray photons but also their spectral shape since it is anticipated that this shape may vary with incident momentum, at least for irregularly spaced radiators as found in foam. Different foam geometries give slightly different excitation curves and it may be necessary to use several different types of foam in the same detector to give coverage over the entire desired dynamic range. We shall also attempt to maximize the signal relative to the noise presented by delta rays.

We will be able to carry out some of these studies in two existing experimental arrangements. In the E791 beam-line TRD, we plan to modify the radiator of a few TRD modules vis-a-vis wall thickness and cell size as a test of our optimizations. Different gas mixtures containing small admixtures of 'fast' gases such as CF_4 and C_2F_6 will be studied to see whether we can reduce the collection time from the present ≈120ns for 3mm drifts by as much as a factor 2. In the E761 TRD, radiator studies using various foam radiator combinations will be performed to determine the shape of the excitation curve for different foam alternatives. In both experiments we will obtain waveform information to confirm that the relative pulse shape is independent of the position of the localized X-ray deposition. If so, simple time over threshold multihit TDC's may be used to measure the spectrum. SSC applications require 100K's of channels. We will develop maximum likelihood techniques to measure γ by measuring pulse height information in addition to X-ray counting.

We are also considering the Bates Linac (Littleton, MA) as a source of electrons with γ in the range $200 \leq \gamma \leq 1800$ for some of the detector development tests.

Construction issues will be studied in an attempt to develop a design that is simple to construct and to maintain. Designs being considered include planar chambers with RO-HACELL walls, straw tube chambers, or carbon coated plastic extrusions with glued or aluminized mylar cathodes. Monte-Carlo studies will be used to define which design strategies are the most promising, and small prototypes of each will be built.

Several large scale implementation issues will also be probed. For large scale construction, we will verify the low outgassing rate of reverse osmosis quality polyethylene and carbon fiber materials. With Union Carbide engineers, we will investigate the large-scale recycling of xenon gas. The following detailed design questions will be addressed:

1) Do activated Cu filters for O_2 scavenging reduce the CO_2 gas buffer to CO? Does the resulting CO remain in the system?
2) Can a simple CH_4 monitor be designed which will function in the presence of isopropyl alcohol, CO_2, H_2O and CH_4 radicals produced by radiation damage?
3) What is the best method to remove CH_4 radicals?
4) How can TRD gas composition be monitored both at the high pressure input to the chamber as well as at the low pressure output?
5) Which safety issues must be addressed to employ 10% C_2H_6 because of its potential flammability?
6) What is the best way to monitor CF_4?

Budget:

Operations	
Engineering support (1 man-year)	$150K
Prototype Liquid scintillator trigger counter	$ 50K
Union Carbide sub-contract	$139K
Travel to FNAL for beam tests (20 man trips)	$ 20K
Gas	$ 30K
Test Radiators	$ 5K
Test Detectors	$ 10K
Equipment	
Test Electronics	$ 20K
Gas Flow Meters	$ 10K
1 Apollo (or equivalent) for simulation and analysis	$ 15K
TOTAL	$449K

BICRON®
20th Anniversary 1969 - 1989

Bicron Corporation
12345 Kinsman Road
Newbury, OH 44065
Telephone: (216) 564-8000
Telex: 980474 BICRON NWBY

Costs of A 16-Month Engineering Program Performed
by Bicron for the
Texas Calorimeter Collaboration

The cost elements are presented in the same sequence as the Statement of Work tasks.

I. Produce and test radiation-resistant plastics and liquid scintillators.

A. Supply approximately 5km of Bicron's latest rad-resistant fibers presently identified by the "RH" designation. RH-1 and RH-2 materials are planned at this time. $10,100

B. Provide several liquids samples of the best formulas. Encapsulate in special ampules. Work on capillary structures. Summary report.

Materials	$ 9,200	
Labor, 40 hrs.	$12,600	$21,800

II. Develop techniques for casting fiber calorimeter modules.

A. Design and Construct Fixtures

-Array Fixtures		
-Fiber Alignment Fixtures		
-Assembly Fixtures		
-Casting Molds	$118,800	
-Concept and Project Engineering, nine man-months	$ 90,000	$208,800

B. Construct projective tower assemblies, 1 each 2 meters long and 1 each 3 meters long. Modules made with developmental fibers Type A, RH-1, and RH-2 as available. Anticipate casting several practice units 4 each demountable PMT assemblies.

Materials and Outside Services:	$ 37,000	
Labor: 2,310 hours	$138,600	$175,600

C. Design and Cost Production Facilities
Engineering: 4 months $ 51,900

III. Develop Simple Optical Interfaces

A. Design and construct fiber mass-coupling splices.

Equipment and Fixtures:		$ 14,240	
Labor and Engineering:	496 hrs.	$ 29,760	$ 44,000

B. Mechanical light coupling for fibers

Materials and Hardware:		$ 2,000	
Labor and Engineering:	2 man-months:	$ 20,760	$ 22,760

C. Optical coupling to liquids

Materials and hardware:		$ 12,000	
Labor and Engineering:	20 weeks	$ 48,000	$ 60,000

Grand Total	$594,960

We estimate that the addition of an extra local contract engineer would enable the work to be completed in 12 months instead of the estimated 16 months. Cost: $150,000

Bicron Rad-Hard Scintillation Development

We are in the process of developing scintillation fibers based on novel new materials. Our first formulation, type RH-1, exhibited improved resistance to discoloration when tested by S. Majewski in December, 1989. That confirmed we were on the right track.

We are presently working on types RH-2 and RH-3. We strong expect that both of these will be improvements over the first material.

Bicron will continue to bear all development costs of the RH-plastics. As we achieve the ability to make fibers of these materials, we will incorporate them in the testing phase of the TEXAS program.

Engineering Development
of Cast Scintillating Fiber Calorimetry

Bicron Corporation

Background:

This statement of work defines an effort to develop materials and construction techniques for scintillating fiber calorimeter production. Specifically, we propose to develop new radiation-hard plastic and liquid scintillators suitable for use in scintillating fibers, to incorporate these materials into cast prototype projective towers for an SSC calorimeter, and to develop techniques for optical coupling of fiber outputs. The specification of requirements for this integrated system will be derived from the needs of scintillating calorimetry within the TEXAS detector, but its application will be more general. A coordinated system-level approach is necessary to design and evaluate radiation-hard materials in their appropriate physical context, to construct and characterize prototype structures with the appropriate component materials, and to compatibly couple calorimeter modules to readout systems.

The SSC will require massive calorimeters with excellent spatial, temporal, and energetic resolution. These devices should be uniform in response, very radiation-tolerant, compact, able to be calibrated, easy to construct, and cost-effective for tens of thousands of channels. We propose to cast a prototype "supertower" (4 towers) of a scintillating fiber calorimeter using lead alloy and scintillating fibers. Vertical casting of plastic fibers within a low-melting point eutectic alloy promises to minimize construction costs by eliminating the need for machining projective towers. The resulting towers will be monolithic, self-supporting, and modular.

In recent months, groups at Bicron and elsewhere have made great progress in developing intrinsically radiation-hard scintillators which are amenable to use in scintillating plastic fibers. Radiation damage to plastic scintillator is a complex physical and chemical phenomenon, as is "annealing" of this damage over time. Both effects are strong functions of fiber material properties, scintillator primary and secondary fluors, radiation dose rates and irradiation environments. Optimization for radiation hardness will be facilitated by specification of several of these variables in the context of a cast fiber calorimeter.

The radiation dose for an SSC calorimeter is most intense in the forward regions near the beampipe. For these regions, which form a small fraction of the total calorimeter volume, a liquid scintillator alternative to plastic scintillating fibers is appropriate. Liquid scintillator has the advantage that it can be circulated past the region of maximal radiation damage (near the electromagnetic shower maximum), or can be removed from the calorimeter and replaced at regular intervals. Light-piping can be accomplished as with scintillating fibers, by piping the liquid through smooth tubes with low refractic index. This method requires radiation hard liquids and especially radiation-hard materials to provide the tubing through which this liquid will flow.

Optical fiber bonding and interfacing to readout devices is extremely important for maintaining the uniformity and resolution of scintillating fiber calorimeters. At SSC energies, systematic errors from these effects will dominate over sampling fluctuations, giving rise to energy-independent limits to the energy resolution. It is thus essential that the fiber coupling and readout techniques be integrated into the overall calorimeter design. Simple and cost-effective manufacturing techniques will be vital for a system involving the readout of many millions of plastic scintillating fibers.

Scope:

* Develop new radiation-hard plastic and liquid scintillator systems suitable for use in cast fiber calorimeters.

* Construct and test several prototype projective towers of cast fiber calorimeters, designed for compatibility with the mechanical requirements of a full-scale SSC calorimeter.

* Design and implement efficient and cost-effective methods for coupling of plastic fibers to output fibers and readout devices.

* Develop manufacturing techniques for large-scale calorimeter module production, including automated assembly and quality control techniques.

Statement of work:

* Produce and test radiation-resistant materials for use in the TEXAS calorimeter.

    * Provide radiation-hard plastic fibers as appropriate for electromagnetic and hadronic calorimeter sections.

    * Provide radiation-hard liquid scintillators and low-index light pipes for use in forward EM and hadronic calorimeters.

* Develop production techniques for cast scintillating fiber calorimeter modules.

    * Design systems and construct prototype fixtures for automated cast fiber calorimeter assembly and quality control.

    * Construct and test prototype projective towers of cast fiber calorimeters, including provisions for device calibration, readout, and mechanical support.

    * Design and cost production facilities for construction of 40,000 cast fiber calorimeter projective towers.

* Develop simple and robust optical interfaces for fiber calorimeter components.

    * Design and construct prototypes of fiber mass-coupling splices.

    * Design and construct prototypes for fiber coupling to light mixers and photomultipliers.

    * Design and construct prototypes for optical coupling to liquid scintillator calorimeter modules.

Deliverable:

* The results of this work will be presented in summary report form. The report shall contain graphic, schematic, and written description of calorimeter materials and manufacturing designs, the basis of design decisions, an assessment of future radiation-hard materials developments which might affect the design, and recommendations for materials-related detector design issues.

* Samples of radiation-hard plastic fibers and other materials will be made available in sufficient quantity for comprehensive tests of their radiation damage susceptibility and other relevant properties.

* A full-scale prototype cast projective calorimeter supertower will be produced, and its performance evaluated in high-energy test beams by TEXAS collaborators.

* An engineering and production cost estimate for the module manufacture of the entire TEXAS calorimeter will be provided, broken down by each major material and labor component and with the basis for each cost estimate indicated.

The Charles Stark Draper Laboratory, Inc.
555 Technology Square, Cambridge, Massachusetts 02139 Telephone (617) 258-3846

TEXAS DETECTOR ENGINEERING DEVELOPMENT

To provide sufficient understanding of the issues involved in the mechanical/structural design of the TEXAS Detector at proposal submission and to assess its viability, a preliminary engineering development study is proposed. Four regions of the detector design would be explored. They include: 1. the structural support of the central tracker, 2. the construction and support of the scintillating calorimeter, 3. the construction and support of the muon tracker system and 4. the integration of all these systems. An assesment will be made of the engineering viability of the detector concept and a plan will be outlined for a following full scale development phase.

1. The central scintillating fiber tracker, would be studied primarily from the point of view of its support inside the calorimeter. The study would lead to a basic mounting and support design consistent with deflection and leadout requirements. A trade-off as to whether the tracker should be built as one unit for optimum alignment or separated at the center for simplicity of access will be performed. Several support system configurations will be evaluated. Some options to be included are: a cantilever support from the central plane of the detector, a cantilever support combined with simple supports at the ends, and suspending the tracker along its length from the inner ends of the calorimeter towers. Details of the interface between the structure and tracker would be finalized. Loads and deflection at the supporting structure would be investigated. Loads and deflections at the structure-tracker interface would also be determined.

2. The scintillating fiber calorimeter, would be studied broadly. A conceptual design would be developed which would maximize performance and optimize issues of assembly, installation, maintenance, cost and safety. Specific issues to be addressed would be: the locating of the scintillating fibers within the towers, the routing of fibers from the towers through the structure to collection points, the interfacing of the lead/bismuth alloy to the sheathing, the attachment of the towers to the support structure and the structural support system. Prime concerns will be structural integrity and the maintenance of the 1/2 cm translational and 2 degree angular stability requirements. Areas of higher technical risk would be identified early and pursued to their resolution. An assembly procedure, with tooling requirements defined, would be developed.

2. (Cont'd) The design of the supporting structure would also be investigated in detail. This study would include stress analysis and optimization for performance safety and cost. Suitable materials for the environment would be selected.

As part of this effort, in cooperation with the tower casting manufacturer, a method will be developed to fabricate the towers. Tooling will be designed to build at least one super tower.

3. The conceptual design of the central muon system (C tanks) and the muon end caps would be supported by extensive stress analysis. As with the calorimeter, problem areas would be isolated early to allow time for in-depth investigation. The design would take into consideration parameters such as materials, inner to outer wall supports, internal gas pressure, maintenance and electronics access. The internal module assemblies would be designed with decisions made on degree of modularity, number of modules and techniques for assembly of the modules between the inner and outer walls. Designs would also be developed for the muon system components such as trigger and tracker and their attachment. The problem of Xenon and CO_2 seals, supply and distribution to the muon system will be addressed.

4. The last area would be a comprehensive study of the complete system and how it can be most effectively integrated. This would include engineering development of the technique for separating and remating the calorimeter halves and the muon system including roller and winch requirements.

Specific issues important to the actual construction of the TEXAS detector would be studied and specifications finalized. The issue of where various components of the TEXAS detector and their support structures would be constructed will receive detailed attention. These issues include decisions on which assemblies or subassemblies would be built remotely and shipped to SSC, which would be built on-site above ground, which on site in the hall and which would be built in place.

Related to where equipment is built is the matter of facility requirements, and services available. Studies would lead to definition of hall size, hall access size (from the surface) and location, hall floor loading requirements, floor level specifications, and floor and wall anchor bolt pull-out requirements. Storage requirements for uninstalled equipment would also be determined.

Truck and rail services from the port of Galveston will be investigated. This study will yield maximum shipable length, width, height and weight parameters. Maximum crane loads would be indentified and service requirements such as electrical power and compressed air will be estimated.

An appropriate vendor list will be started for sources of supply for currently manufactured goods, items to be developed and services.

Estimates of total cost and the cost profile to complete the procurement, transportation, build, and installation of the mechanical assemblies of the TEXAS Detector will be provided. Flow charts will be drawn for the entire system to give managers tools to track schedules, budgets and critical paths of the entire project. The proposed study would last 12 months. The costs of the four studies plus program management are shown below.

TEXAS DETECTOR ENGINEERING DEVELOPMENT WORK BREAKDOWN STRUCTURE	
	COST
Central Tracker Support Configuration Tradeoffs Structural Analysis Interface/Mounting Definition	$130K
Scintillating Calorimeter Tower Design Studies Support Structure Design and Analysis Tooling Design	$425K
Muon Tracker System Gas Containment Tanks Design X-ray detector and Radiator Foam Module Design Xenon Gas distribution system design Design and Attachment of the Liquid Scintillator Tanks and Limited Streamer Tubes Structural Support Analysis	$375K
System Integration Subsystem Interface Control Build, Test, Transportation, Handling and Facility Requirements Definition System Cost and Assembly Schedule Definition	$190K
Program Management	$115K
Total	$1,235K

Contact: Francois Ayer (617) 258-3846

HAMAMATSU CORPORATION

CORPORATE OFFICES
360 FOOTHILL ROAD, BOX 6910, BRIDGEWATER, NEW JERSEY 08807-0910
TELEPHONE: 201/231-0960, FACSIMILE-G3 201/231-1539 TELEX 833-403

7 Whispering Way
Brookfield, CT 06804
May 24, 1990

Prof. David R. Winn
Dept. Physics
Fairfield University
N. Benson RD
Fairfield, CT 06430-7524

Dear Professor Winn:

Hamamatsu Photonics K. K. and Hamamatsu Corporation offer a strong commitment to collaborate with the TEXAS COLLABORATION. Hamamatsu will work toward development of both the "Fast High Pulse Linearity Photodetectors with Gain" and the "Multi-Pixel Photodetectors with Gain for Scintillating Fibers". Hamamatsu will proceed with developing these detectors at its own risk. We look forward to your further negotiation on these subjects.

Sincerely,
HAMAMATSU CORPORATION

Joseph G. Murray

Joseph G. Murray
Sales Engineer

:jgm

PRODUCTION FACILITY AND SHIPPING/RECEIVING DEPT. LOCATED AT:
420 SOUTH AVENUE, MIDDLESEX, NEW JERSEY 08846-0626
TELEPHONE: 201/469-6640, FACSIMILE-G3 201/526-8822

Western Office: 2444 Moorpark Avenue, Suite 312, San Jose, California 95128 U.S.A., Telephone: 408/292-8803
Chicago Office: 1410 Higgins Road, Suite 202, Park Ridge, Illinois 60068 U.S.A., Telephone: 312/825-6046
Asia: Hamamatsu Photonics, K.K. 1126 Ichino-cho, Hamamatsu City, Japan, Telephone. 0534/34-3311, Telex: 04225-185
Europe: Hamamatsu Photonics Europa GmbH, Postfach 1163, MuhlbachstraBe 20, D-8031 Seeleld 1, W. Germany, Telephone: 08152/7705-06, Telex: 527 731
Affiliate: B.H.K., Inc., Monrovia, California

Engineering Development of Fast High Pulse Linearity Photodetectors with Gain

Scintillator Calorimetry at the SSC may require of order 100k-250k ~5 cm diameter bi-alkali photomultiplier-equivalent channels. The demands on these detectors are extreme. These detectors must be linear from ~50-100 MeV equivalent minimum ionizing deposition to ~5-10 TeV deposition, or five decades, with sufficient gain-bandwidth to operate at the 60 MHz beam crossing frequency. Because of the very large number involved, a low unit cost is essential. For some applications radiation hardness at the 10 MRad level may be essential. Stability is also important.

We therefore solicit brief letters indicating a strong Corporate Interest in being further considered for a contract for the following Statement of Work, starting at or near Dec, 1990, and thereby being a member of the TEXAS SSC team.

Statement of Work

(1) "Best Effort" development contract of at least one deliverable prototype high pulse linearity fast low cost photoelectron amplifier with the following target characteristics:

- gain of at least 1,000
- risetime at most 2 ns
- photocathode diameter at least 4 cm
- cathode sensitivity: above 5% Q.E. between 400-600 nm
- rep rate independent gain ±1%, 1,000 p.e. impulses up to at least 10 MHz
- impulse linearity ±1% from 50 p.e. to at least 1,000,000 p.e.
- gain stability ±1% over 1 hour (24 hour warm-up, V±50 ppm power supply)
- Rad hard at 1 MRad

The technology development must keep (2) below as a target cost of less than $150 each in 50k quantity.

Phase I would take one year from award of contract. We expect a cost equivalent to at minimum 2 engineering man-years and at maximum 5 engineering man-years, over 1 year. In the USA, these figures might range from ~$300k - $1,000,000. A report accompanying the prototype work should estimate the success of the technology in meeting the above goals, and propose Phase IIR&D iterations to achieve them if unsuccessful

(2) "Best Effort" Manufacturing Engineering Design Cost Study Contract leading to an Estimated Quote, with at most 15% errors, for the above prototype(s) with the following characteristics:

- Cost in 50k lots of $150 each (or less)
- 50K deliverable in 2 years from order
- 150K deliverable in 3 years from order

The Phase I deliverable Report supporting and detailing a Best Effort Estimated Quote will also include information detailing the estimates of the manpower, resource and time-scales (EDIA/WBS) needed to generate a firm Quote during Phase II.

Phase II, negotiated after the approval of the TEXAS detector, would result in a Quote good for 6 months.

We are impressed by the attention of industry to this problem. We welcome your collaboration as part of our broad industrial team. We are available for Confidential discussions of technology.

Engineering Development of Multi-Pixel Photodetectors with Gain for Scintillating Fibers

SciFi tracking and Pre-radiator detectors at the SSC may require of order 2 million channels of photodetector with sufficient gain to detect signals from 1 mm thick scintillating fibers. We also would like to have a cost below $3 per channel.

We therefore solicit brief Letters indicating a strong Corporate Interest in being further considered for a contract for the following Statement of Work, starting at or near Dec, 1990, and thereby being a member of the TEXAS SSC team.

Statement of Work

(1) "Best Effort" development contract of at least one deliverable pixel detector prototype with the following target characteristics:

- sufficient sensitivity/GainBW to have a S/N level of 10/1 for 5 incident photons on 1 pixel (or pixel cluster) per fiber, crossing a voltage threshold on 50 Ohms of 20 mV (after amplification), or for 2,000 electrons of signal.
- readout time per pixel channel struck of 50 ns, or parallel readout
- cost per channel in mega channel quantity of less than $3.
- rad hard at 1 MRad
- minimum of 1K channels per device for 1 mm diameter fibers

Phase I would take one year from award of contract. We expect a cost equivalent to at minimum 2 engineering man-years and at maximum 5 engineering man-years, over 1 year. In the USA, these figures might range from ~$300k - $1,000,000. A report accompanying the prototype work should estimate the success of the technology in meeting the above goals, and propose Phase.IIR&D iterations to achieve them if unsuccessful

Phase II prototype iteration would be negotiated following approval of an SSC proposal.

(2) "Best Effort" Manufacturing Engineering Design Cost Study Contract leading to an Estimated Quote, with at most 15% errors, for the above prototype(s) with the following characteristics:

- 10K channels deliverable in 2 years from order
- 2 Mega channels deliverable in 3 years from order

The Phase I deliverable Report supporting and detailing a Best Effort Estimated Quote will also include information detailing the estimates of the manpower, resource and time-scales (EDIA/WBS) needed to generate a firm Quote during Phase II.

Phase II, negotiated after the approval of the TEXAS detector, would result in a Quote good for 6 months.

We are impressed by the attention of industry to this problem. We welcome your collaboration as part of our broad industrial team. We are available for Confidential discussions of technology.

The TEXAS SSC Collaboration

May 24, 1990

Background:

This statement of work defines an effort to develop the necessary electronics for a photomultiplier and proportional tube readout system at the SSC as proposed by the TEXAS collaboration. The specification of requirements for this integrated system are derived from the needs of scintillating calorimetry and a muon transition radiation detector spectrometer. A vigorous electronics effort will pays dividends by providing a stable, low power, reliable, and cost effective system. In addition it provides a basis for cost comparison of alternative calorimetry and muon systems. This statement addresses the needs of the first two years of a development program. A careful costing of the actual detector is dependent upon the results of this work. Establishing the technical and financial feasibility to an 80% confidence level is the major goal of the first year's effort.

Scope:

* Estimate and plan for complete electronic systems development, including work breakdown structure, scheduling, manpower and resource allocation, and costing.

* Detailed assessment of the needs of individual detector elements, including electronic performance, system integration, and cost analysis.

* Preliminary design efforts to ascertain optimal electronics techniques for each detector element including the trigger apparatus. This would include simulated designs and prototype circuits to demonstrate feasibility.

Statement of Work:

* A complete analysis of the development project for the data acquisition electronics must be done in order to ascertain the cost, manpower, and scheduling for several years of development. This is also necessary to anticipate large scale manufacturing and assembly of the detector.

* A data acquisition system for a set of 50,000 photomultiplier tubes with 8 bits of resolution and approximately 10^6 dynamic range must be defined. The feasibility of such a system must be carefully studied

LeCROY CORPORATION
700 CHESTNUT RIDGE ROAD
CHESTNUT RIDGE, NY 10977-6499, USA
TELEPHONE: (914) 425-2000

TWX: 710-577-2832
CABLE: LERESCO
FAX: (914) 425-8967

using extensive simulation techniques and prototype circuits.

* A data acquisition system for 250,000 channels of transition radiation detector must be conceived and modelled. This detector is required to provide timing as well as amplitude information. Extensive simulation and circuit prototyping must be done to ensure its utility for the TEXAS detector.

* For the central tracker a system must be created to provide timing information only. The choice of straw tubes or scintillating fibers will be influenced by the necessary electronics. It is thus essential to investigate the electronics options at an early stage. This will be done by the end of the first year so as to finalize the central detector design.

* A triggering system must be conceived which will reject the necessary 10^7 events per second. This key element in the detector must be extensively modelled to characterize its function.

* Develop a preliminary design of a high voltage supply system with integrated calibration and control for photomultiplier tubes. A similar but distinct effort for proportional wire tubes will parallel that for PMTs.

Deliverable:

* The results of this work will be presented in summary report form at the end of the first year of work. The report shall contain graphic, schematic, and textual descriptions of electronics systems designs, the basis of design decisions, and recommendations of electronics related detector design issues. It shall also point the way for the second year's effort. These results are necessary to achieve an 80% confidence in the technical and financial assessment at the time of proposal submission in the fall of 1991. A similar report will be presented at the end of the second year of work which will further specify a development schedule through the manufacturing phase of the various systems.

* Prototype circuits necessary to verify the feasibility in all areas will be specified by the end of the first year, and these shall be designed and produced in the second year.

contact: John Hofteizer, LeCroy Corp.

	1991			1992		
Detector Element	Task	Manpower	Capital	Task	Manpower	Capital
1. System Integration	• Development Plan • Manage/Liason	1		• Plan • Manage/Liason	1	

2. PMT Data Acquisition	• Evaluate Alternatives
	  • ADC Dynamic Range
	  • Non-linear ADC
	• Define Concept
		1	50K	• Finalize ADC Strategy
				• First Prototype ICs
				• Initial ADC Design
					2	75K

3. Muon Chambers	• Concept
	  • 4-Bit ADC
	  • 100 ns Drift
	• Evaluate Alternatives
		1	50K	• Design Prototype System	2	75K

4. HV for PMT & Wires	• System Definition
	  • Generation
	  • Power Distribution
	  • Monitor & Control
	  • ASICs, pcb
	• Modeling & Simulation
		1	50K	• Prototype HV Circuitry
				• Design ASICs
				• Design Control & Monitor
					2	75K

5. Trigger	• Define Concept • Model & Simulate	1	50K	• Demonstrate Feasibility • Initiate Design	2	75K
6. Central Tracker	• Explore Scintillating Fiber Option • Explore Straw Tube Option • Define Concepts • Define ASICs	1	50K	• Finalize Design • Continue ASIC Design • Prototype	2	75K
Budget ($M)						
Manpower	.750 (6 people at .125)			1.430 (11 people at .130)		
Capital Equipment	.250			.350		
Overhead (facility, NRE, technician, support, travel, etc.) 30%	.225			.429		
TOTAL	1.225			2.059		

LeCroy

Innovators in Instrumentation

MECHANICAL DESIGN OF A SCINTILLATING FIBER TRACKER FOR THE TEXAS EXPRESSION OF INTEREST

Background

This statement of work defines an engineering effort to design and evaluate a structural base for the TEXAS Central Tracking System. The engineering effort will be based on the use of conventional technologies which can be implemented cost effectively. A conservative concept based on carbon composite cylinders will be used as the starting point for the structural design.

Carbon composite structures are widely used for lightweight, yet rigid assemblies such as that required for the Scintillating Fiber Tracker. High radiation tolerance, low nuclear interaction mass and excellent stability also point to the use of this material. High quality composite cylinders are available from several domestic vendors using proven winding and lay-up techniques.

Our work within the tracking subsystem collaboration will be coordinated with Northeastern University (A. Grimes).

Scope

Provide a detailed conceptual design for a Scintillating Fiber Tracking Chamber structural assembly.

Statement of Work

1. Develop a conceptual design for a Scintillating Fiber Tracking Chamber support structure;

2. Provide supporting structural analysis for the support structure;

3. Evaluate the use of alternative structural materials, and propose test models for future design, construction, and testing.

This work will be coordinated with an electrical engineer and simulation expert to ensure overall system compatibility and performance requirements.

Budget

The total budget required is listed below:

	FY91
Mechanical Engineer and a Designer	$310K
Electrical Engineer and Simulation Expert	225K
TOTAL ORNL BUDGET	$535K

The work will be administered at ORNL through the Oak Ridge Detector Center.

Terry W. Stapleton /TAG
Head Engineer

Tony Gabriel
Director, Oak Ridge Detector Center

Dr. Reucroft
Northeastern University
High Energy Physics
BOSTON. MASS. 02115

23rd May 1990

Dear Dr. Reucroft,

We have learned from Componix Corp. Mr. Jaquet that you are still very interested by the kind of ribbon samples we have tried to realise for your department in collaboration with Mr. Dave Kaplan last year.

We here at Optectron are more and more involved with scintillating fibers and we believe that the quality of our fibers has definitely improved since the last samples were sent.

We do realise however that your problem is difficult and certain improvements are necessary.

In the Annex to this letter you will find the principal points of research already under study or foreseen by Optectron in the scope of scintillating fibers and which could be useful in your application.

I sincerely hope to renew the relationship and contact between your laboratories and Optectron by the intermediary of Mr. Jaquet and very probably in a short time by OPTECTRON INCORPORATED in the U.S.

Yours sincerely,

Bernard Chiron
President

Adresse Postale
Z.A. COURTABŒUF
BP 535
Avenue du Québec
F - 91946 LES ULIS

OPTECTRON, Société Anonyme au Capital de 2.292.250 Frs
RCS Corbeil-Essonnes B 329 846 828 - SIRET 329 846 828 00013 - Code APE 3404
Z.A. COURTABŒUF - Bâtiment B1 - Avenue de la Baltique - VILLEBON-SUR-YVETTE
Téléphone : (1) 69.28.15.20 - Télex : OPTEC 603635 F - Fax : (1) 69.28.67.40

OPTECTRON
91946 Les Ulis
France

SUBJECT: TOPICS OF RESEARCH ON SCINTILLATING FIBERS FOR THE TRACKER AND THE CALORIMETER OF THE FUTURE S.S.C.

As one of the largest manufacturers of scintillating fibers, Optectron has been involved in the major projects of calorimetry and tracking such as UA2, DELPHI-SAT, NA38, CLEO II and in experiments at Brookhaven National Laboratory and Berkeley.

****

The characteristics of the scintillating fibers which are required in order to be used in the tracker and in the calorimeter of the future S.S.C can be obtained; nevertheless, it would be necessary to carry out studies in order to improve some of the actual characteristics and to optimize the manufacturing process.

We propose the following research program:

- study of a new process for manufacturing the modules of scintillating fibers which will be used in the tracker and in the calorimeter. The aim is to be able to manufacture modules having identical characteristics and to reduce the manufacturing cost.

- improvement of the scintillating fibers behaviour under very high radiation by using, for example, a 3HF dopant and another dye.

- improvement of the coupling between the scintillating fibers and the avalanche photodiode (APD) by using an interface with fluorescent fibers. The goal is to obtain an optical wavelength at the output of the fluorescent fibers which would be close to the wavelength corresponding to the maximum of efficiency of the APD.

- development of new tooling equipments used during the drawing phase of the manufacturing process of the fiber; these new equipments would permit to control very precisely the diameter of the fibers in order to obtain a standard deviation of +/- 4%.

- study of a new process for the metalization of the fibers to avoid the cross-talk between fibers.
  A method using a thin layer of aluminium is possible; another method using a carbon loaded black paint could be developed. An investigation is necessary to decide which one will give the best results.

budgetary cost of this complete program: $300,000.

QUANTUM
RESEARCH SERVICES, INC.

Use of Inverse Monte Carlo in Detector Design Optimization

Quantum Research Services proposes to investigate the use of the powerful Inverse Monte Carlo (IMC) method for detector design optimization studies in support of the TEXAS proposal. The IMC method was developed in 1981 by one of the Quantum investigators; it grew out of the realization that the standard Monte Carlo problem (of estimating a definite integral by a suitable summation) becomes an inverse problem (of the form of a Fredholm integral equation of the first kind) if one or more parameters within the integrand of the definite integral are unknown and if the integral values are known or can be specified. Using a single simulation that carries the unknown parameters in the Monte Carlo scores, the inverse problem can be converted into a simpler form that can be solved for the desired set of parameters by standard procedures, such as matrix inversion or least squares. Design and optimization problems can often be posed in the Fredholm form and can thus be solved by IMC, which has been successfully applied to remote sensing, design of photon beam modifiers, single photon emission computed tomography , and X-ray fluorescence analysis.

In a physical sense, IMC estimates the response of the process being simulated (e.g., detector response) for an arbitrary weighting of the design parameters (e.g., size and composition); the design problem then reduces to finding the parameter weighting that best matches the known, desired, or optimum system response. The desirable features of IMC include: the simulation is noniterative, thus saving immense simulation time; and the method applies, in principle, regardless of the dimensionality or complexity of the problem, in the same sense that direct Monte Carlo applies to multidimensional, energy- and time-dependent transport, etc. On the other hand, IMC requires that the Monte Carlo summation operator decompose into a manageable form for numerical inversion, which is not always guaranteed.

As part of the TEXAS collaboration, Quantum will investigate the application of IMC to the design of the detector, first to determine which design variables are amenable to solution by IMC and then to demonstrate its application to design optimization for those variables. Candidate variables will include the number of layers in the tracker, calorimeter material composition (e.g., the optimum fractions of fiber and lead, or lead eutectic), hermeticity (i.e., locations of support structures to minimize information loss), and subsystem dimensions. Since simulation studies for detectors are very computation intensive, use of the IMC approach – which allows study over ranges of design variables in a single (i.e., noniterative) simulation procedure – could dramatically improve overall design efforts. IMC may also allow an efficient means to test novel design concepts.

Quantum's first-year budget for this study is $120,000, which will include direct labor for Drs. William L. Dunn and A.M. Yacout, fringe and indirect expenses, travel, and other direct expenses.

Beta Building, Suite 340
2222 E. Chapel Hill-Nelson Hwy.
Durham, NC 27713-2208

PO Box 52391
Durham, NC 27717-2391
919-544-4952

AVALANCHE PHOTODIODE DEVELOPMENTS FOR SSC TRACKING DETECTORS

General Electric Canada Inc., Electro Optics Operations
Vaudreuil, Quebec, Canada

PROGRAM OF RESEARCH FOR PHASE II

BACKGROUND

While the suitability of avalanche photodiodes (APD's) as the detector of choice for use with scintillating fibers for an SSC tracking detector still has to be confirmed, GE is confident that such confirmation will be forthcoming during the present feasibility program (Phase I). However, the best (most cost effective) way of using them in this role is still not clear. The object of Phase I is to show that an array of APD's used in the Geiger mode, with periodic and parallel resets, will prove to be an inexpensive and satisfactory approach. A second objective is to determine the radiation sensitivity of an APD used in a photon counting mode.

The main advantage of the Geiger mode is that it eliminates the need for any amplifiers, since the magnitude of the Geiger discharge pulse is more than adequate to directly drive all subsequent signal processing electronics. Other advantages are potentially high (> 50%) single photon detection efficiencies, the need for only moderate (~ ±2°C?) temperature regulation, and high detector-to-detector detection efficiency uniformity.

The main disadvantage of this approach is that detectors operating in the Geiger mode emit light. Thus monolithic arrays of Geiger mode APD's are not practical unless the arrays can be designed with adequate light absorbing regions between the individual elements. While it is too early to rule out the feasibility of this approach, it is probably better to assume for now that the array will consist of individual chips which are carefully optically isolated from one another. Another disadvantage is that each *"fired"* channel will remain *"dead"* until the next reset, likely to be in the 100-200 ns range. However, since it is understood that the expected fiber utilization rate is at most about 10^6/s, the miss rate due to dead time will be a maximum of 10-20%.

If the Geiger mode of operation proves to be unsatisfactory, because of unavoidable crosstalk or for other reasons, a fall-back position is an array of APD's operating in the normal mode, in conjunction with an array of low-noise preamplifiers. The problem with this approach is the cost of the preamplifiers. While suitable low-noise preamps (Equivalent Noise Charge (ENC) of 100-200 electrons rms) having adequately fast time constants (a few ns) have been fabricated in this laboratory, they

are hybrid amplifiers with a GaAs FET as an input stage. It is difficult to see how these could be manufactured at an affordable price for this project. Monolithic InGaAs preamp arrays are a possibility, but these have not yet, to the author's knowledge, been demonstrated. The inexpensive monolithic preamp arrays developed for use with straw tubes (ENC ~ 1000 electrons) are too noisy for use with APD's for photon counting in the normal mode.

PHASE II PROGRAM OUTLINE

The work to be carried out during the next phase of this program will depend on the results obtained during Phase I, but is likely to contain at least some or all of the following tasks:

1. Design and fabricate a linear array of APD's with properties optimized for this application (element size and spacing TBD; number of elements: 32 or TBD) with light barriers between the elements. Evaluate for crosstalk as a monolithic array, photon detection efficiency, element-to-element uniformity, yield, etc. If acceptable, use as an array. If not, cut into individual elements.

2. Develop an inexpensive packaging technique for a linear array of, for example, 32 monolithic or separate detectors and associated electronics. (Center-to-center spacing likely to be about 1-2 mm.) Investigate also inexpensive approaches to making fiber-to-detector couplers.

3. Characterize this array for photon detection efficiency, crosstalk, uniformity, temperature coefficient, etc. With fiber array attached, characterize for MIP detection efficiency as a function of fiber length. Note: This last task could be done by, or in cooperation with, Northeastern University.

4. Consider the feasibility and desirability of a design in which the Geiger discharge is used to directly drive a low-threshold laser so that the module output would be an optical, rather than an electrical pulse. Such an approach appears possible (anticipated optical gain of greater than 10^7) and could be desirable, due to the compactness of fiber cables, if the signal processing electronics is very distant from the detector arrays. An array of low-threshold lasers could be purchased externally or fabricated in-house by GE using a recently-installed AlGaAs/GaAs MOCVD system.

5. Prepare a summary report, indicating remaining problems to be solved, recommended form of the final package, possible further cost reductions, achievable through integration of the remaining circuit elements, etc.

Probable Phase II cost (not including Task 4): about U.S. $300,000.

EXPRESSION OF INTEREST

TEXAS DETECTOR for the

SUPERCONDUCTING SUPERCOLLIDER

TELEDYNE BROWN ENGINEERING
Cummings Research Park
P.O. Box 070007
Huntsville, AL 35807-7007

Teledyne Brown Engineering (TBE) is pleased to submit this expression of interest in the TEXAS Detector Collaboration for the Superconducting Supercollider.

1. Statement of Work

TBE proposes to use its expertise in the following areas for the development of integrated solutions to the design of the scintillating fibre tracking subsystem, the scintillating fibre calorimetry readout system, and the trigger processor for the TEXAS detector:

Optoelectronic readouts. TBE will use its experience in developing fibre-optic data communications networks to develop an optical reader and fibre-optic connection for direct optical readout of the scintillating fibres in the tracking and calorimetry subsystems. The use of optoelectroic connections instead of traditional electronics in these subsystems is expected to significantly enhance radiation hardness and signal processing times. As part of this process, TBE will evaluate the use of this optical repeater for signal preprocessing and timing. Evaluation of a variety of candidate solutions is contemplated.

Optical processors and neural networks. TBE will evaluate the use of the optical readout directly as input to an optical processor, one which uses a neural network algorithm as a high-speed pretrigger. The use of optical computing techniques and neural network algorithms will enhance signal processing times, enabling the TEXAS detector to operate at higher luminosities.

Lasing detection media. TBE will perform further analytic and experimental validation of the use of semiconductor diode, crystalline, and gaseous laser media as primary laser detectors. TBE will determine primary signal strength vs. detector characteristics (bias current, thickness, operational wavelength) and identify signal processing techniques to extract the maximum possible position and particle energy information from the radiation pulse from the ionizing particle interation. Sensitivity studies for both stimulated emission and stimulated absorption detection concepts will be performed.

Detector Design and Development. TBE will perform: design and demonstration of an optical readout system for scintillating fibres; design of single-event threshold optical trigger; design of coincident threshold optical trigger; laboratory-scale demonstration of the candidate trigger systems; and, laboratory scale demonstration of the laser detection media tracking concepts.

2. Facilities and Personnel

Teledyne Brown Engineering, a division of Teledyne, Inc., is an integration and aerospace services company located in Cummings Research Park, in Huntsville, AL. Our 3,000 employees provide a wide variety of services for the Marshall Space Flight Center, U. S. Army Missile Command, and U. S. Army Strategic Defense Command, as well as a variety of other customers. Among our current contracts are:

Payload Missions Integration Contract (PMIC). Responsibility for the

integration of Spacelab missions for the Space Transportation System; the most recent Spacelab mission supported is the ASTRO I high-energy astronomy observatory mission.

Space Station FREEDOM. TBE is responsible for integration and communications of the Crew Module.

Systems Engineering and Technical Assistance (SETAC). As SETAC to Army Strategic Defense Command in Huntsvillle since 1972, TBE has performed work in virtually every area of defense-related technology. Of particular interest are activities related to the radiation hardness of optoelectronics and electronic systems; optical and infrared detection; communications systems; and, large software systems.

TBE possesses an extensive, modern optics laboratory, [illegible] collaborating on optical computer development with the University of Alabama in Huntsville. TBE also has extensive effort devoted the use of neural network algorithms to problems of pattern recognition, classification and target resolution in a high-signal environment. TBE plans to augment this optics facility with a radiation source storage and test facility to support SSC-related activities.

TBE proposes to devote the following personnell to the TEXAS Detector System development effort (resumes/vitas provided on request):

C. E. Kaylor, Ph.D. Program Manager.

J. K. Woosley, Ph.D. Technical manager; event physics, event characteristics, detector and trigger requirements, radiation detection and hardness, signal analysis.

TBD. Deputy Technical Manager; optical system design and test.

A. J. Fennelly, Ph.D. Radiation detection and hardness; signal analysis.

M. B. Johnson. Radiation-hard optical data systems and readouts.

TBD. Optical communications design, test and operation.

TBD. Optical Computers; neural networks.

TBD. Laser systems.

3. Costs

TBE proposes the following cost schedule for supporting research, design, and development on the TEXAS Detector in Fiscal Year 1991.

Government funding. TBE requests funding from the government at the level $600,000 during FY91. This funding estimate should be regarded as preliminary; a detailed cost will be provided on request. This funding will be distributed as follows (all values include overhead, G&A, etc.):

Engineering Labor	
13,000 hours	$520,000
Administrative Labor	
2,000 hours	40,000
Materials	15,000
Travel	25,000

Internal funding. TBE will devote $100,000 of internal capital expenditure and equiptment resources to the upgrade of its optical laboratory for performance of radiation testing, and will devote an additional $50,000 of internal funding to labor.. Expenditure of some of these funds is contingent on receipt of funding above. Ongoing efforts in neural network and optical computing technology will contribute approximately $300,000 (FY90/91) to the technology base in these areas through indirect support of the TEXAS effort.

Thinking Machines Corporation

May 23, 1990

Professor Lawrence R. Sulak
Chairman, Physics Department
Boston University
Boston, MA 02215

Dear Larry:

We have followed with great interest your proposal of using massive parallelism as an integral component of the computational effort required by the TEXAS detector.

We at Thinking Machines Corporation are firmly convinced that massive parallel computations are viable for a large range of applications in experimental particle physics, from the simulation of detector performance to, potentially, the reconstruction and analysis of events. The possibility of using a Connection Machine system in situ for the on line analysis of events after the first levels of triggering may also be envisaged.

As you know, we are providing technical support to several projects in advanced computation at Boston University, including parallel algorithms for the SSC. We will be very pleased to assist you and your group in the application of massively parallel computation to your proposed detector design within the framework of the excellent relationship we have developed with your University.

We wish you the best success for your proposal.

Sincerely,

John Mucci
Vice President

245 FIRST STREET
CAMBRIDGE, MA 02142-1214
TELEPHONE: (617) 876-1111
FAX: 617-876-1823

LINDE
UNION CARBIDE INDUSTRIAL GASES

Union Carbide Industrial Gases Inc.
Linde Division
Post Office Box 44
Tonawanda, N. Y. 14151-0044
Telex 754632

Gas Supply and Recirculation System for the Texas Detector at the SSC
Engineering Design Proposal
May 21, 1990
Prepared by Union Carbide Industrial Gases Inc.

1. Introduction

This document defines the work required to develop a definitive design and cost estimate for the Texas Detector (TD) gas supply and recirculation system. The TD uses a xenon-hydrocarbon gas mixture inside the detector tubes, and a carbon dioxide gas stream as a buffer gas surrounding the tubes. The buffer gas is used to shield the xenon from air contamination during normal operation. Also, the buffer gas is used during initial startup and for long-term shutdown to purge air contaminants from the system and to flush the xenon gas mixture into surface storage facilities. A carbon dioxide buffer gas has been selected because it can be separated relatively easily from the xenon gas mixture. The gas supply and recirculation system consists of storage, supply, recirculation, and purification subsystems for the xenon-hydrocarbon mixture and for the carbon dioxide buffer gas.

2. System Description

A conceptual flow diagram for the gas supply and recirculation system is shown in Figure 1. The overall system consists of separate recirculation loops for the xenon gas mixture and for the carbon dioxide buffer gas. Makeup gas for each loop is provided from on-site high-pressure tube trailers. Both gas streams pass through particulate filters, pressure control equipment, and temperature control equipment prior to being fed to the distribution manifolds. The specifications for the TD feed streams are as follows:

TD Feed Specifications

Xenon Gas Mixture	
Input pressure	3 to 7 millibar
Maximum Flow Rate	75,000 l/hr
Composition	
Xenon	~90 mole %
Hydrocarbon	~10 mole %
Stabilizer	Trace
Oxygen	<100 ppm
Carbon Dioxide	<1000 ppm
Water	<1000 ppm
Temperature Control	±2°F

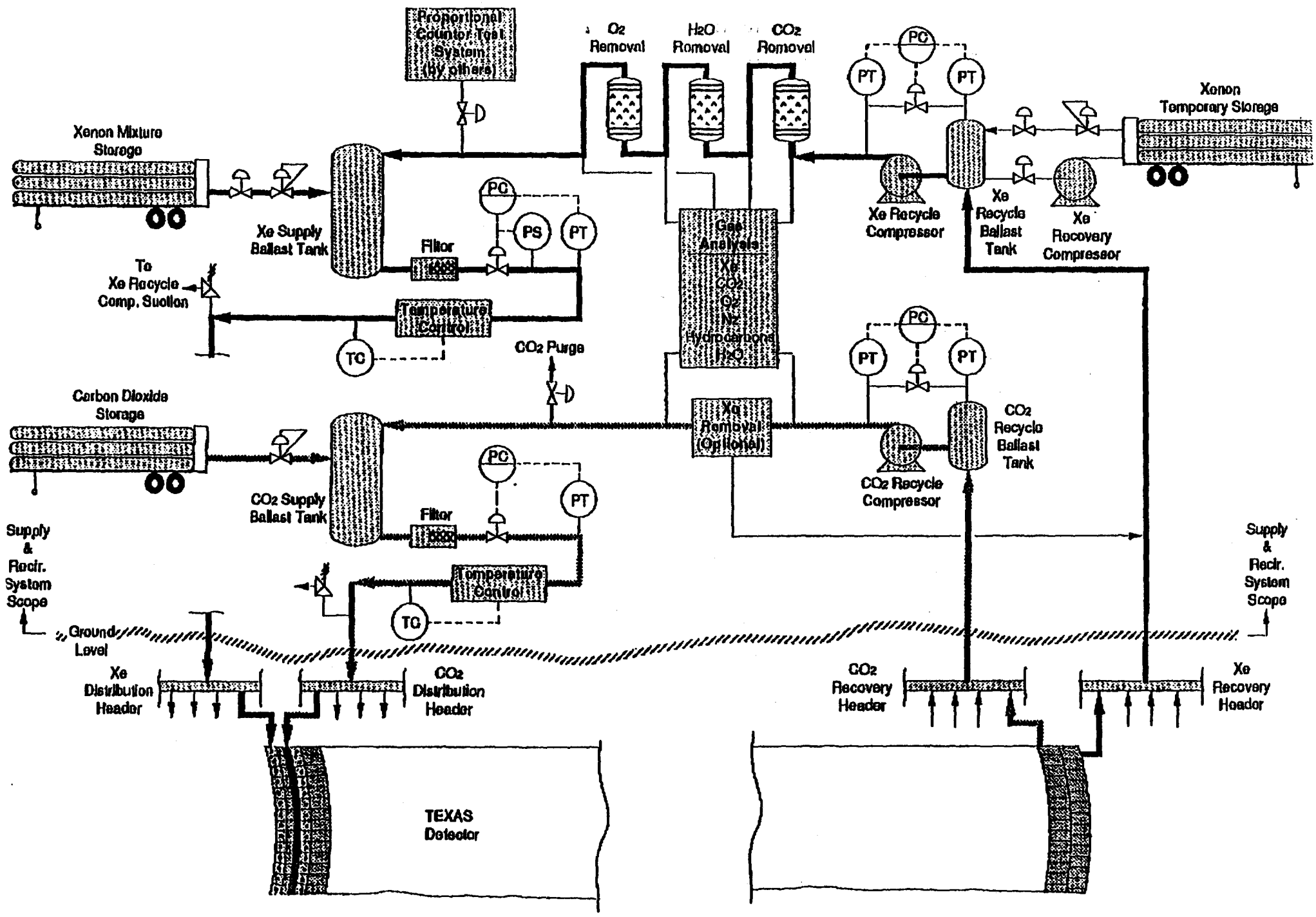

Figure 1 Xenon Supply and Recirculation System Conceptual Flow Diagram

Carbon Dioxide Buffer Gas	
Input Pressure	3 to 7 millibar
Maximum Flow Rate	7,500 l/hr
Purity Requirements	
Water	<1000 ppm
Oxygen	<100 ppm
Temperature Control	±2°F

The carbon dioxide and xenon recovery headers are operated under a slight vacuum (-100 millibar). Gas from each header is compressed prior to being recycled back to the supply systems. Xenon recovery may be provided downstream of the carbon dioxide compressor for xenon that has permeated into the buffer gas. A small CO_2 vent located downstream of xenon recovery is used to limit the buildup of impurities in the buffer gas.

The compressed xenon mixture passes through various stages of purification for removal of CO_2, H_2O, and O_2. These purification stages will likely consist of caustic scrubbing (CO_2 removal), physical adsorption (H_2O removal), and chemical adsorption (O_2 removal). A small proportional-counter test system located downstream of the purification stages is used to test the quality of the recycled gas. A gas analysis system is provided to monitor impurity levels at various points in the process.

A small high-pressure compression system is provided for recovery of xenon prior to shutdown and maintenance of the TD. This is accomplished by flushing the system with CO_2 and collecting the xenon–CO_2 mixture in high-pressure tube trailers for subsequent purification..

3. Scope of Work

The TD gas supply and recirculation system includes the aboveground supply, recirculation, and purification equipment and controls as shown in Figure 1·. The boundary limit for this system is the entrance to and exit from the distribution and recovery manifolds, respectively. This document defines the work required to develop a process and system design in sufficient detail to develop a definitive cost estimate (±10%) for the gas supply and recirculation system. This design effort will not include generation of detailed equipment and construction specifications, construction drawings, or operating procedures.

4. Statement of Work

All activities necessary to provide the scope of work are identified on the Work Breakdown Structure (WBS) presented in Figure 2. This effort will focus on optimizing purification system components while minimizing xenon losses. Specialty components that could have a major impact on cost and operability will be defined as part of this effort.

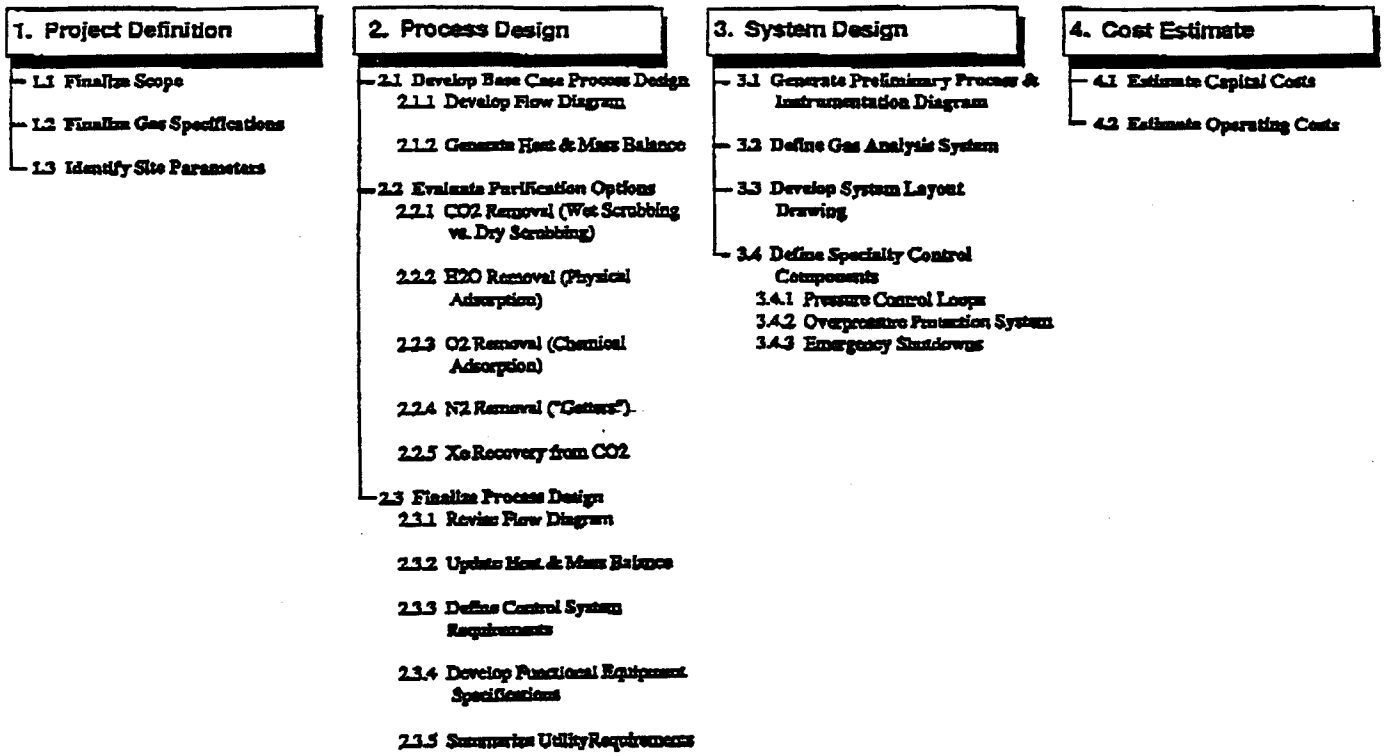

Figure 2: TD Gas Supply & Recirculation System — Work Breakdown Structure

5. Deliverables

The results of this work will be presented in a design report that includes the following:

- Process flow diagram
- Process description
- Heat and mass balance
- Process and instrumentation diagram
- Layout diagram
- Cost estimate

6. Cost

The total cost to complete the scope of work is as follows:

Engineering (140 man days)	75,000
Technical Support (50 man days)	20,000
Travel	10,000
Computer Support	6,000
Subtotal	$111,000
General and Administration (25%)	27,750
Total	$138,750

Union Carbide Contact

Sharon L. Saupp
Union Carbide Industrial Gases Inc.
Linde Division
P.O. Box 6744
200 Cottontail Lane
Somerset, NJ 08875
Phone: 201-271-2613

EOI 11

Expression Of Interest
Answers to Questions from the Program Advisory Committee

A CALORIMETER-BASED HIGH-RATE DETECTOR FOR THE SSC

S. Dye, G. Jones, C. Oh, S. Klein, J.P. Miller, D. Perlman,
M.A. Rahman, B.L. Roberts, J. Stone, L. Sulak**, and W. Worstell†
Boston University

C. Lane
Drexel University

D. Winn
Fairfield University

J. Hofteizer*
LeCroy Research Corp.

G. Alverson, W. Faissler, M. Glaubman, A. Grimes, I. Leedom†,
J. Moromisato, E. Pothier, S. Reucroft**, E. Saletan and E. von Goeler
Northeastern University

W.L. Dunn, F. O'Foghludha, S.K. Myers, J.D. Simpkins, and A.M. Yacout
Quantum Research

T. Kamon and R. Webb**
Texas A&M University

Industrial Affiliates

Bicron
C. Hurlbut*

The Charles Stark Draper Laboratory
F. Ayer*, C. Elder, D. Sullivan, and E. Womble

Hamamatsu Corp.
J. Murray*

Oak Ridge National Laboratory Detector Center
J.W. Stapleton*

Optectron
P. Jacquet*

RCA/General Electric
H. Dautat and R.J. McIntyre*

Teledyne Brown Engineering
J.K. Woosley*

Thinking Machines Corp.
G. Bhanot, J. Mucci, D. Orr and J. Reardon*

Union Carbide Industrial Gases Inc.
S. L. Saupp* and T. Schulte

and SSC Laboratory Participants

M. Hecht and T. Thurston

The TEXAS Collaboration
(Totally hermetic EXperiment At the Supercollider)

July 12, 1990

* Contact person ** Co-spokesman † SSC Fellow

Table of Contents

Preface

An Update on the TEXAS Detector Concept

- Central Tracker/Preradiator Triggering
- e/h Separation
- Calorimeter Triggering
- Radiation Tolerance of Scintillator
- Energy Resolution
- Muon TRD Details
- TEXAS Trigger Details

Answers to the Generic Written Questions

- G1: Higgs Searches in Four Mass Regions
- G2: Quark Compositeness and E_T Measurements
- G3: Top Quark Searches
- G4: Missing E_T Searches
- G5: Detector Staging
- G6: Funds Requested for Systems Integration
- G7: Collaboration Responsibilities

Answers to Questions Specific to TEXAS

- T1: Capabilities at 10^{34} luminosity
- T2: Fiber Calorimetry Performance at High Luminosity
- T3: Current Detector Simulation Program
- T4: $H \rightarrow \gamma\gamma$: Vertex sensitivity, energy calibration etc.
- T5: Quark-Jet Tagging
- T6: High-Mass Higgs and TRD Muon Resolution
- T7: Hermeticity versus Muon Resolution
- T8: Pattern Recognition of the Central Tracker

Answers to the Verbal Questions of TEXAS Subpanel Members

- V1: Is the TEXAS Cost Estimate Realistic?
- V2: Who would Manage TEXAS Construction?
- V3: Why not use an Iron Toroid instead of the Muon TRD?

Appendices

- A: Project Management for TEXAS ... A Draper Lab Report
- B: Critique of Fiber Calorimeter Cost Estimate of SSCL Note # 728 ... Draper Lab Memo EEC-90-693
- C: Cost of MACRO Prototype Muon TRD Spectrometer
- D: TEXAS Calorimeter Tower Assembly Cost Estimate ... Bicron Corp.
- E: Cost Estimate Risk Analysis for Calorimeter Electronics ... LeCroy Research Systems
- F: Intent to Jointly Develop Fiber Calorimetry with TEXAS ... R. DeSalvo, SPACAL

Preface

We answer in this document the questions that the SSC Program Advisory Committee (PAC) addressed to the TEXAS collaboration.

We first present an update on the baseline TEXAS detector concept, a necessary framework to answer the questions in detail. The three most relevant items of progress since our EOI was submitted are the following:

- The $O(\alpha_s)$ corrections to the $H \to \bar{b}b$ decay have been calculated.[1] They decrease the total width of an intermediate-mass Higgs by a factor of two. Thus, the calculated branching ratio for $H \to \gamma\gamma$ *increases* by a factor of two: good news for anybody attempting to exploit this difficult decay channel. $\sigma(pp \to H \to \gamma\gamma) \simeq 0.2\,pb$
- The calculated ionizing radiation dose has decreased by a factor of three.[2] This means that current scintillating fibers would survive – in their TEXAS locations – for ten years of running at $\mathcal{L} = 10^{34}\mathrm{cm}^{-2}\mathrm{s}^{-1}$.
- SPACAL has demonstrated in prototype test beams the outstanding performance of fiber calorimetry in terms of resolution, speed and e/h separation.

The TEXAS Expression of Interest was conceived to bring to the attention of the SSC PAC, and of the physics community, an alternative detector concept. Alternative, that is, to the expensive, large magnetic field, lower luminosity, generalized detector concepts espoused by SDC, EMPACT, and L*. The TEXAS EOI was intended as an expression of interest in the construction of a high-rate, fast, calorimeter-based detector. The TEXAS collaboration was only formed in January 1990; and its details have yet to be fully frozen. That task awaits engineering studies to be performed over the next year. The TEXAS EOI is not yet a proposal for an experiment. Our intention is to attract collaborators and work together over the next few months to develop a complete, detailed, exhaustive proposal. For this we need the support (both verbal and financial) of the SSC management and its advisory bodies.

Compared with the general purpose detectors, TEXAS has the fewest number of major design decisions to be settled prior to the submission of a detailed proposal. This makes it easy for us to provide estimates not only of detailed costs; but also of the physics reach, by using measured resolutions or by employing performances based on Monte Carlos which have successfully modeled real devices. TEXAS has no separate tracking, magnet system, or calorimeter options around which to design the experiment.

The clarity, specificity, simplicity and proven technology of the TEXAS specialized detector-concept makes it easy to envision each of its three major subsystems in a way that is not possible with detector concepts presented as a list of choices, or with untested technology. Each of the three major components has been tested in a major experiment or is being implemented in full scale prototypes. For example, the pre-radiator/tracker has been proven by UA-2, the calorimeter by the SPACAL and SSCINTCAL collaborations and the muon TRD by MACRO.

We must admit that our presently small collaboration could not – in spite of considerable effort – answer in a period of three weeks, and to our own full satisfaction, a long series of

well-taken questions whose fully detailed and complete answers, at the EOI stage, might have normally taken a year of work and simulation. We hope to be able, however, to demonstrate a measure of progress and to convey our conviction that the TEXAS design is not fundamentally flawed, and that our physics and technical claims are entirely tenable.

REFERENCES

1. C.P. Yuan and G. Kane *et al.* private communication.
2. D. Groom *et al.* Draft SSCL-285, June 19 , 1990.

Detector Concept Update

We briefly discuss aspects of the detector concept necessary to answer the questions from the PAC. The limited scope of the EOI, both in format and in intent, did not permit the level of detail we present here.

Central Tracker and Imaging/Preradiator Triggering

Two layers of scintillating tiles precede the imaging preradiator and have ~3 mm thick segmentation to match the calorimeter (0.05 x 0.05, offset by half a cell in both dimensions to achieve 0.025 x 0.025). Fig. 1 shows this in detail. The tiles are read out by a wave-shifting fiber in the manner developed by the SCCINTCAL Subsystem R&D collaboration for calorimetry (see Fig. 1). These trigger pads constitute about 15% of the pixel channels of the tracker/imaging pre-radiator. The tiles

(1) eliminate ghosts in the track reconstruction by constraining the combinatorics;

(2) provide fast (within a crossing) multiplicity information to the trigger;

(3) tag neutrals entering the pre-radiator and calorimeter, when combined with the calorimeter response.

The stereo angles of the fibers in the tracker and preradiator have been increased to 45° to provide more resolution on the track coordinates along the beam direction. (UA-2, for example, has 45° stereo). A combination of uv at different angles is used in adjacent layers to suppress ghosts.

The 6m long tracker module is read out by fibers no more than 3m in length. Since 1mm fibers provided more resolution than needed, the fiber thickness has been increased to 2 mm to give more light and minimize the channel count. In addition, Monte Carlo work shows that a 2 mm grid provides sufficient resolution.

A new option for a support structure without radiation-sensitive epoxy resins has been identified. The tracker/preradiator could be supported by a spun aluminum skin (like a Boeing 747 nose-cone) if radiation damage studies of carbon fiber indicate this is necessary.

Tracking with 2 mm fibers on straight tracks is considerably easier than with the sub-mm fibers proposed for precision tracking in a magnetic field. Light output is greater and the reconstruction hypotheses are limited. Members of the TEXAS collaboration participating in an SSC R&D subsystem task on fiber tracking have developed a design for the central detector and imaging preradiator.

They have built upon the operation of pre-radiators and fiber trackers in existing experiments in designing the fiber orientation, the number of layers, the fiber thickness, etc. This design is being optimized with the aid of Monte Carlo studies.

Preliminary analysis yields a resolution on the vertex in a single event of 4 mm along the beam direction using tracks from minimum bias events. The position of conversion in the pre-radiator of 85% of the gammas above 10 GeV can be determined to $\pm$ 1 mm. Over 90% of the gammas convert in the pre-radiator. Using the SPACAL results on the best fit to the center of gravity of isolated electromagnetic showers ($\pm$ 1mm), the gamma direction is determined to about 0.5 degrees independent of charged track information for the vertex. We shall see that this plays an important role in our search for $H \to \gamma\gamma$.

Calorimeter Segmentation

A conservative baseline calorimeter design was discussed in the EOI. It used separate longitudinal electromagnetic and hadron compartments. This concept is further discussed in Generic Question 5. Since the submission of the TEXAS EOI, the SPACAL collaboration has proven the anticipated performance of a monolithic tower design with combined electromagnetic and hadron compartments. Simplicity and uniformity result from this implementation of fiber calorimetry.

In addition, SPACAL results provide convincing e/π separation available in real time[1] (see Fig. 3) using the following two methods:

In the first method, the pulse shapes for electrons and hadrons are sufficiently different that a full width fifth maximum (FWFM) time measurement of the pulse separates hadrons from electrons (see Fig. 2). When applied to a local cluster of towers large enough to contain hadronic showers, a simple FWFM discriminator gives a direct logic pulse distinguishing electromagnetic from hadronic showers. The cluster must be 30-35 cm in diameter, as shown in Figure 3. From the temporal structure of the phototube signals alone the e/π separation is 10^{-3} without longitudinal segmentation. Improvements on this simple trigger are expected to further enhance this remarkable result.

Secondly, the SPACAL collaboration has also proven the value of fine tranverse segmentation when combined with a prevadiator. The signal from a simple (non-imaging) 1.5 L_{RAD} pre-radiator was independently recorded in front of the SPACAL prototype. Because electron showers have a much narrower core than do hadron showers, transverse shower size also separates shower types. An energy cut on the deposition in the preradiator applied simultaneously with a simple cut

on transverse containment achieved a separation of 4 x10^{-4}, between test beam electrons and pions, as shown Fig. 4.

Fine transverse segmentation achieves much of the same goal as longitudinal segmentation, because showers are correlated in their transverse and longitudinal shapes. While these two methods of e/π separation are not fully independent, the combined e/π separation is 10^{-4}. This is close to the ultimate limit imposed by pion charge exchange scattering in a monolithic calorimeter, and was achieved in preliminary results presented by the SPACAL group at Snowmass '90.

With a monolithic design, the proposed TEXAS calorimeter would be capable of finer hadronic segmentation at a reasonable cost. A segmentation of 0.025 x 0.025 (half that in the EOI) is useful at the 2 meter inner radius when limited by the 22 cm interaction length. It is then comparable to a 1 meter radius calorimeter segmented at 0.05 x 0.05. A design with monolithic lead-fiber towers would require about 160,000 PMTs, 20% fewer than the 200,000 PMTs of the EOI with separate em and hadron compartments.

On the scale of a Molière length (1.9 cm), a fiber spaghetti calorimeter can be treated as a homogeneous mixture of fiber and lead. The degree of homogeneity is dictated by the size of the fibers and the (compensated) ratio of Pb to fiber; this is why this calorimeter is so uniform. Thus, the fineness of the transverse segmentation in the calorimeter is dictated by the shower sizes and the large inner radius and not by physical design considerations. On the other hand, the physical size of the spaghetti calorimeter super-modules is dictated by manufacturing and integration engineering considerations. By simply undoing a fiber bundle and rebundling it into smaller bundles, a spaghetti calorimeter can increase its transverse tower segmentation down to "imaging" dimensions.

Triggering

Following the SPACAL experience, the triggers to separate hadrons from electromagnetic showers are straightforward. As discussed in the TEXAS EOI, signals in adjacent cells are added electronically to form overlapping calorimeter cells. Thus events which cross the boundaries between cells are handled uniformly by the trigger, as in Fig. 5. Triggers have been devised to find hadrons, isolated electrons, and isolated gammas. These use hardwired analysis of the calorimeter pulse shapes, the signal cluster size, and the preradiator trigger information as in Fig. 6. and Fig. 7, from the SPACAL and LAA groups at CERN. These results are due in particular to research by R. DeSalvo.

To give an example, an isolated gamma trigger would require no hit in a tracker tile, hits in the pre-radiator, and an isolated deposition in the tower

cluster aligned with the tile. The cluster trigger is formed from simple pulse height ratios formed electronically with neighboring towers. Indeed, SPACAL beam tests have shown that the overlap of an electron and a hadron separated by only 45 mm can be unfolded, offering a powerful technique for finding electrons even in jets[2]

Imaging Calorimeter Potential

Recent work using neural networks[3] and image recognition techniques[4] has direct implications for spaghetti calorimetry with fine transverse segmentation. Using neural-net algorithms operating on the tower "pixels" of a calorimeter, it may even be possible to discriminate between jets originating from gluons and those originating from quarks. This analysis benefits from fine transverse segmentation, as discussed in the Strong Interactions group at SNOWMASS 1990[5] . Using a fit on adjacent electromagnetic calorimeter cells to find a gamma ray position is an early indication of transverse segmentation being used to derive additional physics information from the shower development[6]

Radiation Damage

Recent recalculation of the ionizing radiation dose expected at the SSC has lowered the previously quoted figure by a factor of 3. At an η of 3, the dose is expected to be about 50 MRad at shower maximum for 10 years of SSC operation at $\mathcal{L} = 10^{34}\mathrm{cm}^{-2}\mathrm{s}^{-1}$. Since fibers available today recover from 30 MR[7] exposures, towers that could be built now can be expected to survive for at least 6 years at high luminosity without further development, even at η of 3.

The boundary between the solid and liquid segments at TEXAS is undecided prior to further studies. In the present EOI, the tungsten absorber matrix for the liquid-calorimeter region of TEXAS starts at $\eta = 3$ to reduce the shower width (from a hadron absorption length of 22 cm to 11 cm). This enhances the jet separation in the forward region to permit triggers from quark spectators in the production of heavy Higgs by WW fusion.

Because of the increased neutron density from a relatively nearby forward calorimeter, the η >3 region may need about 20 cm of polystyrene in front of the calorimeter[8] . However, this may be unnecessary since neutrons have little effect on plastic scintillators. For Si calorimetry, the neutrons at the SSC could be fatal, especially at 10^{34} $\mathrm{cm}^{-2}\mathrm{sec}^{-1}$.

In the answer to Generic Question 5, we discuss a staged implementation of the calorimeter. In stage 1 we would build only the electromagnetic calorimeter,

dedicated to H$\rightarrow \gamma\gamma$ and H$\rightarrow ZZ^*$. Later, this detachable front end could be added to the hadronic tower using the low-cost fiber coupling plates we have developed. See Generic Question 5 for a detailed discussion of this option for constructing the calorimeter.

Enhanced Resolution

The SPACAL collaboration[9] has demonstrated that the Monte Carlo simulation of scintillation calorimetry is fully predictive, having reached $29\%/\sqrt{E}$ for hadrons with a 1% constant term, and $13\%/\sqrt{E}$ with a constant term close to 1/2% for electrons. Using the same Monte Carlo prediction as shown in Figure 9, it is possible to scale to an electromagnetic resolution of $6\%/\sqrt{E}$ with a 1/2% constant term by simply reducing the fiber diameter to 0.5 mm, instead of 1 mm, while maintaining the 20% compensation ratio of lead to fiber. This provides a realistic calorimeter for Higgs $\rightarrow \gamma\gamma$ at the SSC and other physics. With 0.5 mm fibers, t he hadron resolution would reach about $25\%/\sqrt{E}$. (With 4 times the number of fibers, the sampling fluctuations decrease since the mixture becomes more homogeneous.)

To make such high electromagnetic resolution for TEXAS technically possible, fiber technology must improve its dimensional tolerance by a factor of about 3, to 0.5% in the fiber diameter (3-5 microns). This would decrease the attenuation length contribution caused by waveguide non-uniformity. The TEXAS collaboration has been assured by several manufacturers in the US, Europe and Japan as well as by an industrial partner, Bicron, that this is well within the state of the art. For example, common 62.5 micron plastic fibers used in local area networks have a dimensional tolerance of 0.5 microns. More quality control in the pre-form and pulling processing, and installation of the latest fiber equipment manufacturing machinery, is required. The cost of the smaller 0.5 mm fibers is estimated by Bicron to be 30% per meter of the 1 mm fibers. With four times the linear length, the smaller diameter fibers would cost roughly 1.2 times the estimates in the EOI for fiber.

Increasing the number of fibers embedded in the tower is estimated to increase the manufactured cost of a completed tower by about 10-12%. The servos must have a gentler pull and more sensitive feedback mechanism to handle the thinner and more delicate fibers. The matrix insertion (either machine laid-down or cast-in-place) is a major subject of our proposed engineering studies over the next 1.5 years. The factory need not be started for 5 years. We are assured that tooling is relatively straightforward by our industrial affiliates.

An alternative calorimeter implementation uses a separable electromagnetic section, as used by the JETSET collaboration, to achieve $6.5\%/\sqrt{E}$[10] . This option would allow staged operation before installation of the full hadronic calorimeter.

Muon TRD Details

Many proportional wires (about 1,000,000) are required for the muon TRD to reduce drift times to about 150 ns. The wires are not individually read out, but are ORed in projection clusters of about 20-30 for a secondary TRD readout. The 10,000 m^2 of chamber are only about twice the area of the chambers being constructed for MACRO.

The pad readout is segmented at a level equivalent to a tower segmentation of about 0.1 x 0.1, yielding 300,000 TRD channels in 60 layers. The 5000 muon towers thus formed give a direct energy signal without any track fitting. Fine position resolution on muons is provided by the limited streamer tubes and ganged TRD wires. The 60 layers of TRD wires are offset staggered from layer to layer to generate a fast saturation trigger tag in about 25 ns. Muons pass within 25 ns of 1/6 of the wires.

Each layer of xenon TRD detector-wires is backed by about 2-10 mm of structural material for strength and also to scatter and absorb electrons or low energy particles accompanying the muons as they exit the calorimeter. The low-Z layers of liquid scintillator used for triggering reduce the electromagnetic showers exiting the calorimeter. These showers are essentially limited to about 80 MeV for lead, far below the TRD electron threshold of about 250 MeV. In contrast, these showers are a problem for precision trackers with magnetic fields.[11]

A possibility for the TRD "wires" being pursued by the collaboration is a recent development in printed wires - 10 micron lines deposited on an insulating substrate. If this proves to be a low-cost and easily assembled alternative to the existing low-cost techniques used in MACRO, it could be adopted.

Trigger Details

The TEXAS trigger uses "fuzzy" logic to weight the incoming information from the tracker pads, calorimeter, main trigger, *etc.* For example, if the an E_T deposition is large enough, it may override a veto or the absence of other trigger requirements. In the electron trigger, the isolation requirement may be softened; for a hard muon trigger, +6 logic may over-ride a muon signal in the calorimeter. The first level trigger will output numerical values corresponding

to the robustness of the trigger. Custom fuzzy logic chips will evaluate that information in the second level.

The details for implementing the imaging reconstruction of the cells of the calorimeter to find electromagnetic or hadronic energy were described earlier in the calorimeter update section. Each cell of the calorimeter is connected logically to its nearest neighbors to form these quantities and to avoid bias on the basis of the physical segmentation of the calorimeter.

The basic first level trigger signals are the following:

(1) high transverse hadronic cluster energy: the calorimeter cluster ASIC fires above threshold;

(2) high p_T electron trigger: pulse shape discriminator tracker tile pre radiator-tile angle-scaled energy isolation override, ASIC/ROM on calorimeter cluster;

(3) gamma trigger: same as electron trigger but with tracker tiles in veto, and a different p_T threshold;

(4) high p_T muon trigger: TRD + calorimeter tower ASIC + Tracker tile central detector isolation evaluation.

The basic second level trigger signals are the following:

(1) Global total E_T and global missing E_T: an ASIC looking at the global pipeline;

(2) Lepton multiplicity, E_T, and patterns: an ASIC looking at the global pipeline;

(3) Trigger clusters: evaluation of the total trigger patterns.

FOOTNOTE: Many results used here were presented by Michele Livan at BU on 6/18/90, and by Ricardo DeSalvo at Snowmass 1990, for the SPACAL collaboration. Note that e/h is slightly larger than 1.0 in these preliminary results; Monte Carlo predictions indicate that a slight shift downward in the fiber diameter, or a slight shift upward in the fiber spacing will be able to tune e/h to 1.00+ 0.01.The results were taken in the first week of June without calibration data; the phototubes were simply balanced to about 3% with a source, and these calibration errors gave rise to an effective constant term of 2.6% in these preliminary results.

REFERENCES

1. SPACAL: separation available in real time recently shown by SPACAL.
2. H. Parr, Private Communication.
3. Recent work using neural networks.
4. Image recognition techniques.
5. Snowmass-90: fine transverse segmentation.
6. GAMS collaboration: how to derive additional physics information from the shower development.
7. Fibers available today recover from 30 MR.
8. We thank Don Groom of LBL for advice in this matter.
9. Demonstration by SPACAL that the Monte Carlo simulation of spaghetti calorimetry is fully predictive.
10. The JETSET collaboration expects to achieve 5%–6.5%/$\sqrt{E}$. Dave Hertzog, private communication.
11. EMPACT: precision trackers in magnetic fields (Adair).

Figure Captions

Fig. 1 TEXAS tracker/preradiator with trigger pads.

Fig. 2a Pulses from the SPACAL spaghetti calorimeter. Note the differences between e^- and π^-.

Fig. 2b Pulse width (Full width at one fifth maximum) distribution (fixed offset of 6 hs).

Fig. 3a, 3b (SPACAL) e/π separation electronics for pulse shape discrimination.

Fig. 4a (SPACAL) Containment definitions.

Fig. 4b (SPACAL) e/π separation with containment vs pre-radiator signal.

Fig. 5 Electronic overlapping towers for trigger. (From SPACAL).

Fig. 6a-g SPACAL concept for fiber calorimeter electronics (courtesy of R. DeSalvo).

Fig. 7 Ionizing dose at electromagnetic shower maximum at SSC design luminosity for one year and (in parenthesis) at $\mathcal{L} = 10^{34}\mathrm{cm}^{-2}\mathrm{s}^{-1}$.

Fig. 8 TEXAS projected resolutions with 0.5mm fiber option.

Fig. 9 TEXAS potential energy resolution, but with 1% constant term. (Data from 6/90 without calibration).

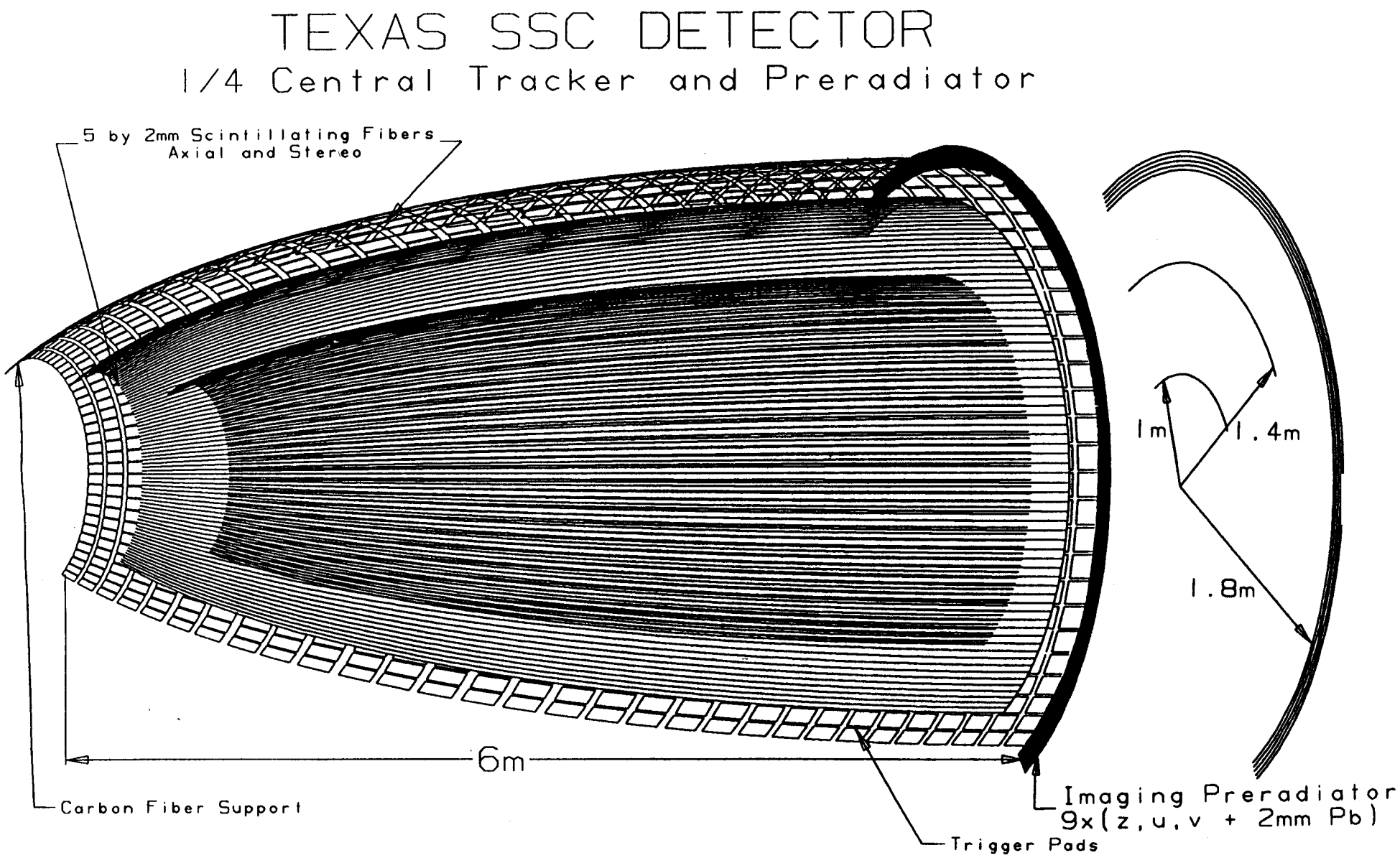
TEXAS SSC DETECTOR
1/4 Central Tracker and Preradiator
5 by 2mm Scintillating Fibers
Axial and Stereo
1m
1.4m
1.8m
6m
Carbon Fiber Support
Trigger Pads
Imaging Preradiator
9x(z,u,v + 2mm Pb)

Figure 1

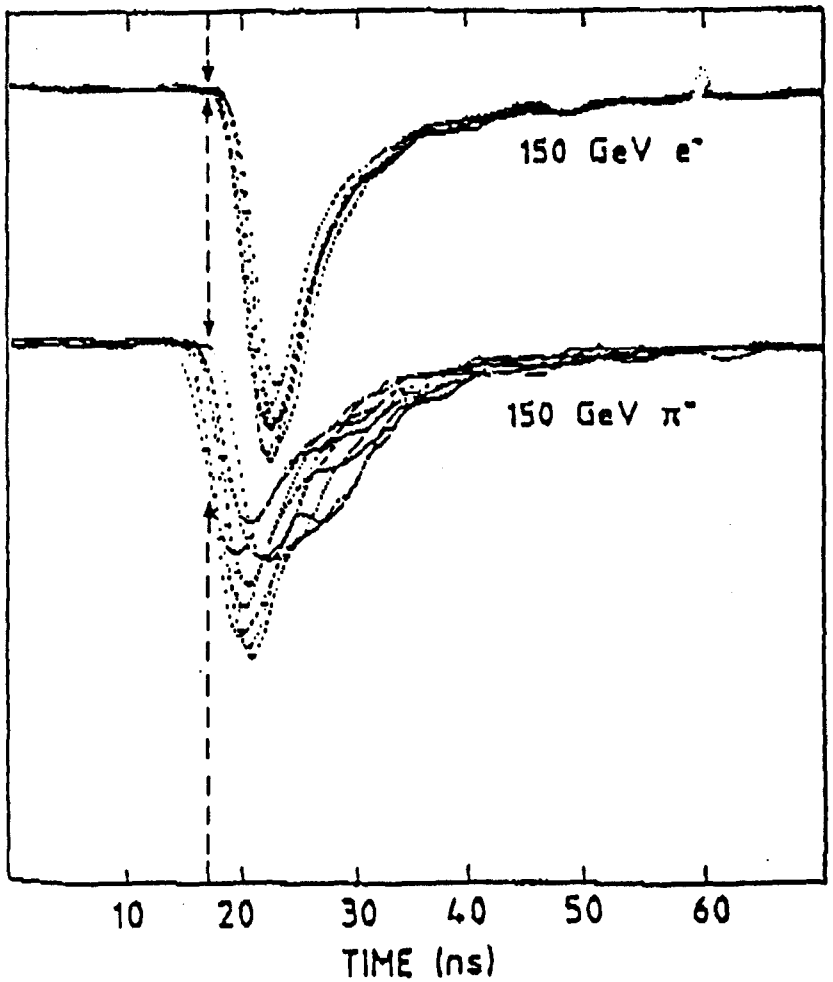

Figure 2a

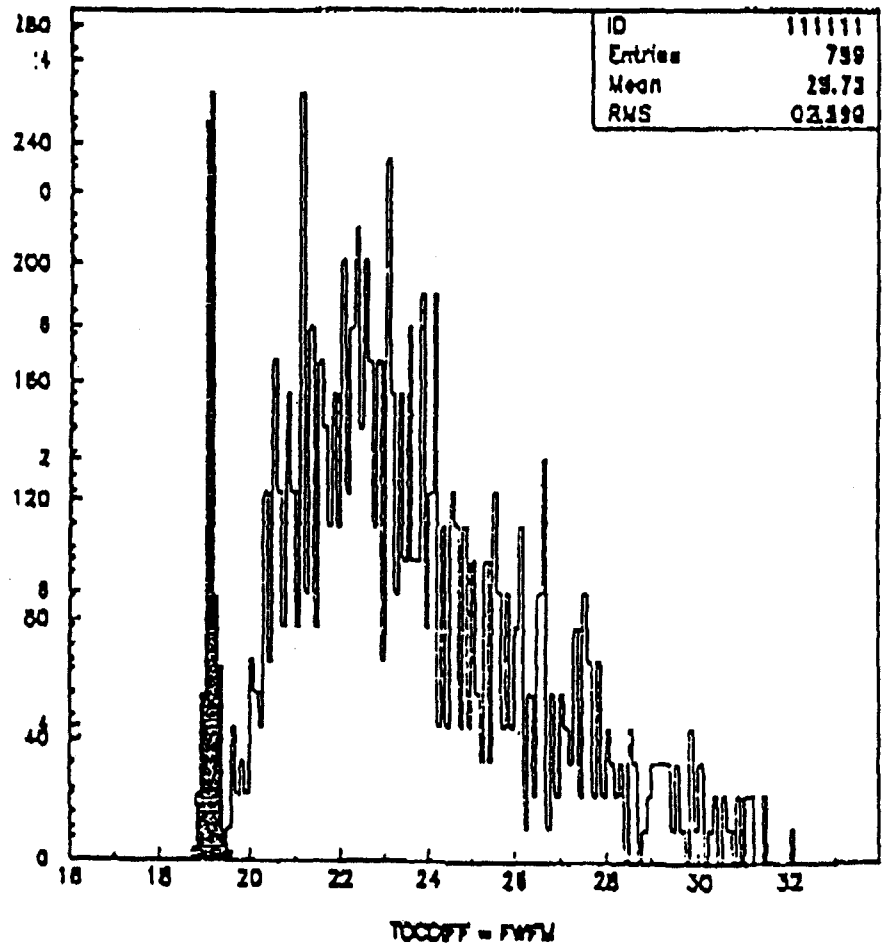

Figure 2b

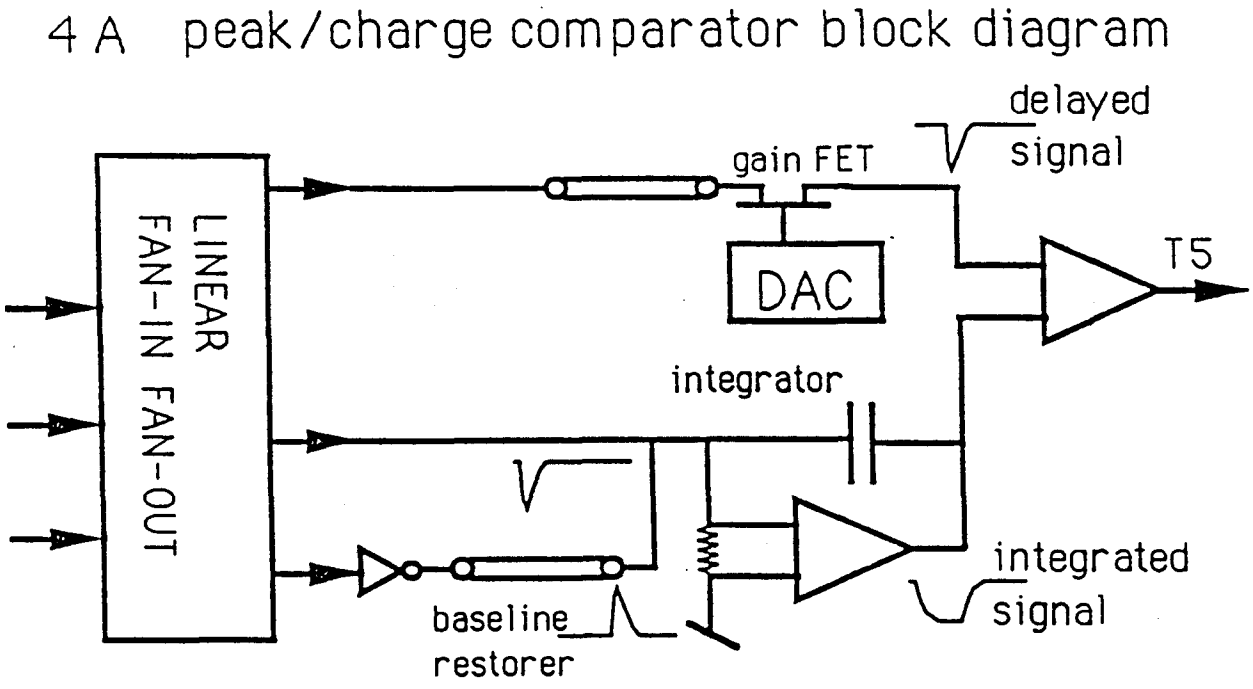

Figure 3a

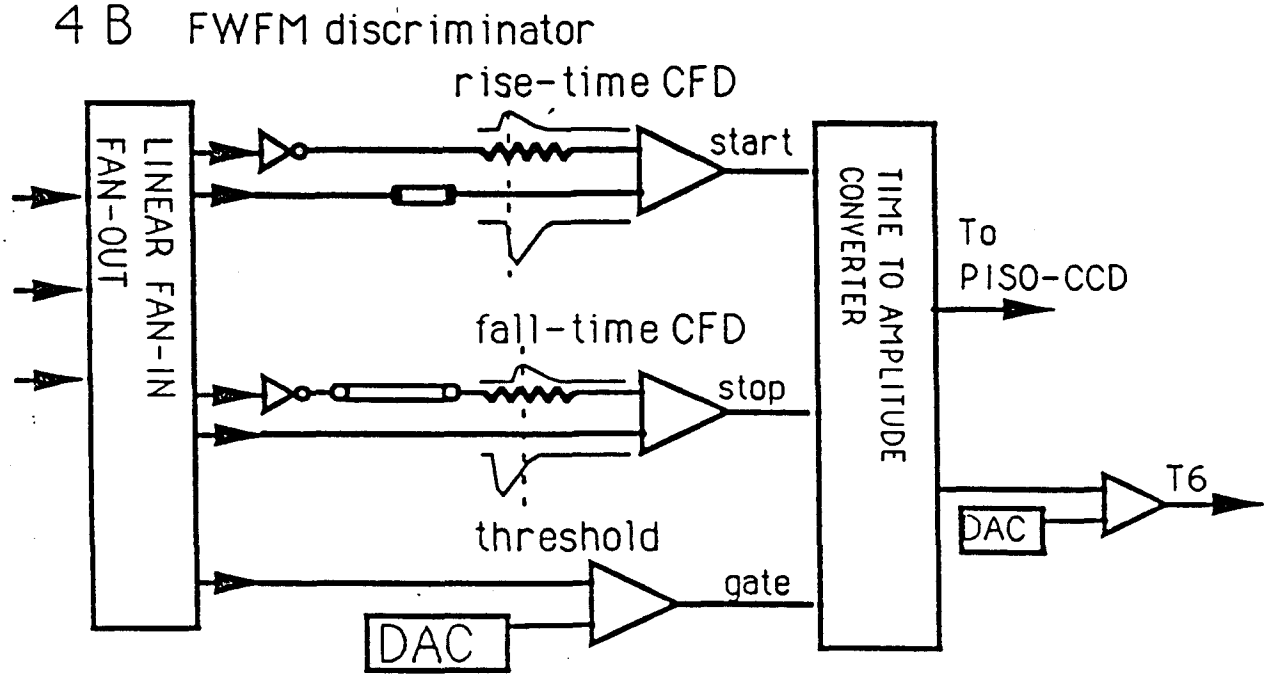

Figure 3b

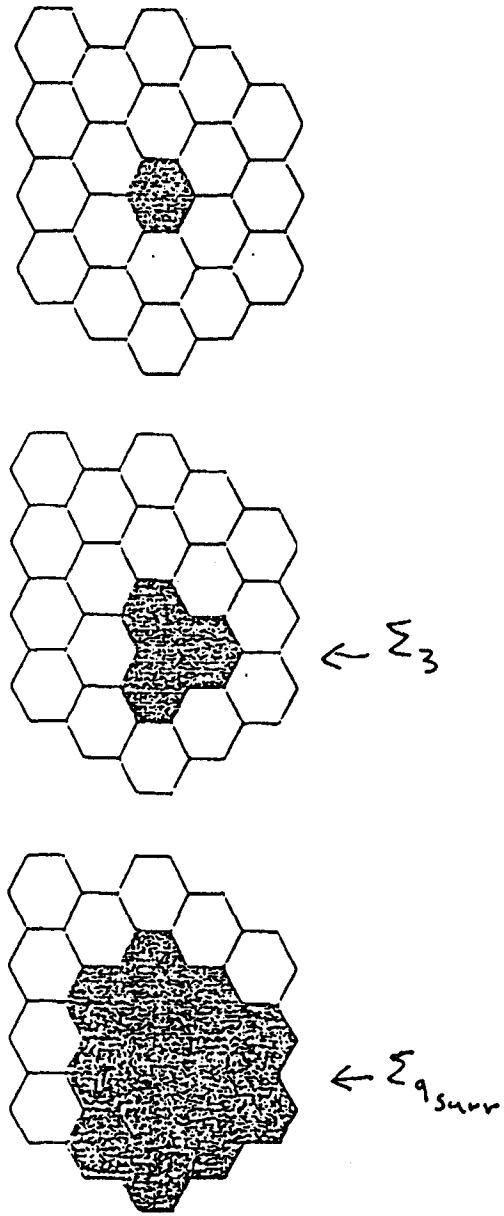

Figure 4a

e/π separation with preshower

$$C = \Sigma_3 / (\Sigma_3 + \Sigma_9^{surr.})$$

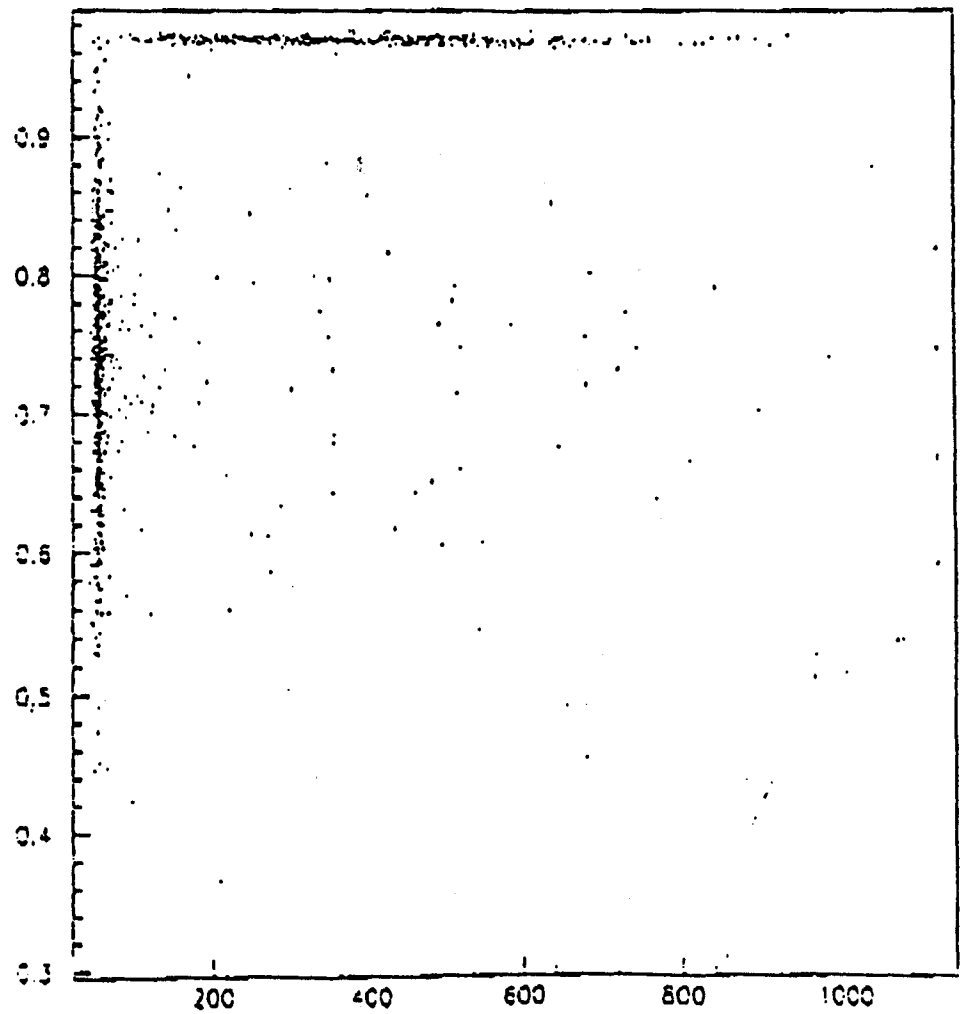

C vs preshower signal

Figure 4 b

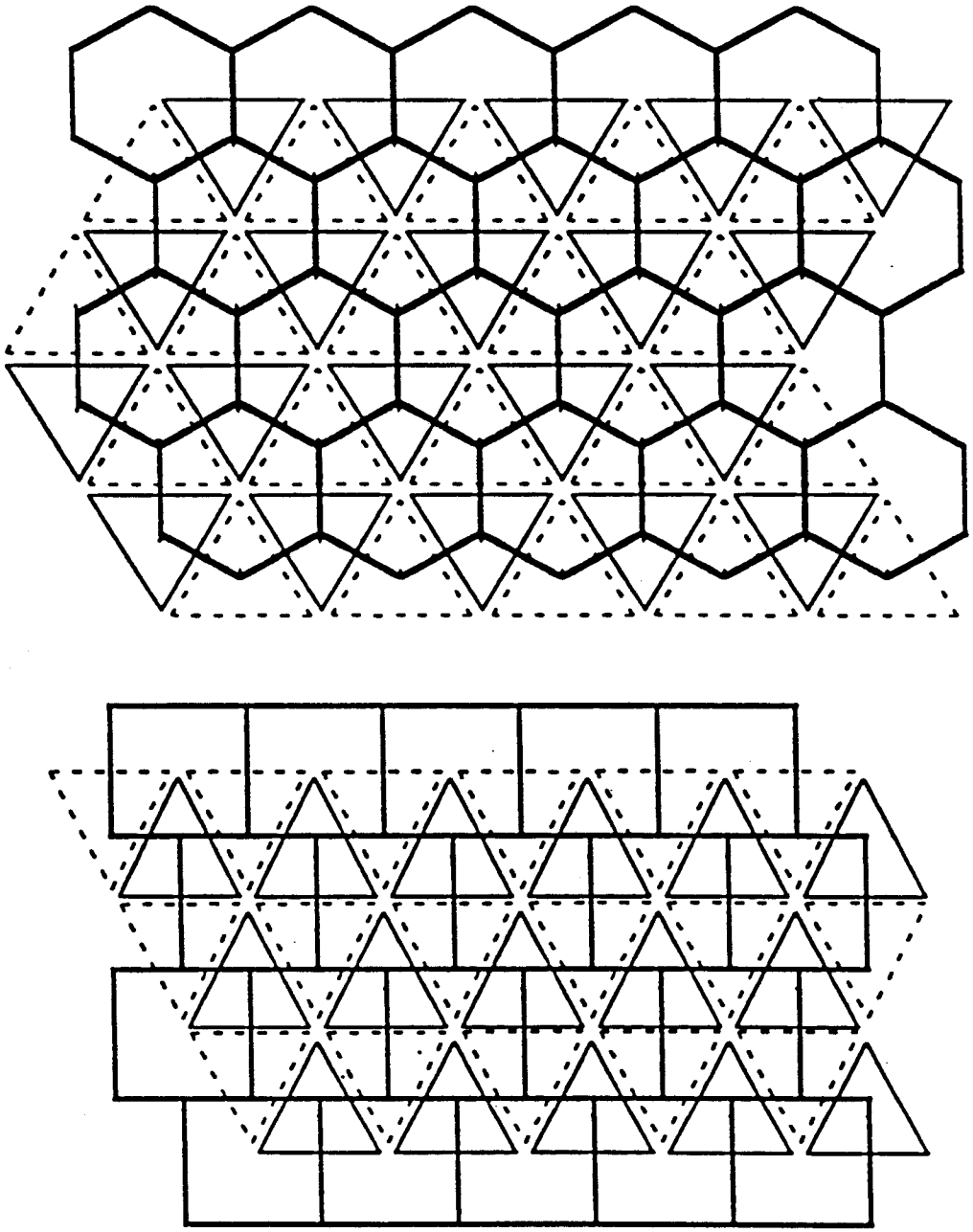

Figure 5

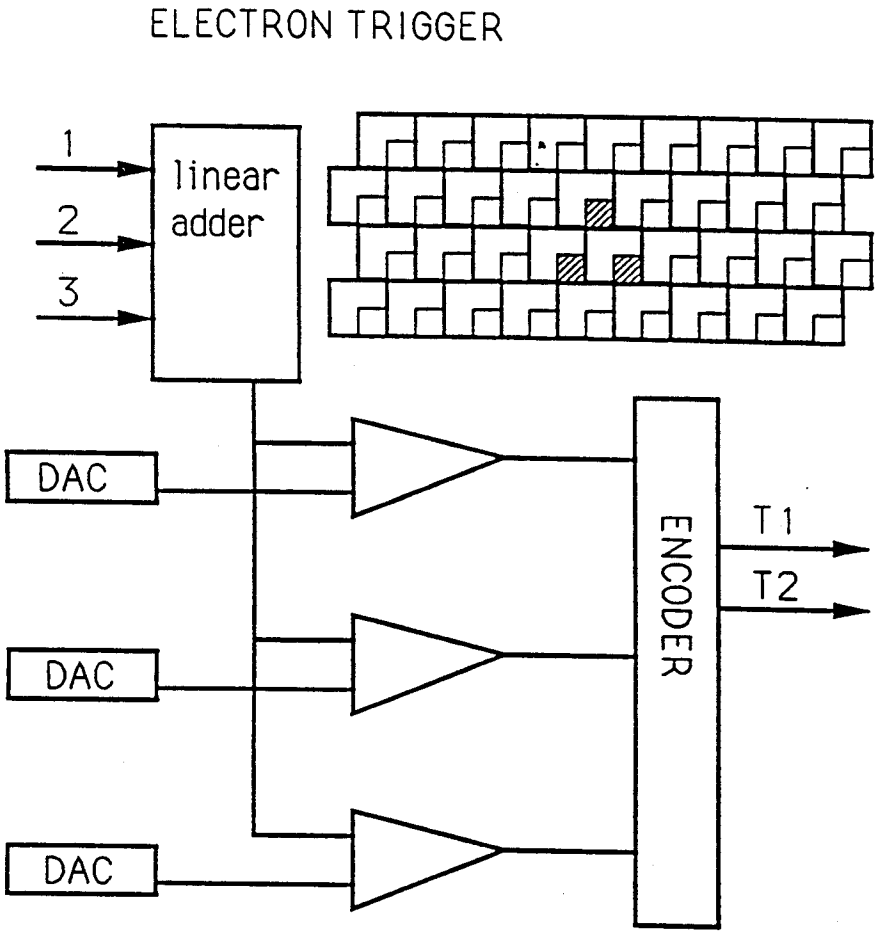

Figure 6a

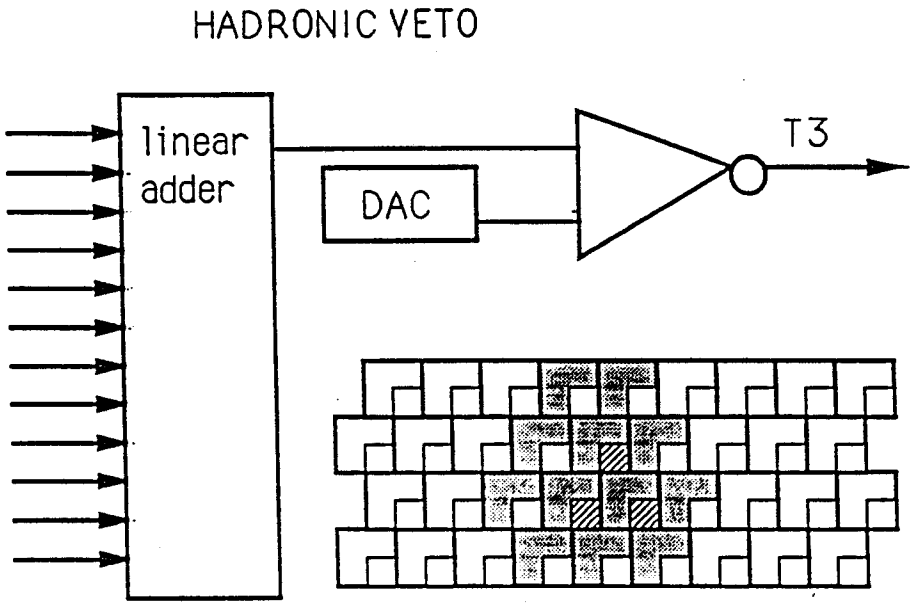

Figure 6b

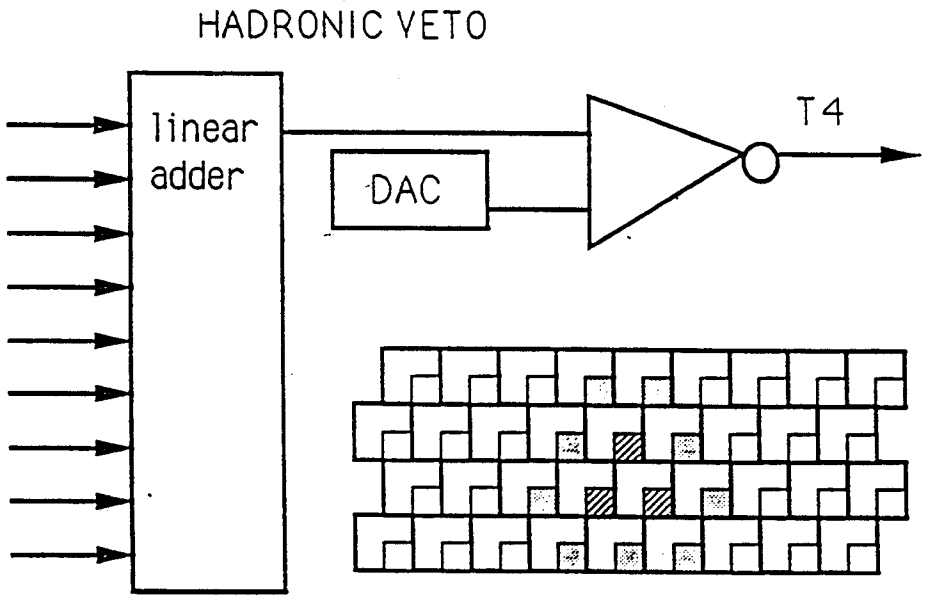

Figure 6c

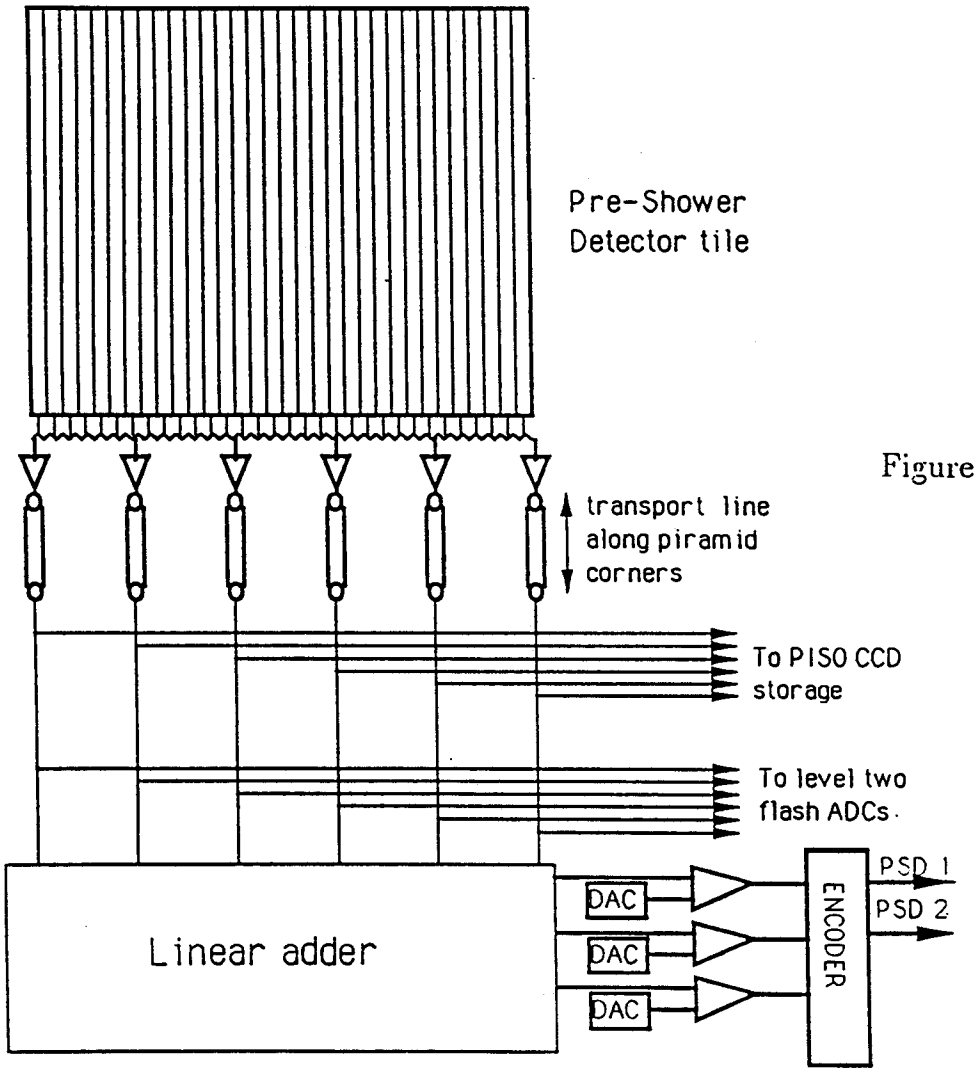

Figure 6d

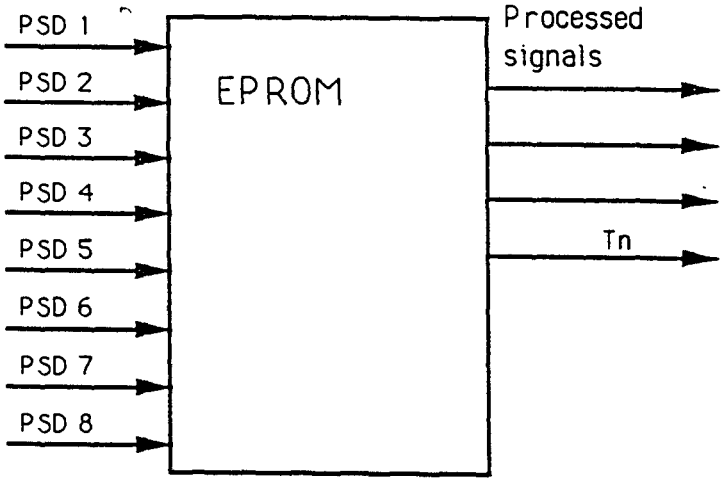

Figure 6e

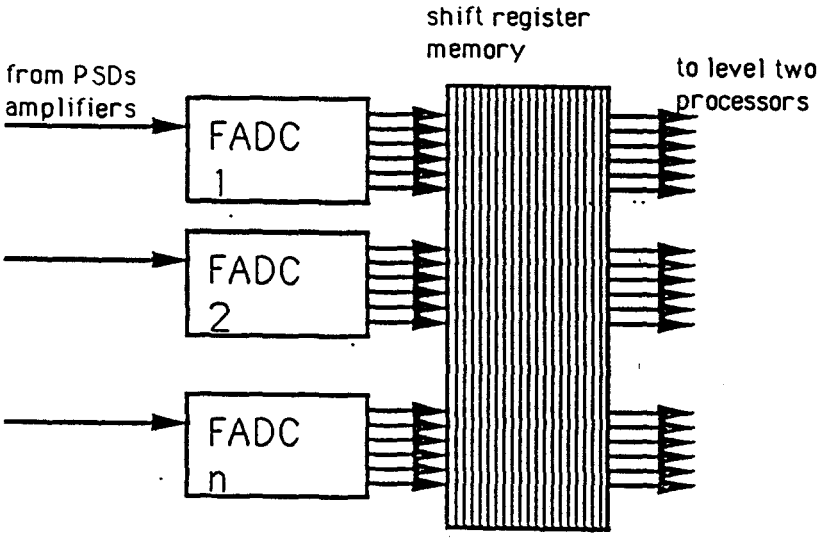

Figure 6f

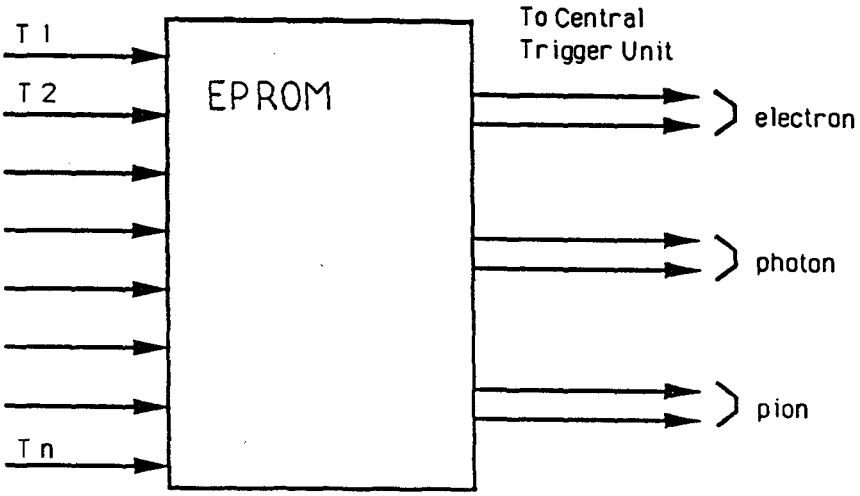

Figure 6g

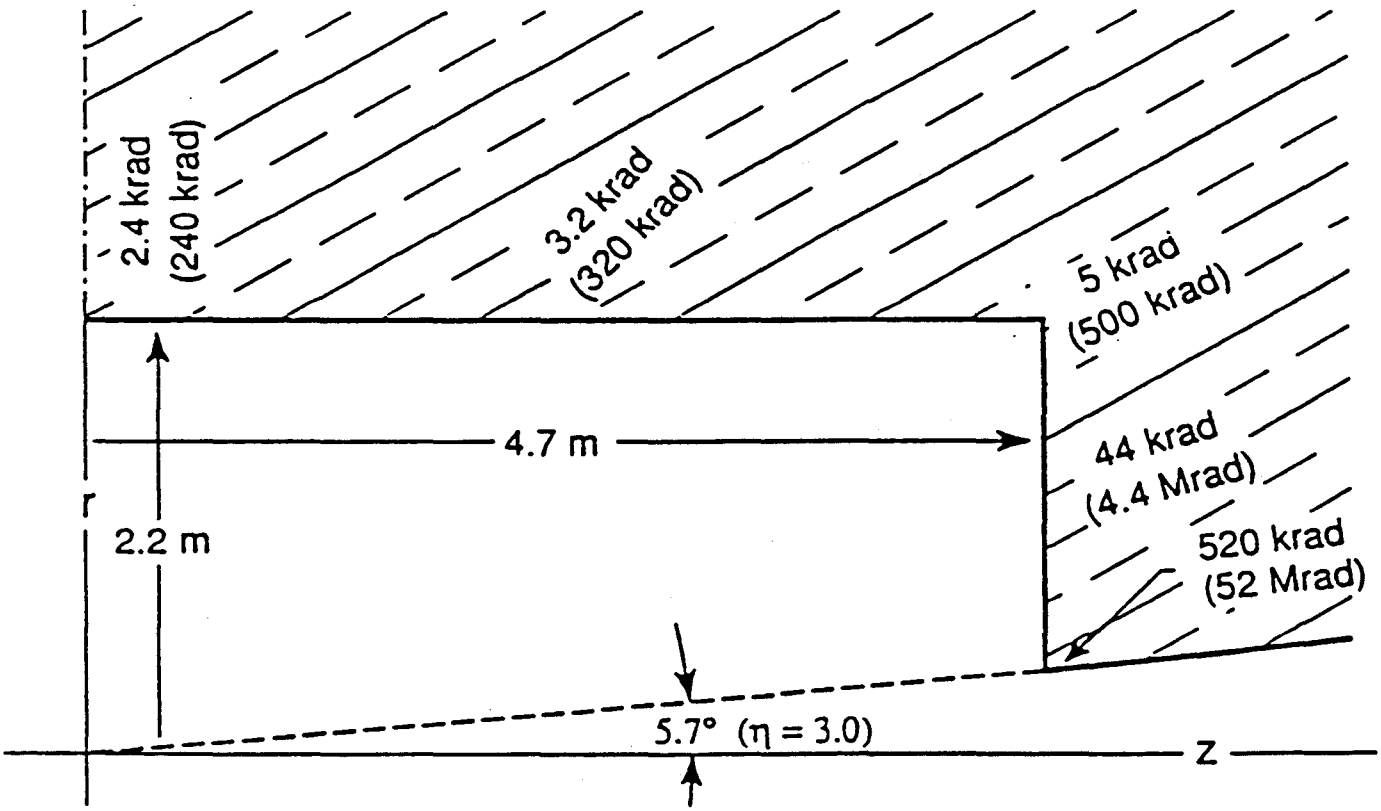
2.4 krad
(240 krad)
3.2 krad
(320 krad)
5 krad
(500 krad)
4.7 m
r
2.2 m
44 krad
(4.4 Mrad)
520 krad
(52 Mrad)
5.7° (η = 3.0)
z

Figure 7

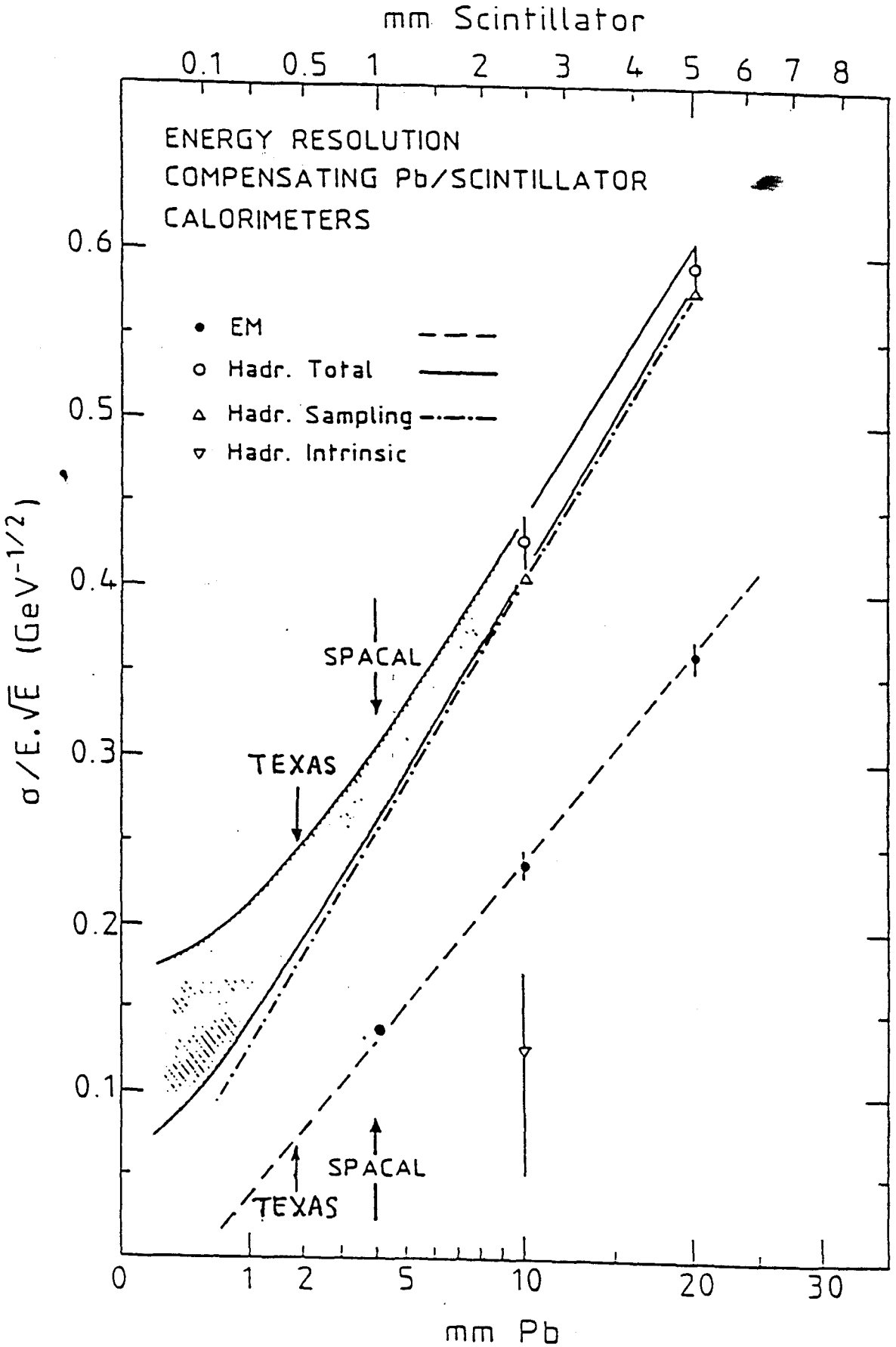
mm Scintillator
0.1
0.5
1
2
3
4
5
6
7
8
ENERGY RESOLUTION
COMPENSATING Pb/SCINTILLATOR
CALORIMETERS
EM
Hadr. Total
Hadr. Sampling
Hadr. Intrinsic
0.6
0.5
0.4
0.3
0.2
0.1
σ/E.√E (GeV^-1/2)
SPACAL
TEXAS
SPACAL
TEXAS
0
1
2
5
10
20
30
mm Pb

Figure 8

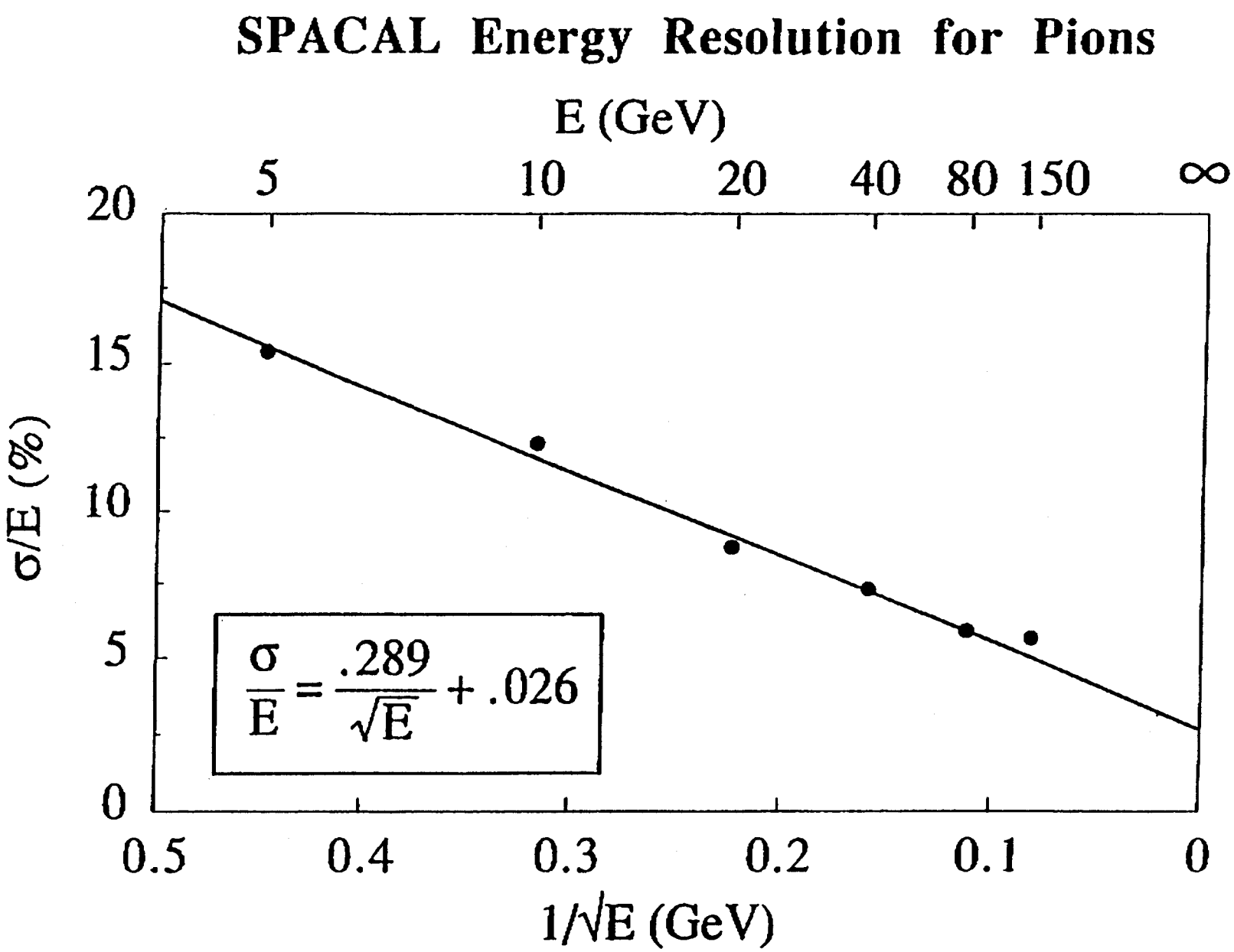
SPACAL Energy Resolution for Pions
E (GeV)
5
10
20
40
80
150
∞
20
15
10
5
0
σ/E (%)
$\frac{\sigma}{E} = \frac{.289}{\sqrt{E}} + .026$
0.5
0.4
0.3
0.2
0.1
0
1/√E (GeV)

Figure 9

G1: Higgs Searches

Describe the capabilities of TEXAS for searching for a standard model Higgs from 90 to 800 GeV/c^2.

A: Intermediate Mass Higgs (80 GeV/c^2 to 180 GeV/c^2)

$H \rightarrow \gamma\gamma$

The decay $H \rightarrow \gamma\gamma$ appears to be the most promising channel in the intermediate mass region. The measurement of the $H \rightarrow \gamma\gamma$ branching ratio is widely recognized[1] as a fundamental tool to elucidate electroweak symmetry breaking no matter what the underlying mechanism is. The signal is clean: a pair of isolated high p_T photons and no missing E_T. However, excellent energy resolution for photons is required for this channel. Also, due to the low signal to noise ratio, high luminosity (10^{34} cm^{-2}sec^{-1}) may indeed be helpful.

Recent theoretical calculations, including QCD α_s corrections,[2] show $\Gamma(H \rightarrow b\bar{b})$ to be half the value we used in the calculations for the TEXAS EOI. This implies that the cross section for Higgs decaying into two γ's is two times larger than anticipated. This extends the sensitivity of the TEXAS search for the Higgs down to a mass of 100 to 120 GeV/c^2.

An important aspect of the TEXAS detector for the $H \rightarrow \gamma\gamma$ search is its rejection power against QCD jets that fragment into π^0's. Typically the background to a single γ is a jet of several lower energy π^0's that overlap. These are easily identified in the imaging preradiator. A problematic background for other detectors is fragmentation to a single π^0. A simulation of a typical event is shown in Fig. G1-1.[3] The conversion of the two gammas is quite distinct due to the large radius of the TEXAS calorimeter and the fine granularity of the preradiator. The separation of the photon conversion points is 1 cm transverse to the π^0 direction.

The cross-section for $\bar{q}q$ to $\pi^0\pi^0$ reconstructing into the invariant mass range of the light Higgs is about 1 mB (a 1MHz rate). The cuts and the trigger must therefore reduce this rate by six orders of magnitude. The preradiator tiles and the electromagnetic energy signal allow an isolation cut of R<0.6. This rejects the background by a factor of 10^{-4} to 10^{-5} at level 2 of the trigger. (Unfortunately, the real SSC fragmentation function needed to determine this rejection to better precision in hadron collisions with initial state gluon bremsstrahlung is not known). The resulting 10-100 Hz trigger rate is still high compared with the required rate of 1 Hz. However, the gammas from a π^0 are separated by 0.3–1.2 cm at the imaging preradiator. The third level trigger will lower the rate by at least a factor of 25.

Another performance specification of TEXAS is its ability to identify the vertex associated with a $H \rightarrow \gamma\gamma$ event. As discussed in the Detector Update section, the TEXAS detector has two methods of determining the vertex:

1) central tracker pointing back to the vertex, using the underlying charged particles of the event, and

2) calorimeter/preradiator pointing, using the center-of-gravity of the em shower (σ = 1mm)[4] and the photon conversion point in the preradiator ($\sigma = 0.6$mm).

The first technique determines a vertex, at both low and high luminosity, to < 1 mm, the second to 0.6 cm. Both of these numbers are smaller than the typical vertex separation, the interaction diamond length ($\sigma = 5$ cm) divided by the number of overlapping events, even at high luminosity (10cm/15 $\sim$ 1cm). The second technique is crucial for 10^{34} cm^{-2} sec^{-1} operation where typically 15 minimum bias vertices could be confused with the $H \rightarrow \gamma\gamma$ vertex. It insures that a $H \rightarrow \gamma\gamma$ candidate is a "quiet" event.

Two instrumental effects contribute to the width of the mass peak, energy resolution and vertex uncertainty. Without any vertex fitting, the mass resolution smearing from the size of the interaction diamond is comparable to that due to the energy resolution. With either of the pointing techniques, the energy resolution dominates the error. This is summarized in Table 1.

Table 1: Mass Resolution for H$\rightarrow \gamma\gamma$

Higgs Mass	Diamond smearing	σ/E + Diamond smearing	σ/E smearing + Vertex pointing
100	99.98±1.03	99.93±1.33	99.94±0.89
120	120.00±1.25	120.00±1.58	120.00±1.02
130	130.00±1.34	130.00±1.71	130.00±1.09
140	140.00±1.45	140.00±1.86	140.00±1.18
150	150.00±1.57	150.00±1.95	150.00±1.22

The mass resolution for a 150 GeV/c^2 mass Higgs is 1.22 (1.95) GeV/c^2 at 10^{33} (10^{34}) cm^{-2}sec^{-1} luminosity as shown in Fig. G1-2. A worse resolution[5] , 1.91 GeV/c^2, is sufficient to see the mass peak with 7.6 σ of statistical significance.

Based on an ISAJET (V6.31) Monte Carlo and a TEXAS detector simulation with Z vertex pointing we have studied the decay $H \rightarrow \gamma\gamma$ and $gg, q\bar{q} \rightarrow \gamma\gamma$. The total cross sections for signal and background are about 0.15 pb and 3.6 $\times$ 10^3 pb with $p_T(\gamma) \geq 10$ GeV/c. We have generated 5000 events for each Higgs mass and 1.1 $\times$ 10^5 events for background. Figure G1.3, for example, shows the distribution in E_T for signal (a) and the QCD to two photon background (b). These distributions have motivated the following selection criteria:

O.K.

$$E_T(\gamma) \geq 20\ GeV$$
$$|\ \eta(\gamma)\ | \leq 3.0$$
$$|\ \cos\theta^*_\gamma\ | \leq 0.8$$
$$|\ M(\gamma\gamma) - M(Higgs)\ | \leq 2.5 GeV/c^2$$

Here θ^*_γ is the polar angle of photons in the $\gamma\gamma$ rest frame. These cuts reduced the signal to $\sim$ 0.075 pb and background to $\sim$ 3.6 pb. Thus the signal-to-background ratio is estimated

to be around 0.02 for the intermediate mass Higgs in a ± 2.5 GeV/c^2 mass window. To obtain the background for 1 and 10 standard SSC year equivalents we fit the mass spectrum from the background sample (1.1×10^5 events) to a single exponential function. Then the equivalent number of background events is generated using the fitted slope. Figure G1-4 shows the background subtracted 2 photon invariant mass spectrum with signals for a Higgs mass of 100, 120, 130, 140, and 150 GeV/c^2 for 1 SSC year of operation. The vertex pointing accuracy is 0.5 cm.

An independent evaluation of the TEXAS detector response has been carried out by R. Partridge.[6] Figure G1-5 shows the signal on top of the background for Higgs masses of 80, 100, 120, and 150 GeV/c^2. The histogram is fit with an exponential and four Gaussians. In this independent analysis the statistical significance of the signal is determined to be 3.6σ at 80 GeV/c^2, 6.2σ at 100 GeV/c^2, 9.5σ 120 GeV/c^2 and 10.2σ at 150 GeV/c^2. Figure G1-5a shows (clockwise from upper left) the accepted transverse energy, gamma pseudorapidity, digamma pseudorapidity, and c.m. opening angle spectra.

In our analysis, the statistical significance for discovery is simply expressed as

$$SS = \frac{N - B}{\sqrt{B}} \quad ,$$

where N is the total number of events in the mass bin with B background events fitted under it. A summary of this study is given in Table 2.

Table 2: Significance of $H \rightarrow \gamma\gamma$ Detection

Higgs Mass	$N - B$/SSC Yr	B/SSC Yr	Discovery Significance/SSC Yr	Branching Ratio Precision at High $\mathcal{L}$
100	677	9.7×10^4	2.1	46%
120	877	5.0×10^4	3.9	25%
140	952	4.3×10^4	6.0	22%
150	712	4.0×10^4	3.6	28%

Here one standard (high $\mathcal{L}$) SSC year is equivalent to an integrated luminosity of 10^{40} (10^{41}) cm^{-2}. At a luminosity of 10^{33} cm^{-2}sec^{-1}, we will be able to discover a Higgs in the mass region between 120 and 150 GeV/c^2. At high luminosity, the reach extends down to 100 GeV/c^2 (where the discovery significance is SS=6.6).

After discovery of the $H \rightarrow \gamma\gamma$, it will be important to measure the branching ratio to verify the model, independent of the Higgs mechanism.[1] The error in measuring the rate of the signals for $H \rightarrow \gamma\gamma$ is given by

$$\frac{\sigma_S}{S} = \frac{\sqrt{N}}{S}$$

This is also shown in Table 2. Clearly, high luminosity is necessary to make even a relatively modest 30% measurement of the branching ratio.

A potential difficulty at high luminosity is the pile-up of 15 minimum bias events. Figure G1-6 shows the transverse energy flow in cones of 0.1 and 0.2 around each γ in the environment expected at a luminosity of 10^{34} $cm^{-2}sec^{-1}$.

Table 3: Underlying event energy flow within a cone

# of pile-up events	E_T(cone=0.1)	E_T(cone=0.2)
0	0.6 ± 0.8GeV	0.8 ± 2.1
15	2.1 ± 3.3	8.0 ± 8.0

Table 3 shows that the summed E_T within a cone of 0.1 around the photon is 2 GeV. Since the TEXAS calorimeter has high segmentation (0.025 × 0.025), we can require such a stringent isolation cut. Most of the electromagnetic shower is contained in one tower (5cm ^{2}). The underlying event energy in the signal tower is 0.2 GeV ± 0.3 GeV, in addition to the real signal energy. This underlying energy and its fluctuation shift the mass measurement by 400 MeV and broaden the mass resolution by 0.7 GeV. The mass shift will be resolved by subtracting the average underlying event energy. The mass resolution worsens, for example, from 1.22 GeV/c^2 to 1.95 GeV/c^2 for 150 GeV/c^2 Higgs.

The isolation cut around the gamma directions is superior in TEXAS because of the fine segmentation and large radius. This allows us to operate at high luminosity more easily. Because a tower is only 0.025 wide, an energy cut of 6 GeV electromagnetic energy per crossing (17 events) in an annulus of R=0.1 to 0.2 about the gamma direction is easily made. Since this sets the baseline for the electromagnetic energy measurement, a tighter annular cut of R from 0.05 to 0.1 would be preferable. In TEXAS this is possible because the towers for η <2.5 are at least 3 radiation lengths across, reducing the energy cut to 1.5 GeV. The ability to lower this isolation energy cut is essential to preserve the electromagnetic energy resolution for the $H \rightarrow \gamma\gamma$ search.

Because the Higgs events are reasonably high q^2 events, there will be initial gluon radiation. In principle, these events will therefore have different multiplicity and topology from the minimum bias ones, or low jet E_T events. Cuts are being devised to attempt to enhance the Higgs signal using a multiplicity cut. This depends on a complete knowledge of the fragmentation function, and ISAJET and Pythia give substantially different answers. We are exploring this cut, but are still wary of its effectiveness.

$H \rightarrow ZZ^*$

Another decay mode, $H \rightarrow ZZ^*$, also has a narrow mass width. The mass resolution for a 150 GeV/c^2 Higgs is 1.16 GeV/c^2 in the TEXAS detector for the four electron mode. The

cross section for $H \rightarrow ZZ^* \rightarrow eeee$ is 4.2 fb. The event selection criteria are

$$E_T(e) \geq 20\text{GeV for two leading electrons,}$$
$$E_T(e) \geq 10\text{GeV for other non} - \text{leading electrons}$$
$$|\,\eta(e)\,| \leq 3.0,$$
$$|\,M(ee) - M(Z)\,| \leq 5.0\text{GeV/c}^2 \text{ for a pair of electrons,}$$
$$20\text{GeV/c}^2 \leq \text{M}(\text{Z}^* \rightarrow \text{ee}) \leq 80\text{GeV/c}^2 \text{ for another pair of electrons.}$$

Half of the events pass these cuts. We expect 21 events for a standard SSC year. Clearly, higher luminosity, such as 10^{34} cm^{-2}sec^{-1} would be helpful. The potential problem is again a pile-up of up to 15 events at high luminosity. As mentioned above, it is important to require isolation within a ΔR cone of 0.1 or smaller. This isolation cut is also powerful for reducing Z+$b\bar{b}$ events, since leptons from b quark decays are not well isolated. Detailed simulation studies are in progress.

B: Heavy Higgs (300 GeV/c^2 to 800 GeV/c^2)

We consider here the cleanest signature for Higgs hunting: H→ZZ→ 4 leptons. The energy resolution of the TEXAS detector is $6.5\%/\sqrt{E} + 0.5\%$ for the EM calorimeter. Figure G1-7 shows the muon momentum resolution.

A study has been made of the trigger acceptance. Optimized geometrical/kinematic cuts for four leptons appear to be:

$|\,\eta(lepton)\,| \leq 3$

$E_T(l) \geq 20$ GeV

$P_{Total}(\mu) \geq 40$ GeV/c and $P_T(\mathbf{Z}) \geq 25$GeV/c.

The efficiency of these cuts is summarized in Table 4.

Table 4: Geometrical/Kinematic Cut Efficiency for Higgs Events

Higgs Mass	$\sigma \cdot$ BR [fb]	eeee	ee$\mu\mu$	$\mu\mu\mu\mu$
300	67.0	0.46±0.013	0.24±0.008	0.14±0.009
400	34.7	0.53±0.013	0.37±0.009	0.29±0.012
600	16.4	0.64±0.012	0.57±0.009	0.51±0.013
800	7.6	0.72±0.012	0.66±0.009	0.61±0.013

For the standard SSC luminosity, the total number of events produced and the number of events that trigger the detector are shown in Table 5.

Table 5: Number of Events Triggering Detector in Standard Year

Higgs Mass	N_{total}	$N_{trigger}$		
		eeee	ee$\mu\mu$	$\mu\mu\mu\mu$
300	670	76	82	26
400	347	46	64	25
600	164	26	46	21
800	77	14	25	13

Table 6 shows the detection efficiency for Z's for a reconstructed mass cut of $\pm$ 15 GeV/c^2 (76 to 106 GeV/c^2). No other kinematic or geometrical cuts are applied. The errors are statistical.

Table 6: Detection Efficiency for Z's in Higgs Events

Physics	Z $\rightarrow$ ee	Z $\rightarrow$ $\mu\mu$
H=300	1.00	0.67$\pm$0.006
400	1.00	0.71$\pm$0.006
600	1.00	0.70$\pm$0.006
800	1.00	0.67$\pm$0.006
ZZ continuum	1.00	0.53$\pm$0.003

Clearly, at this stage of our simulations we should make a tighter cut on the Higgs mass for the 4e mode, and perhaps a loosercut on the 4μ mode. The reconstructed mass distribution for Z$\rightarrow$ee and for the 400 GeV/c^2 Higgs is shown in Figure G1-8. The total momentum distribution for the 4μ mode is shown in Figure G1-9; it is important for the optimization of the design of the muon TRD.

The statistical significance (SS) of a fluctuation of the total number N ($=B+S$) of events above the fitted background (B) to give a signal (S) is defined as

$$SS = (N - B)/\sqrt{N}\,.$$

N, B and SS values for each decay mode and mass are tabulated below:

Table 7: Expected Number of Higgs Events

Higgs Mass	eeee			ee$\mu\mu$			$\mu\mu\mu\mu$			Combined		
	N	B	SS	N	B	SS	N	B	SS	N	B	SS
300	47	13.7	4.8	43	9.3	5.1	12	2.3	2.5	100	25.3	7.5
400	27	5.8	4.0	35	6.2	4.8	12	2.0	2.9	74	14.0	6.9
600	17	4.1	3.2	23	3.4	4.0	8	0.9	2.4	47	8.3	5.6
800	12	4.4	2.0	13	3.6	2.6	5	1.3	1.6	29.5	9.4	3.7

The results shown in the above table include a uniform lepton identification efficiency due to cuts on isolation, hadronic to electromagnetic ratio, position matching, etc. Using the experience of CDF, we assume an efficiency of 85% per lepton to make a realistic decision. The efficiency for all four leptons has therefore been taken to be 0.52 ($= 0.85^4$) in the results of Table 7.

From the table, we conclude the following:

1. A heavy Higgs, up to a mass of 600 GeV/c^2, can be seen independently in two four-lepton modes, eeee and ee$\mu\mu$.
2. For the 4μ mode, the current high P_{Total} threshold degrades the Higgs detection efficiency; conversely, the background reduction power is large. We are therefore simulating the dE/dx measurements in both the calorimeter and in the muon TRD to exploit a lower P_{Total} cut. Nevertheless, after two standard years of integrated luminosity of 2×10^{40} cm^{-2}, the 4μ signal would be significant for the full mass range between 300 and 600 GeV/c^2.
3. A heavy Higgs with a mass of 800 GeV/c^2 could be found by combining all three modes at $\mathcal{L} = 10^{40}$ cm^{-2} to obtain 30 signal events.

The expected mass distribution for a 400 GeV/c^2 Higgs decaying to 4e (2e 2μ) after all cuts is given in Figures G1-10(11) for M(top) = 120 GeV/c^2. In conclusion, in one standard SSC year a Higgs with mass between 300 and 800 GeV/c^2 could be discovered using the TEXAS detector. With a luminosity of $\mathcal{L} = 10^{34}$cm^{-2}s^{-1} the measurement of the $H \rightarrow ZZ$ branching ratio would become significant.

For a very massive Higgs, we run out of rate (especially at $\mathcal{L} = 10^{33}$ cm^{-2} s^{-1}) into the 4-lepton channels. For this reason, we must turn to the larger branching fractions available in $H \rightarrow ZZ \rightarrow ee\nu\nu$ and $H \rightarrow ZZ \rightarrow eejj$. The signal-to-noise ratio in each of these channels is a strong function of detector performance parameters, with an emphasis on hermeticity for the neutrinos and hadronic energy resolution and fine segmentation for the jets. Our simulation work on these channels is still in its preliminary stages, and we still must do careful studies of backgrounds with high statistics. All the tools are now in place for this work, but we have been limited by the time and computer power available since EOI submission.

Our preliminary studies of the signals in these channels are nonetheless promising. Figure G1.12 shows the invariant mass reconstruction of an ISAJET Z (generated with zero width, so that the displayed width is entirely from reconstruction errors) from $H \rightarrow ZZ \rightarrow eejj$ for an 800-GeV Higgs. The cluster-finding algorithm used $R \leq 0.5$ and the fine segmentation at large radius of the TEXAS calorimeter to resolve the narrow opening angle between the jets from the decay of high-P_T Z's. This study will explore the sensitivity of the Z reconstruction from 2 jets as a function of calorimeter segmentation, radius, resolution and speed.

For both the neutrino and the jet decays of Z's from very massive Higgs bosons, there are several other experimentally accessible cuts which can improve the signal-to-noise ratio. One is to use the quark-jet tagging signature which is discussed in section T5. Another is illustrated in Figure G1.13. The Z's which are produced in the decays of a very massive Higgs tend to be nearly equal in P_T, since they are produced back-to-back in the Higgs rest frame. This is in contrast to continuum production of pairs of Z bosons, where the production cross section is heavily skewed toward smaller P_T. (One high-P_T Z is required to produce a large invariant mass for the ZZ system.) This points out the need for precise measurement of missing P_T in the neutrino channel, and we will exploit this characteristic in our simulations of the hermetic TEXAS calorimeter.

REFERENCES

1. For recent discussions, see J. Gunion and G. Kane, contribution to Snowmass '90 proceedings.
2. C.-P. Yuan and G. Kane, private communication.
3. G.P. Melese and G. Russack, private communication.
4. Experimental result of SPACAL in test beams, R. DeSalvo, private communication.
5. Barter *et al.* in Snowmass '88.
6. R. Partridge, contributions to Snomass '90 proceedings.

FIGURE CAPTIONS

G1.1 Potential for separation of the 2 γ's of a 75 GeV π^0 in the TEXAS imaging preradiator, shown in actual size.

G1.2 Effects of detector smearing on the invariant mass peak in the $\gamma\gamma$ decay of a 150 GeV Higgs. The dots reflect the size of the interaction diamond. The dashed line is the actual expectation that exploits the TEXAS capability to reconstruct the γ direction.

G1.3a Transverse energy distribution of the QCD direct-photon background.

G1.3b Transverse energy distribution of photons from the $H \rightarrow \gamma\gamma$ signal, for $M_H = 150\text{GeV/c}^2$.

G1.4 Background-subtracted M($\gamma\gamma$) signal for various indicated Higgs masses.

G1.5 Partridge's results for the $H \rightarrow \gamma\gamma$ hunt in TEXAS, for a standard 1 year running at the SSC.

G1.5a Partridge's results for various characteristics of the accepted $\gamma\gamma$ signals. Clockwise from upper left: Transverse energy, gamma pseudorapidity, digamma pseudorapidity and center of mass opening angle.

G1.6 Sensitivity to the cut in ΔR around the observed photons, as a function of transverse energy.

G1.7 Muon momentum resolution, discussed in the TEXAS EOI.

G1.8 Effect of calorimetric resolution on the reconstruction of a $Z \rightarrow ee$ peak in the $H \rightarrow ZZ$ decays of a Higgs of mass 400 GeV/c^2.

G1.9 Total momentum distribution for muons in the $H \rightarrow ZZ \rightarrow 4\mu$ decay chain of a 400 GeV/c^2 Higgs.

G1.10 Reconstruction of the invariant mass of an 800 GeV/c^2 Higgs in its $H \rightarrow 4\mu$ decay, for a one year run at high luminosity.

G1.11 Same as G1.10 in the $H \rightarrow 2e2\mu$ channel.

G1.12 Invariant mass reconstruction for $Z \rightarrow jj$, from $H \rightarrow ZZ \rightarrow eejj$, for an 800 GeV/c^2 Higgs.

G1.13 Momentum balance for the two Z's in the decay $H \rightarrow ZZ$ of an 800 GeV/c^2 Higgs. The abscissa is the ratio of the reconstructed transverse momentum of the lower-p_T Z to that of the higher-p_T Z.

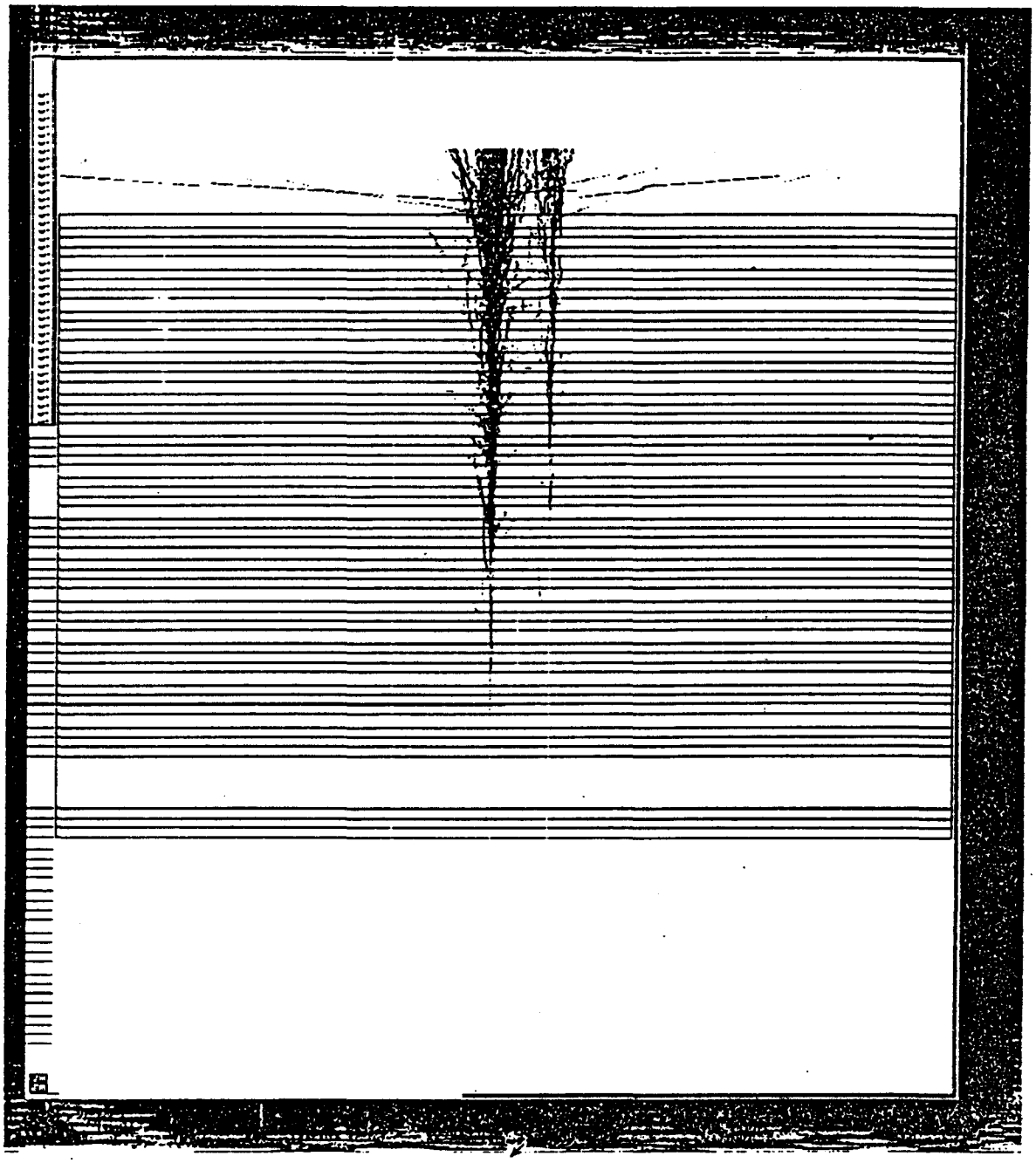

Figure G1.1

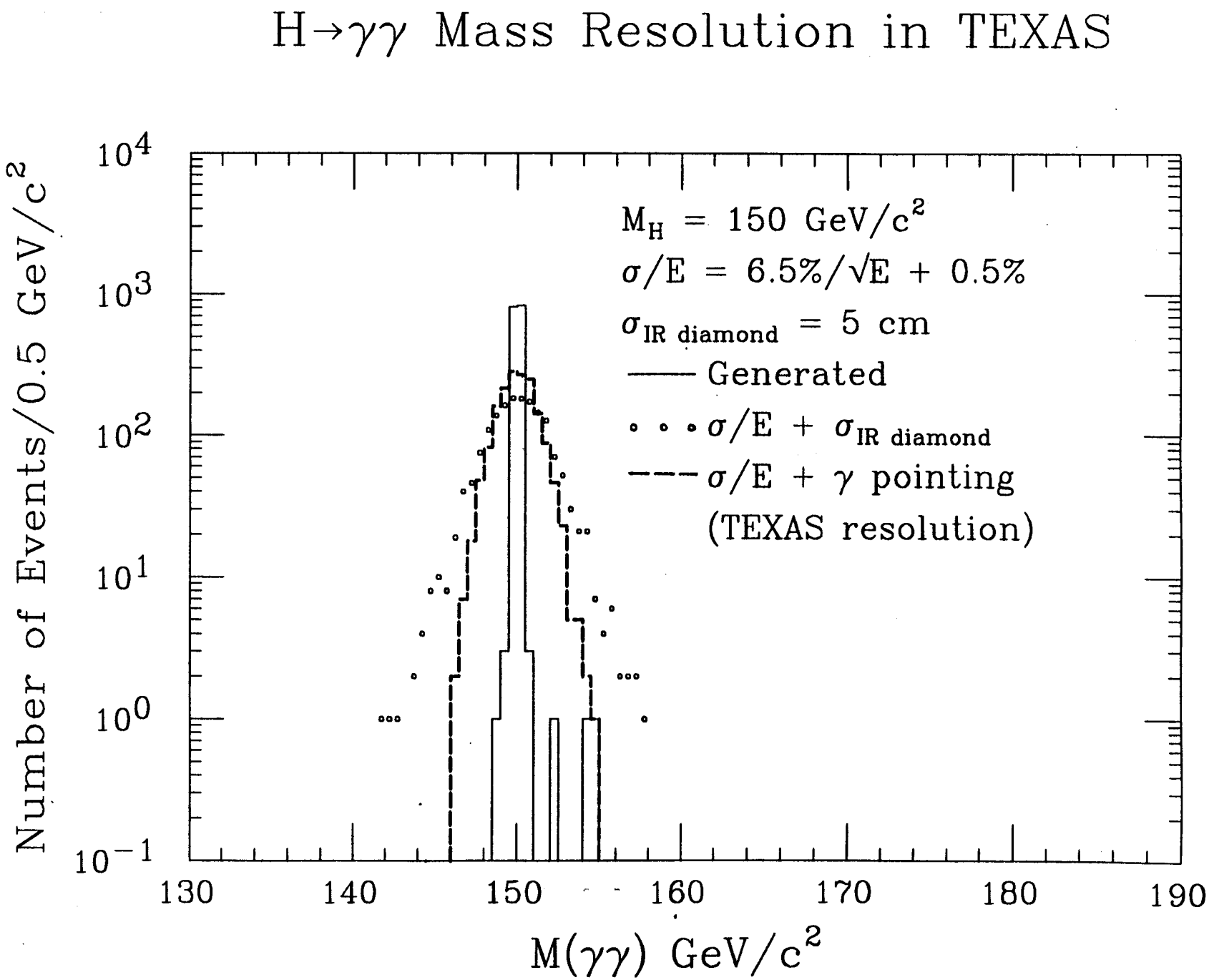
H→γγ Mass Resolution in TEXAS
M_H = 150 GeV/c^2
σ/E = 6.5%/√E + 0.5%
$\sigma_{IR\ diamond}$ = 5 cm
Generated
σ/E + $\sigma_{IR\ diamond}$
σ/E + γ pointing
(TEXAS resolution)
Number of Events/0.5 GeV/c^2
M(γγ) GeV/c^2
10^4
10^3
10^2
10^1
10^0
10^{-1}
130
140
150
160
170
180
190

Figure G1.2

E_T Distribution of γ for $H \rightarrow \gamma\gamma$.

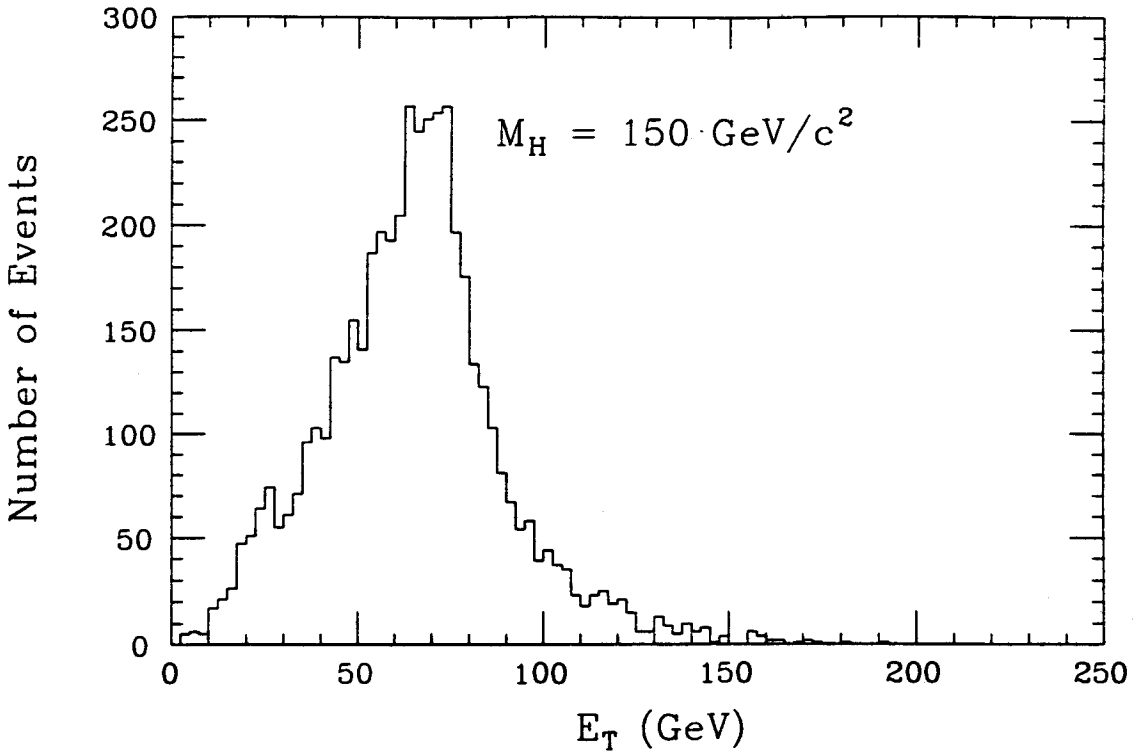

Figure G1.3a

E_T Distribution of γ for QCD $\rightarrow \gamma\gamma$

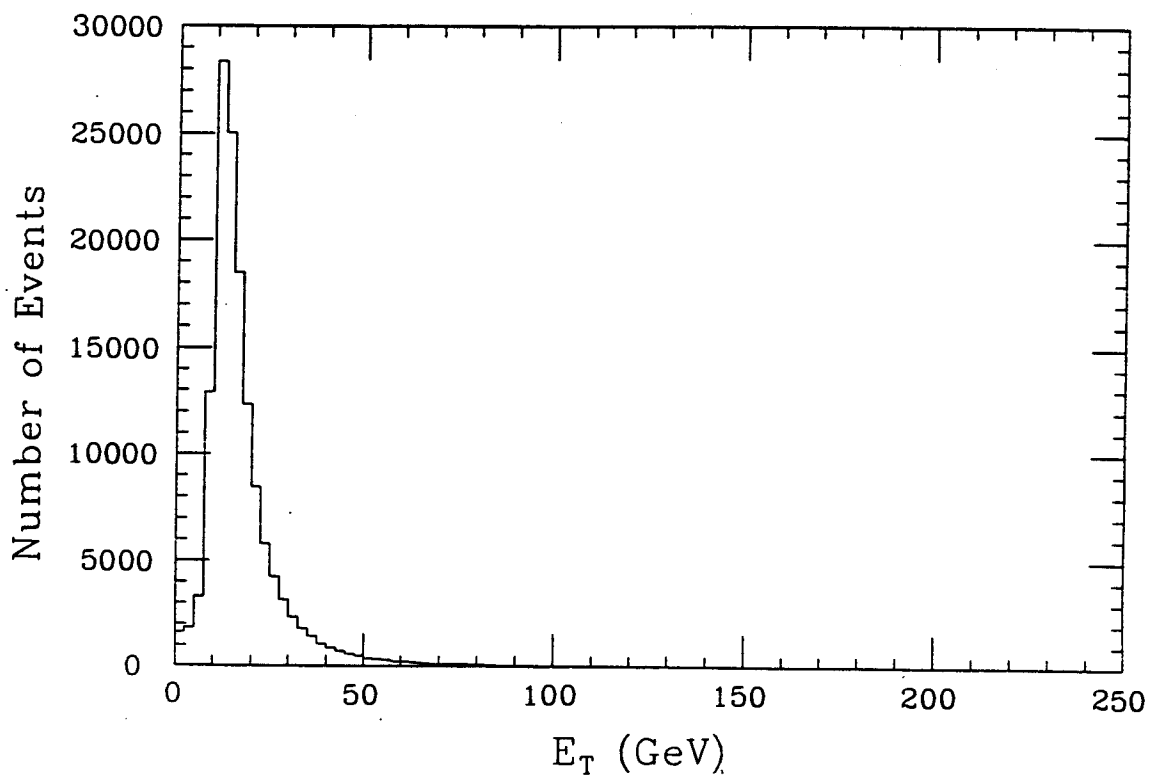

Figure G1.3b

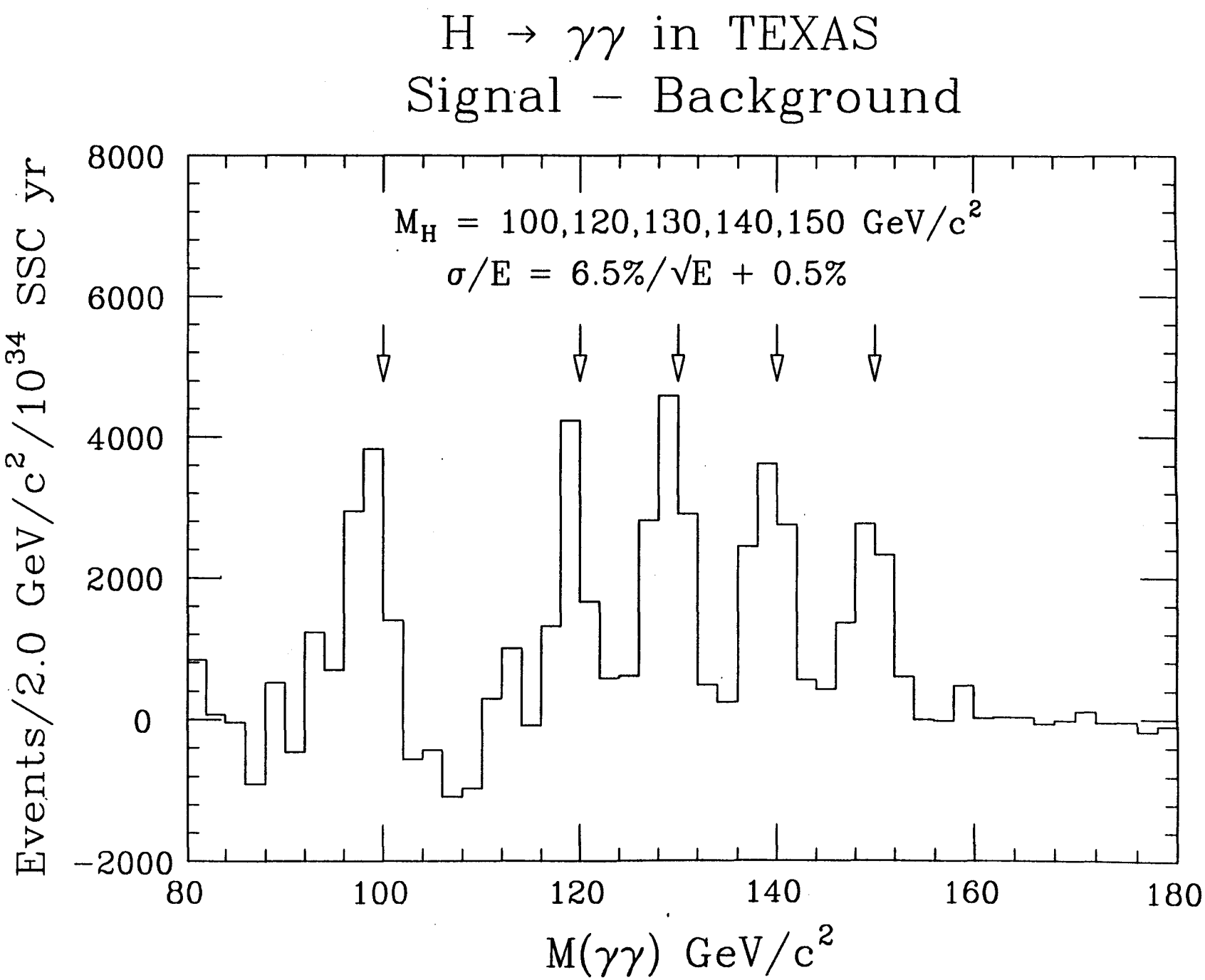
H → γγ in TEXAS
Signal − Background
M_H = 100,120,130,140,150 GeV/c²
σ/E = 6.5%/√E + 0.5%
Events/2.0 GeV/c²/10³⁴ SSC yr
8000
6000
4000
2000
0
−2000
80
100
120
140
160
180
M(γγ) GeV/c²

Figure G1.4

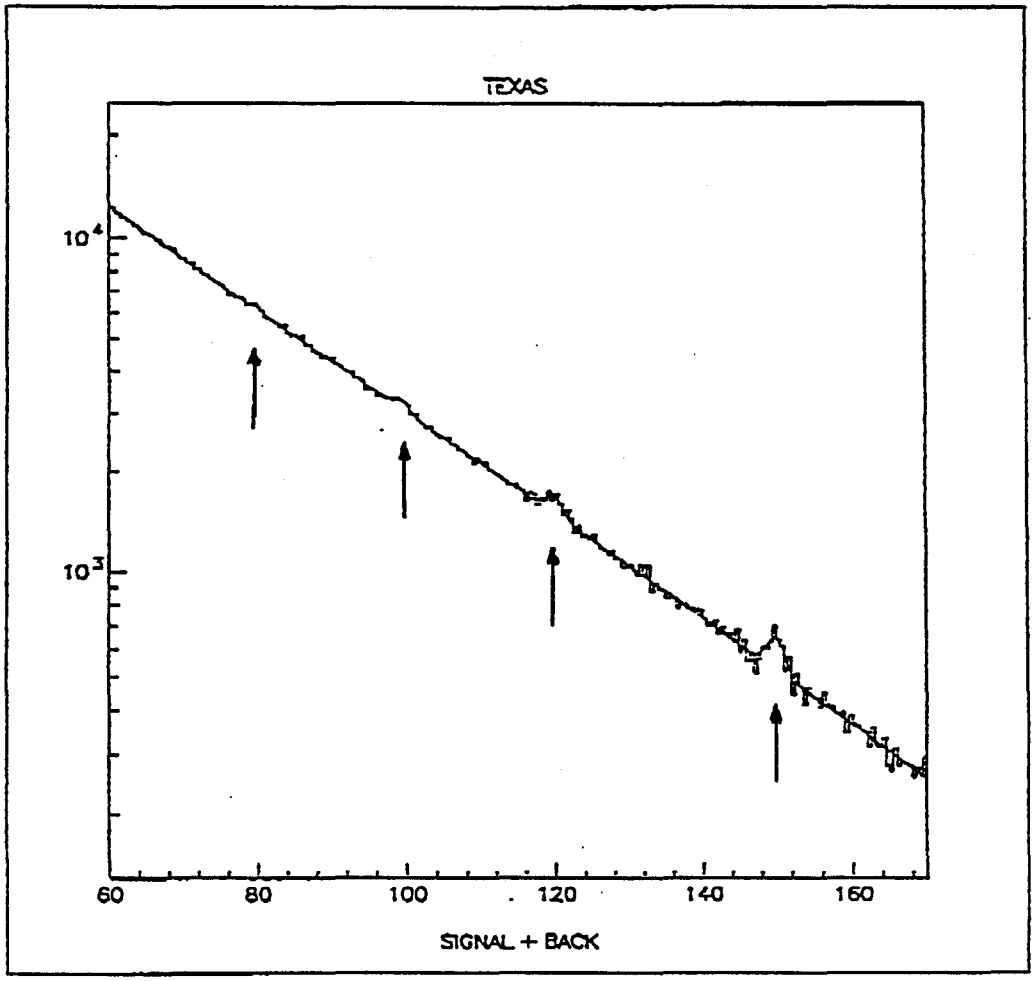

Figure G1.5

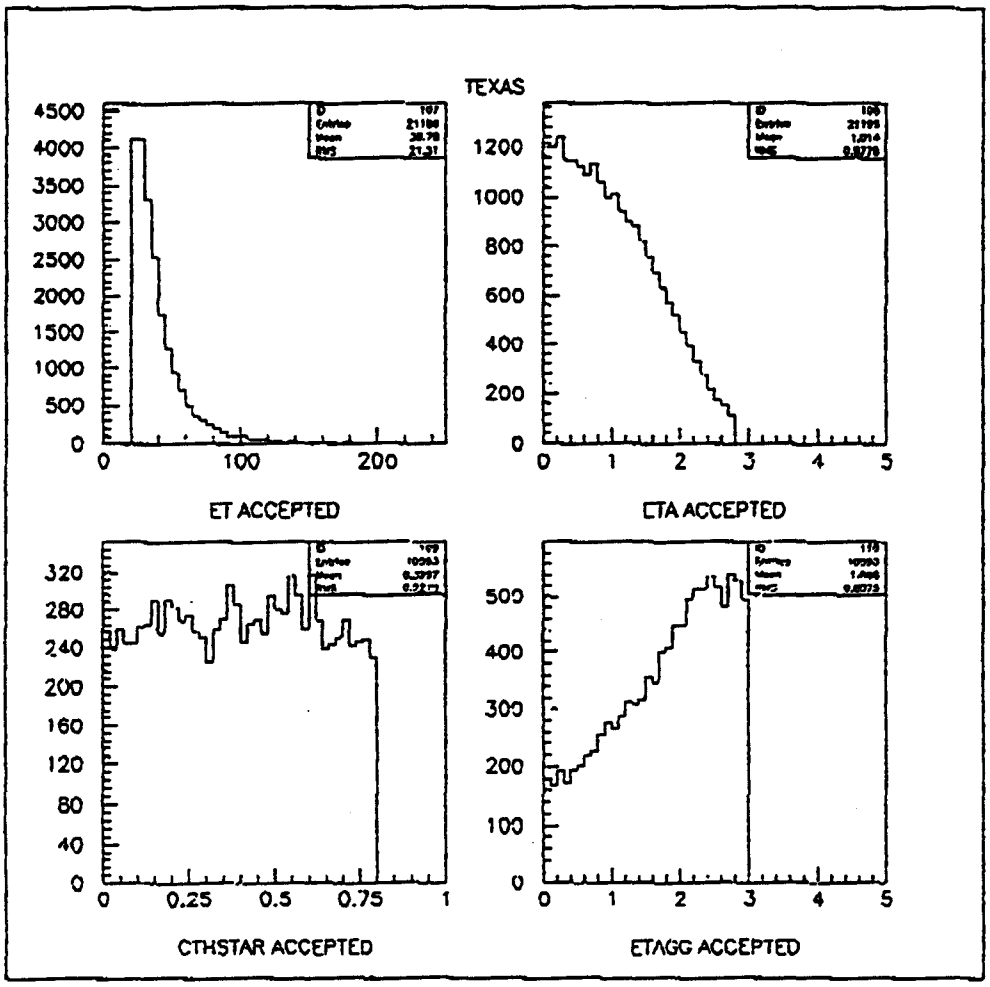
TEXAS
ET ACCEPTED
ETA ACCEPTED
CTHSTAR ACCEPTED
ETAGG ACCEPTED

Figure G1.5a

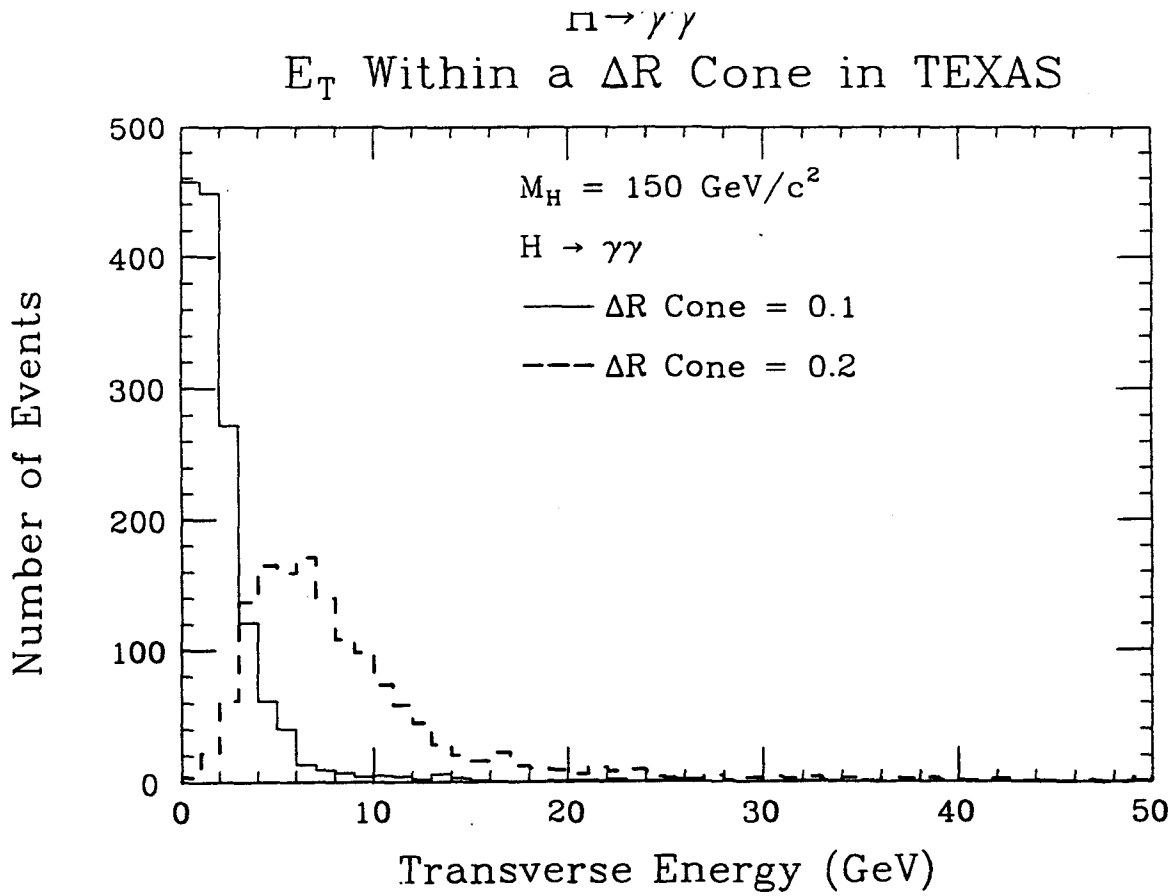

Figure G1.6

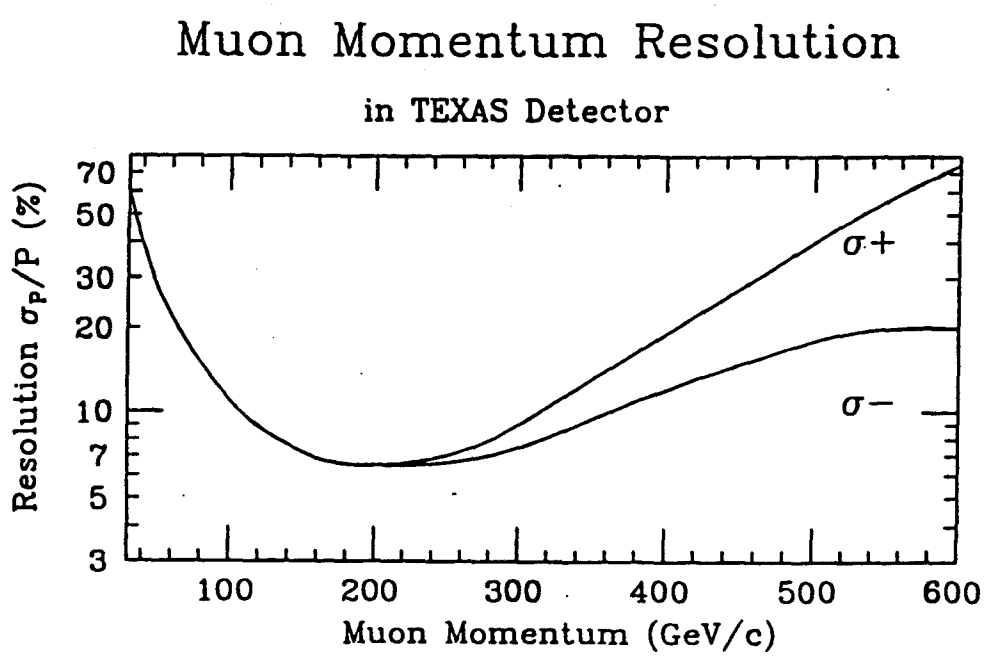

Figure G1.7

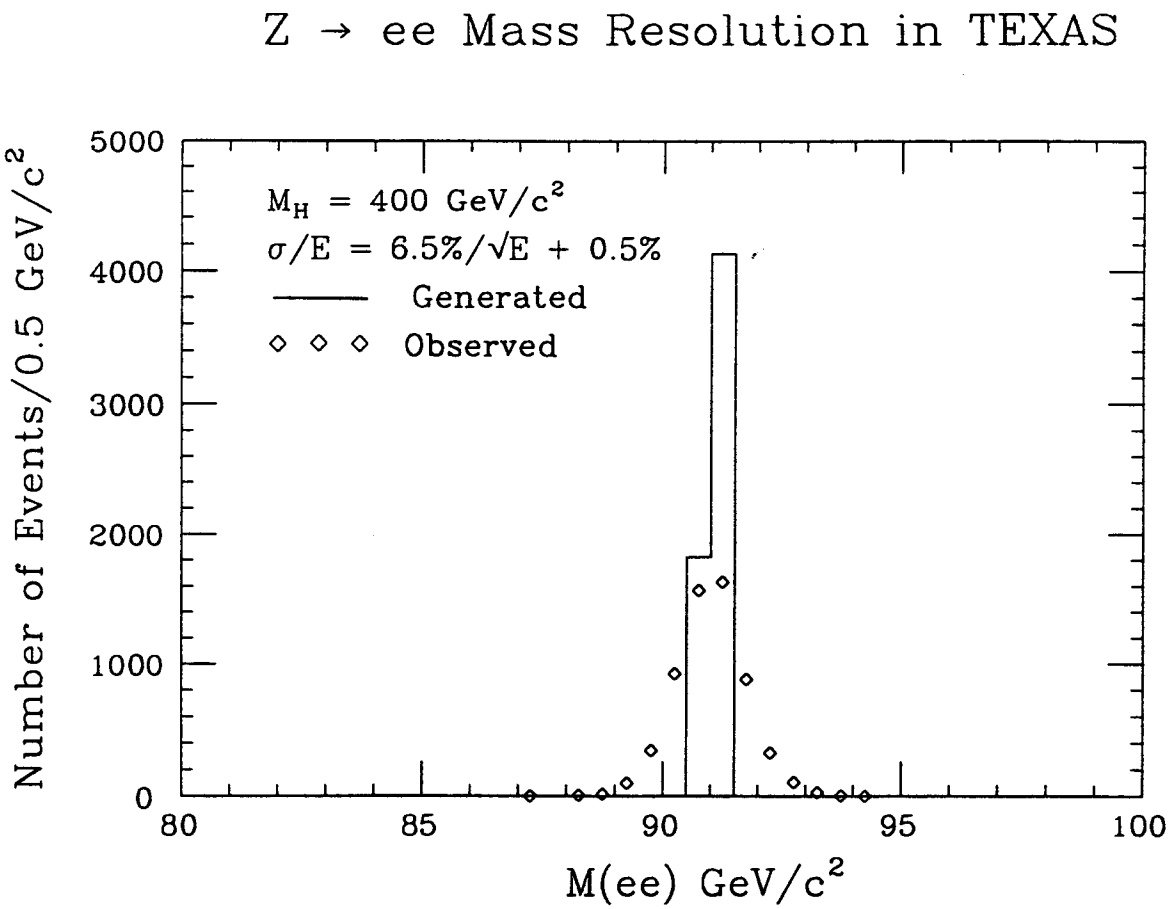

Figure G1.8

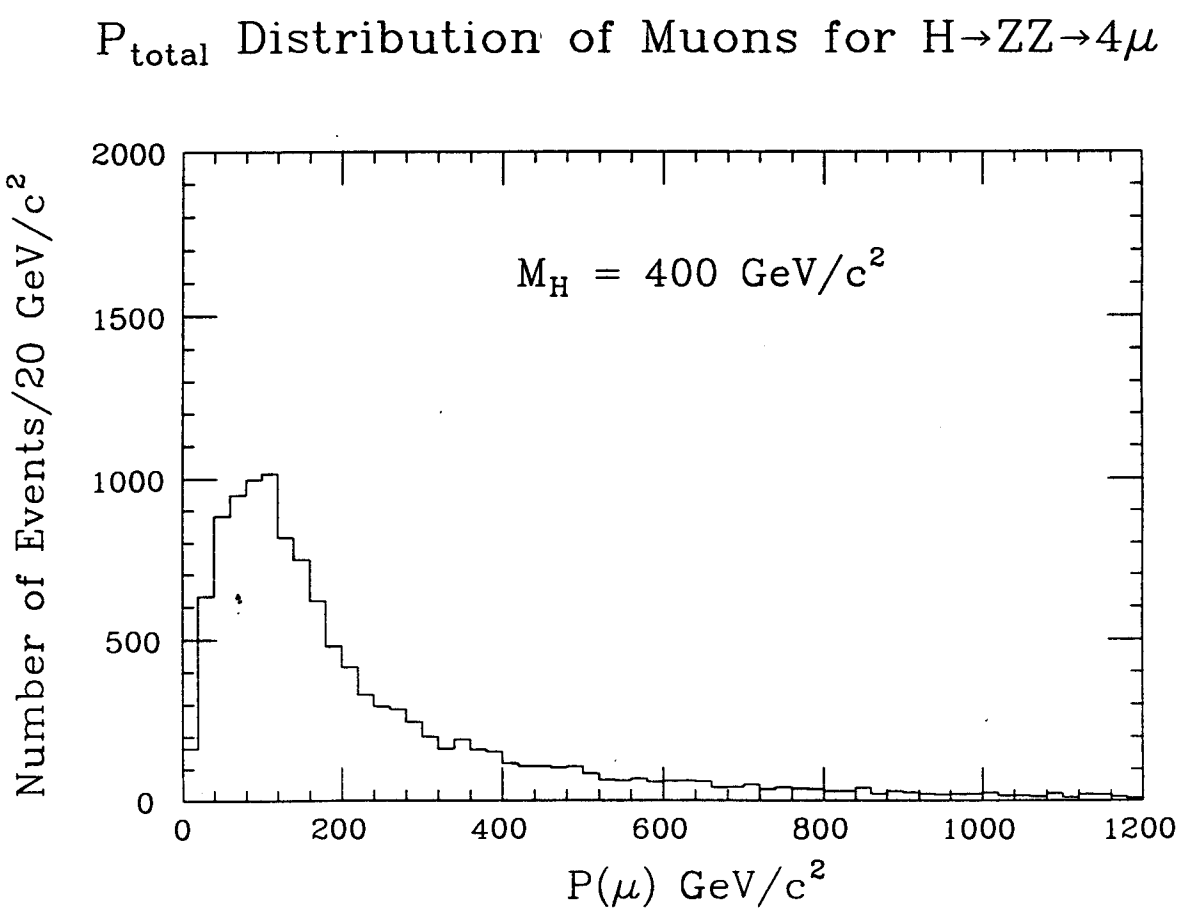

Figure G1.9

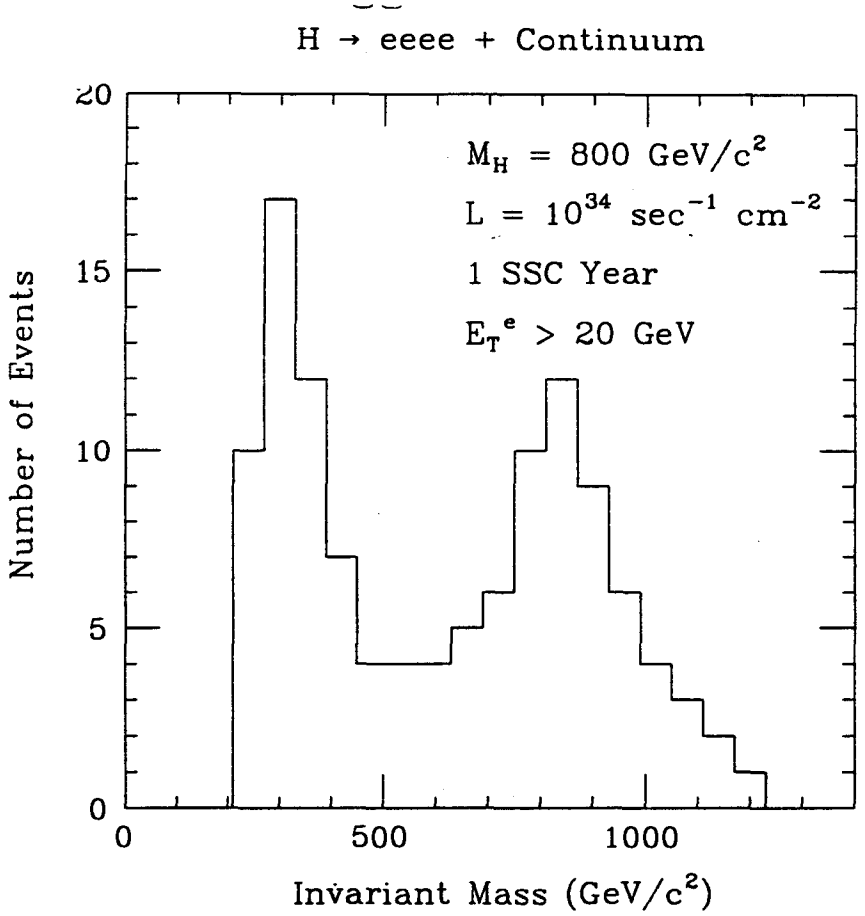

Figure G1.10

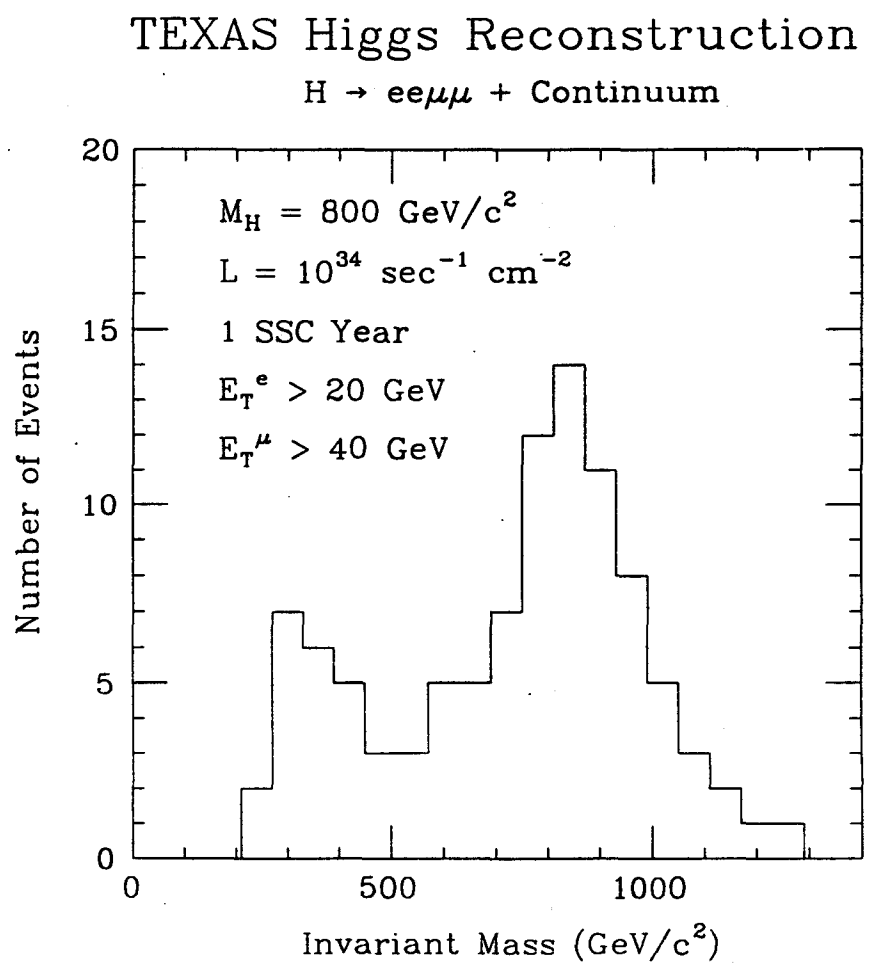

Figure G1.11

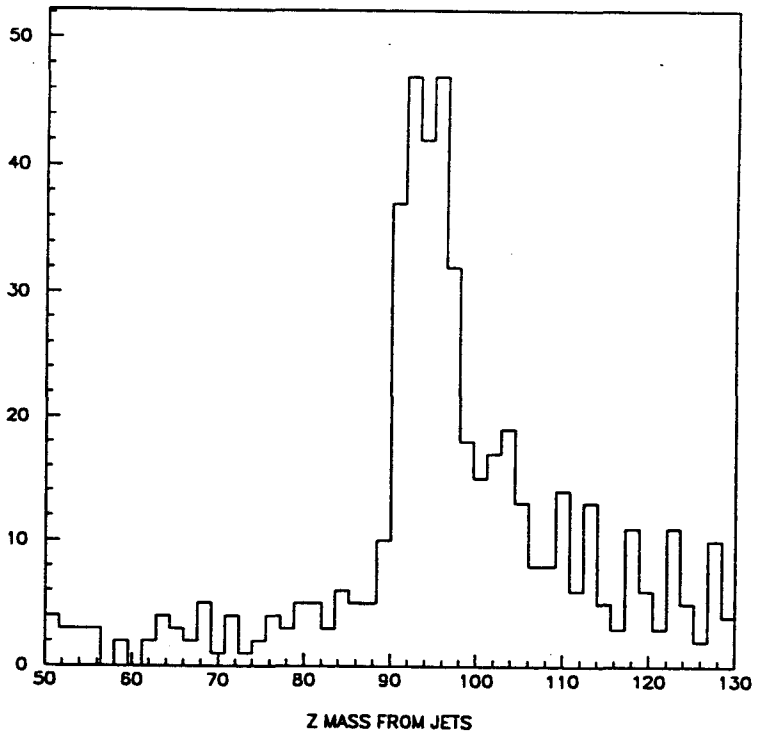

Figure G1.12

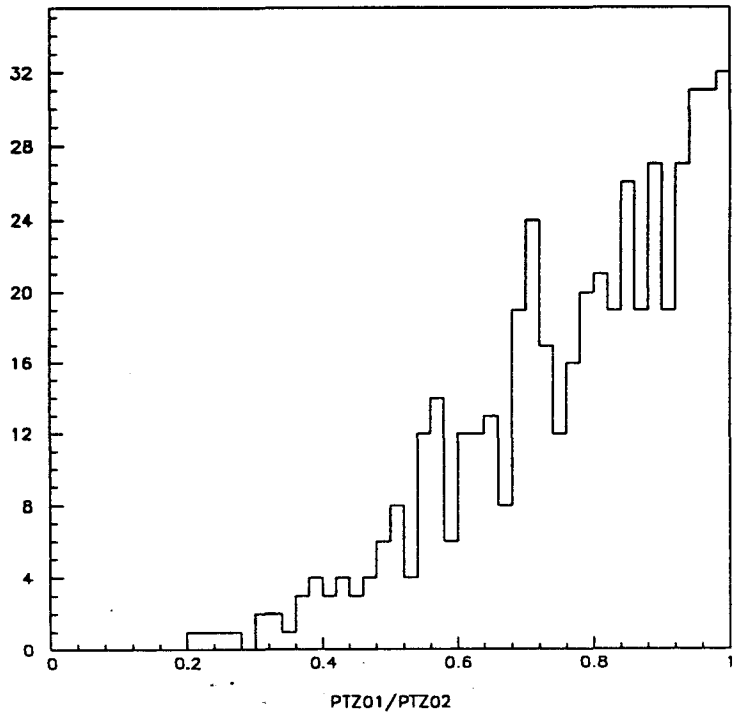

Figure G1.13

G2: Quark Compositeness and E_T Measurements

With a view to studies of quark compositeness, what are the systematic errors on the measurements of the inclusive jet cross section as a function of E_T?

The limits on compositeness are given by the ability to generate a perfectly linear and Gaussian response to jet energy deposition. The SPACAL group has shown that e/h can be tuned to 1.00 within 1%, which essentially guarantees the Gaussian response of the calorimeter. A study by Geoffrey Fiorden, U. of Arizona, (reported at the Tucson Meeting on SSC Detectors in Feb., 1990) showed the systematics of e/h on jet energy resolution up to 5 TeV. If e/π is 1.0, there is essentially no systematic error in the jet resolution up to 5 TeV E_T from the calorimeter response. Fig. G2.1 shows the linear single particle response for $e/\pi = 1$, giving $\frac{E_{response}}{E_{incident}} = 1$, independent of energy. This single particle response is folded into a jet energy Monte Carlo. A compensating calorimeter response is linear in jet energy, as shown in Fig. G2.2. The systematic error on the jet energy from calorimeter physics is therefore negligible, and less than 0.2% for a calorimeter with $|e/\pi - 1| \leq 0.01$.

The systematic effects will therefore be limited by statistics, and by instrumental effects such as phototube and electronic linearity and fiber attenuation (each of which may give an energy-dependent effect). Since the effective fiber attenuation will be greater than 5 m, and the showers grow only like log E, this effect is less than 1%. The effect from the photomultiplier linearity is serious but can be controlled. The recent results from a test of a hybrid diode anode phototomultiplier tube (Fig. G2.3) made by DEP for R. DeSalvo and the LAA project at CERN have shown linearity over 3.5 orders of magnitude, see Fig. G2.4. The costs of this type of tube will be no more than for normal PMTs in quantity, because the dynode cost in a typical PMT is about 20% of the cost of the tube, or \$20-\$30. Typical large area fast Schottky diodes with a depletion region thickness of 10 microns cost about \$10 a piece in the quantity we would need.

Compared with the SDC detector group, which accepts non-Gaussian tails, the limitations on compositeness in TEXAS may reach $\Lambda = 50$ TeV, at a luminosity of $10^{34}\text{cm}^{-2}\text{s}^{-1}$, producing 100 events in excess of the QCD background at an E_T of 5 TeV.

There are a number of non-standard top decays one can look for. One possibility involves flavor-changing neutral currents, a possible signature of walking technicolor. A 250 GeV top quark may decay into c and a real Z, which can as usual be detected via its decay to lepton pairs. The signature is then a 91 GeV lepton pair plus a jet, adding up to the top quark mass, opposite a top tag. The major background is Z plus jets, with a negligible 50 pb cross section. With the constraint of the top quark mass, and suitable cuts, the accidental backgrounds could be reduced to a very low level, and a signal of a few 10's of events could be detected in a year's running, giving an accessible branching ratio of

$$BR(t \to Zc) \sim 0.1\%.$$

There is no known background that would produce a peak at the top quark mass for the Z plus one jet combination. Again, because this signal produces a mass peak, a luminosity of $10^{34}\mathrm{cm}^{-2}\mathrm{s}^{-1}$ would triple our sensitivity.

Figure Captions

G3.1. P_t spectrum for leptons from top quark decays.

G3.2. Mass spectrum of dijet masses reconstructed opposite a lepton tag in the top events. The UA.1 jet finding algorithm is used; jets are required to have 15 GeV of energy in a ΔR cone of 0.7. All combinations of the three highest energy jets in the opposite hemisphere are used. This reconstruction clearly gives less than the W mass.

G3.3. Mass spectrum of W candidates (in a 40-100 GeV mass range) combined with the third jet in an event. The combination is required to have a momentum of at least 30 GeV. The broad peak from 100-200 GeV is from the top.

G3.4. Mass spectrum of dijet masses reconstructed opposite a lepton tag in events of the form $pp \rightarrow t\bar{t}$, $t \rightarrow e\nu b$, $\bar{t} \rightarrow H^+b$, $H^+ \rightarrow c\bar{s}$, using the same analysis as in Figure G3.2. Only the two highest jets in this event are selected here.

G3.5. Mass spectrum of top candidates reconstructed using the Higgs in Figure G3.3, and adding a third highest energy jet opposite the lepton tag.

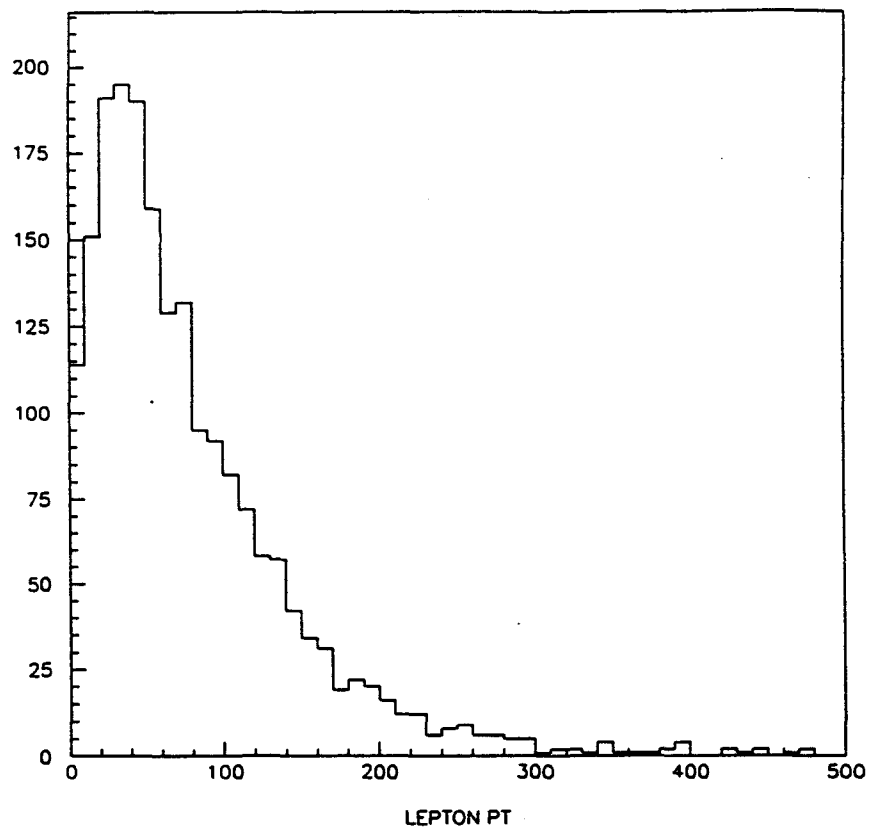

Figure G3.1

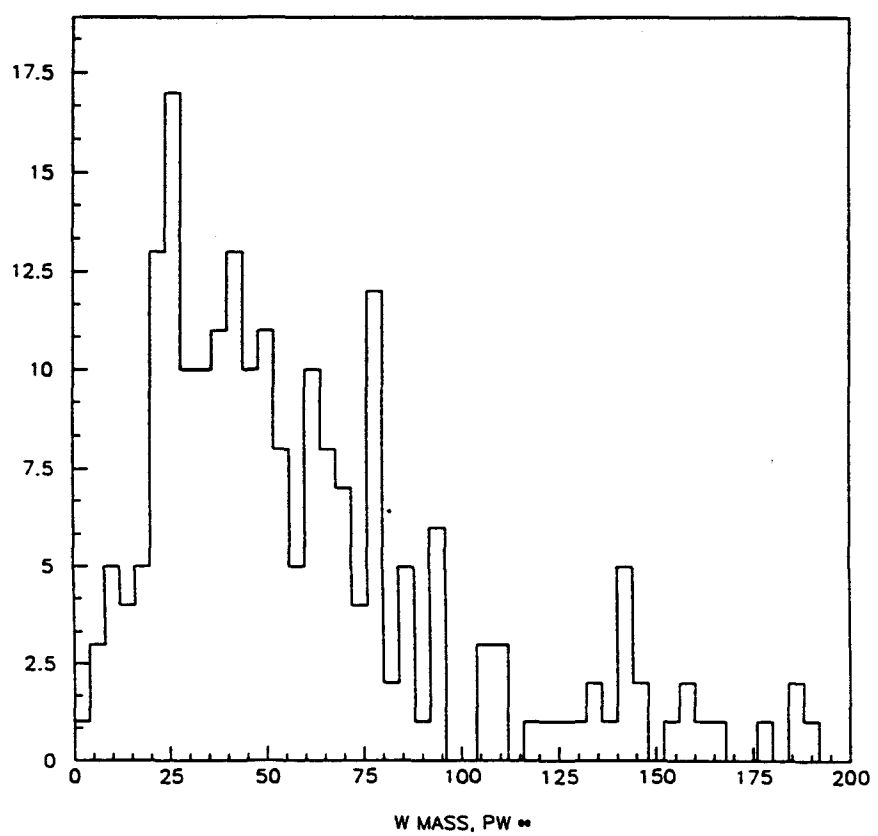

Figure G3.2

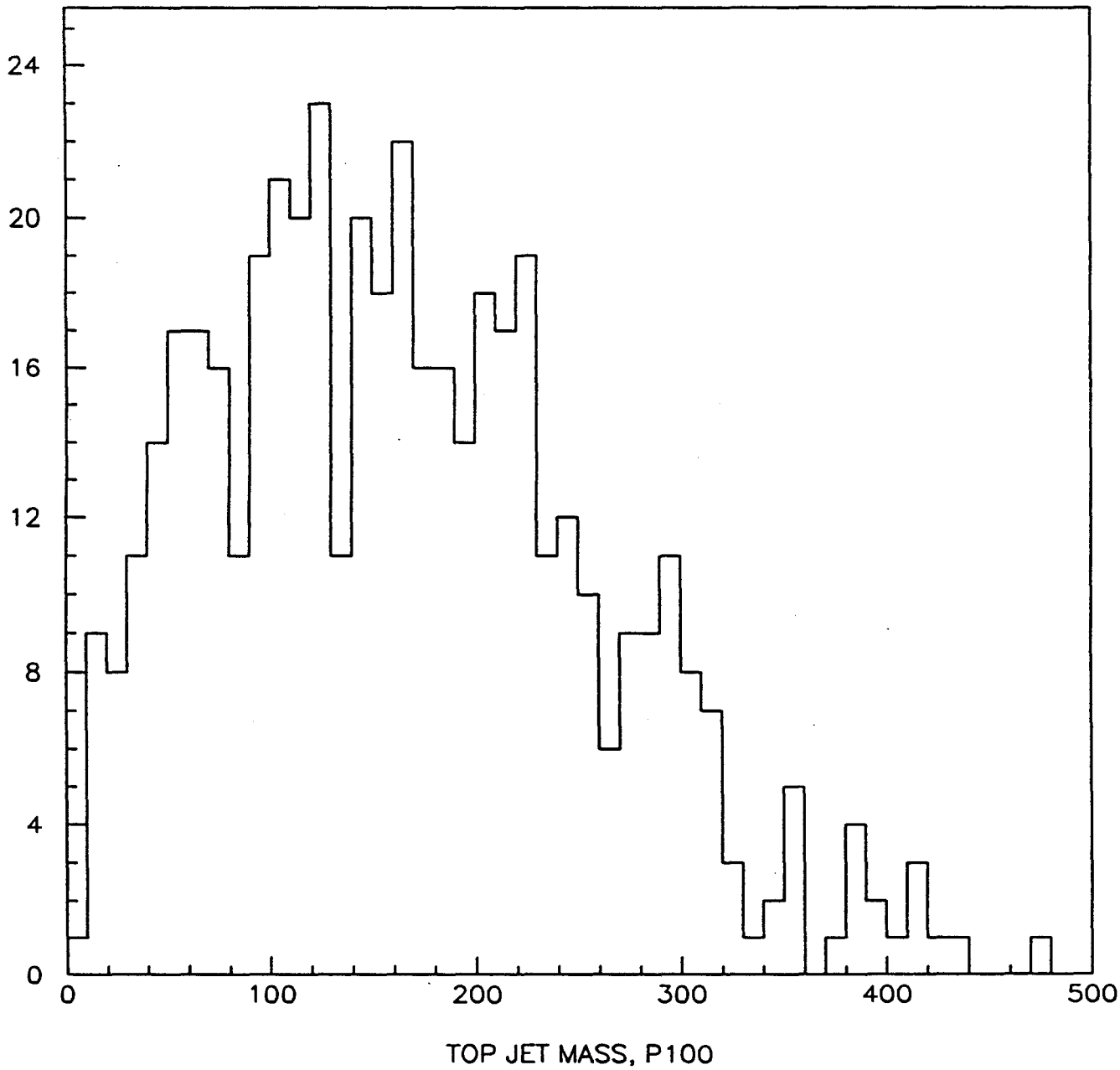

Figure G3.3

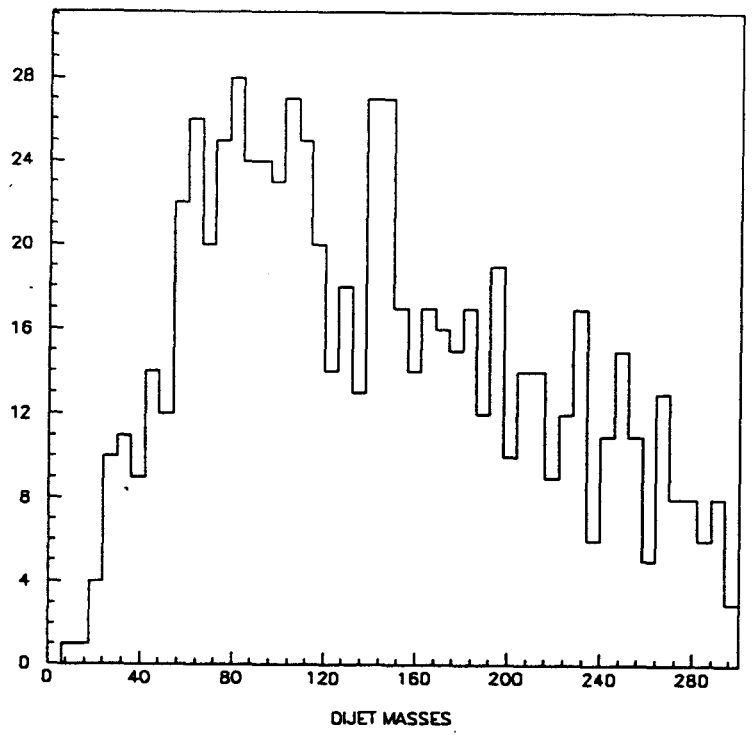

Figure G3.4

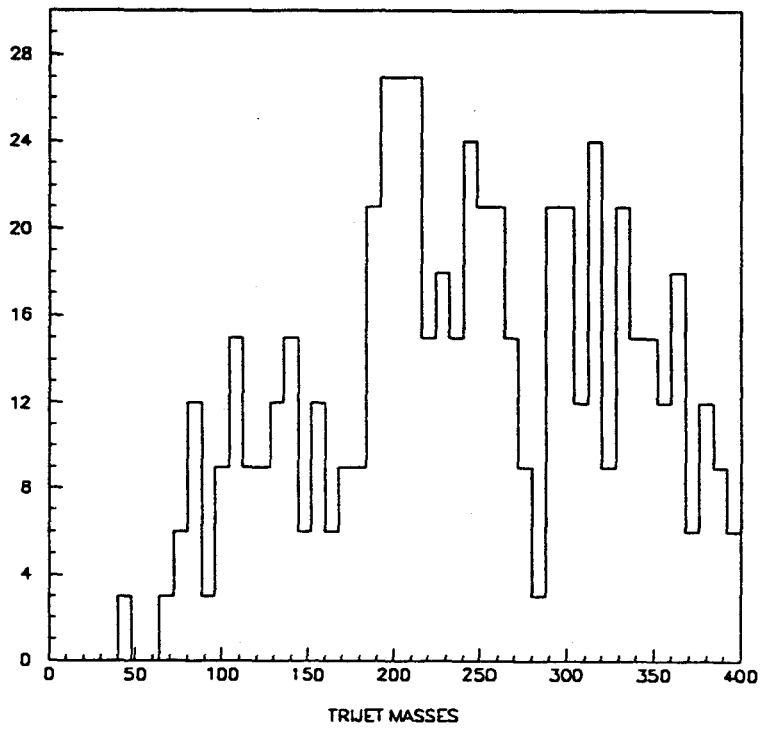

Figure G3.5

G4: Missing E_T Searches

The committee is interested in better understanding the missing E_T capability of the detector. Please address the discovery capability for:

- *A 400 GeV fourth generation quark decaying into W+b.*

Our strategy in a search for a t' quark decaying to Wb is the same as for the top quark search described in the answer to an earlier question; the main differences are the higher mass and the t-induced backgrounds. At 400 GeV, the cross section is about 300 pb, corresponding at $\mathcal{L} = 10^{33}$ to about 3×10^6 $\overline{t'}t'$ pairs per SSC year. The (m_t= 150 GeV) top quark production rate is 10 times higher. To reduce the t-background, stringent lepton-momentum cuts must be used. For a $p_T > 400$ GeV lepton cut, the signal to noise ratio is about 1:4. Adding a missing energy cut of $E_{miss} > 200$ GeV will raise this S/N to roughly 1:1. At this stage, we would proceed along the lines of the top analysis, looking for a W plus a third jet to reconstruct the 400 GeV object.

The missing energy spectrum expected for TEXAS is shown in Figure G4.1. For this analysis, the detector smearing plays a minor role. The major background is from $t \rightarrow c\,W(\rightarrow l\nu)$. The missing energy carried by these neutrinos smears out the detector-resolution effects.

As with the 250 GeV top quark, rare decays of the new quark could be detected by tagging one side of the event, and looking for a rare decay on the other.

- *A 300 GeV gluino*

Since supersymmetry has such a large parameter space, we have had to make some assumptions in answering this question. To begin with, we have assumed that the gluino is lighter than the squark; otherwise we would presumably be asked to look for the lighter squark. With this proviso, the gluino decays to any of a number of charged SUSY states, which then decay through any of a variety of cascades. The major salient feature is that these decays will eventually end with the production of the lightest supersymmetric particle (LSP), most likely the photino. Since this LSP is non-interacting, the major signature is missing energy, with the average amounts depending on the exact masses and branching ratios.

To detect this missing energy, an extremely hermetic detector is needed. TEXAS has two holes in it. The major one is for the beampipe; those regions with $|\eta| > 5.5$. This hole is unavoidable; at larger η, the energy deposited by the beam becomes immense, and radiation damage becomes intolerable. The other hole is a crack at $\eta = 0$, with width less than ±0.05. This hole is needed to bring out the signals from the inner tracker. It will likely be lightly instrumented to detect the presence of jets, even if their energy cannot be measured. In any case, this crack is narrow enough that a jet passing through the middle will deposit significant energy on both sides of the crack. Although the energy would not be accurately known, these events could be easily vetoed in missing energy searches. Since the muon system will also cover this crack, the only possible problem is with electrons. Since these elecrons are likely to be detectable through the simple counters mentioned above, and since most high p_T electrons are from W's, the event is likely to already have significant missing energy, and we do not view this crack as a significant problem.

Since our simulations of these processes have been done on a parton level (with calculations kindly provided by M. Barnett) we have not simulated the crack at $\eta = 0$. Instead, we have concentrated on the beam-pipe hole. The simulation results are shown in Figure G4.1. The curve in G4.1(a) shows the losses due to the beam hole; the solid histogram in G4.1(b) gives the expected signal from the chosen gluino model seen towering over the major physics background (from the semileptonic decay of a 150 GeV top). The other significant physics background is from the process $pp \rightarrow Z + 3j, Z \rightarrow \nu\nu$; it is the lowest histogram, shown with a dot-dashed line in G4.1(b). A cut on event sphericity is applied to reduce the background from top events; otherwise top decays would dominate the plot and hide possible new physics. Since the plot begins at 100 GeV of missing energy, the detector resolution plus hole contribution is not even visible on the plot. The major point to be made here is that above 100 GeV missing energy, physics backgrounds are dominant over detector contributions.

Figure Captions

G4.1 (a) Missing energy due exclusively to the holes in the endcaps. Notice that the effect vanishes before 100 GeV. Losses due to the crack at $\eta = 0$ are not simulated; events with energy spread across the crack would be vetoed, leaving the missing energy spectrum unaffected. (b) Missing energy distributions above 100 GeV. The solid histogram shows the expected gluino signal and the dotted and dashed curves are backgrounds.

Effect of Beam Hole Losses in TEXAS

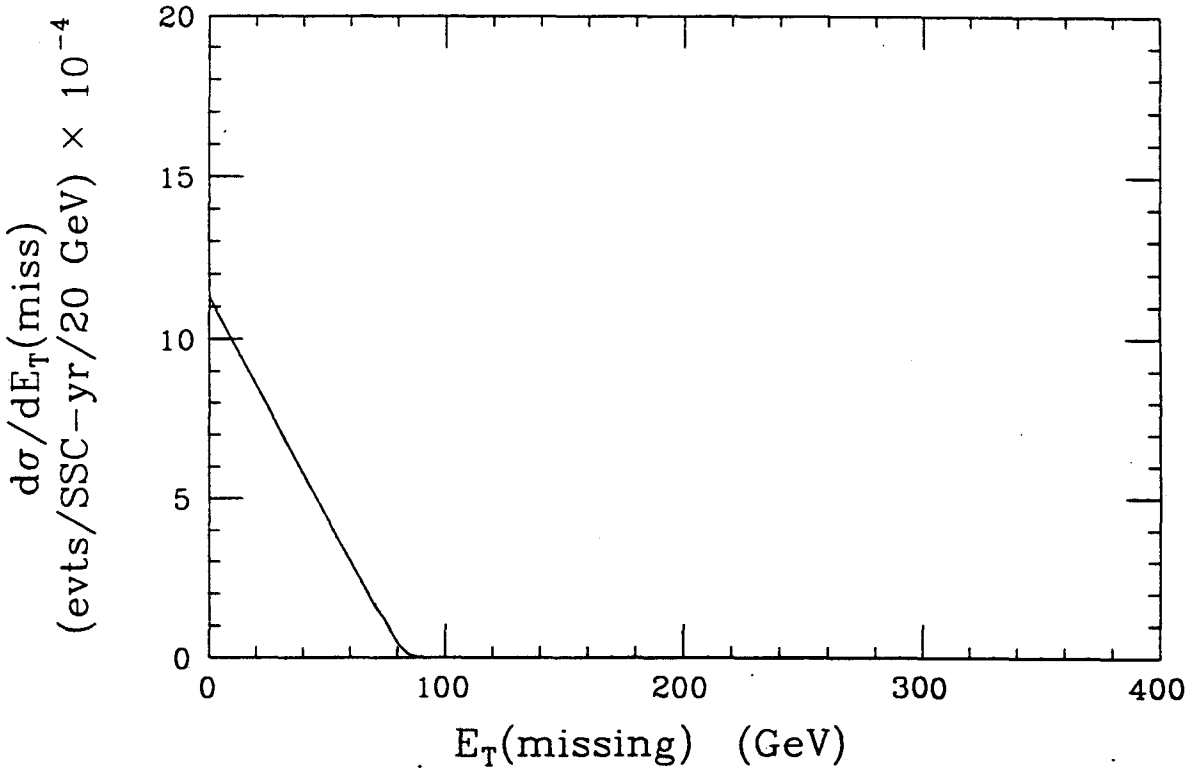

Figure G4.1a

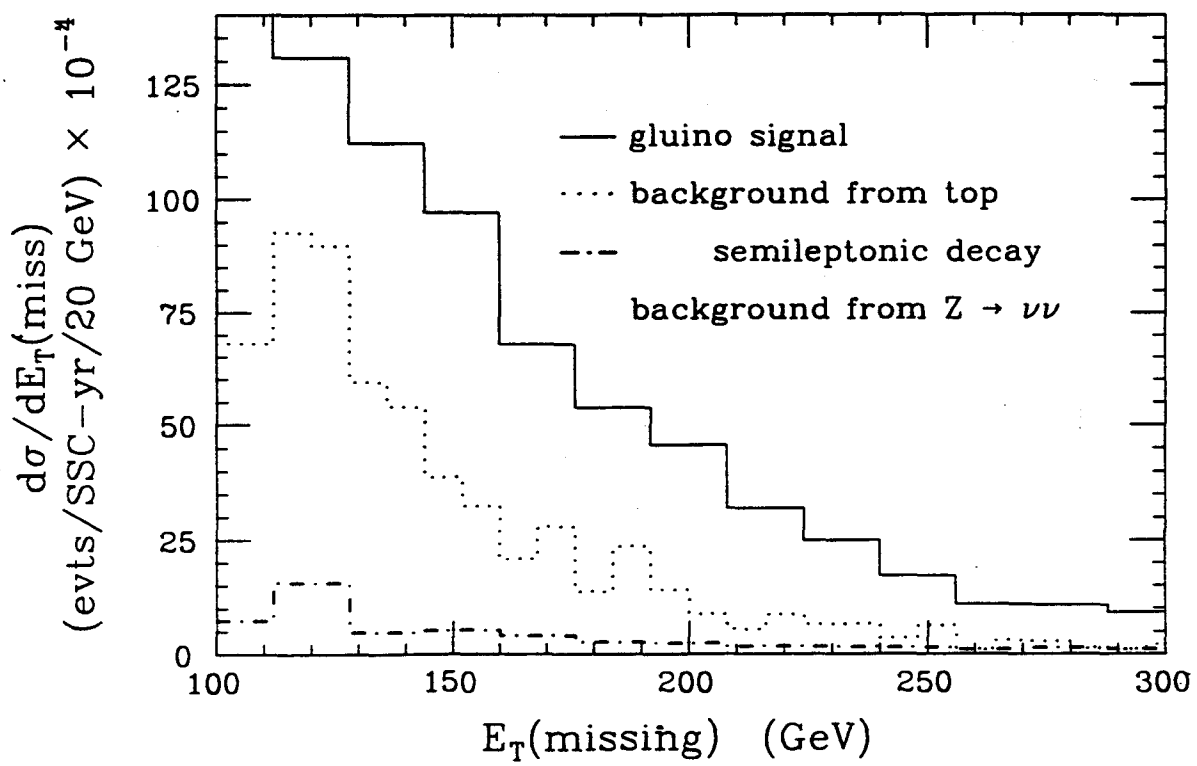

Figure G4.1b

G5: Detector Staging

- *It is unlikely that there will be enough money to meet all requests initially. How can this detector be staged? What costs can be deferred? What are the physics capabilities at each stage?*

The physics of the TEXAS detector lends itself to a two staged approach. The focus on H$\rightarrow \gamma\gamma$ at standard luminosity requires an excellent electromagnetic calorimeter with a good charged particle veto at the front. This can be achieved in Stage 1 by the tracking tagger, the imaging preradiator, and the electromagnetic compartment of the calorimeter. These elements can also search for high mass Higgs to four electrons and other physics. They can be installed independent of the rest of the detector with little extra cost, by utilizing the final structural system.

It is important to veto on hadrons that exit the em section. This can be achieved by an extra element: scintillator veto pads located after the em section. These pads would not be utilized in the final detector; however, the phototubes, light diffusers, electronics, etc. would be eventually used on the final hadron calorimeter. The final calorimeter support structure would be installed in Stage 1. Figures G5-1 and 2 show this Stage 1 implementation of TEXAS.

Stage 2 of the detector would be the mounting of the hadron calorimeter for jet physics. Lastly the physics of missing E_T and muons would require the installation of the muon TRD. This approach requires a calorimeter that is constructed in two physical depths. The front 20-25 L_{RAD} electromagnetic section can be separated from the hadronic compartment by using a precision matching plate technique. The matching plates align the fibers in the two compartments. Members of the TEXAS collaboration have successfully demonstrated this technique at BNL for the G-2 experiment. A detachable front end is part of our SSCINTCAL subsystems studies.

Matching plate prototypes for the G-2 experiment (see Figure G5.4) connect an electromagnetic module to a clear fiber light-guide readout, as would be done in Stage 1 of TEXAS. These plates and light pipes were displayed to the PAC during the June presentation at the SSC laboratory. They add less than 1% fiber-fiber non-uniformity to the light-transmission, similar to the 1/2 dB insertion loss quoted in typical optical fiber connectors. In addition, a potential advantage of a detachable front end is that the towers could be replaced if radiation damaged, at a cost of about 10% of the calorimeter bulk cost. The 30cm detachable electromagnetic towers serve as a radiation shield for the remaining 2.2 meters of calorimeter. Fig. G5.4 shows prototypes of the detachable towers with a removable optical light-guider in place.

The cost of the materials of the em lead fiber shell is 8% of the full calorimeter. We estimate that the assembly cost will be one quarter that of the full calorimeter because of the short fibers and the size-to-weight ratio of a tower. The assembly task could easily be handled by a single worker. Estimates by Bicron indicate that a worker in a team of 4 with the appropriate tooling can assemble 1,000 full hadron towers/year. Under the same conditions, a team worker should be able to assemble 4,000 of the 30-L_{RAD} towers per year. We estimate that the total cost to assemble and stage the e-m shell mechanics to be $20

million. This would include much of the special automation to build the full detector. The Pb/fiber/lightguide cost would be $5.2 million. This includes an upward change of 25% for increased costs per fiber length because of the lower volume. The increased cost of the hadron veto tiles would be about 10% of the pre-radiator cost, or about $2.5 million. The mechanical support structure would be reduced by about a factor of 0.6. It would be upgradable to the full support. The data acquisition system is less expensive by a factor of 0.6. The total cost of the Stage I detector is the following:

E-M Calorimeter Mechanics:	$25.3M
Hadron Veto:	$2.5M
Imaging Preradiator/Tracker:	$24.4M
Mechanical Support:	$8.0M
Data Acquisition:	$4.0M
Lightguide, PM's Electronics, Calibration etc.	$394/channel
(A) Calorimeter Electronics without (0.025)segmentation	$63.0M
(B) Calorimeter Electronics with (0.05) segmentation	$17.0M
Total Low Segmentation	$81.7M
Total High Segmentation	$123.7M

The staged detector cost would range between $82 and $124 million, depending on the segmentation used for the electromagnetic calorimeter. The light guides at the end of the fiber towers would be designed so that the segmentation could be upgraded simply by implementing additional electronic readout channels (symmetrically) as down-time permits. The pmt, HV, electronic, and calibration channels of the electromagnetic shell would be retained and mounted on the monolithic hadronic towers during the staging.

We have considered making a smaller radius calorimeter. As can be seen, that results in only modest savings in Pb and fiber (total is $5-6 million, so saving a factor of 4 would save only $3-4 million), at a large compromise in radiation damage probability, the imaging pre-radiator performance, and π^0 separation.

In conclusion, while staging TEXAS is not one of our goals, we have the flexibility to do it, if necessary.

FIGURE CAPTIONS

G5.1 Side view of Stage 1 TEXAS detector.

G5.2 Beam view of Stage 1 TEXAS detector.

G5.3 Prototype fibers alignment matching-plate.

G5.4 Prototype calorimeter tower.

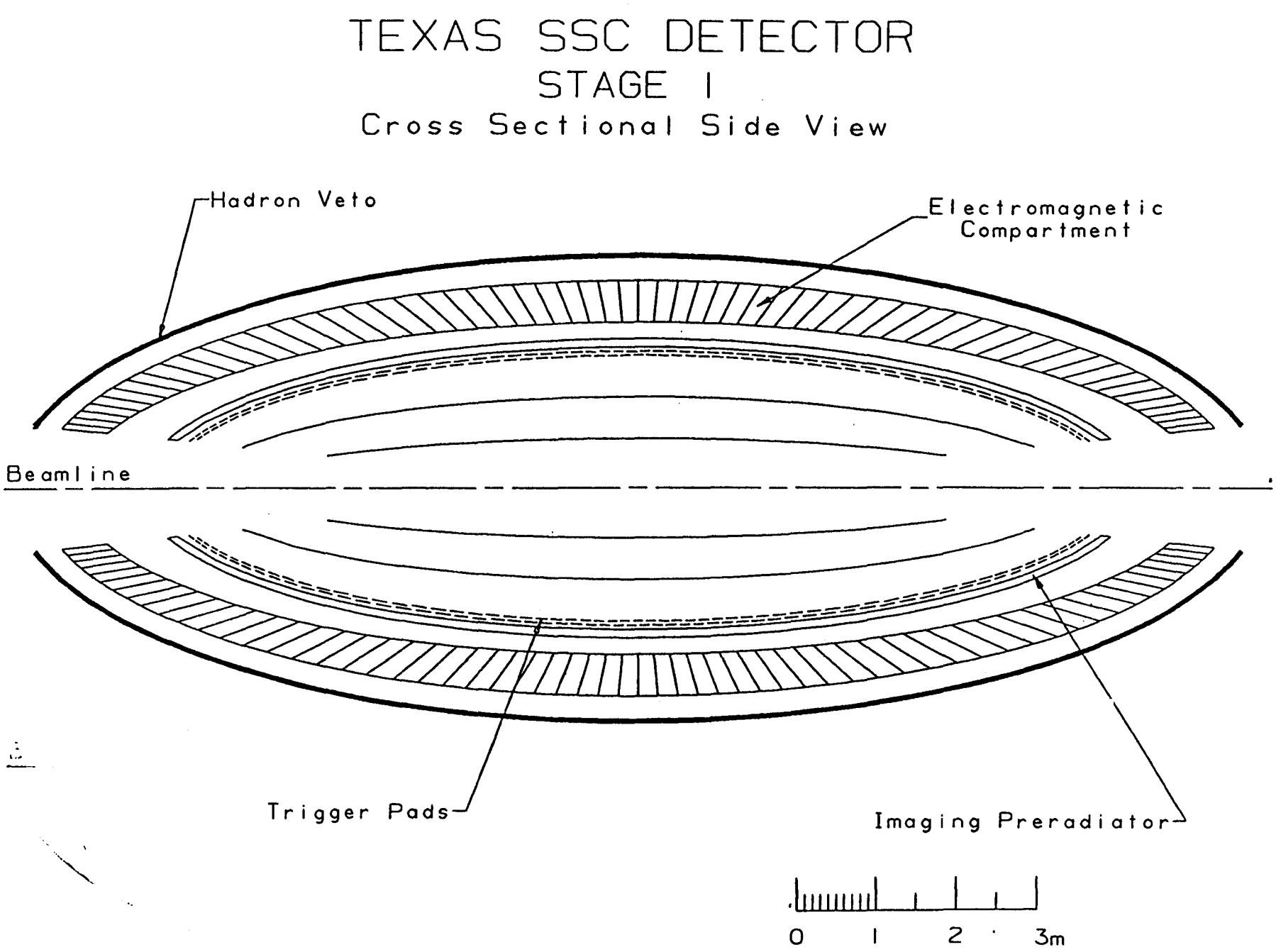
TEXAS SSC DETECTOR
STAGE I
Cross Sectional Side View
Hadron Veto
Electromagnetic Compartment
Beamline
Trigger Pads
Imaging Preradiator
0
1
2
3m

Figure G5.1

TEXAS SSC DETECTOR

STAGE I

Axial View

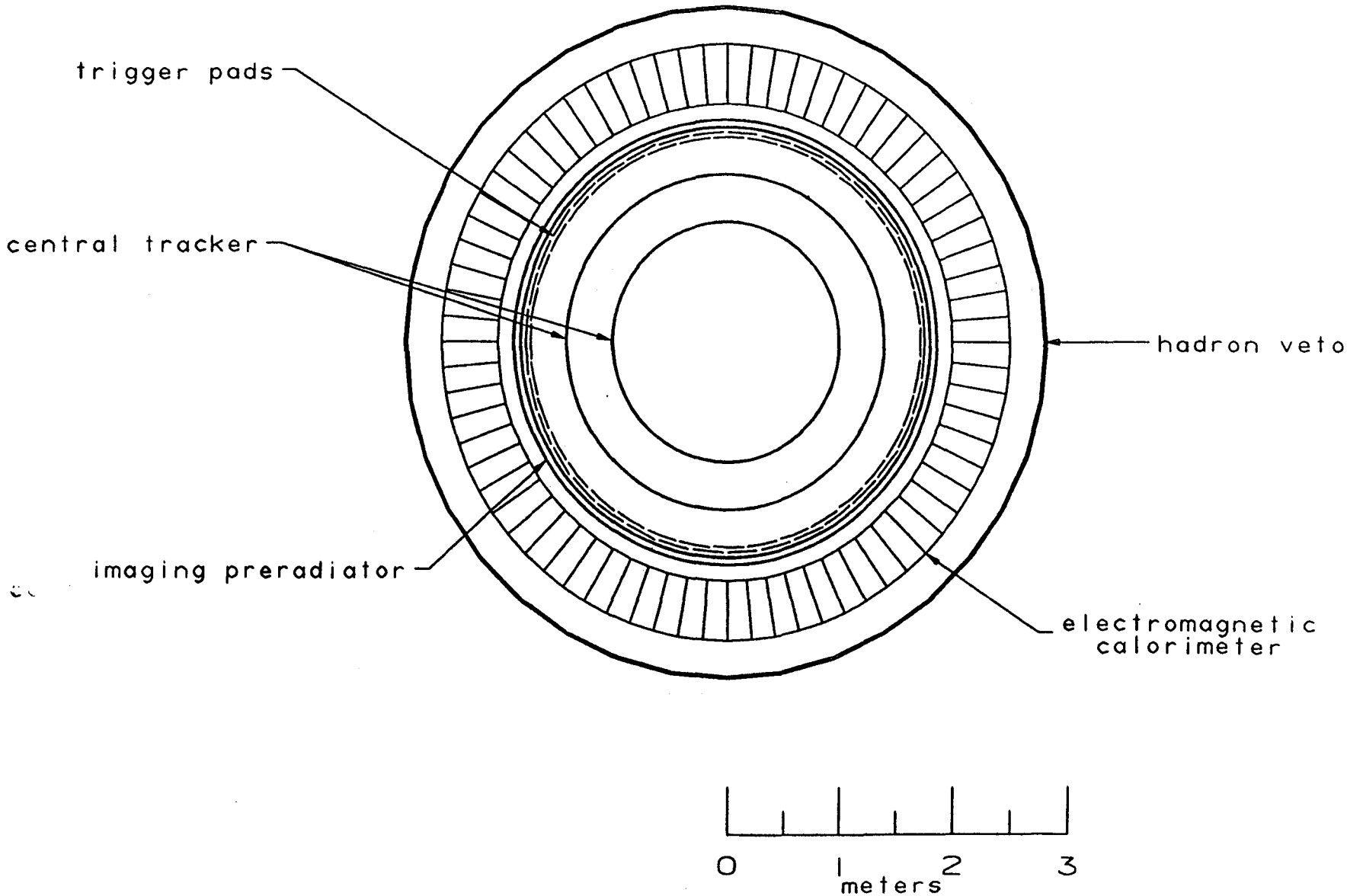

Figure G5.2

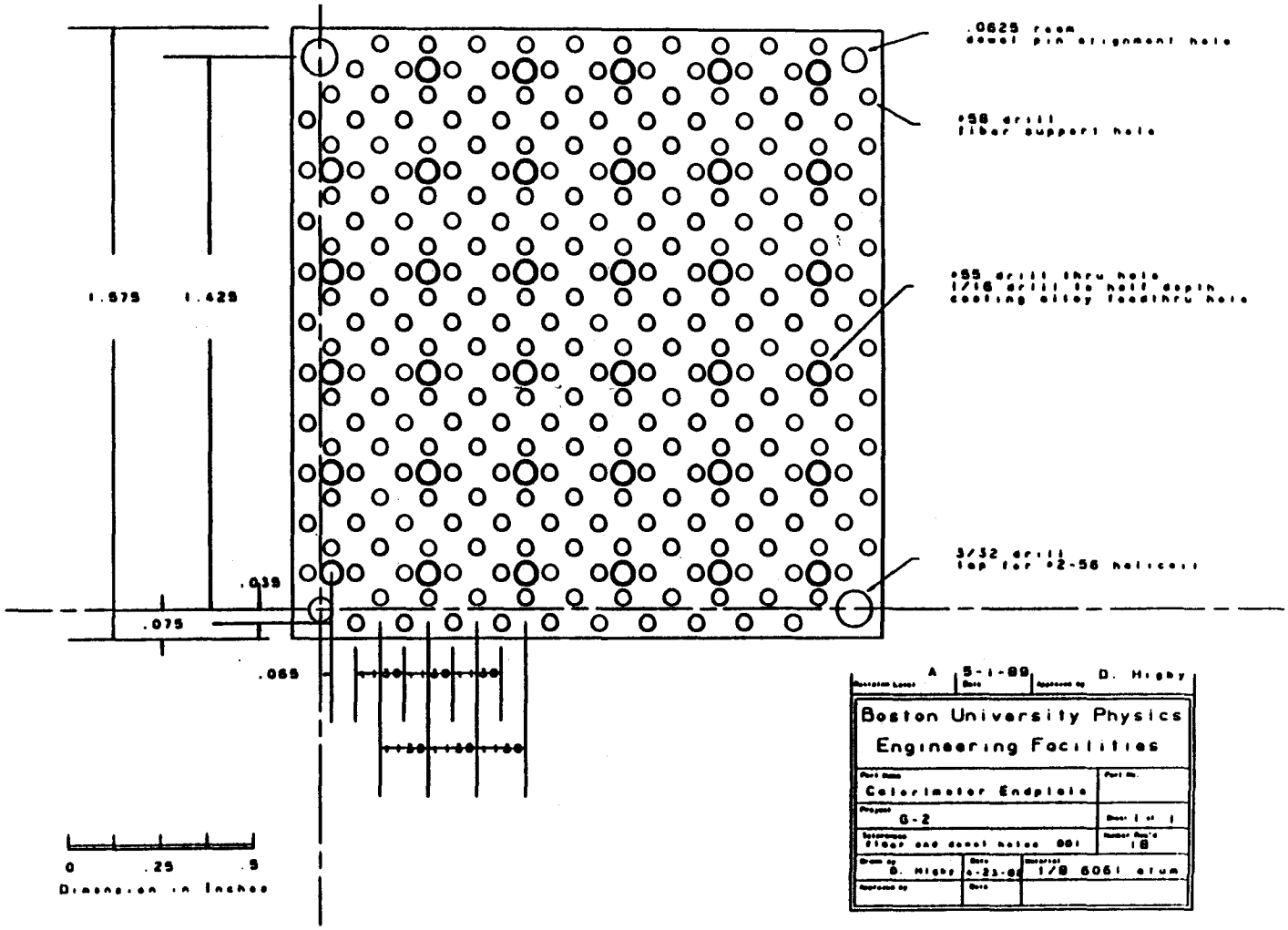
.0625 ream
dowel pin alignment hole
#58 drill
fiber support hole
#55 drill thru hole
1/16 drill to half depth
cooling alloy feedthru hole
3/32 drill
tap for #2-56 helicoil
1.575
1.425
.035
.075
.065
.30
.30
.30
.30
.30
.30
0
.25
.5
Dimension in Inches
A
5-1-89
D. Higby
Boston University Physics
Engineering Facilities
Calorimeter Endplate
G-2
Floor and dowel holes 001
18
D. Higby
6-23-89
1/8 6061 alum

Figure G5.3

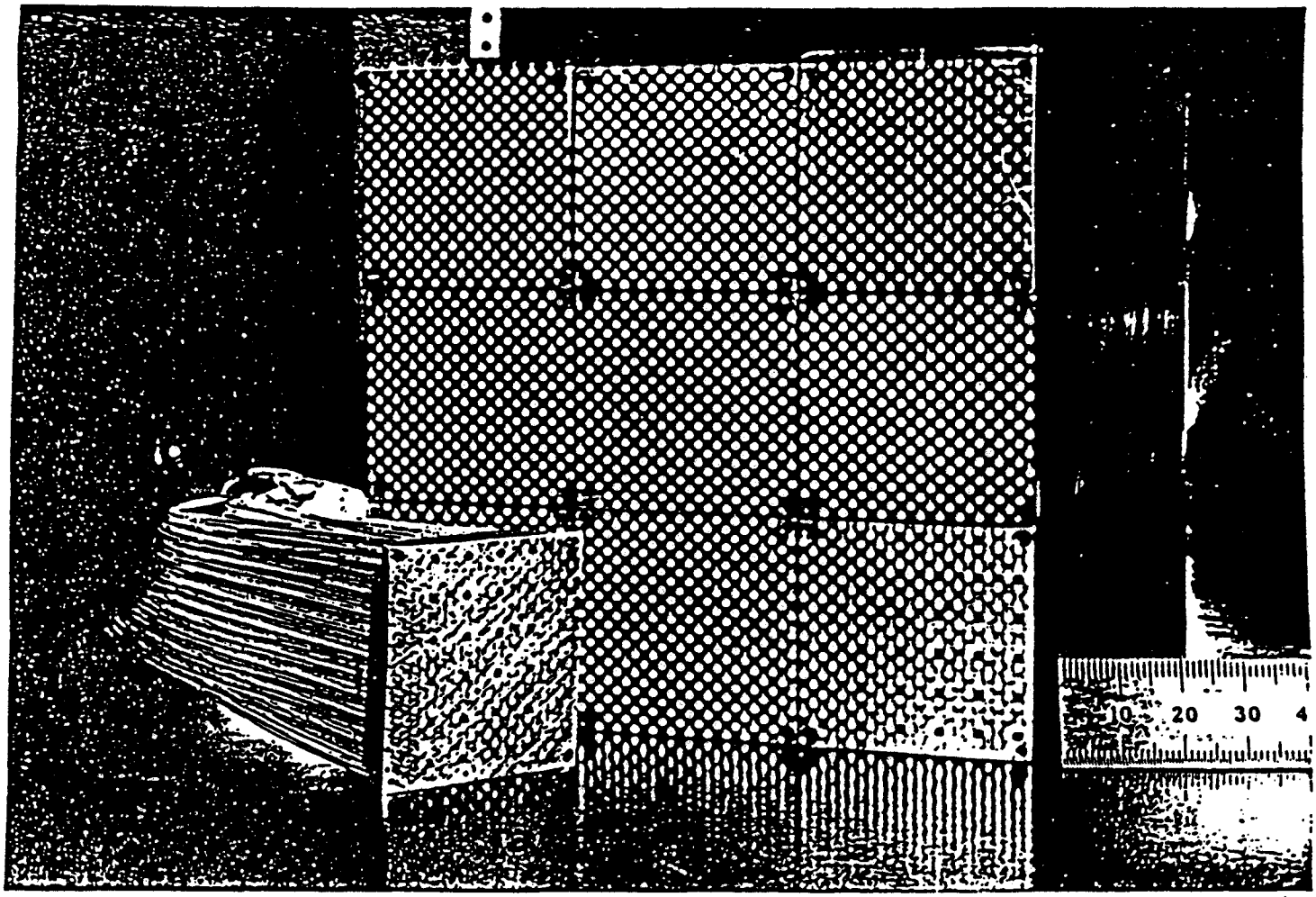

Figure G5.4

G6: Funds Requested for Subsystem Integration

- *The total funds requested in the EOIs for FY91 exceed the total funds available. It is assumed that most of the funds to be provided for detector R&D will follow through the subsystem R&D program. For those funds requested in your EOI for systems integration and proposal preparation, please give a plan including a list of tasks in order of priority and with a detailed justification for each.*

Subsystem Research and Development Tasks

Members of this collaboration play major roles in two subsystem research and development programs, one on scintillation calorimetry (SSCINTCAL) and one on fiber tracking and preradiators. Currently neither have funds allocated for the work explicitly needed to develop the TEXAS proposal. Without a budget dedicated to this task, the proposal cannot be prepared. Even if the level of the funding currently allocated to our institutions for SSC research and development in fiscal year '90 for other tasks were diverted ($220,000 for 26 active Ph.D.'s, an average of $8,500 per person) the value is grossly inadequate.

New Subsystem Proposal for Muon TRD Spectrometer

The TEXAS EOI contains an explicit proposal in the Appendix (page A8) to pursue engineering studies on the underdeveloped concept of a muon TRD spectrometer. There is currently no SSC system task on this subject. This request for a prototype and beam test work ($449,000) is a high priority for a final decision before proposal submission.

System Integration/Proposal Preparation Costs

Table I summarizes by task and by institution the TEXAS request for FY91 made in the EOI. The fourth column shows the breakdown of the Systems Integration request, a total of $1.25 million. The engineering design by Draper Lab necessary for proposal preparation for each subsystem is tabulated as the following: Calorimeter ($495 k), Tracker ($130 k) and Muon TRD ($375 k). These requests for Integration and for Proposal Preparation are our highest priority. Without them the SSC Lab request for "90% confidence level that the detector can be built," and that "the costing is accurate to 90%" cannot be met.

The plan for the projected disbursement of these funds appears in the chapter on "Request for Funds for Engineering Studies" of the TEXAS EOI. Explicit proposals for the use of these funds by each of our industrial affiliates are included in the eleven Appendices of the EOI. The detailed justification of each task is indeed expressed throughout the EOI and this set of Answers to the PAC.

Table I: Engineering Studies and Integration

Funding Request FY91

	Calorimeter	Tracker	Muon TRD	Integration Management #1 Priority	Total
Boston	750	-	210	200	1160
Drexel	-	-	100	-	100
Fairfield	30	95	-	-	125
Northeastern	-	550	265	150	965
Texas A&M	400	-	-	150	550
Subtotal	1180	645	575	500	2900
LeCroy	450	225	225	325 min.	1225
Quantum Research	-	-	-	120	120
3 Bicron	495	100	-	-	595
#1 → priority Draper	425	130	375	305	1235
Hamamatsu	-	-	-	-	0
Oak Ridge	-	535	-	-	535
Optectron	150	150	-	-	300
RCA/GE	150	150	-	-	300
Teledyne	300	300	-	-	600
Thinking Machines	-	-	-	-	0
Union Carbide	-	-	140	-	140
Subtotal	1970	1590	740	750	5050
Total	3150	2285	1315	1250	7950

½-3M. minimum

G7: Collaboration Responsibilities

• *How would your collaboration deal with the circumstances that would arise if a major collaborator could not fulfill its planned obligations?*

Once more the key to the answer to this question lies in the inherent simplicity of the TEXAS concept. Each of the TEXAS sub-systems uses well understood technology and is built of materials that are all available in the United States. Our list of US industrial affiliates testifies to this. None of the TEXAS sub-systems uses particularly unusual know-how and therefore several groups will be able to effectively participate to a given sub-system. Thus no single group is indispensable.

It goes without saying that we are anticipating the TEXAS collaboration to eventually involve non-US collaborators. However, we are not *dependent* upon the participation of foreign groups or upon unreliable foreign sources of expensive or rare materials.

To summarize: we wish this was our main problem!

T1: Capabilities at 10^{34} luminosity

• *Why is your experiment better than the other experiments at 10^{34} luminosity?*

This rather blunt question forces us into giving a blunt answer, an uncomfortable position that we would not otherwise have spontaneously taken; we apologize in advance for our criticism of the work of others, *honi soit qui mal y pense.*

Broadly speaking, the characteristics of the TEXAS detector that make high luminosity operation a realistic goal, are the following: tracking and calorimetry based on scintillator techniques; large calorimeter inner radius; very fine calorimeter segmentation; radiation hardness; no magnetic field and therefore straight tracks.

It is important to emphasize that the TEXAS design, which permits running at $\mathcal{L} = 10^{34}\text{cm}^{-2}\text{s}^{-1}$, is also a valuable research tool for operation at lower luminosity. Indeed, operating a non-magnetic detector from day one, in parallel with a magnetic detector, is desirable on physics grounds (remember the UA2, UA1 experience at CERN). It also ensures that the non-magnetic device is fully operational and debugged when high luminosity becomes available.

In the following we expand on the high $\mathcal{L}$ TEXAS characteristics and wherever possible we compare with other Expressions of Interest.

• Calorimeter Integration Time

We use the measured scintillating spaghetti calorimeter integration times recently reported by the SPACAL collaboration for the expected temporal response in the TEXAS detector at the SSC (see Appendix). To achieve an energy dependent resolution term of $29\%/\sqrt{\text{E}}$, with e/h of 1.00±0.05, the pion integration time in a spaghetti calorimeter only needs to be 35-40ns (see figs. T1.1 and T1.2. These were presented by Michele Livan at BU on 6/18/90, and by Riccardo DeSalvo at Snowmass 1990, for the SPACAL collaboration. Note that e/h is slightly larger than 1.0 in these preliminary results; Monte Carlo predictions indicate that a slight shift downward in the fiber diameter, or a slight shift upward in the fiber spacing will result in a tuning of e/h to 1.00±0.01. The results were taken in the first week of June without calibration data; the phototubes were simply balanced to about 3% with a source, and this is the origin of the large constant term of 2.6%)

The peaking time appropriate for a jet trigger is about 6-8ns. Furthermore, as can be seen from the above figures, at a 16ns integration time SPACAL has achieved a $40\%/\sqrt{\text{E}}$ resolution, with e/h of ~1.25 in 16ns, comparable to or better than competing proposed calorimeters with integration times of ~ a few hundred ns.

The myth of long compensation time comes from the use of liquid Argon, or Uranium, or both. Moderation is longer by a factor of 5 in liquid Argon than in plastic, and Uranium produces 3 times the neutrons of lead, and has a 1μs time-scale and a γ-capture cross-section about 30 times that of lead. According to estimates by SPACAL colleagues, the integration

time may be improved by about 5ns with improved electronics and the slightly faster plastic scintillator produced by Bicron. (The cables in the SPACAL tests were about 100m long - adding to the dispersion and to the time to discharge the cables into the ADC). In the forward liquid scintillator calorimeter plugs planned for TEXAS, the light pulse decay time may be made as short as 0.9ns with marginal loss of energy resolution.

At the highest luminosity TEXAS will be able to integrate over a single beam crossing, with only 20-30% of the deposited energy of a crossing contributing to the following crossing, with a somewhat degraded energy resolution of $40\%/\sqrt{E}$. At the standard luminosity, the TEXAS calorimeter will be a precision device, measuring a 500GeV pion to better than 2.5%. It is very doubtful that any technology may beat either this temporal response or this energy resolution.

We emphasize that the temporal performance of the calorimeter we are proposing is *measured*, and that the TEXAS design for the SSC is a straightforward, practical and minimal extrapolation of this proven technology. It also capitalizes on our own experience with electromagnetic spaghetti (both liquid and plastic) modules for the G-2 experiment at BNL, and our generic and subsystem R&D work on spaghetti and liquid scintillator calorimeters.

At the SSC starting luminosity of $10^{33}\mathrm{cm}^{-2}\mathrm{s}^{-1}$ the strategy to find a heavy Higgs is to use the calorimeter both for missing E_T (neutrino decays of the vector bosons) and for dijet reconstructions of the vector bosons, in order to have enough signal events. As an example of how important it is to have clean events without overlap even at a luminosity of $10^{33}\mathrm{cm}^{-2}\mathrm{s}^{-1}$, fig. T1.3 shows a potential degradation by a factor of 1.5 in the $W \rightarrow jj$ mass resolution even with only 3 minimum bias overlapping events (the Monte Carlo was for a calorimeter with cruder segmentation - 0.05 x 0.05- and lower energy resolution than the TEXAS design). CERN LHC studies show similar dijet mass signal degradation effects due to event overlaps; 10 minimun bias event pile-up produces a factor of 2 degradation in the dijet mass resolution.

At $10^{33}\mathrm{cm}^{-2}\mathrm{s}^{-1}$, it is difficult for liquid Argon calorimetry or even Si calorimetry (with its 30ns charge collection time and much longer compensation integration time) to avoid a significant event overlap, with resulting noise in the jet-jet mass signal. For a heavy Higgs search using $H \rightarrow ZZ \rightarrow lljj$, or $H \rightarrow WW \rightarrow jjl\nu$, our ability to avoid event overlaps will lower background and enhance the signal in the dijet mass reconstruction. This yields a factor $\sim$2 reduction in the mass cut necessary at the W or Z mass as compared to calorimeters integrating over 10 or so events. At $10^{34}\mathrm{cm}^{-2}\mathrm{s}^{-1}$, TEXAS will have a dijet mass resolution degraded by a similar factor because of event overlaps. In other words, at $10^{34}\mathrm{cm}^{-2}\mathrm{s}^{-1}$, the TEXAS peaking time of about 6-8ns compares to the 80 ns peaking time in liquid Argon at $10^{33}\mathrm{cm}^{-2}\mathrm{s}^{-1}$, and the 40ns integration time compares to the 400ns integration time of liquid Argon at $10^{33}\mathrm{cm}^{-2}\mathrm{s}^{-1}$.

The strategy to find technicolor and compositeness also requires minimal overlap noise in order to preserve the linearity of the jet energy signals.

Lastly, the monolithic calorimeter allows fast trigger decisions at an early level on electrons, γ's (when combined with the pre-radiator) and hadrons.

• Segmentation and Inner Radius

Because the TEXAS calorimeter has a large (2m) inner radius (twice as large as that of EMPACT and 2.7 times as large as that proposed for L*), a segmentation of 0.05×0.05 at 1m in alternative proposed calorimeters is equivalent to a segmentation of 0.025x0.025 at 2m in TEXAS (for the same number of cells), in terms of shower spreading to adjacent cells for calorimeters of the same effective absorption length. TEXAS has chosen a segmentation of 0.025×0.025 for its monolithic spaghetti calorimeter, therefore consisting of ~160,000 towers. The singles rate in each tower is reduced by about a factor of 4, compared with most of the other proposed SSC calorimeters. This is better for operation at higher luminosity. The activity per tower at 4 x $10^{33}cm^{-2}s^{-1}$ in TEXAS is roughly equivalent to most of the other EOI's at $10^{33}cm^{-2}s^{-1}$.

The large radius also allows survival at high luminosity operation. Compared with a calorimeter starting at 75cm (L*) or 1m (EMPACT), the TEXAS calorimeter has a radiation dose 7 or 4 times lower, respectively.

Fine segmentation is also important for operation at the standard luminosity of $\mathcal{L} = 10^{33}cm^{-2}s^{-1}$. In order to understand the QCD backgrounds to new physics, the stability of jet algorithms needs to be checked. One crucial check is to plot $F = E_T(r)/E_T(R)$ as $r \rightarrow 0$, with the limit $F = -\ln 2R/r$. Finer segmentation allows a complete check of this limit as long as the segmentation is effective and not blurred by the physics of shower spreading. Furthermore, the large inner radius and fine segmentation allows finer separation of overlapping jets.

The ability to use this fine segmentation is preserved in the TEXAS detector partially because of the absense of a magnetic field. Monte Carlo results from UA2 indicate that 1GeV particles, which may be eliminated from a calorimetric jet reconstruction by the sweeping in a magnetic field, contribute substantially to the energy resolution of a jet. Fig. T1.4 demonstrates this effect. Similarly, fig. T1.5 shows the magnetic field broadening effect on $W \rightarrow jj$; a 30kG-m field broadens the W signal by about a factor of 1.5 (the p_T of the W is 500 GeV/c).

• Radiation Damage

Because the TEXAS calorimeter starts at a radius of 2m, and has a design for the forward region that uses liquid scintillator, the radiation dose from electromagnetic sources to the scintillating fibers is less than for competing designs. For example, EMPACT is proposing a spaghetti design with a 1m radius, at 4 times the radiation dose of TEXAS, without a clearly proposed plan in the forward regions, with considerably more cracks and with half the segmentation. Furthemore, the Bicron fibers which recover from 30MRad are part of a TEXAS development program which will continue to improve the radiation potential of this design.

Neutron doses are not problematic for scintillator at the levels predicted for the SSC. Compared with liquid Argon, where recent results indicate serious neutron damage to the

pre-amp electronics buried in the detector, the absence of active devices inside the spaghetti calorimeter offers the possibility of long term operation at standard and high luminosity running. Silicon hadron calorimeters (as proposed by L*) will have a survival problem at $10^{34}cm^{-2}s^{-1}$ resulting from the neutrons produced in them by the event rate alone.

In the very unlikely circumstance that radiation damage were to prove to be an obstacle to plastic spaghetti, the forward liquid canelloni would simply be extended to the entire calorimeter, with some slight increase in complexity. (Note that modern scintillating liquids have optical attenuation lengths of some 20m, and preliminary work by us indicates that the light yield from a capillary spaghetti calorimeter is equal to or exceeds that of the normal plastic spaghetti).

Lastly, we note that in the baseline design, no active components are inside the calorimeter, and there is therefore no possibility of radiation damage to the electro-optical readout.

• Leptons

As shown by SPACAL with high energy electrons (see fig. T1.1), the full integration time for an electromagnetic signal is 15ns, completely consistent with high luminosity operation. Liquid Argon devices cannot compete with this. Furthermore, the TEXAS electromagnetic segmentation (0.025×0.025) is superior to that proposed for BaF_2 by L* (0.04×0.04). The singles rates and overlapping event occupancy per tower in TEXAS will be lower than L* by a factor of 2.6 in the 16 event per beam crossing environment at $10^{34}cm^{-2}s^{-1}$.

The scintillating fiber tracker/preradiator signal is also fast in the intrinsic response, about 15ns, merely requiring a sufficiently deep pipeline to collect the data. Using the scintillating tiles in the tracker/preradiator for isolation reduces the higher-level trigger-pipeline depth necessary for pixel readout. The scintillator tiles have an integration time of a few ns at most. Unlike straw tracker tubes proposed for other experiments, such as SDC, EMPACT, and L*, with drift times typically in the 30-40ns range, the electron (or muon) isolation signals necessary for lepton definition are available in 1 beam crossing, and integrate over the minimum possible number of event overlaps. Using tiles at the segmentation level, it would even be possible to abandon the tracking at very high luminosity, and simply use the tile system to set electron isolation trigger requirements without track finding.

Without an imaging pre-radiator, it is likely that an experiment like L* with crude electromagnetic segmentation at the calorimeter level (and with a tracker integrating over several beam crossings) will have trouble isolating (identifying) electrons with high efficiency at $10^{34}cm^{-2}s^{-1}$ because of the difficulty of isolating a single track into a calorimeter cell. The probability of finding an isolated electron tower cell (no surrounding towers with charged tracks identified by the tracker) integrated over 2 beam crossings in L* is only 75%. (Loopers, which we have not considered, will be an additional problem).

The muon TRD is designed to be a fast-trigger muon device and to operate where other systems would be confused by punchthrough and by the flux of low energy muons at the luminosity extreme of the SSC. At a luminosity of $10^{34}cm^{-2}s^{-1}$, the muon/punchthrough rate after 12 interaction lengths into $0 \leq \eta \leq 3$ is 180MHz, not counting the extra electrons

and γ's accompanying the particles exiting the calorimeter (energies limited to about 80-100MeV) which further cloud chambers. It is relatively easy to mismeasure a track point and move a low energy muon on the steeply falling muon distribution to high energy in a precision chamber system. It is difficult to imagine how that could happen to tracks below 40-50GeV in a TRD system.

- Calorimeter Calibration

Using the simulated annealing or global entropy surface techniques to perform relative calibration actually becomes easier at high luminosity. In this technique, the symmetry of the calorimeter system and the deposited energy are used to calibrate. In a zeroth approximation, with N identical cells, N-1 are used to form an average, and the Nth is adjusted to the average. The process is then iterated over every cell. Remarkably, statistical mechanics shows that this process converges quickly. It would first be used on every ring in constant η. Then the cells would be redefined as the difference in adjacent η towers at constant ϕ. (The profile in η should be identical for every stripe in constant ϕ). More sophisticated adaptive algorithms of a similar nature can be designed to do this globally (simulated annealing) much more rapidly, with many towers adjusted simultaneously.

Long-term absolute energy calibration, tied to global calibration, would be performed continuously using event signals (such as electron decays of the Υ and Z). Periodically, compact accelerators and radiosource wires would be used off-line. The phototube average currents, voltages, and temperatures would be recorded by a highly multiplexed low rate spy system integrated into the phototube electronics.

For short term calibration, high stability ring dye lasers phase-locked to the accelerator RF serve as a precision light-source (with the intensity monitored by radiosources and cryogenic negative electron affinity photodiodes - typical cost about $150-250k/laser). A sub-ns laser pulse would be periodically delivered into the calorimeter towers on quartz injection fibers (4 per tower, embedded with the other fibers, injected into Silica diffusers at the front and back of each tower - note the front mirrors on the fibers are 85% reflective/15% transmissive) about 1 ns before a beam crossing, creating a prepulse in the quietest time before an event. The normal event pipeline would be used to look backwards and accept only towers which had least count energy for at least 3-4 beam crossings.

The laser pulse wavelength and intensity are tunable. By injecting in the near UV (330-390 nm) some of the the scintillator energy transfer mechanisms can be monitored. By tuning the laser to longer wavelengths the transmission properties of the fiber base can be monitored (radiation damage is often wavelength dependent). By injecting in the back just in front of the photodetector, the photodetector can be separately monitored from the fibers. By detecting the reflected pulse during back-injection, and comparing that pulse with the front pulse at several wavelengths, the fiber properties along the length of the fiber can be unfolded. The laser intensity can be precisely varied by electro-mechanical cavity tuning and by mechanically switchable sets of metallized neutral density filters. It is therefore possible to measure the linearity of the calorimeter system over 6 orders of magnitude with an error

of 0.1%. The capability of near UV-visible light injection to simulate the properties of energy deposition is unique to visible light scintillators.

• Central Tracker

The all-scintillating fiber central tracker in TEXAS integrates over just one beam crossing, unlike most drift detectors. Since curved tracks are not an issue, the track fitting and finding are rapid and simple, with far fewer pixels necessary to buffer than in L* or SDC, which must use high precision tracking. While the absence of a magnetic field is shared by EMPACT, the radiation dose will draw too much current from the drift tubes in the TRD system inside. The inner TRD is likely to be lit up by the low energy γ's from neutron captures. Furthermore, the pre-amps neccessary on the drift tubes in all the other proposals will suffer neutron damage at $10^{34}\mathrm{cm}^{-2}\mathrm{s}^{-1}$, within 1m of the beam pipe. The absence of active devices close to the beam pipe is a major advantage of the TEXAS detector for high luminosity operation.

The scintillating tiles matched to the finely divided calorimeter segmentation are a fast method to determine isolation for electron and γ triggers, unique to TEXAS for high rate operation.

Generally speaking, wire gas and Silicon tracker systems at $10^{34}\mathrm{cm}^{-2}\mathrm{s}^{-1}$ will not operate effectively. Detectors such as L* which may rely on them for electron isolation will cease to operate at high luminosity.

• Conclusion

We conclude this discussion by emphasizing that for TEXAS to operate sucessfully, at $10^{34}\mathrm{cm}^{-2}\mathrm{s}^{-1}$ it must also operate at $10^{33}\mathrm{cm}^{-2}\mathrm{s}^{-1}$ more cleanly than the calorimeters proposed for the other large experiments. It is not likely that the other experiments could fully utilize the advantages of a homogeneous lead-scintillator (spaghetti) calorimeter because of design restrictions. Liquid Argon calorimeters will have difficulty avoiding integrating over less than ~10 events and Si calorimeters will not be able to integrate over fewer than ~4-5 beam crossings (because of a raw collection time of ~30ns, and a longer time to compensation), at the standard luminosity. The bipolar proposed shaping is dangerous; a given pulse contributes both positively and negatively to the following.

The SDC and L* calorimeter designs, both in a large solenoidal magnetic field, are not conducive to scintillator-calorimeter readout. The phototubes in these EOI's must operate linearly over a very large dynamic range in a magnetic field, most efficiently at large angles to the field direction, with the potential for decreased jet energy resolution from the magnetic field effects. Typical high magnetic field mesh dynode phototubes are intrinsically less linear than other photomultipliers. Systematic effects over the full jet dynamic range are likely.

In the EMPACT design, minimal calorimeter space is imposed by the price of the muon toroid coil and dewar, whose size is made as small as possible to reduce costs, resulting in a compromise on the calorimetry in several respects: shower containment, access, hermeticity

and projectiveness. No optimization has occurred for what would follow from this choice. The dimensions for the EMPACT calorimeter were designed for a liquid Argon device, and a spaghetti design was fit into the same volume. The considerable space needed for phototube readout, cables and thermal dissipation make it difficult to fit a thick spaghetti calorimeter inside the support tube space provided in EMPACT, and lower the potential hermeticity of the spaghetti design, one of its major potential features. Furthermore, it will be almost impossible to change phototubes or phototube/jet trigger electronics over the course of the experiment. Perhaps most difficult for the EMPACT spaghetti requirements is to find the $3 million worth of adhesives budgeted in their design which will hold the calorimeter super-rings together under the radiation dose. The TEXAS support is specifically designed to avoid this problem and is feasible because of the open space around the calorimeter. It is not unlikely that EMPACT will choose non-projective liquid Argon calorimetry around which the toroids and support tube were originally designed (a choice which will make the best possible energy resolution/compensation and high rate operation very unlikely).

L* is proposing an unproven silicon hadron calorimeter, likely to have inhomogeneities, both in the light collection and in the complex construction. Waveshifter calorimeter designs provide inhomogeneous responses unless considerable tuning is performed on the modules. Furthermore, the shifter fibers proposed are no more inherently radiation hard than other fibers, and some of the huge number of individual glue joints required for assembly and sealing of the individual fiber shifters may prove to fail in the radiation environment at the small proposed inner radius (there is essentially no difference in the hardness of shifter and scintillating fibers). Most problematic is the very high precision or uniformity required of an individual readout fiber, as contrasted to a spaghetti design where typically hundreds of fibers contribute to the hadronic energy, averaging out individual variations in fiber thickness or composition. The L* alternative hadron calorimeter is an untested Silicon design, fraught with uncertainty in almost every aspect of its performance; survival, price and ability to be delivered. Both L* calorimeter designs have relatively low expected performance and compensation, especially with the BaF_2 front end (which is also problematic in its advertised performance - see Higgs$\rightarrow \gamma\gamma$ discussion in the answer to question T4).

In terms of a combination of energy resolution, segmentation, speed, and radiation resistance, none of the current proposals offers in our opinion a realistic calorimeter that favorably compares with TEXAS. In terms of hermeticity, none of the other designs matches TEXAS. They are not as simple to construct or maintain, particularly for the local readout and trigger electronics. TEXAS is the only design where repairs can be contemplated, or where the trigger electronics on the calorimeter shell can be changed or upgraded. We are confident at this juncture of the TEXAS calorimeter performance at $10^{33}cm^{-2}s^{-1}$, and that it can approach $10^{34}cm^{-2}s^{-1}$ much more comfortably than other EOI's, with only the noise of 1 or 2 beam crossings. We note that even a luminosity 4 x $10^{33}cm^{-2}s^{-1}$ accumulates a large statistical advantage very quickly.

Furthermore, the TEXAS systems which must operate in concert with the calorimeter are all designed with the high rate in mind. All of the systems inside the muon TRD operate with electro-optic technology, and with active devices shielded by the calorimeter. This rapidly advancing technology is at the forefront of high rate-signal detection and generation.

Lastly, the TEXAS technology and design chosen are to lower the risk of radiation damage to any component.

The very heavy Higgs searches use calorimetric measurements or high luminosity or both, to provide enough statistical power to extract a signal. The TEXAS detector is uniquely suited to this role, when compared with the other detectors. However, TEXAS is committed to the notion that the standard model Higgs is hopefully not all there is to look for. Indeed, one might speculate about the end of high energy physics if the only discovery of the SSC is a 400 GeV Higgs, which would leave more questions than answers about the nature of the fundamental forces, the origin of the particle spectra, and the ultimate simplicity of nature. We must therefore be prepared for SUSY or Technicolor or Compositeness or Something Else, with most of the important signals exploiting the potential of calorimeters. At least one SSC detector should therefore provide an optimal calorimeter, and be prepared for high luminosity operation, in order to cover the maximun ground in the search for new physics at the SSC.

Figure Captions

T1.1 SPACAL Compensation Time Structure; e/π ratio.

T1.2 SPACAL Time Structure; resolution.

T1.3 W mass resolution *vs.* number of superimposed background events.

T1.4 Effect of B-field on dijet reconstruction (after P. Jenni).

T1.5 Effect of B-field on $W \rightarrow jj$ (after Freeman and Newman-Holmes).

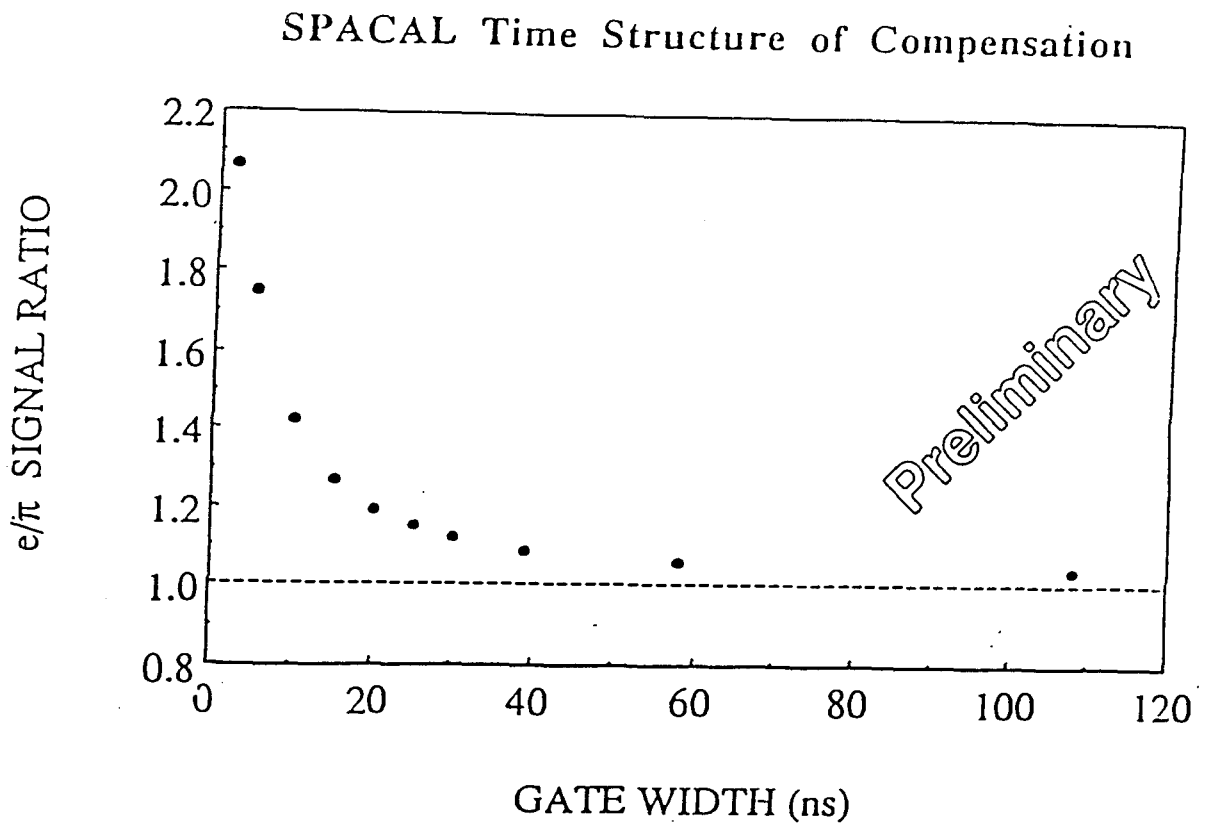

Figure T1.1

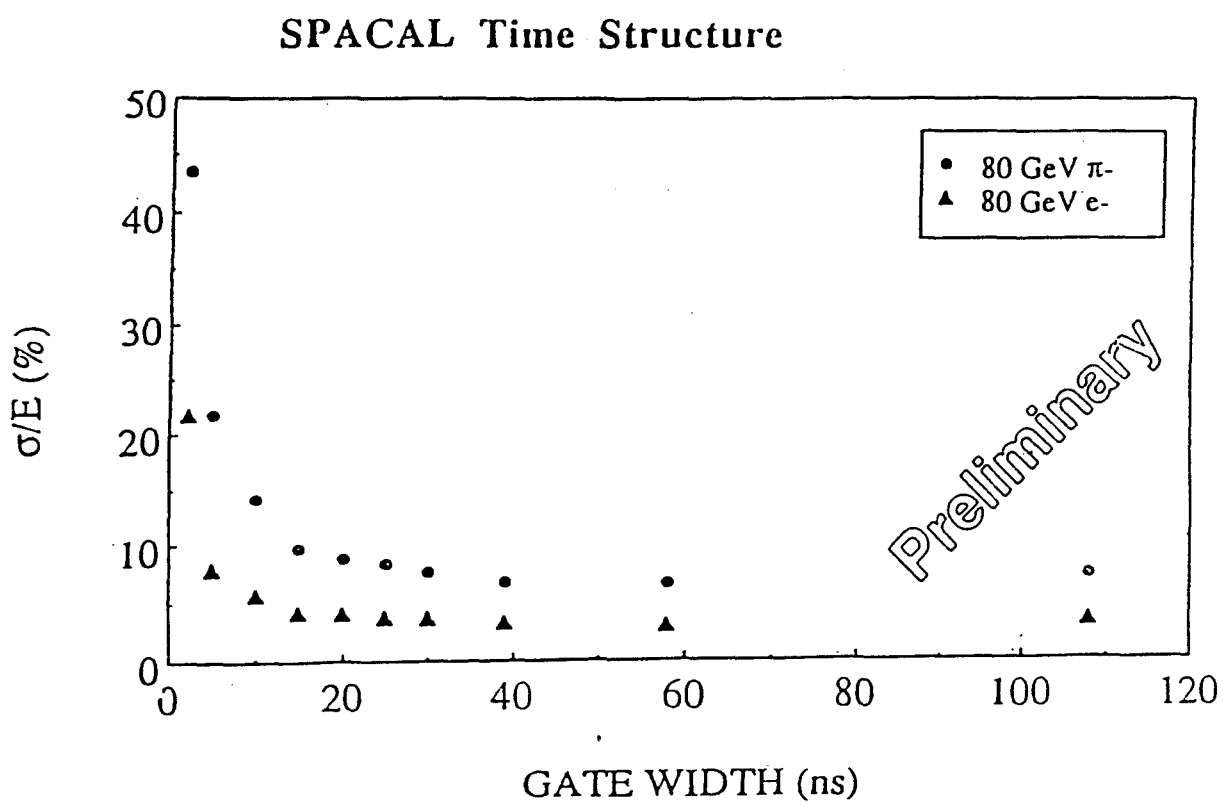

Figure T1.2

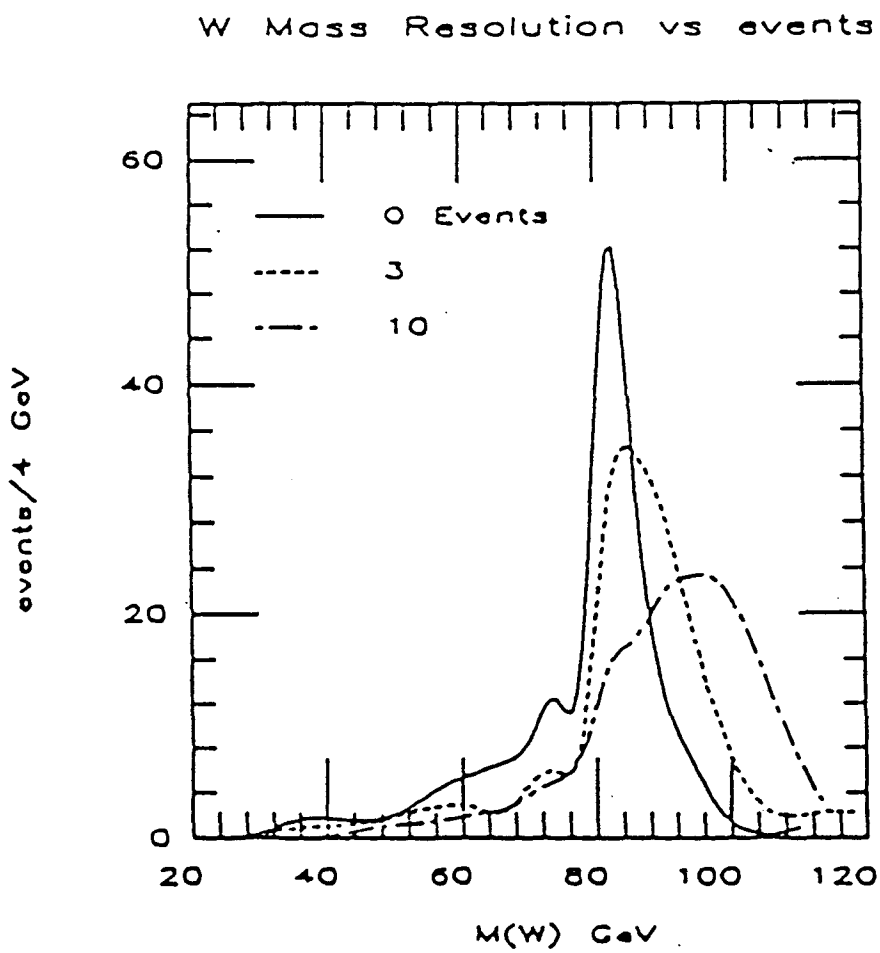

W mass resolution vs number of superimposed background events.

Figure T1.3

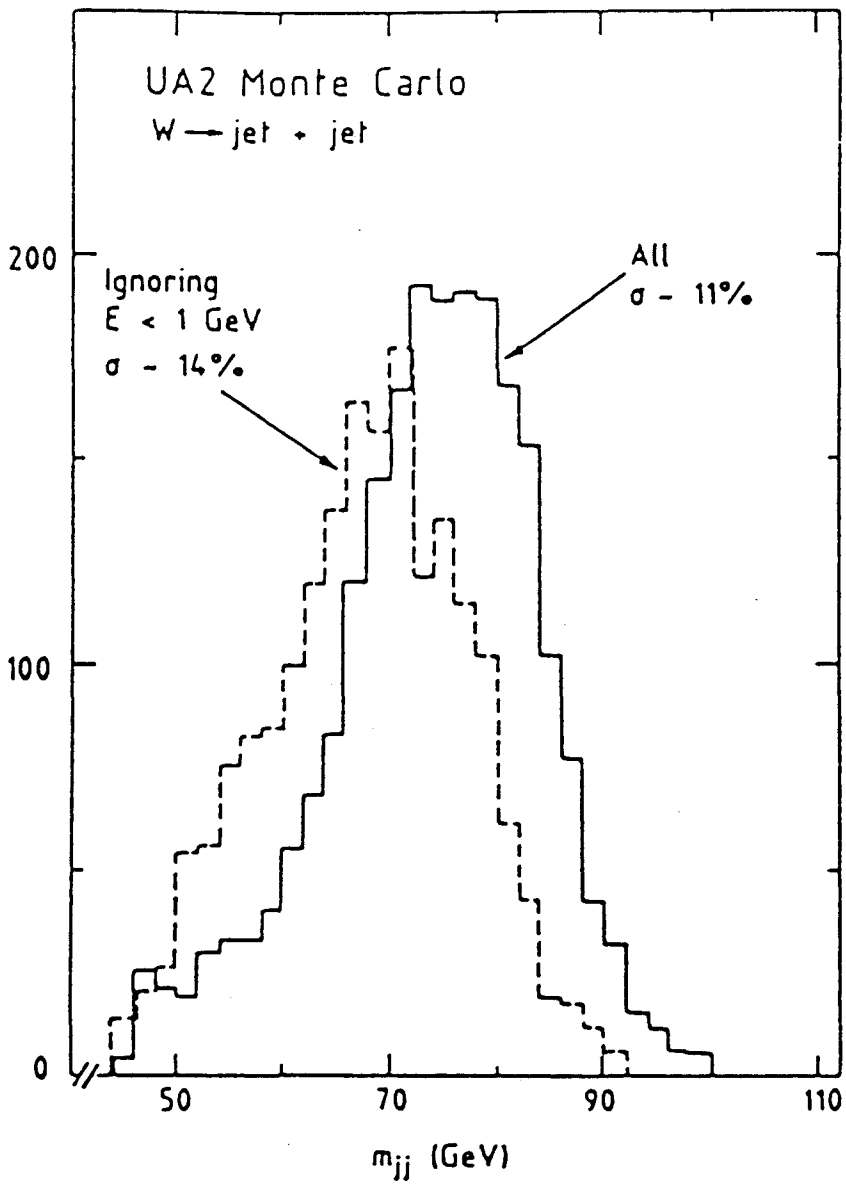

W → 2-jet simulations (UA2 calorimeter) including (solid histogramme) and excluding (dashed histogramme) particles with E < 1 GeV.

Figure T1.4

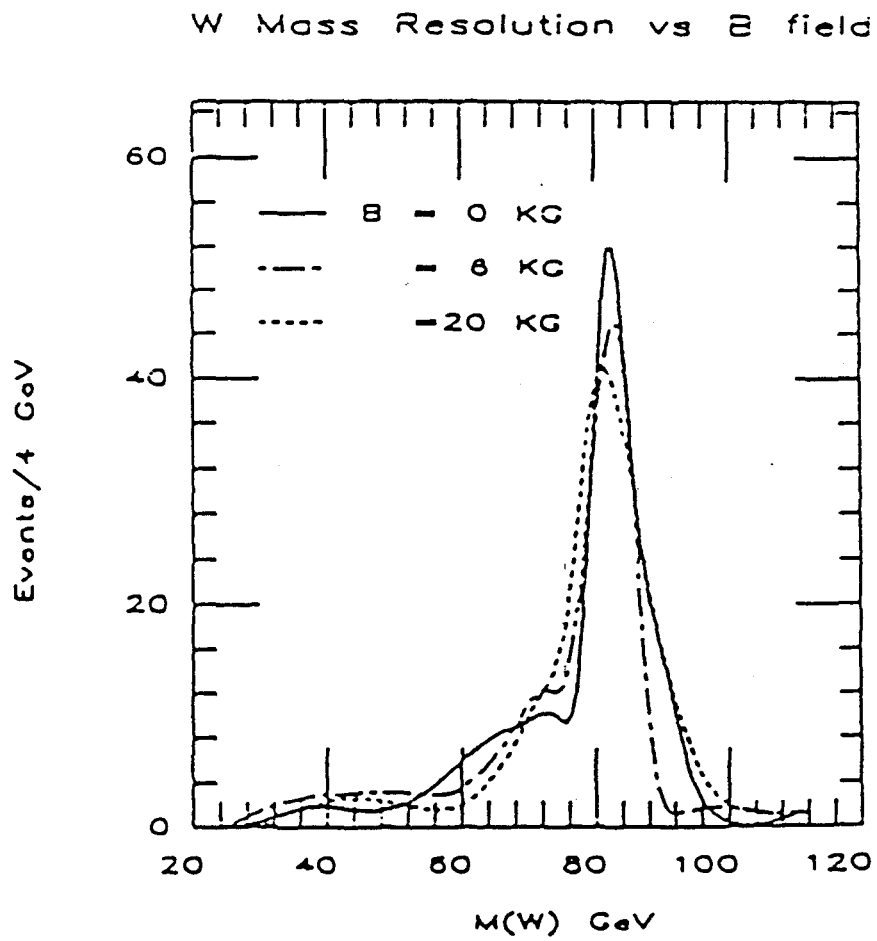

W mass resolution as a function of magnetic field.

Figure T1.5

T2: Fiber Calorimetry Performance at High Luminosity

- *How is the high-$\mathcal{L}$ performance of the hadron calorimeter consistent with the collection time needed for compensation?*

The internal consistency of the answer to a previous question (T1) required that we answer there the present question (T2) *en passant.* To simplify the PAC's effort in dealing with our answers, we take the liberty of repeating here the relevant paragraphs *verbatim.*

We use the measured scintillating spaghetti calorimeter integration times recently reported by the SPACAL collaboration for the expected temporal response in the TEXAS detector at the SSC (see Appendix). To achieve an energy dependent resolution term of $29\%/\sqrt{E}$, with e/h of 1.00±0.05, the pion integration time in a spaghetti calorimeter only needs to be 35-40ns (see figs. T2.1 and T2.2. These were presented by Michele Livan at BU on 6/18/90, and by Riccardo DeSalvo at Snowmass 1990, for the SPACAL collaboration. Note that e/h is slightly larger than 1.0 in these preliminary results; Monte Carlo predictions indicate that a slight shift downward in the fiber diameter, or a slight shift upward in the fiber spacing will result in a tuning of e/h to 1.00±0.01. The results were taken in the first week of June without calibration data; the phototubes were simply balanced to about 3% with a source, and this is the origin of the large constant term of 2.6%)

The peaking time appropriate for a jet trigger is about 6-8ns. Furthermore, as can be seen from the above figures, at a 16ns integration time SPACAL has achieved a $40\%/\sqrt{E}$ resolution, with e/h of ~1.25 in 16ns, comparable to or better than competing proposed calorimeters with integration times of ~ a few hundred ns.

The myth of long compensation time comes from the use of liquid Argon, or Uranium, or both. Moderation is longer by a factor of 5 in liquid Argon than in plastic, and Uranium produces 3 times the neutrons of lead, and has a $1\mu s$ time-scale and a γ-capture cross-section about 30 times that of lead. According to estimates by SPACAL colleagues, the integration time may be improved by about 5ns with improved electronics and the slightly faster plastic scintillator produced by Bicron. (The cables in the SPACAL tests were about 100m long - adding to the dispersion and to the time to discharge the cables into the ADC). In the forward liquid scintillator calorimeter plugs planned for TEXAS, the light pulse decay time may be made as short as 0.9ns with marginal loss of energy resolution.

At the highest luminosity TEXAS will be able to integrate over a single beam crossing, with only 20-30% of the deposited energy of a crossing contributing to the following crossing, with a somewhat degraded energy resolution of $40\%/\sqrt{E}$. At the standard luminosity, the TEXAS calorimeter will be a precision device, measuring a 500GeV pion to better than 2.5%. It is very doubtful that any technology may beat either this temporal response o r this energy resolution.

We emphasize that the temporal performance of the calorimeter we are proposing is *measured*, and that the TEXAS design for the SSC is a straightforward, practical and minimal extrapolation of this proven technology. It also capitalizes on our own experience

with electromagnetic spaghetti (both liquid and plastic) modules for the G-2 experiment at BNL, and our generic and subsystem R&D work on spaghetti and liquid scintillator calorimeters.

At the SSC starting luminosity of $10^{33}cm^{-2}s^{-1}$ the strategy to find a heavy Higgs is to use the calorimeter both for missing E_T (neutrino decays of the vector bosons) and for dijet reconstructions of the vector bosons, in order to have enough signal events. As an example of how important it is to have clean events without overlap even at a luminosity of $10^{33}cm^{-2}s^{-1}$, fig. T2.3 shows a potential degradation by a factor of 1.5 in the W$\rightarrow jj$ mass resolution even with only 3 minimum bias overlapping events (the Monte Carlo was for a calorimeter with cruder segmentation - 0.05 x 0.05- and lower energy resolution than the TEXAS design). CERN LHC studies show similar dijet mass signal degradation effects due to event overlaps; 10 minimun bias event pile-up produces a factor of 2 degradation in the dijet mass resolution.

At $10^{33}cm^{-2}s^{-1}$, it is difficult for liquid Argon calorimetry or even Si calorimetry (with its 30ns charge collection time and much longer compensation integration time) to avoid a significant event overlap, with resulting noise in the jet-jet mass signal. For a heavy Higgs search using H$\rightarrow ZZ \rightarrow lljj$, or H$\rightarrow WW \rightarrow jjl\nu$, our ability to avoid event overlaps will lower background and enhance the signal in the dijet mass reconstruction. This yields a factor $\sim$2 reduction in the mass cut necessary at the W or Z mass as compared to calorimeters integrating over 10 or so events. At $10^{34}cm^{-2}s^{-1}$, TEXAS will have a dijet mass resolution degraded by a similar factor because of event overlaps. In other words, at $10^{34}cm^{-2}s^{-1}$, the TEXAS peaking time of about 6-8ns compares to the 80 ns peaking time in liquid Argon at $10^{33}cm^{-2}s^{-1}$, and the 40ns integration time compares to the 400ns integration time of liquid Argon at $10^{33}cm^{-2}s^{-1}$.

The strategy to find technicolor and compositeness also requires minimal overlap noise in order to preserve the linearity of the jet energy signals.

Lastly, the monolithic calorimeter allows fast trigger decisions at an early level on electrons, γ's (when combined with the pre-radiator) and hadrons.

Figure Captions

T2.1 SPACAL Compensation Time Structure; e/π ratio

T2.2 SPACAL Time Structure; resolution

T2.3 W mass resolution vs. number of superimposed background events

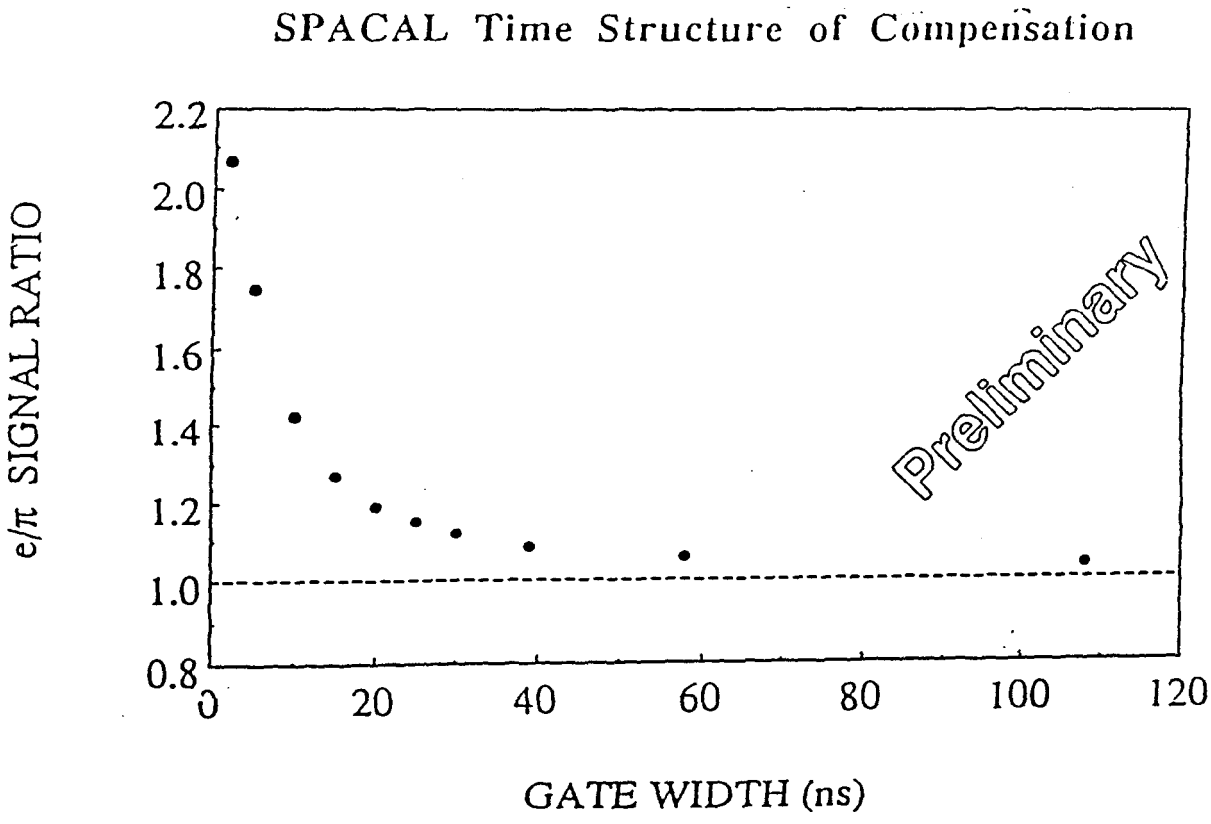

Figure T2.1

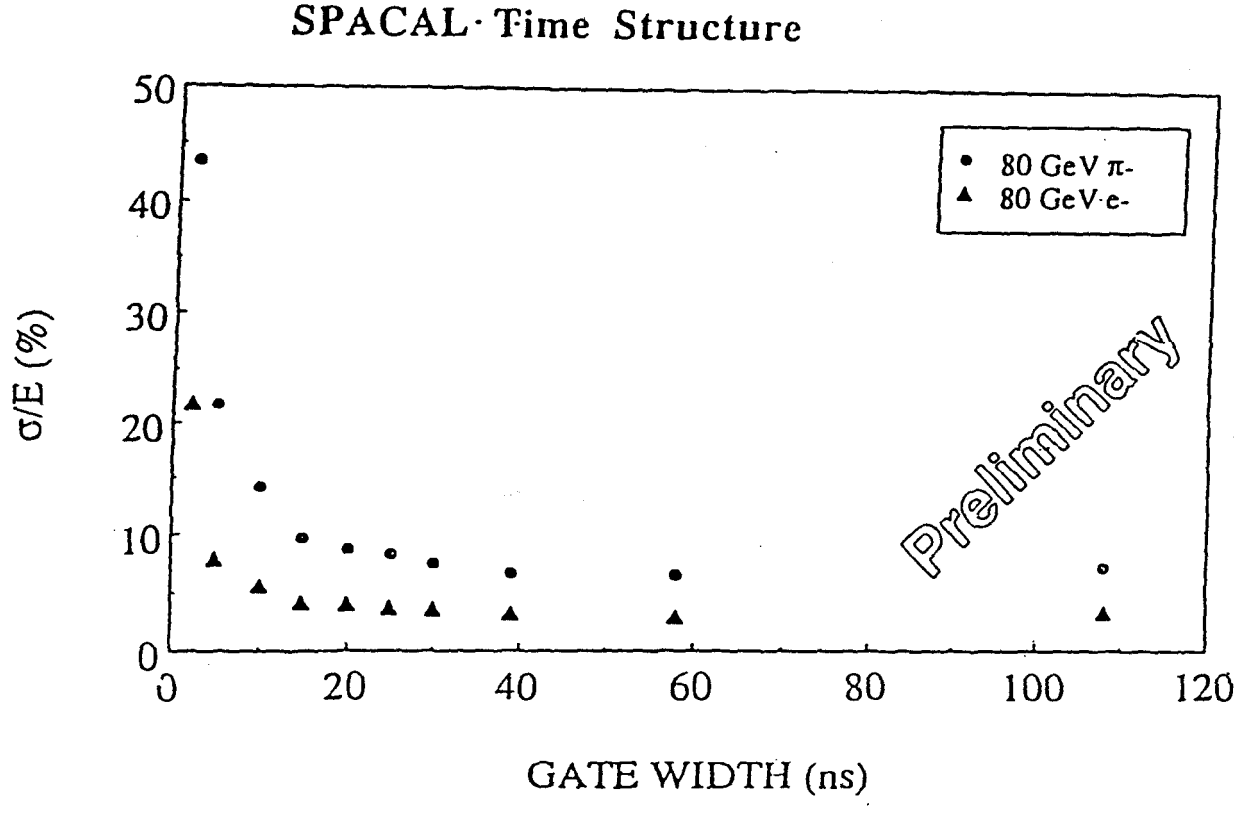

Figure T2.2

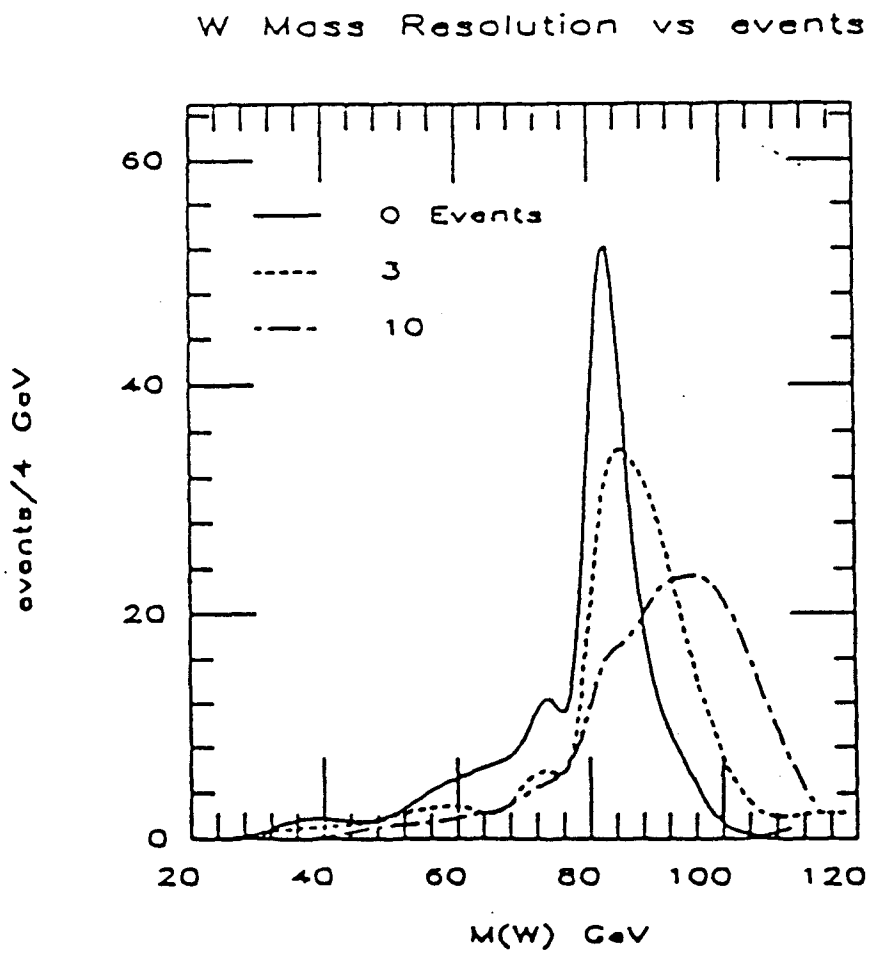

W mass resolution vs number of superimposed background events.

Figure T2.3

T3: Current Detector Simulation Program

Outline the simulations you are doing to complete the analysis of your detector's capabilities

The overall TEXAS simulation scheme is summarized in the box/flow diagram. All of the simulation sections exist in one form or another. Of course, there is still a large amount of optimization and fine-tuning to perform before we have a full and detailed analysis of the TEXAS detector capabilities. One of the more important features of the TEXAS simulation involves the ability to incorporate new results from test-beam work, etc. wherever necessary to update individual detector element performance characteristics.

Event generators include ISAJET, HERWIG and PYTHIA. In all cases, files of generated signals and backgrounds are saved before sending the events through the detector simulation. ISAJET provides a very flexible user interface for a wide variety of physics processes. HERWIG (Hadron Emission Reactions with Interfacing Gluons) is especially well-suited to process and signatures which are sensitive to QCD jet production and fragmentation.

Each of the TEXAS subsystems has its own simulation package. These are the central calorimeter, forward calorimeter, tracker/imaging pre-radiator and muon transition radiation detector. Examples of the results of using these packages are contained in many of the other answers to the PAC questions that are included in this document.

The calorimeter simulation is handled at several different levels of detail. Parameterizations are included for energy resolution effects (including the constant term and tails), lateral shower spreading and both lateral and longitudinal shower development. Naturally enough, the present version of the central calorimeter simulation contains many simplifications. Monolithic towers are assumed for jet studies. We use a simplified version of the CDF/UA1 parameterizations which thereby incorporates optimal longitudinal development/fluctuation. We treat the calorimeter as a uniform mixture of materials. We assume no angular dependence (as is confirmed by the experience of the SPACAL group, for hadronic showers at least). We assume a linear calorimetric response (except with some explicit longitudinal development). We assume e/h=1. Wherever possible we make detailed comparisons with the SPACAL test-beam results. On-going central calorimeter work includes a detailed study of the effect of speed and event pile-up on the high luminosity operation (including shower spreading) with particular emphasis on electron isolation cuts. The forward calorimeter simulation includes a full GEANT shower generation into segmented tungsten and liquid scintillator. Present studies include missing E_T versus η and the effect of e/h=1. Spectator quark jet tagging work is being performed to establish the forward calorimeter response parameterization, to determine granularity effects and to optimize jet-finding and clustering algorithms to yield efficient separation of signal from background.

The tracker/imaging pre-radiator simulation uses both GEANT and EGS. Ray tracing has given valuable pattern recognition information and allowed a computation of track finding and vertex finding efficiencies. On-going studies include conversion rate versus η, pre-radiator rejection of low energy conversions and Dalitz pairs, pre-radiator identification of e/h and

π^0/γ overlaps, event vertex resolution, high-luminosity track-finding capability and trigger pad performance.

The muon transition radiation detector simulation incorporates a parameterization of the muon momentum resolution versus momentum based on test-beam results and theoretical calculations. Studies include the effect of the muon system response on Higgs search capabilities and on missing p_T determinations.

TEXAS STIMULATION

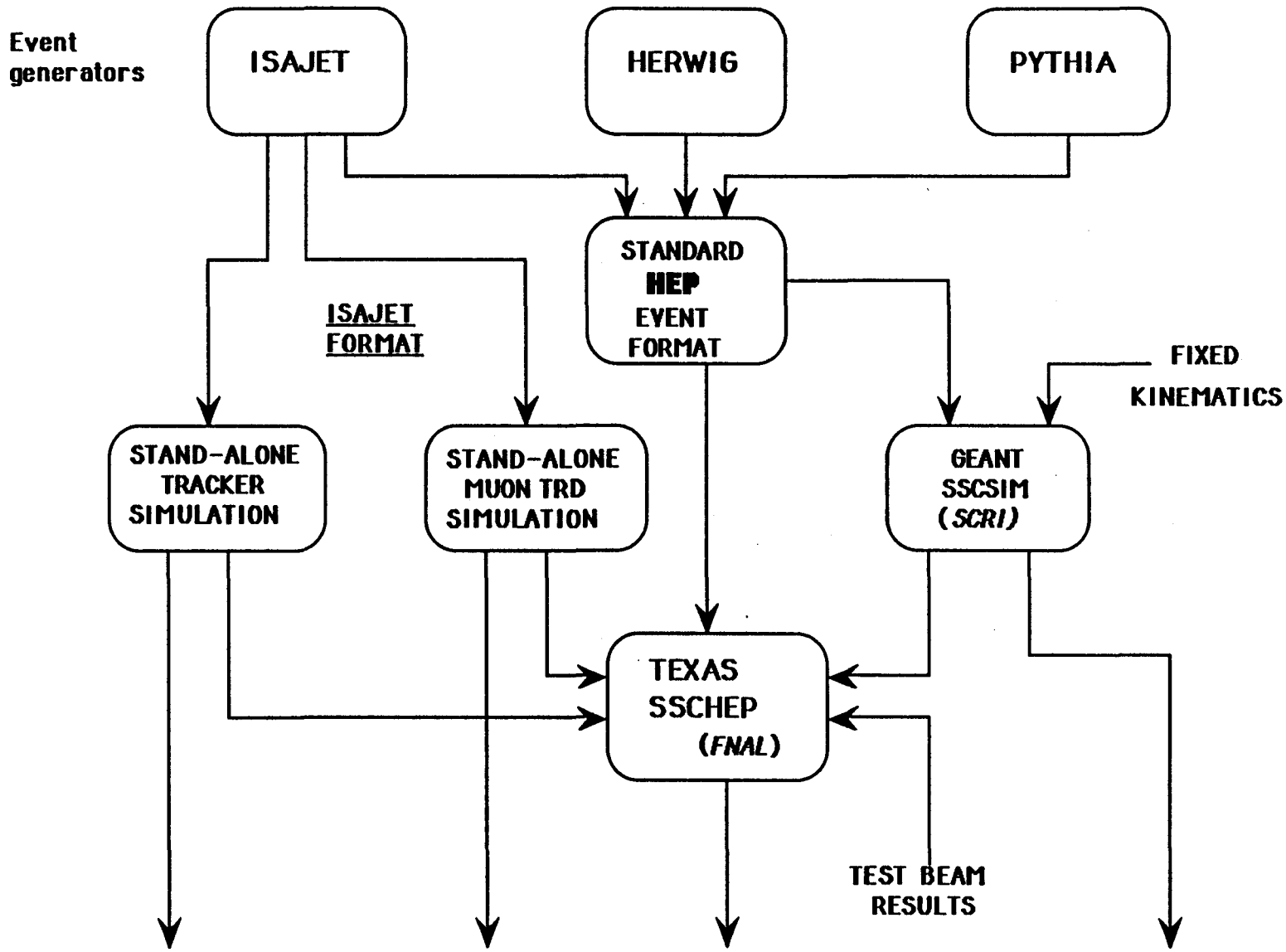

T4: $H \rightarrow \gamma\gamma$: Vertex Sensitivity, energy calibration, etc.

- *You emphasize searching for intermediate-mass* $H \rightarrow \gamma\gamma$. *Please simulate the response of your detector to this process, including effects of vertex resolution along the beam.*

For a Standard Model Higgs with mass between ~100-110GeV and $2M_W$, $H \rightarrow \gamma\gamma$ is a signal that TEXAS has the unique capability to detect. This signal is very important because the coupling to $\gamma\gamma$ is the only channel not available to the Z. Regardless of the initial Higgs discovery method, the branching ratio of the $H \rightarrow \gamma\gamma$ is an important figure which probes the existence of new particles in the quantum loop that mediates this decay.

This signal consists of 2 γ rays roughly back-to-back in ϕ, separated by about 1 unit of rapidity. The average opening angle is typically larger than 135°. The energies are such that the $E_T(\gamma)$ >20-30GeV.

The origins of the dominant backgrounds are the processes qq$\rightarrow \gamma\gamma$, gg$\rightarrow \gamma\gamma$, gq$\rightarrow \gamma$+q-jet($\rightarrow$ leading π^0), and qq$\rightarrow \gamma$+g-jet($\rightarrow$ leading π^0). A cut on E_T of 20-30 GeV reduces the qq and gg background. A cut on the $\gamma\gamma$ rapidity of η <2.5-3 reduces the qq background by a factor of ~2. A cut on the γ rapidity of <2-3 also enhances the signal. A cut on the polar angle of the 2 photons in the $\gamma\gamma$ rest frame of θ^*>35° is also of help.

To eliminate the serious backgrounds from accompanying jets that produce a leading π^0, an isolation cut about the γ direction is imposed in a cone of radius R of 0.4-0.8, requiring less than 10% of the $E_T(\gamma)$ in cells surrounding the γ in the cone. Unfortunately this cut is very uncertain, because of the uncertainty in jet fragmentation into isolated π^0's at SSC energies. Estimates from ISAJET suggest that a rejection of about 10^{-4} per γ can be achieved with the isolation cut, but this is merely preliminary.

To study and eliminate this π^0 contamination from a jet that fragments into a single hard neutral pion, the pre-radiator is used to measure a single π^0. The minimum opening angle for a π^0 is given by $\theta_{min}=2M_\pi/P_\pi$. Thus, for a 100(50)GeV neutral pion, the two decay photons are separated by more than 2.6(5.2)mm per m of flight path. In TEXAS, they are separated at minimum by 5(10)mm at the pre-radiator, easily detected in our imaging pre-radiator. This is demonstrated in fig. T4.1 which shows a simulation of the showers from the two γ's of a π^0 decay. Furthermore, as mentioned previously, SPACAL has shown that it is possible with a spaghetti calorimeter to detect the presence of an electromagnetic shower and a hadron separated by as little as 45mm in the calorimeter. TEXAS is thereby able to measure in detail the fragmentation of a jet into γ's, electrons and ultimately, by extrapolation, into isolated π^0's. TEXAS will be able to directly measure π^0 background fakes to the $H \rightarrow \gamma\gamma$ signal.

Even after the above cuts, a mass resolution of at worst ~1% is necessary over this mass range to reject the single photon background. Therefore the energy resolution for a ~50GeV γ must be ~1% or better. A resolution of $6\%/\sqrt{E}+0.5\%$ is adequate for this channel provided that the calibration can be held. This is the design goal for TEXAS (with two methods in the spaghetti calorimeter to achieve this goal).

The mass resolution also has a contribution from angular errors given by dM/M = $d\theta/2$ for approximately back-to-back photons. The γ position resolution is at most $\pm$1mm in the pre-radiator. SPACAL has measured a resolution on the position of electromagnetic showers of less than 1mm using centroid fits in towers larger than those proposed for TEXAS. Therefore, in TEXAS, with 2m inner radius, the crudest angular error is given roughly by the size of the interaction diamond. In this case, $d\theta$ would be 5cm/200cm, giving a 1.25% contribution to dM/M. At a luminosity of $10^{33}\mathrm{cm}^{-2}\mathrm{s}^{-1}$ the other tracks in the event can be used to improve this vertex determination by at least a factor of 10. Using the tracker system for vertexing therefore implies that the angular error contributes a negligible amount to the mass error.

At high luminosity with overlapping events, the photon direction given by the combination of the pre-radiator and the calorimeter may be used to constrain the possible vertex. For a γ conversion in the pre-radiator, the position of 85% of the γ's above 10GeV can be determined to better than $\pm$1mm. Over 90% of the γ's convert in the pre-radiator. Taking the calorimeter and the pre-radiator together (and using the SPACAL result of a position determination of $\pm$ <1mm for isolated γ's), the typical γ direction can be determined to $\sim$5mrad without using any event vertex information. Each γ then projects back to the beam axis with resolution along the beam direction of $\sim\pm$1cm. This can be used to constrain γ's (and pairs of γ's) to specific vertices. It should thereby be possible for TEXAS to explore this channel at luminosities exceeding $10^{33}\mathrm{cm}^{-2}\mathrm{s}^{-1}$.

We have simulated the response of TEXAS to the H$\rightarrow \gamma\gamma$ process and the results are given below. In the guideline example with 5cm vertex resolution along the beam (the length of the beam crossing diamond) we assume the worst-case scenario of no vertex reconstruction. The 0.5cm vertex resolution assumes excellent shower position determination in both calorimeter and pre-radiator and, as can be seen below, is unnecessarily good since the energy smearing term dominates at all Higgs masses.

H$\rightarrow \gamma\gamma$ events were generated with ISAJET and selected according to the following criteria:

$$\begin{aligned} E_T(\gamma) &\geq 20 \text{ GeV} \\ |\,\eta(\gamma)\,| &\leq 3 \\ |\cos\theta_\gamma| &\leq 0.8, \end{aligned}$$

with the following detector parameters assumed in the event simulation:

EM calorimeter energy resolution	: 6.5%/ $\sqrt{E}$+ 0.5%
Position resolution for showers in the preradiator	: 0.6 mm
Z vertex smearing	: 5.0 (0.5) cm

Figure T4.2 shows the $\gamma\gamma$ mass distributions for 150 GeV Higgs generation (solid line) and $\sigma_E + \sigma_{Z\,vertex}$ smearing. The dotted curve is computed under the assumption that the vertex resolution is $\pm$5cm and the dashed curve with the assumption that the vertex resolution is $\pm$0.5cm. The rms widths for dashed and dotted curves are 0.8% and 1.3%, respectively. The

table below is a summary of the mass resolutions for different assumed Higgs masses. All quantities are given in GeV. The last two columns give the computed error on M($\gamma\gamma$) with the assumption of 5 (0.5)cm vertex error. The total mass smearing is ~1.3% (0.8%) in the mass region between 100 and 150 GeV/c^2 for the 5.0 (0.5) cm vertex resolution.

Higgs Mass	Generated	σ_E smearing	Vertex smearing	σ_E + Vertex smearing
100	100.00 ± 0.006	99.94 ± 0.88	± 1.03 (0.25)	± 1.33 (0.89)
120	120.00 ± 0.007	120.00 ± 1.00	± 1.25 (0.27)	± 1.58 (1.02)
130	130.00 ± 0.007	130.00 ± 1.08	± 1.34 (0.27)	± 1.71 (1.09)
140	140.00 ± 0.008	140.00 ± 1.13	± 1.45 (0.28)	± 1.86 (1.18)
150	150.00 ± 0.008	150.00 ± 1.20	± 1.57 (0.38)	± 1.95 (1.22)

More details on the Higgs $\rightarrow \gamma\gamma$ channel are given in the answer to generic question number 1.

Also it seems that excellent γ energy resolution is needed for $H \rightarrow \gamma\gamma$. *How does one calibrate the calorimeter sufficiently well?*

The energy resolution possible with a spaghetti calorimeter has been measured as $6.5\%/\sqrt{E}$ by the JETSET collaboration, with a double fiber loading. The Monte Carlo which completely predicts the resolution in SPACAL shows that a $6\%/\sqrt{E}$ resolution is easily obtainable with 0.5 mm fibers in a spaghetti calorimeter, as shown previously in the introductory section on the calorimeter design. On the basis of the SPACAL results, a constant term of 0.5% is also a realistic goal, provided the availability of proper calibration, a crucial item that we proceed to discuss.

A basic technique for calibrating a homogeneous compensated tower is to use the simulated annealing or global entropy surface. This technique for relative calibration actually becomes easier at high luminosity. In this technique, the symmetry of the calorimeter system and the energy deposited is used to calibrate. In a zeroth approximation, with N identical cells, N-1 are used to form an average, and the Nth is adjusted to the average. The process is then iterated over every cell. Remarkably, statistical mechanics shows that this process converges quickly. It would first be used on every ring in constant η. Then the cells would be redefined as the difference in adjacent η towers at constant ϕ. (The profile in η should be identical for every stripe in constant ϕ). More sophisticated adaptive algorithms of a similar nature can be designed to do this globally (simulated annealing) much more rapidly, where many towers are adjusted simultaneously.

Long-term absolute energy calibration, tied to the global calibration, would be performed continuously using event signals (such as electron decays of the Υ and Z). Periodically, compact accelerators and radiosource wires would be used off-line. The phototube average currents, voltages, and temperatures would be recorded by a highly multiplexed low rate spy system integrated into the phototube electronics.

For short term calibration and linearity calibration, high stability ring dye lasers phase-locked to the accelerator RF serve as a precision light-source (with the intensity compared to radiosources and cryogenic negative electron affinity photodiodes - typical cost about \$150-250k/laser). A sub-ns laser pulse would be periodically delivered into the calorimeter towers on quartz injection fibers (4 per tower, embedded with the other fibers, injected into Silica diffusers at the front and back of each tower - note the front mirrors on the fibers are 85% reflective/15% transmissive) about 1 ns before a beam crossing, creating a prepulse in the quietest time before an event. The normal event pipeline would be used to look backwards and accept only towers which had least count energy for at least 3-4 beam crossings.

The laser pulse wavelength and intensity are tunable. By injecting in the near UV (330-390nm) some of the scintillator energy transfer mechanisms can be monitored. By tuning the laser to longer wavelengths the transmission properties of the fiber base can be monitored. (Radiation damage is often wavelength dependent). By injecting in the back just in front of the photodetector, the photodetector can be separately monitored from the fibers. By detecting the reflected pulse during back-injection, and comparing that pulse with the front pulse at several wavelengths, the fiber properties along the length of the fiber can be

unfolded. The laser intensity can be precisely varied by electro-mechanical cavity tuning and by mechanically switchable sets of metallized neutral density filters. It is therefore possible to measure the linearity of the calorimeter system over 6 orders of magnitude with an error of 0.1%. The capability of near UV-visible light injection to simulate the properties of energy deposition is unique to visible light scintillators.

• Comparison of $H \rightarrow \gamma\gamma$ with other EOI's: Barium Fluoride Critique

We now contrast our electromagnetic system with that of L*, the only competition in this important Higgs channel.

L* has no Imaging Pre-radiator device, and therefore no formal way to measure π^0 contamination in the isolation cut. Furthermore, the only constraint on the γ direction is given by the fit to the position of the γ by the BaF_2 crystal, whereas TEXAS has 2 contraints. The BaF_2 crystals are relatively large for an electromagnetic calorimeter, covering 0.04 x 0.04 in segmentation, and therefore are more subject to stray backgrounds than the towers in TEXAS.

For example, because the BaF_2 crystals are slightly larger than the Molière radius, background energy in neighboring crystals will degrade the γ point resolution (only 2-3 crystals participate in a coordinate fit in each direction). The large segmentation of 3 crystals together (0.12 in each direction) has a larger probability of extra tracks, only 75cm from the beam, compared with TEXAS. A single looper in the magnetic field through a crystal degrades the point resolution by about a factor of 2.

The larger electromagnetic segmentation makes it harder to study and identify electrons in jets in L*. This is important to fully understand the potential backgrounds to this Higgs channel, as well as for other SSC physics.

Furthermore, it is more difficult for L* than for TEXAS to trigger on an isolate d γ without interrogating all of the tracker system pixels. Because TEXAS has tile sections in the tracker/preradiator system matched to the cell-size of the calorimeter and a fast electromagnetic identification in a more highly segmented monolithic calorimeter, it is easier to trigger on isolated γ's.

The BaF_2 resolution claimed by L* has never been obtained in beam tests. The best resolutions obtained have used both the long and the short wavelength components (the long component has about 5 times the light output at a much more tractable wavelength). One group obtained $4.2\%/E^{1/4}$, and another group obtained $1.8\%/E^{1/3}$ on electrons up to 40GeV. (R-Y Zhu, CALT-68-1566 (1979)). With low energy electrons (1-4GeV) and using mainly the short wavelength component, the G-2 group (BNL AGS E821) never achieved better than $6\%/\sqrt{E}$.

The number of photoelectrons per GeV quoted by L* was obtained using 0.662MeV γ's from Cs^{137} on crystals of a maximum size of 14 x 3 x $3cm^3$ (62 photoelectrons/MeV) with 80-90 photoelectrons/MeV obtained on small (2-5cm diameter, 2-7cm long) crystals and with

a 55 ns gate. It is probably worthy of note that a GEANT calculation quoted in the L* proposal simply generates the energy deposited in the crystal (with no assumed loss from leakage, etc.) which is then converted into photoelectrons by a multiplicative constant (80K photoelectrons/GeV) without the correct Birk's constant. This estimate does not properly include photon propagation, spectral reflection, spectral absorption in a 50cm long crystal, coupling properties, etc., especially as a function of energy. These are the most important factors dominating the energy resolution of a large shower counter detector, and also the ones that will contribute to a constant term. We note that the Crystal Ball collaboration obtained a best resolution of $2.7\%/E^{1/4}$ using NaI (operating at 410nm peak light output wavelength), with more than 15 times the detected photoelectrons than in the fast component of BaF_2. Despite the superb photon statistics, the best resolution obtained with a large NaI crystal (20 radiation lengths) is $2\%/E^{1/4}$ in a test cell. (The best resolution obtained in a small NaI crystal with γ rays is about $1\%/\sqrt{E}$ effective.)

If we use the two experimentally measured resolutions for BaF_2 (which used both wavelength components) and include a constant term of 0.5%, to bracket the potential respone of the BaF_2, then for the 2 energy resolutions, $1.8\%/E^{1/3}+0.5\%$ and $4.2\%/E^{1/4}+0.5\%$, we obtain resolutions of 0.96% and 2.0% at 60 GeV for the BaF_2. and if we use $6\%/\sqrt{E}+0.5\%$ for the TEXAS spaghetti, we obtain an energy resolution of 1.27%. These energy resolutions are similar enough that the price of the BaF_2 surely cannot be justified.

In addition, several other factors mitigate against BaF_2, especially when used only with the fast component for the best energy resolution, and which may make even the experimentally obtained resolutions using smaller crystals and the long component overly optimistic, especially in a large system close to the beam at the SSC:

(1) Far UV emission: The 180-220nm light in the fast component is very difficult to work with and to exploit uniformly, for several reasons. Optical Coupling is difficult - even a fingerprint will absorb a large fraction of the light. Very accurate dimensional control must be maintained to preserve uniform UV transmission. Furthermore, the silicone optical fluids proposed are known to suffer radiation damage. UV photocathodes seem to be notoriously spatially non-uniform in their response. Reflectors are necessary to smooth out the response of a 50cm long crystal. Teflon film would be ideal for this purpose, but suffers severe radiation damage at 75cm from the SSC beam. Unfortunately, Aluminium coating on the BaF_2 crystal has been shown not to be sufficient to reflect this short wavelength light effectively enough. The surface quality and polish at 200nm is also more critical than at longer wavelengths (NaI - 410nm - blue, BGO - 480nm - green). It will be a difficult job to perfect a uniformly responding BaF_2 crystal and reflector system to the level claimed by the proposal, and maintain the small inter-crystal gap claimed to be possible in L*. This is contrasted to the good results obtainable in BGO, where the light emission (480nm) can be easily reflected at tunable levels of reflectivity in a low radiation damage environment with very thin materials (as shown by the results in tests by the L3 group). The far UV properties of the fast component will almost certainly contribute to a decrease in the energy resolution than might be predicted from photon statistics alone.

(2) Crystal Size and Quality: In the past, BaF_2 crystals have been very difficult to grow water-clear in large sizes, without wave or film imperfections. We have seen no data on crystals longer than 14 cm; in the tests by the Caltech group, the largest crystal was the poorest performer. Data on the large crystal (22cm long - 44% of the size needed in L*) recently delivered to Caltech has not been provided. While SIC may be able to solve the large crystal problem, it is a risky claim indeed for 26,000 crystals, despite the success of BGO; UV transmission is much more susceptible to a small amount of impurities.

(3) Radiation Damage: Both the coupling fluids and the reflectors normally used with BaF_2 damage easily; since L* would be in a radiation environment 7 times higher than the TEXAS calorimeter, this may a be a problem. Furthermore, the Carbon fiber/epoxy support structure proposed will not hold up the 50tonnes of crystal after a year of exposure at 75cm from the beam. While the BaF_2 is radiation hard, the system components necessary to allow it to operate are not; these will not only reduce the energy resolution, but may physically give way. Other solutions may introduce inhomogeneities in the system which are not desirable. Already in the existing L* design there are 1% dead regions.

(4) Magnetic Field Readout: There is no good solution at the present time for the phototubes which would be most naturally oriented transverse to the magnetic field direction. No existing phototube operates with reasonable gain in this mode at 7.5kG; furthermore, the tubes that operate at low gain up to 45° to the field are not noted for high linearity. These tubes will also receive the dubious benefits of hadron showers; the crystals provide 1.7 interaction lengths.

(5) Low Segmentation and Short Inner Radius: As previously noted, the ionization rates in these crystals will be high not only because they are 75cm from the beam (again, compare with the TEXAS inner radius of 200cm), but also because the 26,000 Towers in L* subtend 0.04 x 0.04 (as contrasted with TEXAS at 0.025 x .025 with ~160,000 towers). The background radiation and minimum bias event noise will be higher in L* by a factor of 7 or more.

(6) Calibration: Most importantly, short-term and linearity calibration of the BaF_2 will be very difficult if not impossible. It is not practical to provide a light pulse with a wavelength of ~220nm to crystals/phototubes in a tight array sandwiched between a tracker and a hadron calorimeter (the phototube has to be blind to light with wavelength longer than 220nm to avoid the slow component). This is contrasted to the spaghetti design, where tunable optical pulses can calibrate both the dynamic range response and the full operation of the calorimeter.

The calibration methods proposed by L* have serious short-comings for on-line, linearity, and short-term stability calibration. Whether the method to use minimum ionizing hadrons will work for BaF_2 as suggested by L* is not clear. We point out that 81% of the hadrons will undergo an inelastic interaction, and 93% will undergo some type of a nuclear collision (including elastic and quasi-elastic collisions), in the 50cm long BaF_2 crystals. While this may give a relative calibration, there will be a widening of the 0.33GeV MIP deposition by quasielastics, elastics, low-q inelastics, charge exchange etc. and will require a larger

sample and therefore much longer than the 12 hours claimed in the L* EOI. Even multiple scattering on the 25 radiation length crystals will widen the MIP distribution by ~1%. The use of accelerator and radiosources in off-line running is important, but does not fully solve the on-line and large dynamic range problems.

The ease of calibration together with the quiet operation of the large inner radius and finely segmented calorimeter that is proposed by TEXAS is therefore a good compromise solution to the problem of detecting $H \rightarrow \gamma\gamma$, with an energy resolution fully adequate for Higgs masses larger than ~100-110GeV. Indeed, it may be argued that the difficulty of operation, calibration, and production of BaF_2 in the UV in a large magnetic field is not solved, and is not a prudent solution at this time. Moreover, the lack of fine electromagnetic segmentation, the short radius, and the absence of an imaging preradiator in L* detract from the capability to measure and/or reduce background.

Figure Captions

T4.1 Tracker/Preradiator simulation of the two γ showers from a 50GeV π^0 decay 2m from the detector. The figure shows a 10cm section of the imaging preradiator; the horizontal lines represent plastic scintillating fiber layers and lead sheets. (Private communication, P. Mélèse).

T4.2 $M(\gamma\gamma)$ distributions for a 150GeV Higgs. The explanation of the symbols and plotting characters is given in the text.

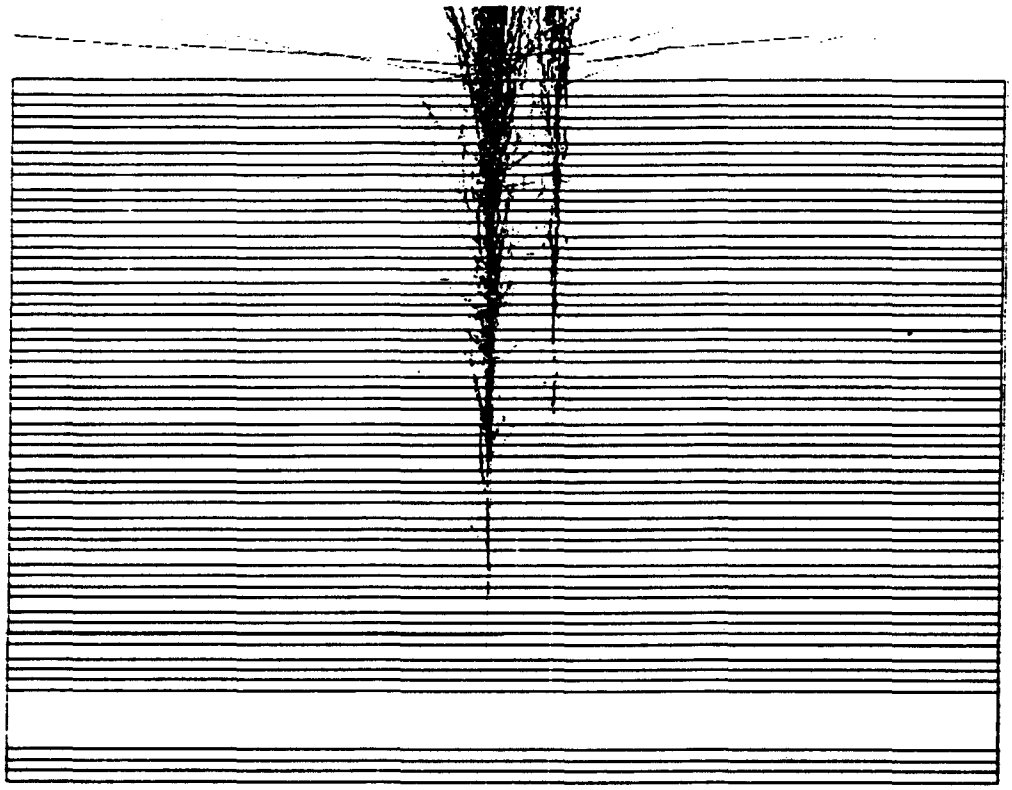

Figure T4.1

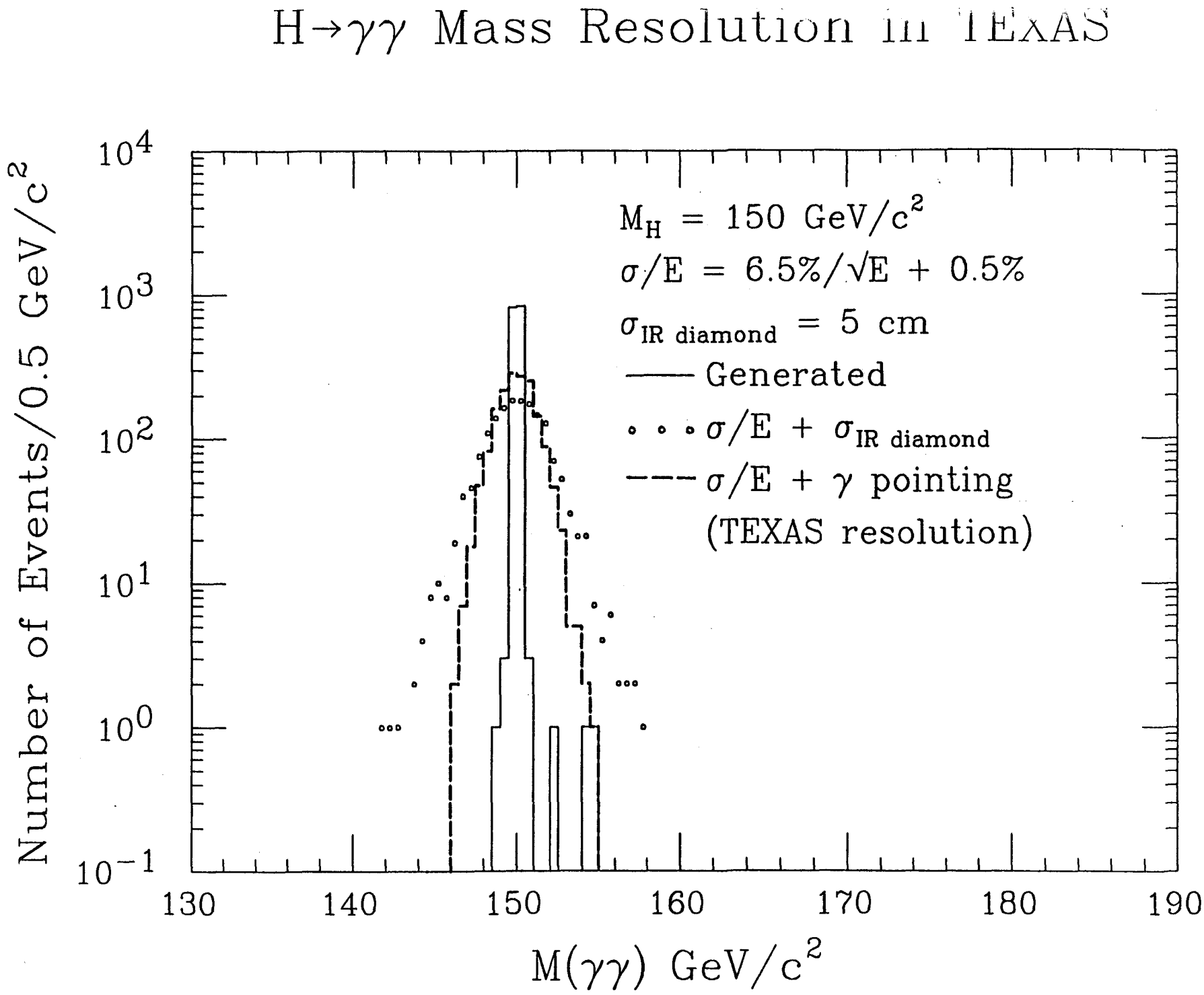
H→γγ Mass Resolution in TEXAS
M_H = 150 GeV/c^2
σ/E = 6.5%/√E + 0.5%
$\sigma_{IR\ diamond}$ = 5 cm
Generated
σ/E + $\sigma_{IR\ diamond}$
σ/E + γ pointing
(TEXAS resolution)
Number of Events/0.5 GeV/c^2
10^4
10^3
10^2
10^1
10^0
10^{-1}
130
140
150
160
170
180
190
M(γγ) GeV/c^2

Figure T4.2

T5: Quark-Jet Tagging

- *Describe in detail the role of quark-jet tagging for your Higgs searches. Your simulation should include effects of resolutions, cracks, initial-state gluon radiation, clustering, and pileup. In particular, can this method be used given the QCD background of high-p_t Z production?*

The TEXAS calorimeter provides high-resolution hadronic energy measurement over a large rapidity range ($|\eta| < 5$). Preliminary studies, both at the parton and QCD jet level, have indicated that high-p_t processes which are mediated by W-W fusion (which dominates Higgs production at high energies) are much more likely to give energetic jets in forward calorimetry than are background processes mediated by g-g fusion. Detection of these forward jets (typically with $3 < |\eta| < 5$) can thus complement other cuts in providing signal-to-background discrimination for such processes as $H \rightarrow ZZ \rightarrow ee\nu\nu$, $H \rightarrow ZZ \rightarrow eejj$, and $H \rightarrow WW \rightarrow e\nu jj$. Each of these processes has a signal to QCD background ratio of order 1:100, with the $H \rightarrow ZZ \rightarrow ee\nu\nu$ having the benefit of a missing p_t signature in addition to two electrons reconstructing to the Z mass. Accessing these modes increases the statistics over that available in the 4-lepton final state by accessing larger branching ratios in the Z decays.

For our studies of quark-jet tagging in high-mass Higgs searches, we have used the HERWIG event generator program and our TEXAS-SIM detector simulation program. HERWIG (Hadron Emission Reactions With Interfering Gluons) performs a detailed QCD interaction and fragmentation simulation, including the effects of initial-state gluon radiation.[1] The TEXAS-SIM detector simulation includes the hadronic energy resolutions (including the constant term) appropriate to both the central and forward calorimetry, the effect of our material transition at $\eta = 3$, the effect of the hole at $\eta = 5$ (with shower spreading and cross-over), hadronic shower profiles matched with test-beam data and GEANT calculations, pileup of minimum-bias events, and a modified UA1-type clustering algorithm.

Figure T5.1 illustrates typical quark-jet tags in the TEXAS forward calorimeter, with and without the effects of shower spreading. As is evident in the figure, shower spreading has a small effect on jet-finding and jet energy measurement for $|\eta| < 4.5$. This is because of the relatively large distance of the forward calorimeter from the interaction point (> 7 meters) and the relatively short interaction length (< 12 centimeters) of the tungsten-liquid scintillator composite. More than 90% of the hadronic shower energy is deposited within 15 centimeters of the shower axis in this material. For the TEXAS forward calorimeter geometry, this corresponds to the following rapidity and azimuthal spread as a function of jet rapidity:

η	$d\eta$	$d\phi$
3.0	.12	.15
3.5	.21	.28
4.0	.37	.50
4.5	.63	.87
5.0	1.04	1.46

Because of limited statistics and computer time, our results thus far are only preliminary (but quite promising). We place rapidity constraints of $3 < |\eta| < 4.5$ (1.3 to 5.7 degrees) and an energy requirement of $E_{jet} > 1$TeV. Of the WW signal events, 35% had at least a quark-jet tag, while 4% had two tags. For the gg background, 8% of the events had one tag, with 0.25% of the background events generating two tags. The signal-to-background ratio is thus improved by a factor of 4.5 for the single-tag and a factor of 15 for the double-tag requirements. Information from the central calorimeter has not yet been correlated with that from the forward calorimeters. The effects of pile-up from minimum bias events at high luminosity have not yet been studied with sufficient care, although preliminary indications are that the spectator-quark jet tags are sufficiently prominent to stand out well above this background. In combination with our central calorimeter studies of $H \rightarrow ZZ \rightarrow ee\nu\nu$, and $H \rightarrow ZZ \rightarrow eejj$, these quark-jet tagging results indicate both channels can yield signals significantly above background in the TEXAS detector.

Figure Captions

T5.1 Quark-jet tags in the TEXAS forward calorimeter with and without the effects of transverse shower spreading.

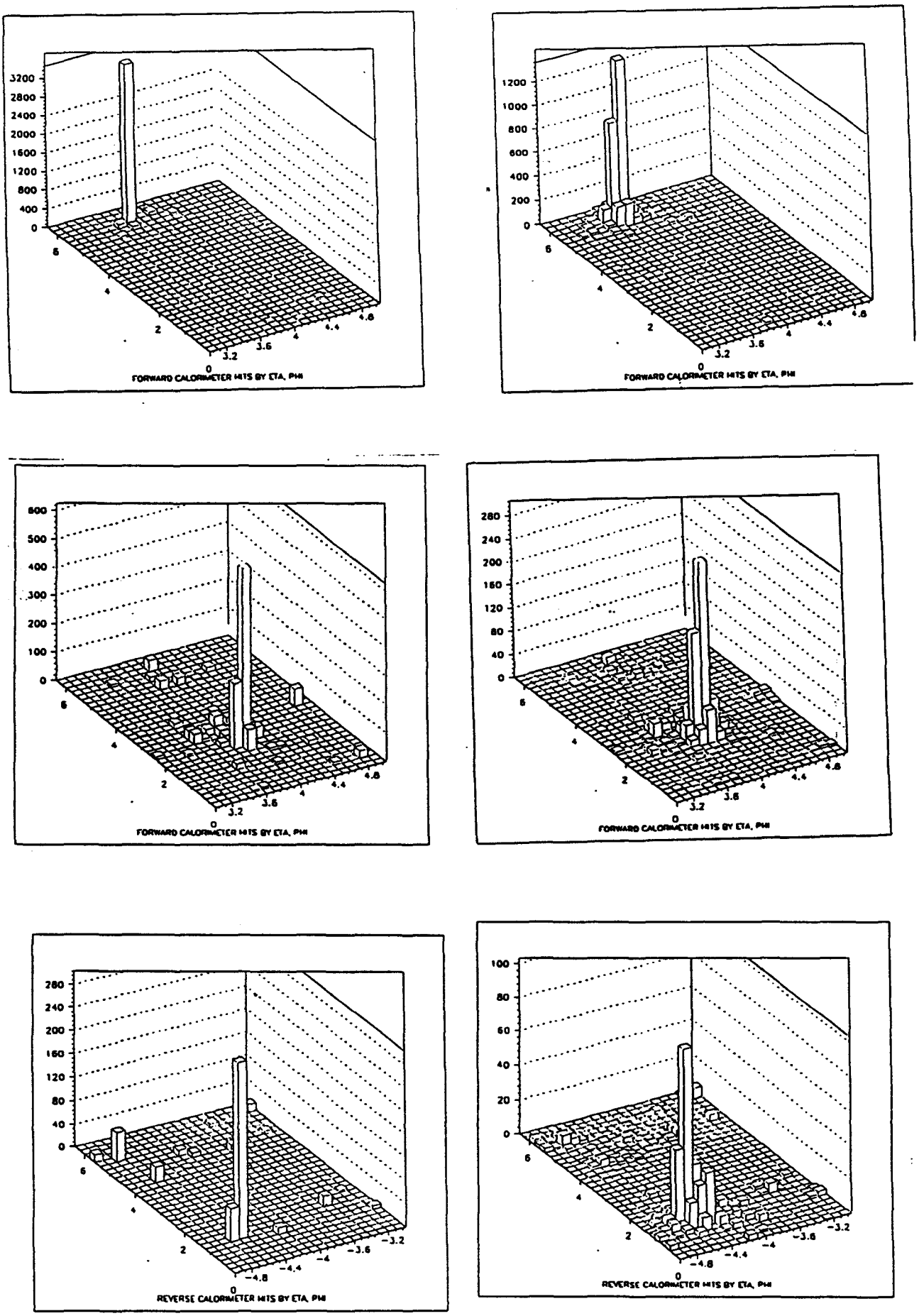
FORWARD CALORIMETER HITS BY ETA, PHI
FORWARD CALORIMETER HITS BY ETA, PHI
FORWARD CALORIMETER HITS BY ETA, PHI
FORWARD CALORIMETER HITS BY ETA, PHI
REVERSE CALORIMETER HITS BY ETA, PHI
REVERSE CALORIMETER HITS BY ETA, PHI

Figure T5.1

T6: High-Mass Higgs and TRD Muon Resolution

In looking for a high-mass Higgs, how does the uncertainty in measuring muon momenta affect the backgrounds from uncorrelated muons?

We have investigated Higgs discovery by the 4-lepton channel in TEXAS. Table 1 below shows the lepton energy resolution necessary to match the Higgs width.

Higgs mass	200 GeV	400 GeV	600 GeV	800 GeV
Higgs width (Γ)	4 GeV	32 GeV	108 GeV	256 GeV
Lepton resolution	1.8%	6.3%	13.5%	26%

In TEXAS, for the 200 GeV Higgs, the electron energy resolution, $6.5\%\sqrt{E} + 0.5\%$, matches or exceeds the Higgs natural width for electrons with energies greater than 20 GeV (this provides nearly 100% acceptance). Since the production rate is high for the 200 GeV Higgs even at standard luminosity, the muon mode is not needed in this case.

For a 400 GeV Higgs, the muon TRD momentum resolution is optimal, (7% at 200 GeV momentum) as in Fig. T6.1 and the electron resolution is more than adequate, so all 4-lepton modes are easily detectable. For a 600 GeV Higgs, we rely on the 4e and $2e2\mu$ modes. The 4μ mode would be used only to check the consistency of the other measurements; this represents at most a 25% loss in the four lepton modes. Muon energy resolution is important in rejecting background from continuum ZZ production, by requiring that muon pairs reconstruct to give the Z invariant mass. The results of our signal and background simulations including TEXAS electron and muon resolution functions were given earlier, but we repeat them here to simplify the reader's task.

A study has been made of the trigger acceptance. Optimized geometrical/kinematic cuts for four leptons appear to be:

$| \eta(lepton) | \leq 3$

$E_T(l) \geq 20$ GeV

$P_{Total}(\mu) \geq 40$ GeV/c and $P_T(Z) \geq 25$GeV/c.

The efficiency of these cuts is summarized in Table 2.

Table 2: Geometrical/Kinematic Cut Efficiency for Higgs Events

Higgs Mass	σ BR [fb]	eeee	ee$\mu\mu$	$\mu\mu\mu\mu$
300	67.0	0.46±0.013	0.24±0.008	0.14±0.009
400	34.7	0.53±0.013	0.37±0.009	0.29±0.012
600	16.4	0.64±0.012	0.57±0.009	0.51±0.013
800	7.6	0.72±0.012	0.66±0.009	0.61±0.013

For the standard SSC luminosity, the total number of events produced and the number of events that trigger the detector are shown in Table 3.

Table 3: Number of Events Triggering the Detector in a Standard Year

Higgs Mass	N_{total}	$N_{trigger}$		
		eeee	ee$\mu\mu$	$\mu\mu\mu\mu$
300	670	76	82	26
400	347	46	64	25
600	164	26	46	21
800	77	14	25	13

Table 4 shows the detection efficiency for Z's for a reconstructed mass cut of ± 15 GeV/c^2 (76 to 106 GeV/c^2). No other kinematic or geometrical cuts are applied. The errors are statistical.

Table 4: Detection Efficiency for Z's in Higgs Events

Physics	Z → ee	Z → $\mu\mu$
M_H=300	1.00	0.67±0.006
M_H=400	1.00	0.71±0.006
M_H=600	1.00	0.70±0.006
M_H=800	1.00	0.67±0.006
ZZ continuum	1.00	0.53±0.003

Clearly, at this stage of our simulations we should make a tighter cut on the Higgs mass for the 4e mode, and perhaps a loose cut on the 4μ mode. The reconstructed mass distribution for Z→ee and for the 400 GeV/c^2 Higgs is shown in Figures T6.2. The total momentum distribution for the 4μ mode is shown in Figure T6.3; it is important for the optimization of the design of the muon TRD.

The statistical significance (SS) of a fluctuation of the total number N $(=B+S)$ of events above the fitted background (B) to give a signal (S) is defined as

$$SS = (N - B)/\sqrt{N}$$

N, B and SS values for each decay mode and mass are tabulated below:

Table 5: Expected Number of Higgs Events

Higgs Mass	eeee			$ee\mu\mu$			$\mu\mu\mu\mu$			Combined		
	N	B	SS	N	B	SS	N	B	SS	N	B	SS
300	47	13.7	4.8	43	9.3	5.1	12	2.3	2.5	100	25.3	7.5
400	27	5.8	4.0	35	6.2	4.8	12	2.0	2.9	74	14.0	6.9
600	17	4.1	3.2	23	3.4	4.0	8	0.9	2.4	47	8.3	5.6
800	12	4.4	2.0	13	3.6	2.6	5	1.3	1.6	29.5	9.4	3.7

The results shown in the above table do not include any lepton selection efficiency due to cuts on the isolation, HAD/EM cut, position matching cut, etc. Using the experience of CDF, we take an efficiency of 85% to make a realistic decision on any one lepton. The efficiency for four leptons is expected to be 0.52 $(= 0.85^4)$.

We could classify several grades for potential discovery

A : SS $\geq$ 7 and S $\geq$ 20 : Discovery at $\mathcal{L} = 1 \times 10^{40}$ cm^{-2}

B : SS $\geq$ 5 and S $\geq$ 10 : Discovery at $\mathcal{L} = 2 \times 10^{40}$ cm^{-2}

C : SS $\geq$ 3.5 and S $\geq$ 5 : Discovery at $\mathcal{L} = 4 \times 10^{40}$ cm^{-2}

The grade for the each mode is summarized in the following table:

Table 6: Summary of Higgs Hunting Capability

Higgs Mass	eeee	$ee\mu\mu$	$\mu\mu\mu\mu$	Combine
300	A	A	B	A
400	A	A	A	A
600	A	A	B	A
800	B	B	C	A

From the above table, we see the following:

1. The maximum sensitivity for hunting the Higgs is around 400 GeV/c^2.

2. A heavy Higgs up to a mass of 600 GeV/c^2 can be studied with each four-lepton mode, i.e. eeee, ee$\mu\mu$, or $\mu\mu\mu\mu$.

3. For the 4μ mode, the high P_T threshold largely degrades the Higgs detection efficiency, while the background reduction power is very large. If the SSC can achieve an integrated luminosity of $4 \times 10^{40}\text{cm}^{-2}$, the 4μ mode would be given an "A", for the mass range between 300 and 800 GeV/c^2.

4. A heavy Higgs with a mass of 800 GeV/c^2 could be found by combining the three four-lepton modes at $\mathcal{L} = 10^{40}$ cm^{-2}.

Finally, an expected mass distribution for each Higgs mass and each decay mode after the final cut is given in Figs. T6.4 for $M_t = 120$ GeV/c^2.

For standard model Higgs masses above 600 GeV, the TEXAS detector would begin to use the jetjet and $\nu\nu$ decay modes at standard luminosity, and the lepton modes at higher luminosity, because the rate of production is becoming marginal. (The following sections include a more detailed discussion of the TEXAS detector's high-luminosity capability, its ability to find missing E_T as in the gluino search, and to reconstruct W,Z masses from jets.

Since the Higgs width grows as the cube of the mass, at 800 GeV, the muon resolution becomes much less important. Because of the increased Higgs width, the TEXAS TRD resolution contribution is smaller than the Higgs natural width. At the same time, the production rate drops. After acceptance cuts on lepton ID efficiency of 90% (80%) and isolation efficiency of 85% (75%), typically only 22(11) 4-lepton events remain per SSC year at the standard luminosity in a bump 30% wide. Thus, the 4-lepton mode search at M_H >800 GeV/c^2 is marginal at $\mathcal{L} = 10^{33}\text{cm}^{-2}\text{s}^{-1}$; higher luminosity is needed.

Because the TEXAS muon system can operate in the TRD threshold mode, the fog from low energy showers and punch-through entering large area precision muon drift chambers following a calorimeter is reduced. The electron identification and energy measurement continues to operate in this environment. With a scintillating calorimeter, the full electromagnetic energy in a tower cluster is collected in less than 15 ns. Even at $\mathcal{L} = 10^{34}\text{cm}^{-2}\text{s}^{-1}$ (16 events per crossing), the occupancy in a monolithic 0.025 x 0.025 tower is 1.8%. Electron isolation also continues to function in the pileup. On the average, only 2 GeV of electromagnetic energy is deposited in a ring cone around the electron direction between R=0.1 to 0.2. This band is chosen because the electron will occupy the region below R=0.1; the region from 0.1 to 0.2 can be used as a veto. Isolation and triggering uses the tile tracker/preradiator electron tag together with the electromagnetic energy trigger from the spaghetti calorimeter.

REFERENCES

1. SPACAL: separation available in real time recently shown by SPACAL
2. technique for finding electrons even in jets
3. recent work using neural networks
4. image recognition techniques
5. Snowmass90: fine transverse segmentation
6. GAMS collaboration: derive additional physics information from the shower development
7. fibers available today recover from 30 MR
8. LBL: We thank Don Groom of LBL for advice in this matter
9. SPACAL: has demonstrated that the Monte Carlo simulation of spaghetti calorimetry is fully predictive
10. Dave Hertzog: JETSET collaboration to achieve $6.5\%/\sqrt{E}$, private communication
11. Green & Hedin: estimates from muon rate calculation
12. Adair, EMPACT: precision trackers in magnetic fields

FIGURE CAPTIONS

T6.1 Momentum resolution of the TEXAS muon TRD spectrometer.

T6.2 Effect of calorimetric resolution on the reconstruction of a $Z \rightarrow ee$ peak in the $H \rightarrow ZZ$ decays of a higgs of mass 400 GeV/c^2

T6.3 Total momentum distribution for muons in the $H \rightarrow ZZ \rightarrow 4\mu$ decay chain of a 400 GeV/c^2 Higgs.

T6.4 Reconstruction of the invariant mass of an 800 GeV/c^2 Higgs in its $H \rightarrow 4\ell$ decay, for a one year run at high luminosity.

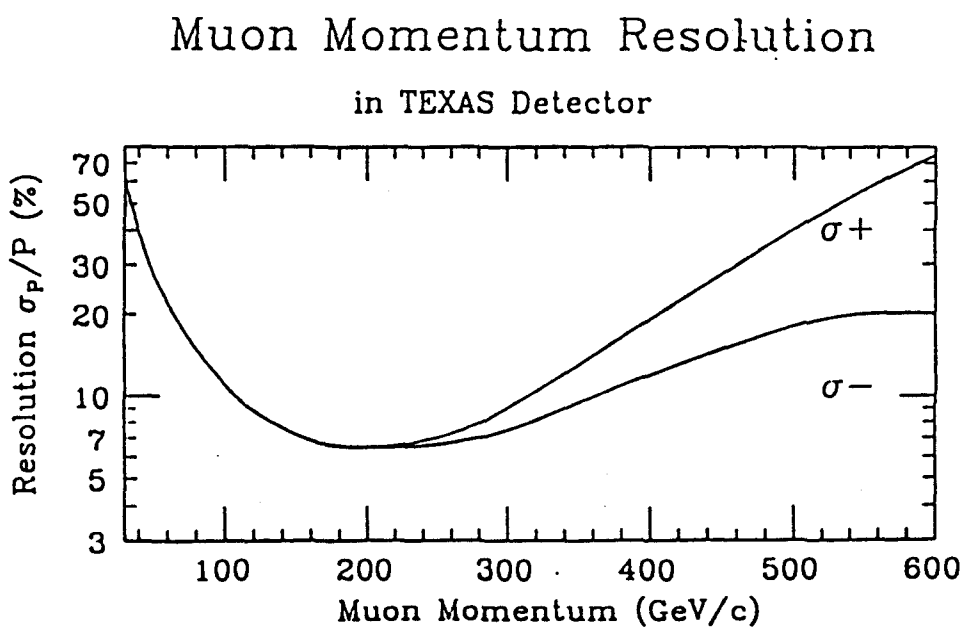
Muon Momentum Resolution
in TEXAS Detector
Resolution σ_P/P (%)
70
50
30
20
10
7
5
3
100
200
300
400
500
600
Muon Momentum (GeV/c)
$\sigma+$
$\sigma-$

Figure T6.1

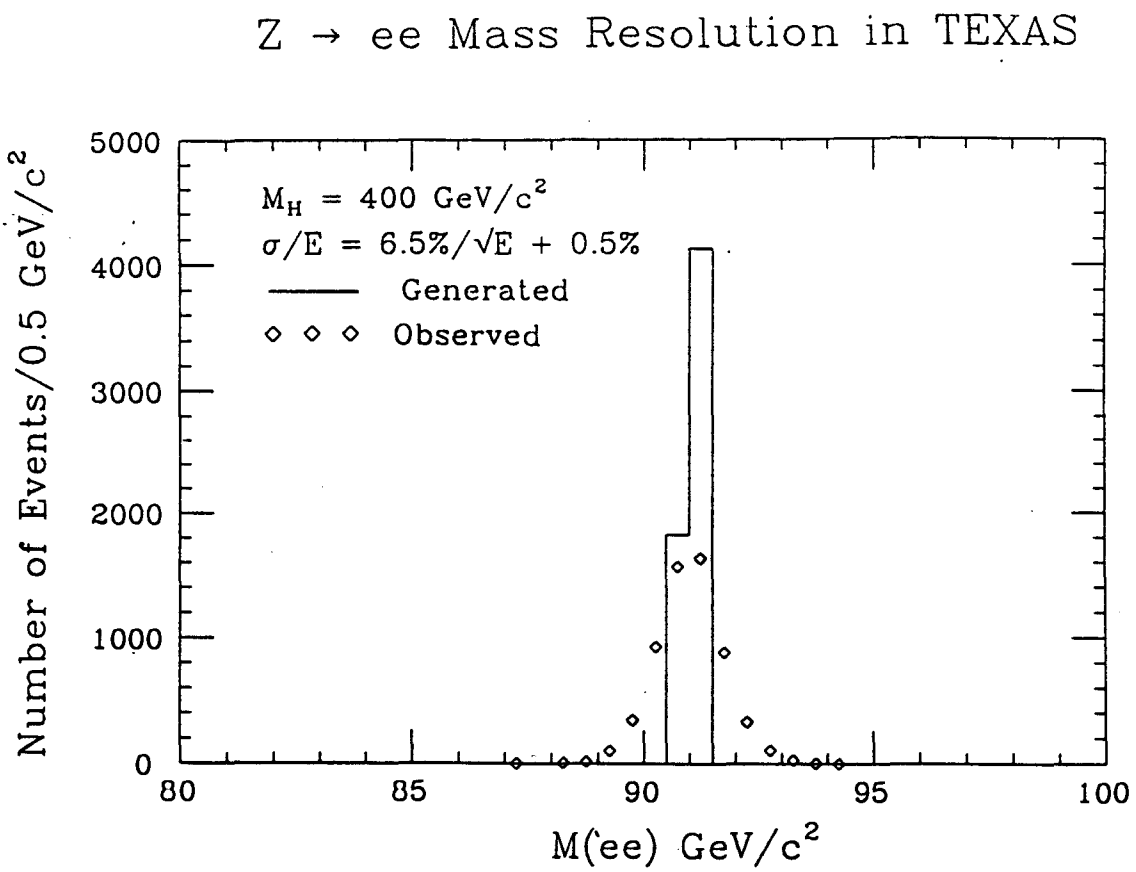

Figure T6.2

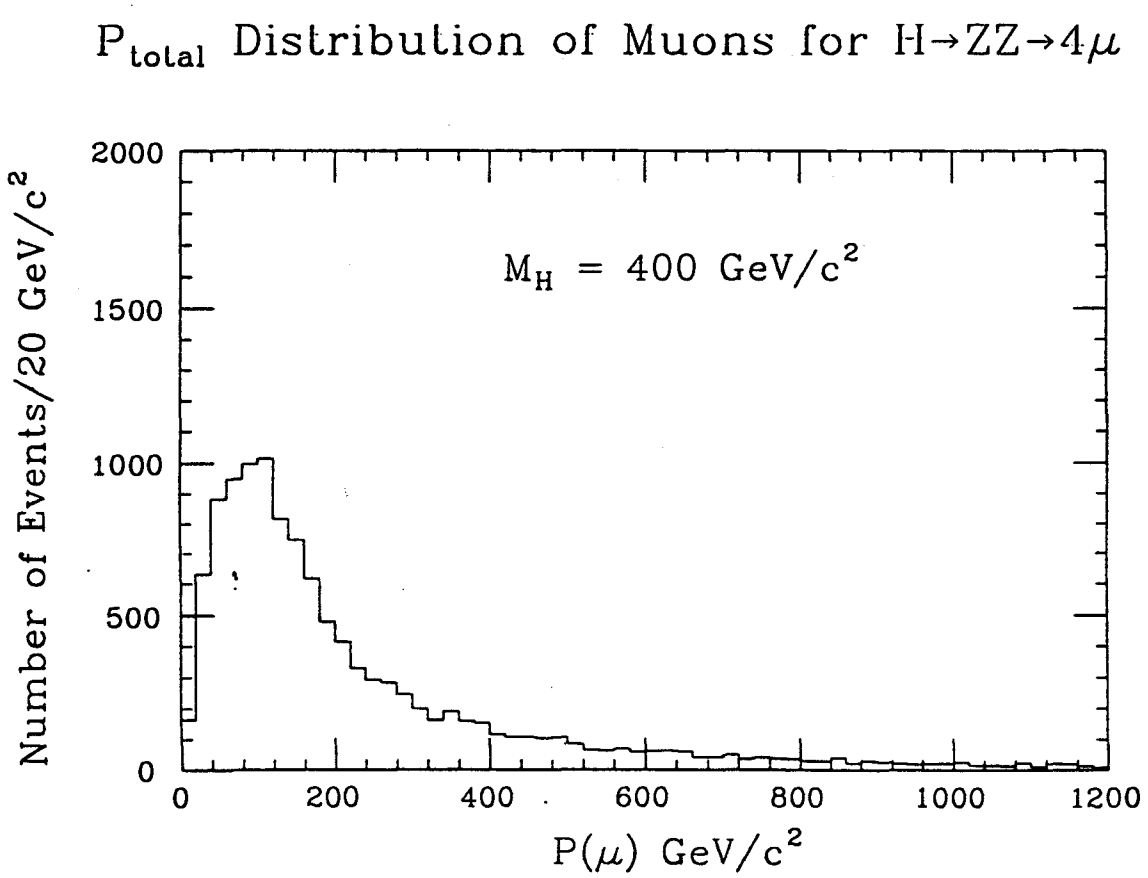

Figure T6.3

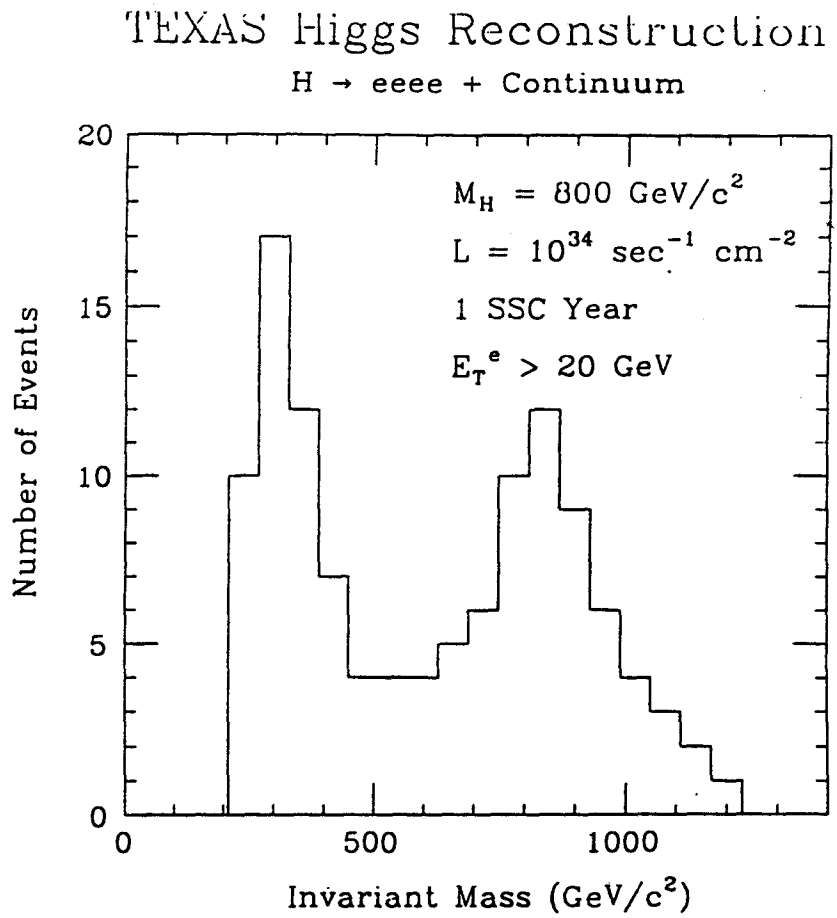
TEXAS Higgs Reconstruction
H → eeee + Continuum
M_H = 800 GeV/c^2
L = 10^{34} sec^{-1} cm^{-2}
1 SSC Year
E_T^e > 20 GeV
Number of Events
Invariant Mass (GeV/c^2)
0
5
10
15
20
0
500
1000

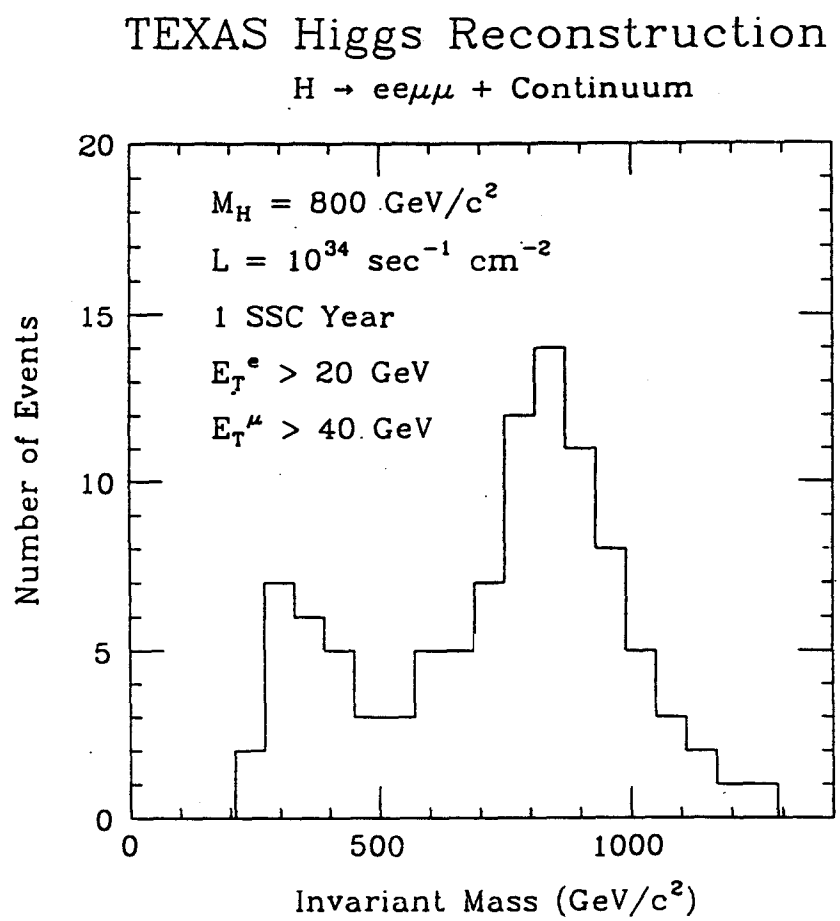
TEXAS Higgs Reconstruction
H → ee$\mu\mu$ + Continuum
M_H = 800 GeV/c^2
L = 10^{34} sec^{-1} cm^{-2}
1 SSC Year
E_T^e > 20 GeV
E_T^μ > 40 GeV
Number of Events
Invariant Mass (GeV/c^2)
0
5
10
15
20
0
500
1000

Figure T6.4

T7: Hermiticity versus Muon Resolution

- *You stress the importance of the hermeticity of the TEXAS calorimeter, especially for measuring missing P_t. At what level is this advantage compromised by your uncertainty in measuring muon energy?*

High P_t muons are primarily produced in the prompt semileptonic decays of heavy quarks. The muon TRD spectrometer is very effective in removing muon backgrounds from hadronic punch-through, since the latter will be below the TRD threshold. The 2m inner radius of the calorimeter will add slightly to the rate of muons from decays in flight over those in a smaller-radius calorimeter, but these muons are dominated by prompt muons for P_t >20 GeV. We thus exclusively consider prompt muons in our high P_t background discussion below.

We have followed Green and Hedin[1] in analytical and ISAJET calculations of the muon P_t spectrum as a function of rapidity. We have then convoluted this source sprectrum with the muon resolution function of the TEXAS muon TRD spectrometer, where this resolution function was derived from measurements and Monte Carlo calculations and discussed earlier. For comparison, we have also convoluted this source spectrum with the response of a steel toroid with resolution $\sigma_{P_t}/P_t = 0.2$ (1.5 meters thick) and with a magnetic tracking system with resolution $\sigma_{P_t}/P_t = 0.54P_t$ for P_t in TeV/c. The results are illustrated in Figure T7.1 with the vertical axis indicating the number of events per GeV bin of missing energy per unit of rapidity collected in 10^7 live seconds of SSC operation at 10^{33} luminosity. For no muon system at all, one has 1 event with missing P_t = 1 TeV per GeV of missing P_t per unit of rapidity in one "live" standard SSC year.

It is important to note that these missing P_t background events have a very distinctive signature in the TEXAS detector: they are accompanied by a muon with a very large TRD signal. At high P_t, all the missing P_t background from muons in TEXAS arises from the asymmetric errors in the muon TRD system response. Large P_t errors arise from the large TRD signals obtained for muons which nearly saturate the TRD. The reconstructed azimuth of the apparent missing P_t vector will be precisely opposite that of the energetic muon. Since we anticipate using missing P_t signatures in conjunction with electromagnetic and hadronic calorimetry, rejecting events containing high P_t muons opposite apparent missing P_t entails no loss of signal. We are not interested in such channels as $H \rightarrow ZZ \rightarrow \mu\mu\nu\nu$, since they afford no advantages over channels like $H \rightarrow ZZ \rightarrow ee\nu\nu$ in our detector.

The energy threshold of the muon TRD system, and thus the energy scale of the abrupt change in the differential P_t spectrum shown in figure T7-1, is entirely determined by the choice of TRD parameters. Note that above this threshold the apparent missing P_t background is less for the TEXAS muon system than for the iron toroid system out to $P_t > 200$ GeV/c, beyond which the muon rates are quite small. Similarly, the TEXAS muon system is superior in this regard to the magnetic tracking system between the TRD threshold and $P_t > 400$ GeV/c.

Figure Captions

T7.1 Comparison of false missing P_T event rate from mis-measured muons in TEXAS and other muon systems.

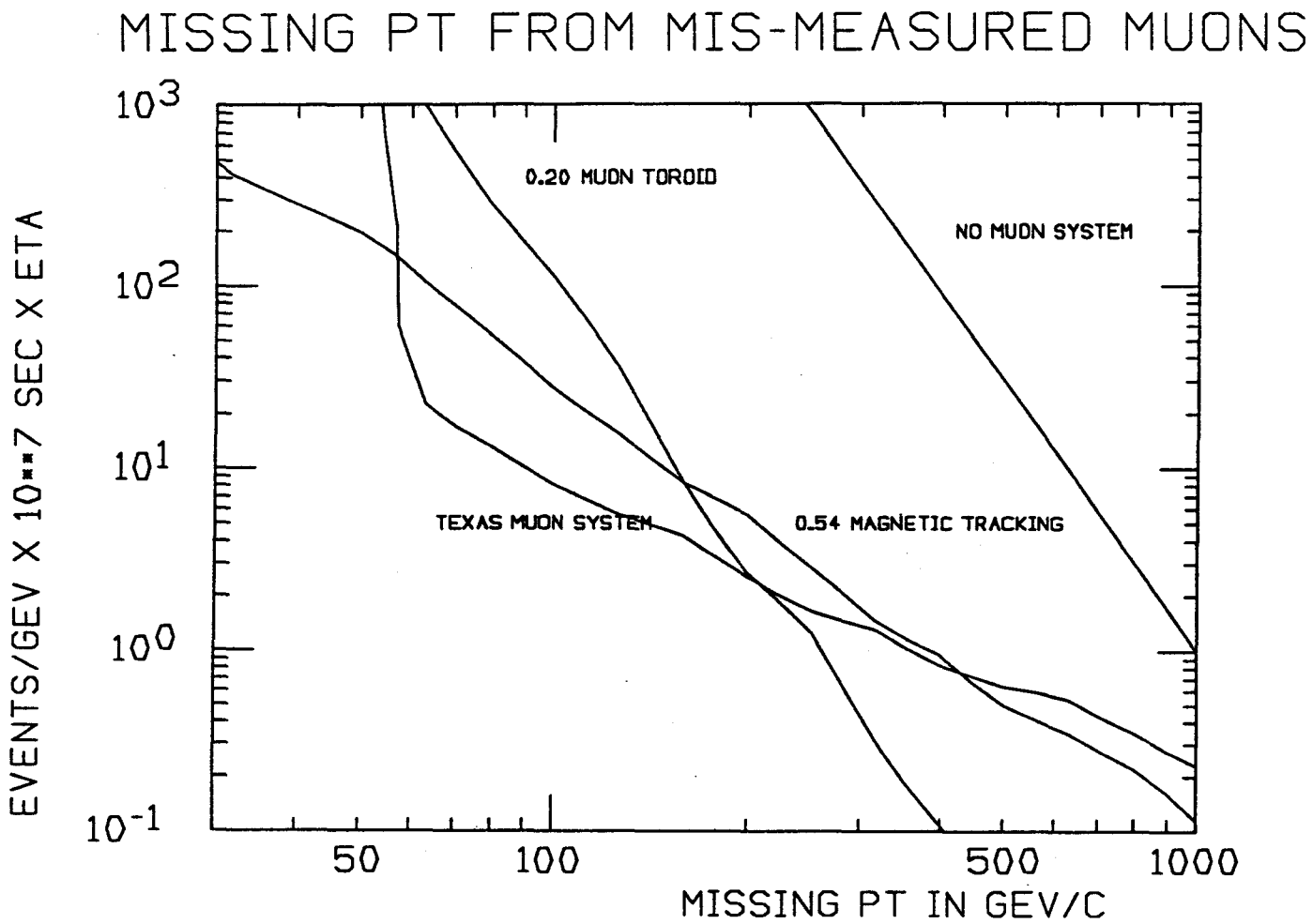
MISSING PT FROM MIS-MEASURED MUONS
EVENTS/GEV X 10**7 SEC X ETA
10^3
10^2
10^1
10^0
10^-1
0.20 MUON TOROID
NO MUON SYSTEM
TEXAS MUON SYSTEM
0.54 MAGNETIC TRACKING
50
100
500
1000
MISSING PT IN GEV/C

Figure T7.1

T8: Pattern Recognition of the Central Tracker

- *Please simulate the pattern recognition efficiency of the tracking system as a function of luminosity.*

In this section we make a simple simulation in order to demonstrate the fact that the reconstruction of tracks in a highly segmented non-magnetic detector such as TEXAS is straightforward even in the high-luminosity SSC environment.

In order to investigate the pattern recognition efficiency as a function of the SSC luminosity we have used GEANT to produce a first order simulation of the tracker/pre-radiator system (including pads) and electromagnetic calorimeter. Instead of modelling the actual cigar shape of the tracker/pre-radiator system, for the sake of simplicity, we have assumed a series of right, concentric cylinders for these detector elements, as shown in fig. T8.1. Since we shall not need to exploit here the segmentation in η of the pad system, this simplification is not misleading. The plastic scintillating fibers (PSF) are circular in cross section of 1mm diameter. The tracker layers are at radii of 1m, 1.4m and 1.8m. The electromagnetic calorimeter has inner radius 2m and has 250 segments in ϕ and 560 segments in η ($\Delta\phi \times \Delta\eta = 0.025 \times 0.025$).

ISAJET events can be plotted as either tracks of all particles, of only charged particles, etc or as simply a set of space points. Fig. T8.2(a) shows an $r - \phi$ projection of the full set of charged particle tracks from a 150GeV H $\rightarrow \gamma\gamma$ event and fig. T8.2(b) shows the corresponding hits. The two Higgs photons are also noted on figure T8.2(b). In order to investigate the charged particle track pattern recognition efficiency, each electromagnetic calorimeter segment plus associated pad is used with the beam crossing vertex to define a triangular road of apex angle 25mr. Each triangular road which has an associated pad signal is scanned for hits. For the first iteration the segmentation in η is ignored (in other words, the entire detector is projected into one $r - \phi$ plane), and unused hits are passed to a second iteration. For the second iteration the η range is divided into two halves, for the third iteration into quarters, and so on until roads contain isolated tracks.

Appropriate multiple coulomb scattering, particle decays, etc. are built into the simulation and, as a first approximation, individual tracker element and pad efficiencies are assumed to be 100%. Based on our experience with 1mm plastic scintillating fibers this is a realistic assumption. In addition, the tracker is presently assumed to have negligible noise; we are presently testing fibers in a reactor environment to evaluate the magnitude of any neutron-albedo noise.

Fig. T8.3 shows a close-up of a road which has just one track in it. A successfully recognised track is one which has all three hits in a straight line $\pm$ one entire PSF diameter at each tracker plane. All tracks such as the one seen in fig. T8.3 have 100% pattern recognition efficiency. It is worth emphasising that we have not yet exploited the additional track hit provided by the electromagnetic calorimeter pad system. Tracks in the same road which are separated by at least 3 PSF diameters also have 100% recognition efficiency. Since the outer tracker layer fibers each subtend an angle of $\sim$0.5mr, this means that only tracks within $\sim$1.5mr are potentially mutually confused.

Fig. T8.4 shows $r - \phi$ views of a 150 GeV H $\rightarrow \gamma\gamma$ event plus 2 minimum bias events (thereby simulating one beam crossing at $\mathcal{L} = 10^{33}\text{cm}^{-2}\text{s}^{-1}$) and fig. T8.5 shows a 150 GeV H $\rightarrow \gamma\gamma$ event plus 15 minimum bias events (simulating $\mathcal{L} = 10^{34}\text{cm}^{-2}\text{s}^{-1}$). Even at the high luminosity the situation is very clean and all charged tracks are easily found.

Fig T8.6 shows $r - \phi$ views of a two-jet event. Even this event is clean and tracks are easily found. This becomes convincing when we look at the blow-up view of the jet region in fig. T8.7.

The combination of no magnetic field (and therefore straight, single-pass tracks) and very fine segmentation in the tracker and pad system yields unbeatable efficiency for recognising and reconstructing charged particle tracks even at the highest possible SSC luminosity.

Figure Captions

T8.1 Views of the tracker/imaging pre-radiator and electromagnetic calorimeter sectors as used in the simulation: (a) Perspective view; (b) $r - \phi$ view.

T8.2 (a) $r - \phi$ view of all the charged particle tracks of a 150 GeV H$\rightarrow \gamma\gamma$ event. After all decays, etc. the event contains 547 charged tracks.

(b) The tracker (points) and calorimeter (crosses) hits corresponding to the H$\rightarrow \gamma\gamma$ event of fig. T8.2(a). Also shown are the directions of the two γ's from the Higgs decay.

T8.3 A blow up of a small region of fig. T8.2(b). The small oval at the right shows the beam-pipe; it is oval because of a slight distortion in the blow-up.

T8.4 (a) $r - \phi$ view of all the tracks of a 150 GeV H$\rightarrow \gamma\gamma$ event superimposed on 2 minimum bias events. Charged particle tracks appear as solid lines.

(b) The tracker (points) and calorimeter (crosses) hits corresponding to the H$\rightarrow \gamma\gamma$ event plus 2 minimum bias events of fig. T8.4(a).

T8.5 (a) $r - \phi$ view of all the tracks of a 150 GeV H$\rightarrow \gamma\gamma$ event superimposed on 15 minimum bias events. Charged particle tracks appear as solid lines.

(b) The tracker (points) and calorimeter (crosses) hits corresponding to the H$\rightarrow \gamma\gamma$ event plus 15 minimum bias events of fig. T8.5(a).

T8.6 (a) $r - \phi$ view of all the tracks of a two-jet event. Charged particle tracks appear as solid lines.

(b) The tracker (points) and calorimeter (crosses) hits corresponding to the two-jet event of fig. T8.6(a).

T8.7 A blow up of a small region of fig. T8.6(b). The small oval at the right shows the beam-pipe; it is oval because of a slight distortion in the blow-up.

TEXAS

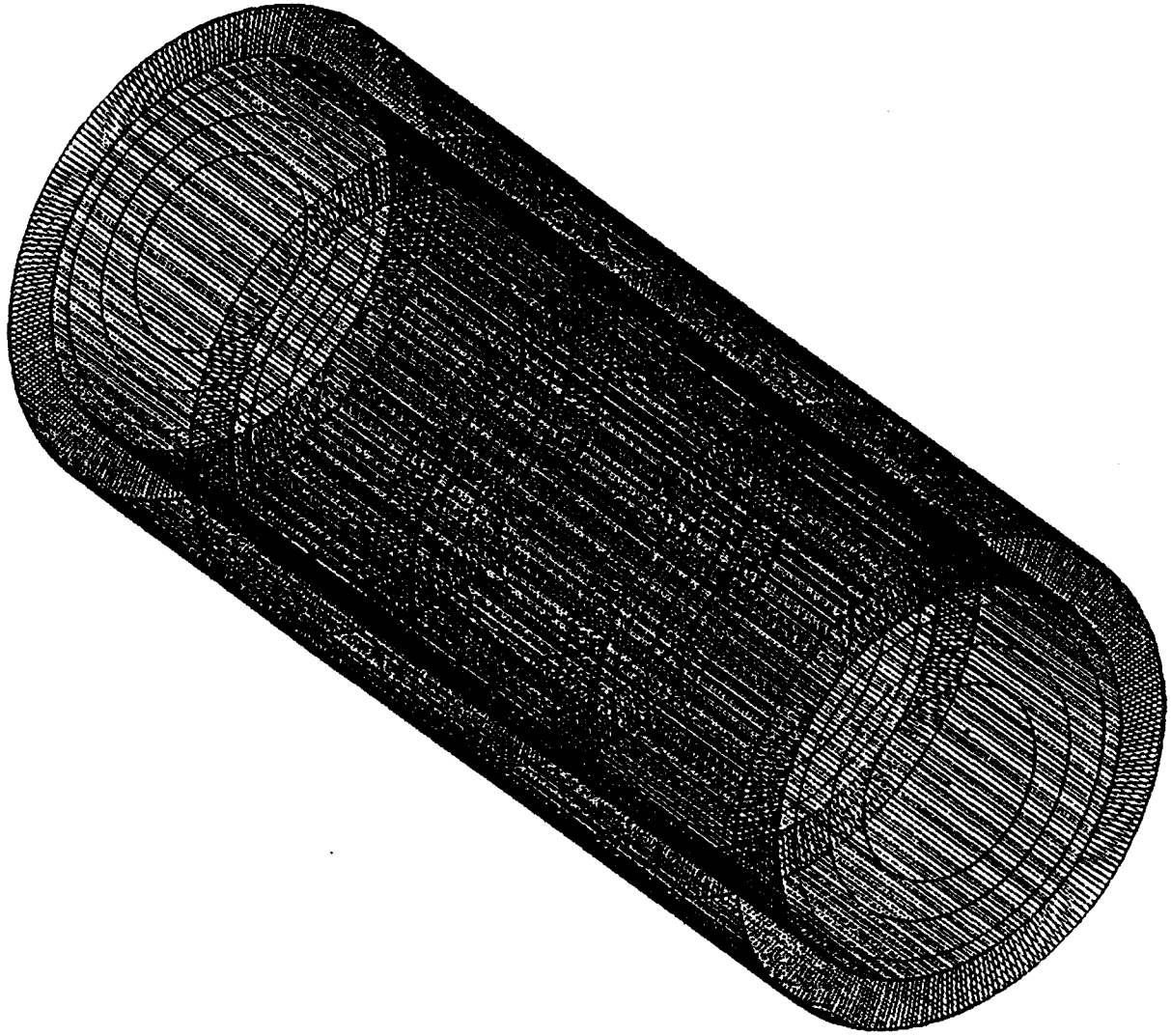

Figure T8.1a

TEXAS

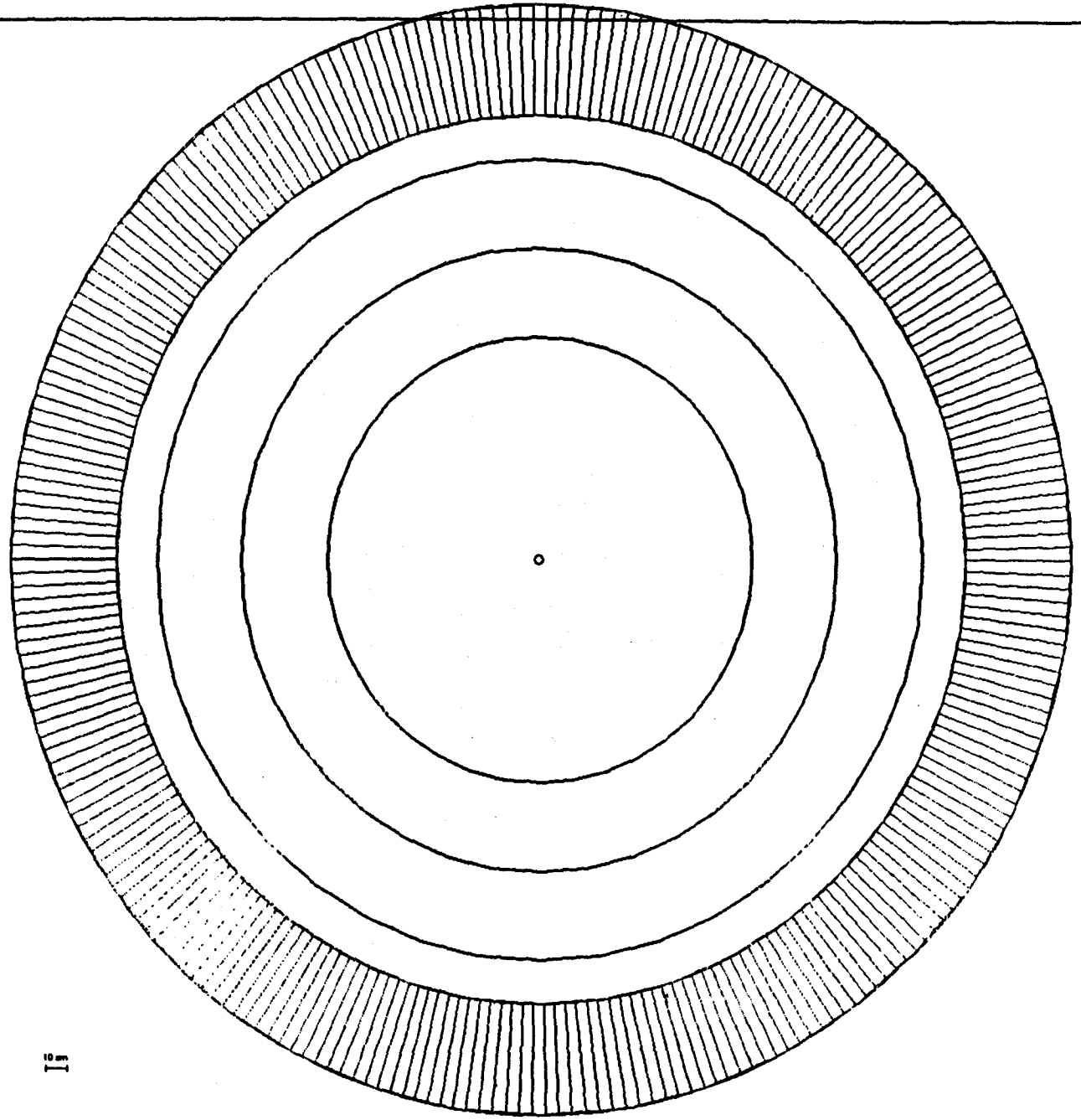

Figure T8.1b

Higgs $\rightarrow \gamma\gamma$

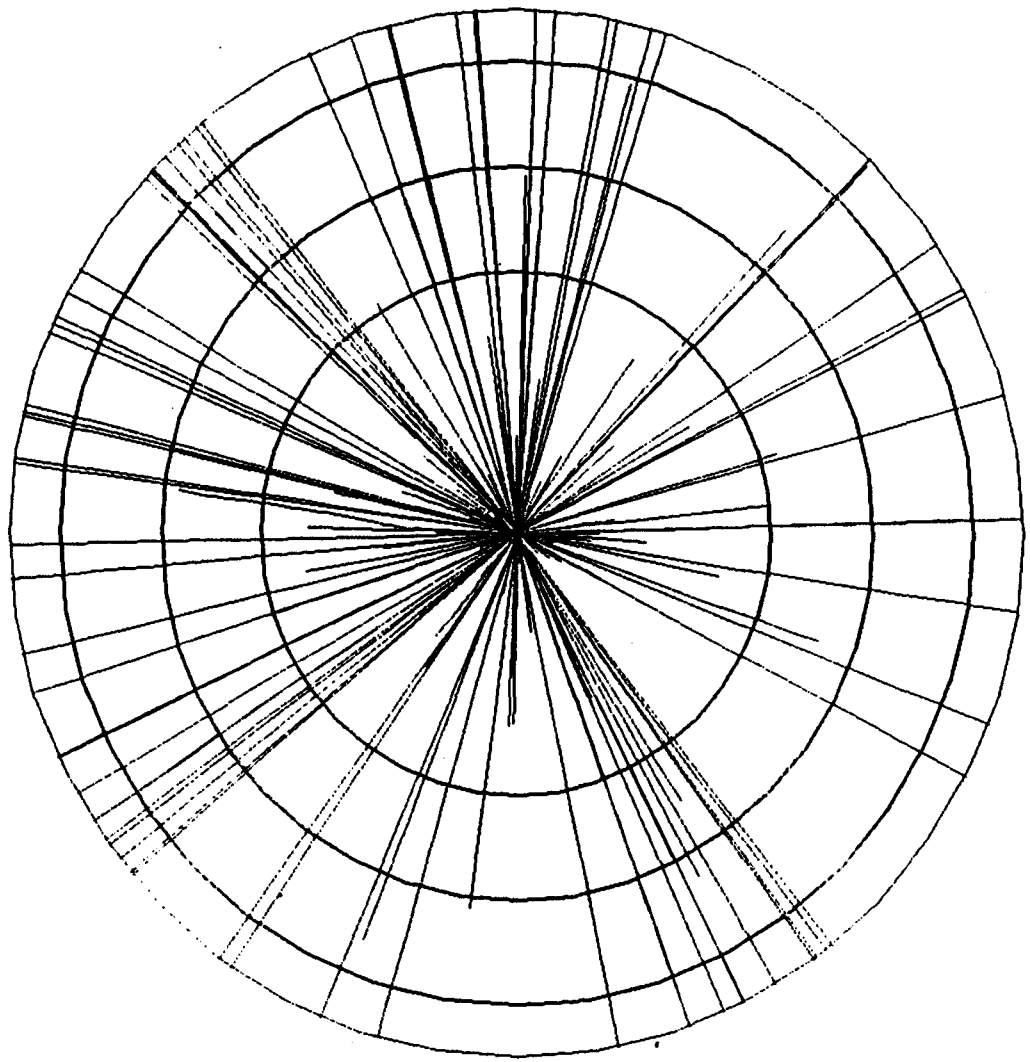

Figure T8.2a

Higgs $\rightarrow \gamma\gamma$

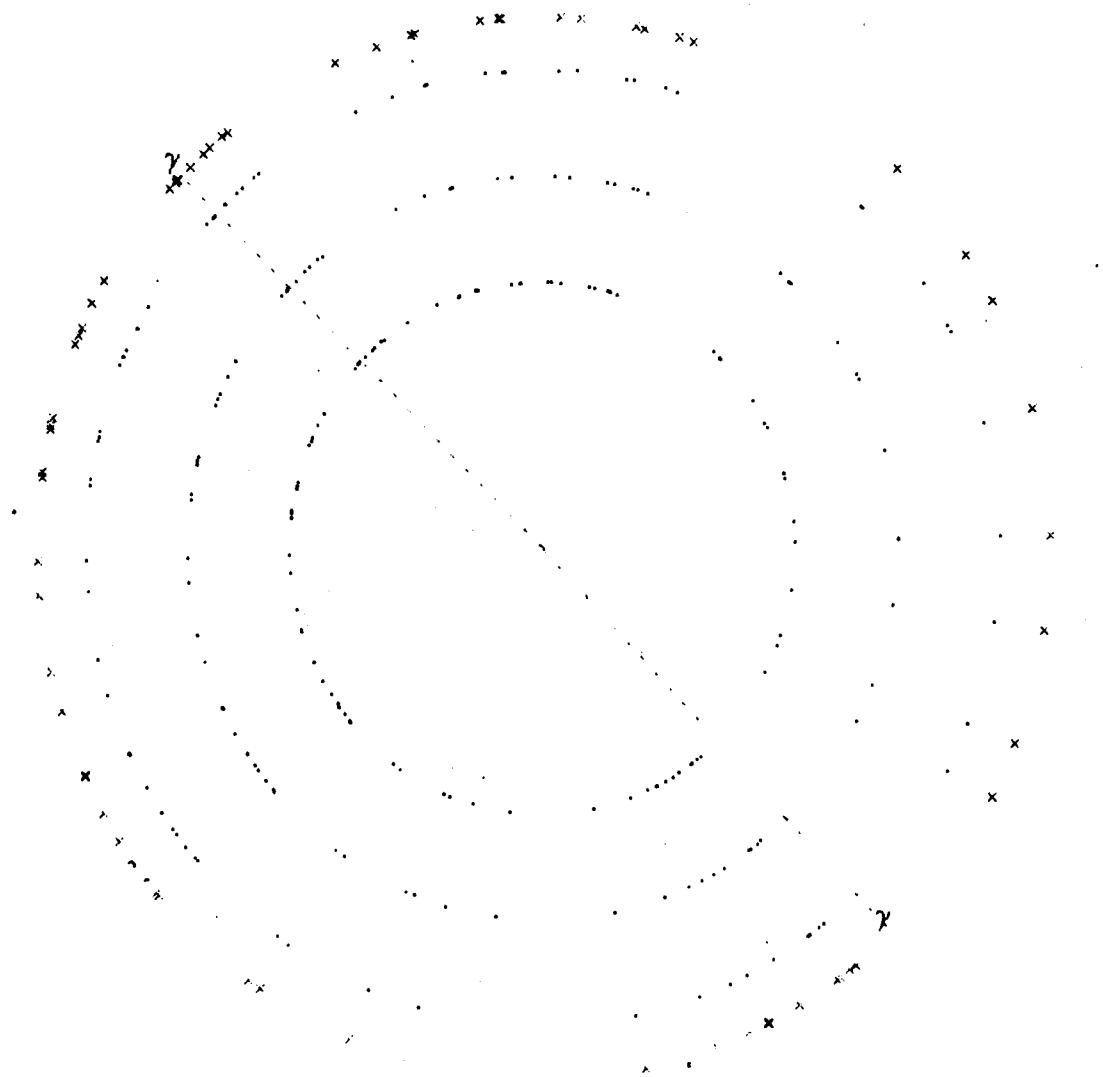

Figure T8.2b

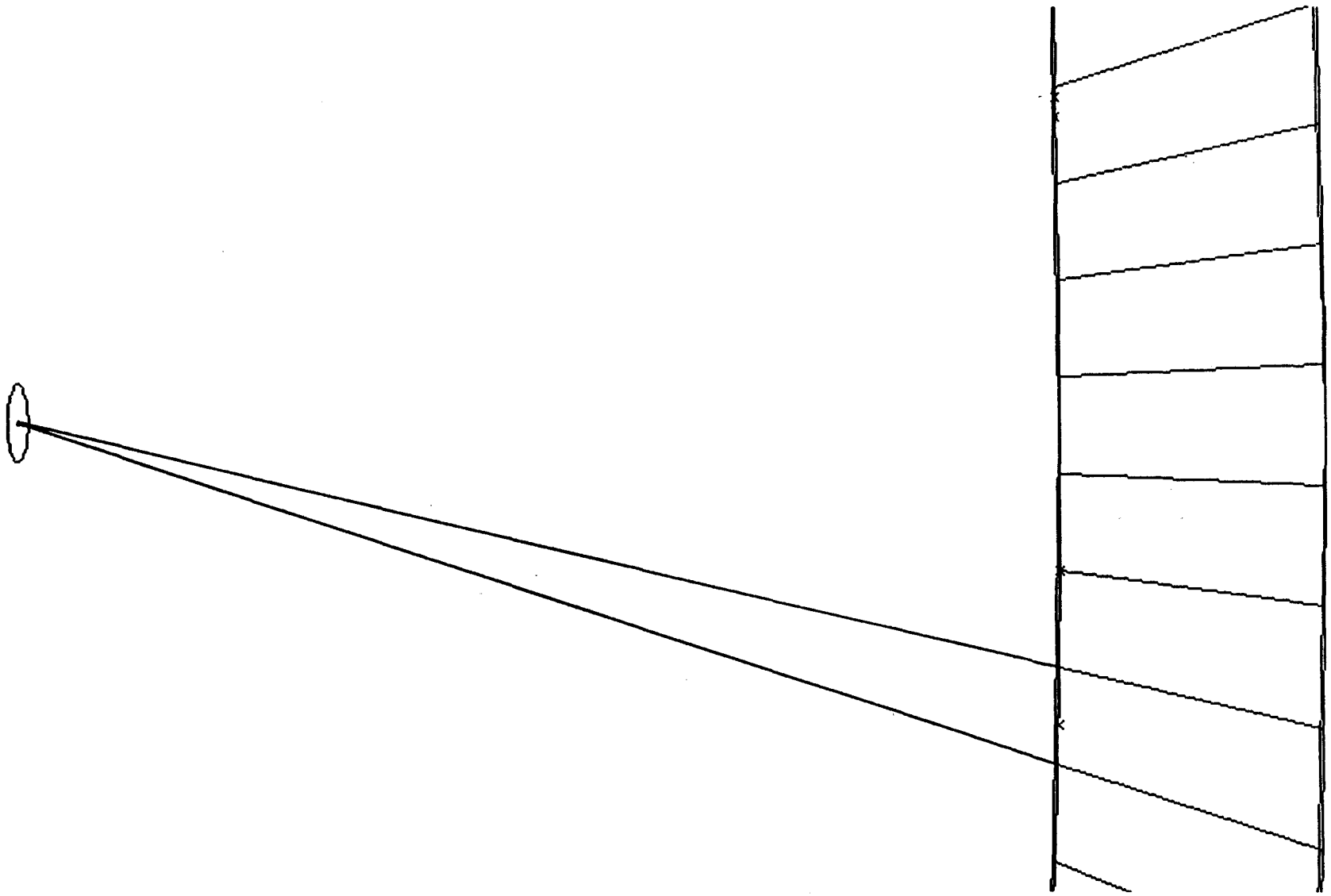

Figure T8.3

Higgs $\longrightarrow$ $\gamma\gamma$ + 2 Minbias

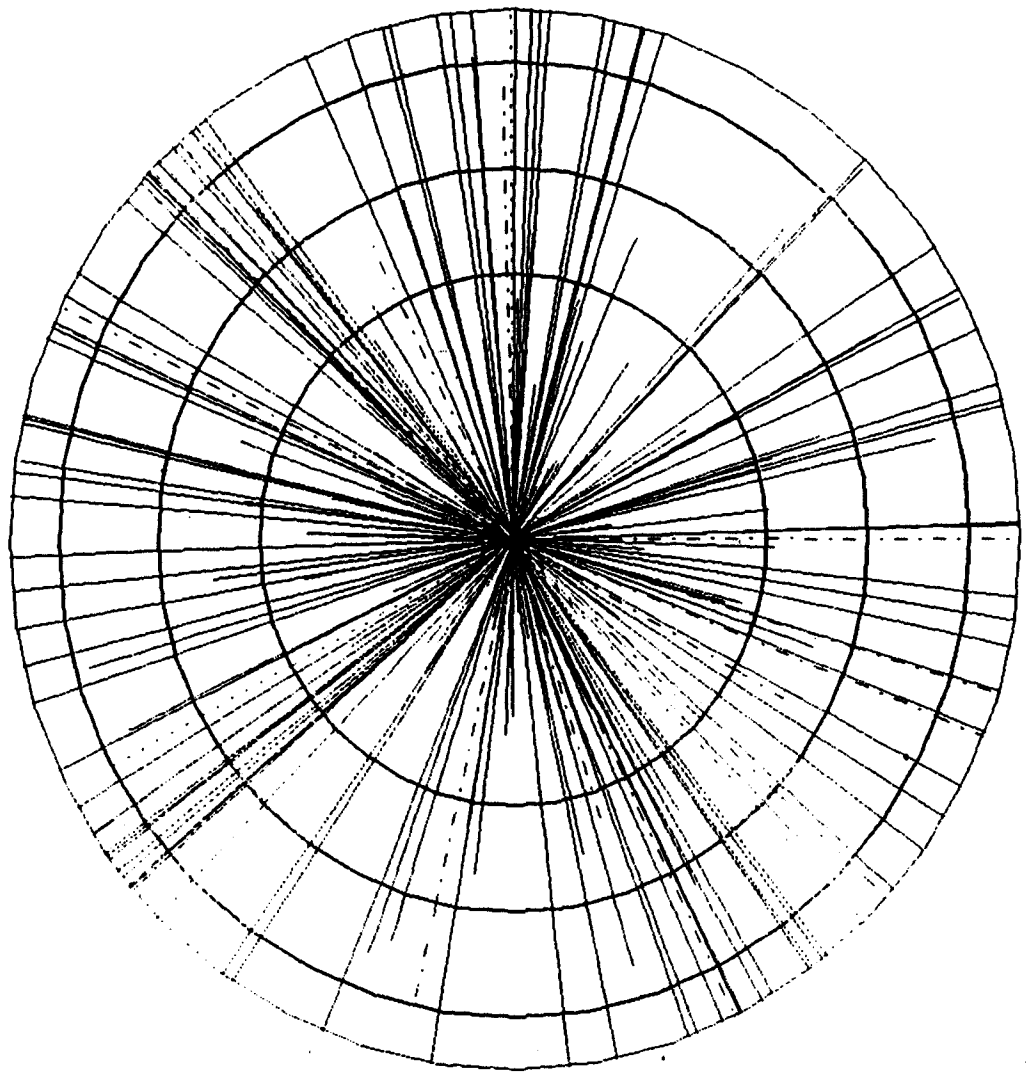

Figure T8.4a

Higgs $\longrightarrow \gamma\gamma$ + 2 Minbias

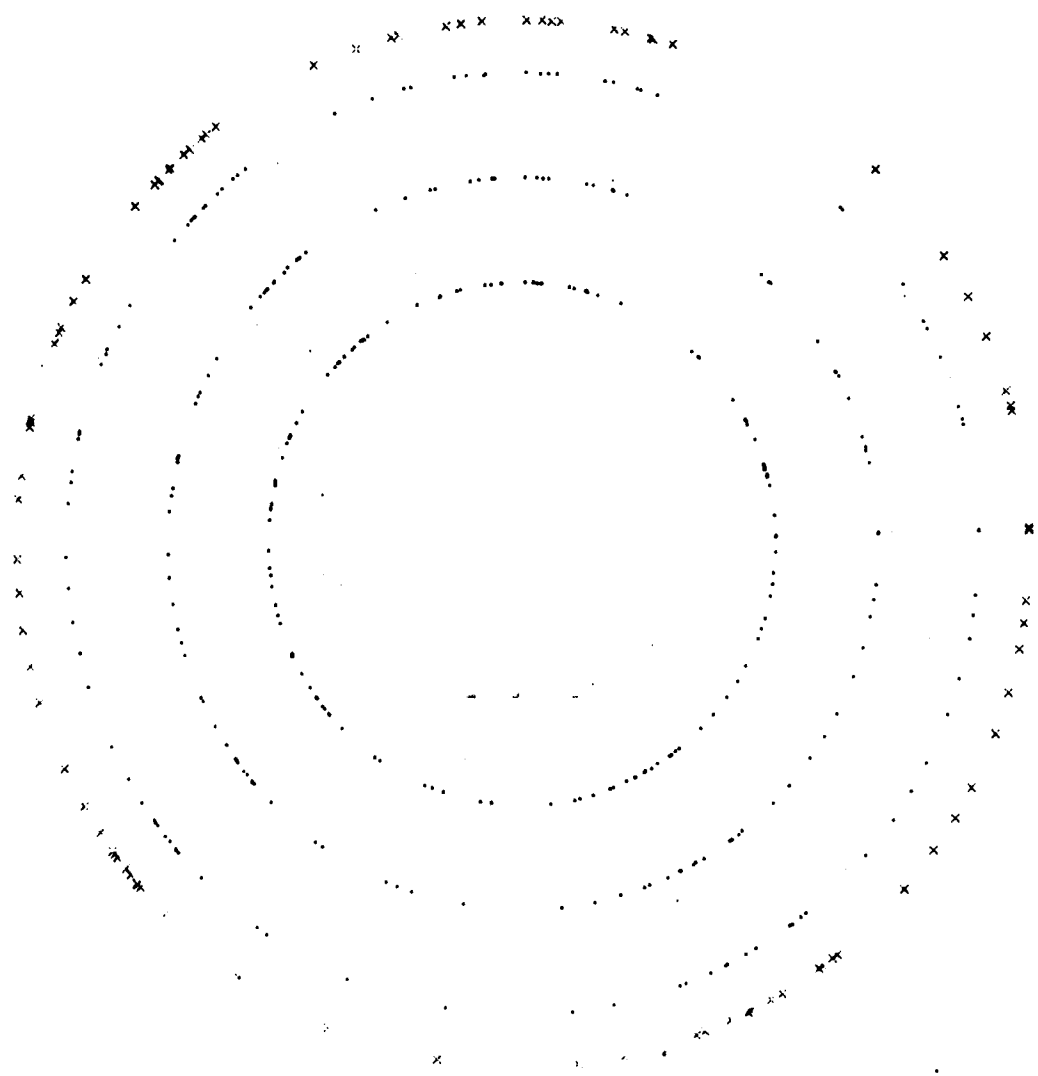

Figure T8.4b

Higgs $\longrightarrow$ $\gamma\gamma$ + 15 Minbias

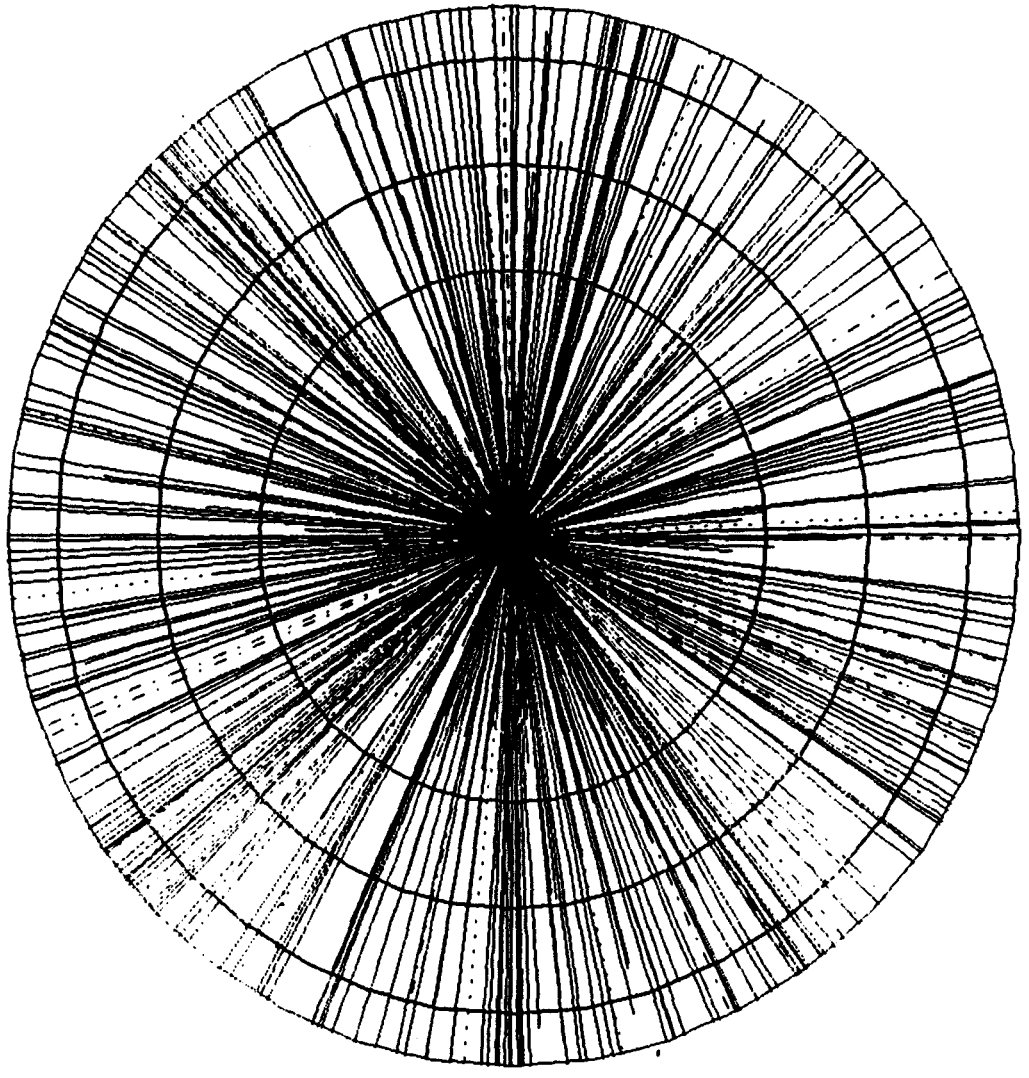

Figure T8.5a

Higgs $\longrightarrow$ $\gamma\gamma$ + 15 Minbias

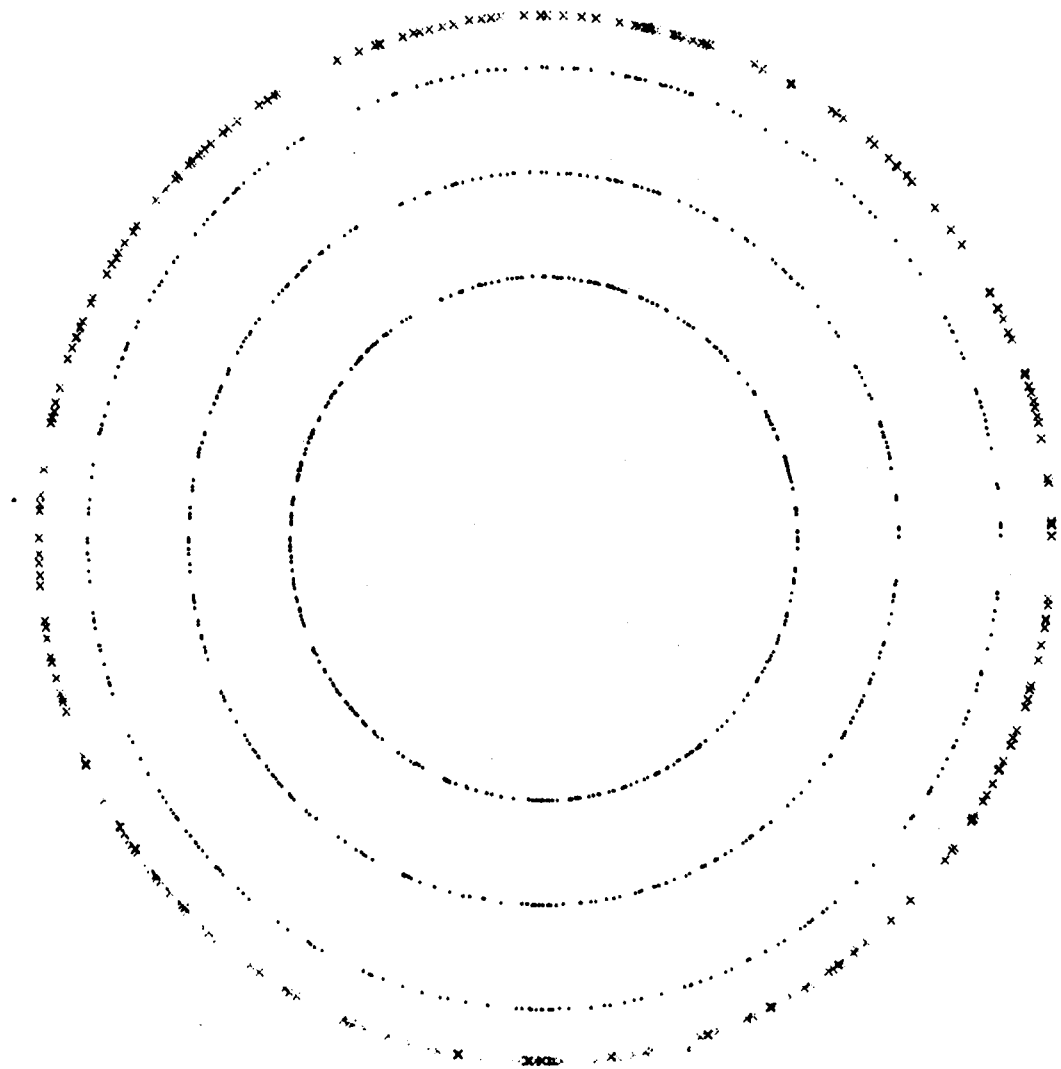

Figure T8.5b

Twojet

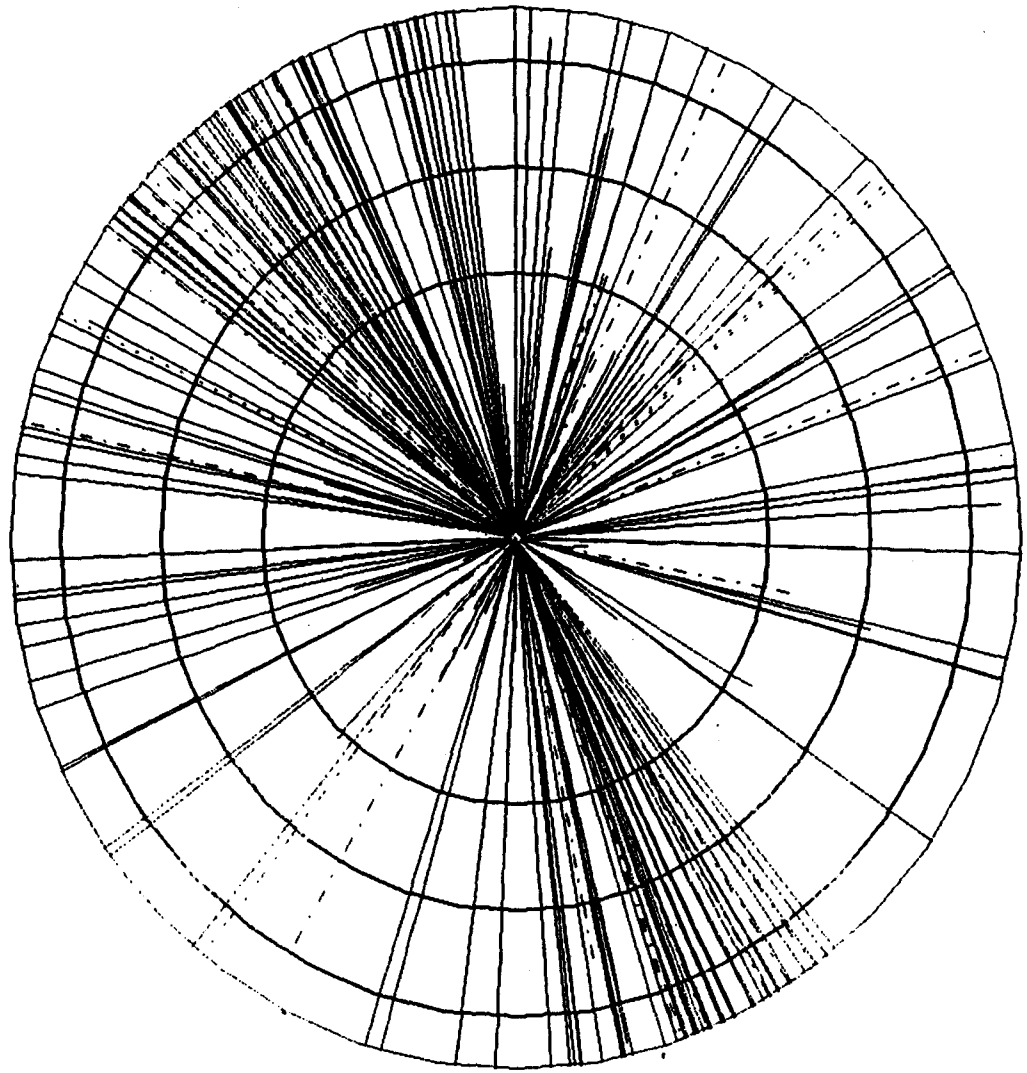

Figure T8.6a

Twojet

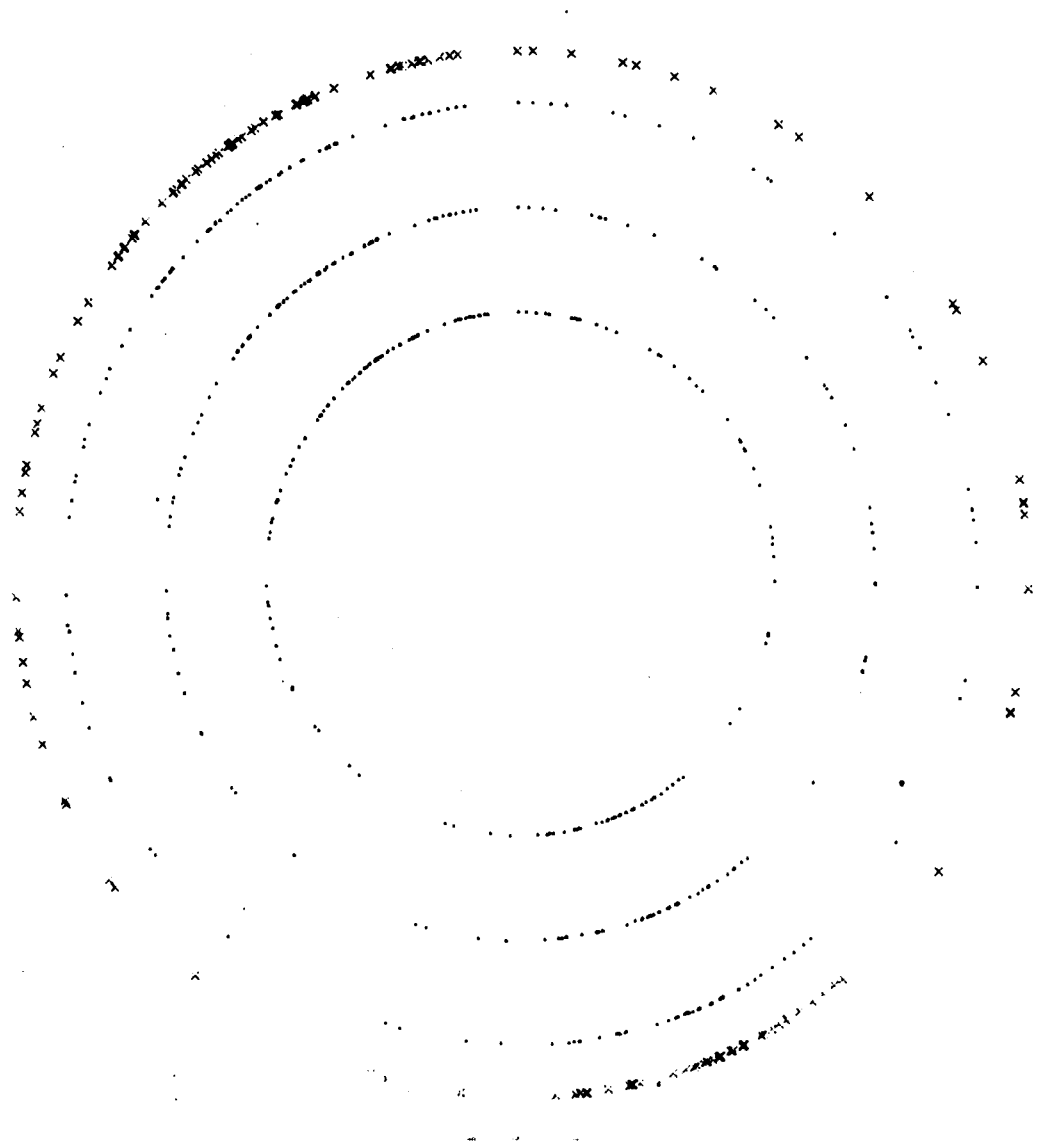

Figure T8.6b

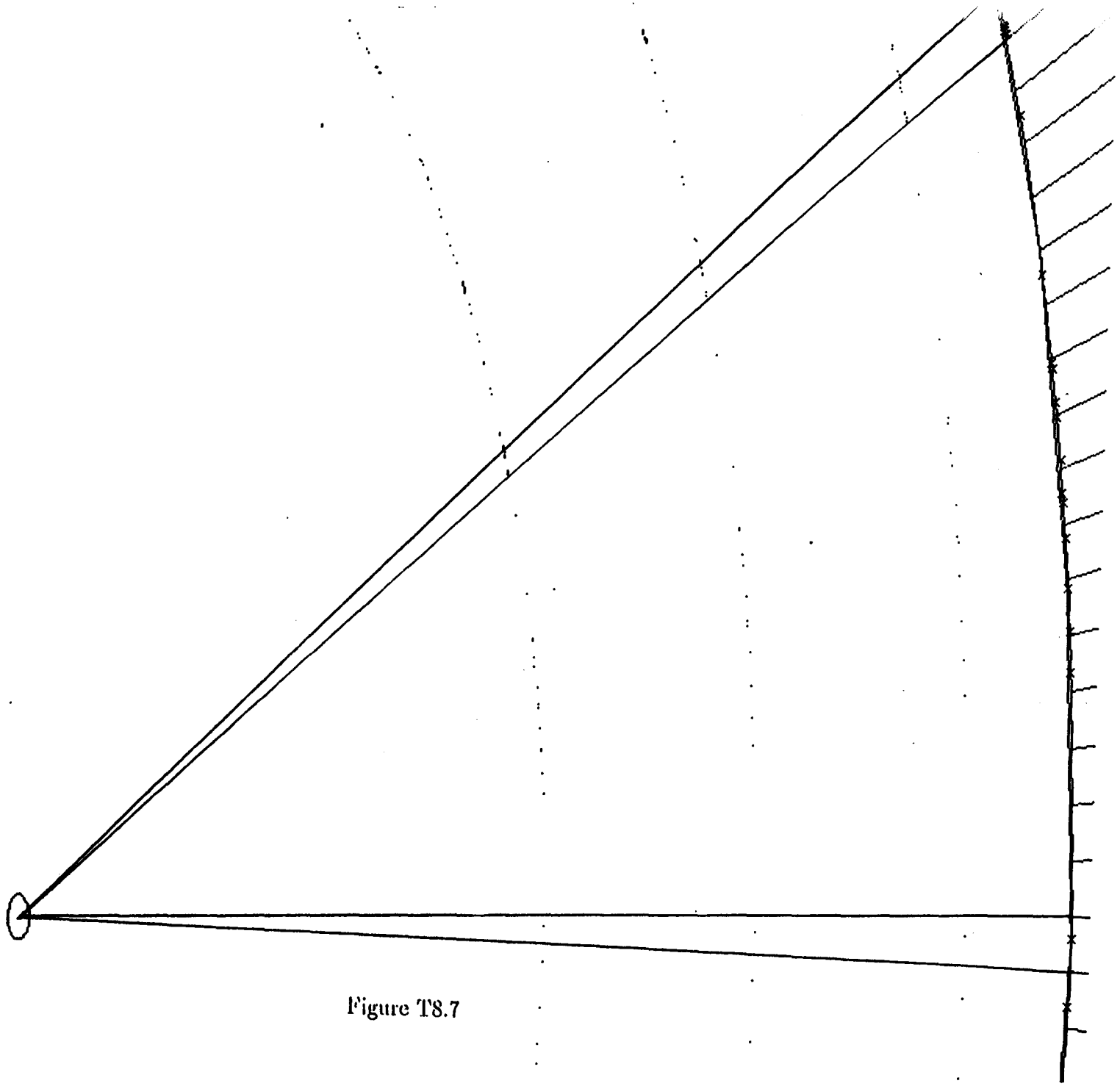

Figure T8.7

V1: Is the TEXAS Cost Estimate Realistic?

Appended to this document are four Appendices (B to E) directed at this question. The numbers in the EOI, which appear there in the chapter entitled "Preliminary Cost Estimate", derive almost exclusively from current experience. For example, the cost of the TRD system is taken directly from the actual costs of the MACRO group. A breakdown of this appears in Appendix C, justifying our cost estimate.

Recently an independent costing of a fiber calorimeter has been performed (SSC Note SSCL-N-728, Martin-Marietta, May 30, 1990). The cost of assembly of the TEXAS calorimeter is considerably lower than the Martin-Marietta analysis. They assume the equivalent of 1,000 man-years simply to assemble the calorimeter towers. Furthermore, they assume that each of the 40,000 towers is individually engineered. In contrast, the TEXAS design needs only 60 individual tower cell designs. Independent estimates by Bicron in Appendix D and by Draper Lab in Appendix B arrive at a cost for all design labor and assembly under $30 M. Appendix B presents a direct critique of the Martin-Marietta costing by Draper Lab. The Draper Lab manufacturing technique is summarized in Appendix A1 of the EOI. Their detailed work appears as an SSC Note, SSCL-N-727, 31 May, 1990. Draper Lab and Bicron reaffirm the cost estimates in the EOI for the calorimeter manufacture.

A last question on the cost estimate concerns the calorimeter electronics. G. Blanar of LeCroy Research Systems has performed a cost estimate risk analysis. You will find a summary of this in Appendix E. He concludes that the TEXAS projection of $100/channel of calorimeter electronics is realistic.

V2: Who would manage the TEXAS Construction?

TEXAS, a University industry consortium, has an industrial affiliate, Draper Lab, with extensive experience in project management. Their plan for management appears in Appendix A, "Project Management for TEXAS." The current management structure of TEXAS (see chart) has a technical committee (see table) with a physicist responsible for each subsystem. The decisions of that team are implemented by several liaison physicists (see Table III) each of whom works intimately with one of our industrial partners. Draper Lab, as project manager, would form a team of engineers to work with the liaison physics and industry to assure the production of each subsystem, on time, on budget, and within its engineering envelop.

TEXAS Management Structure
FY91

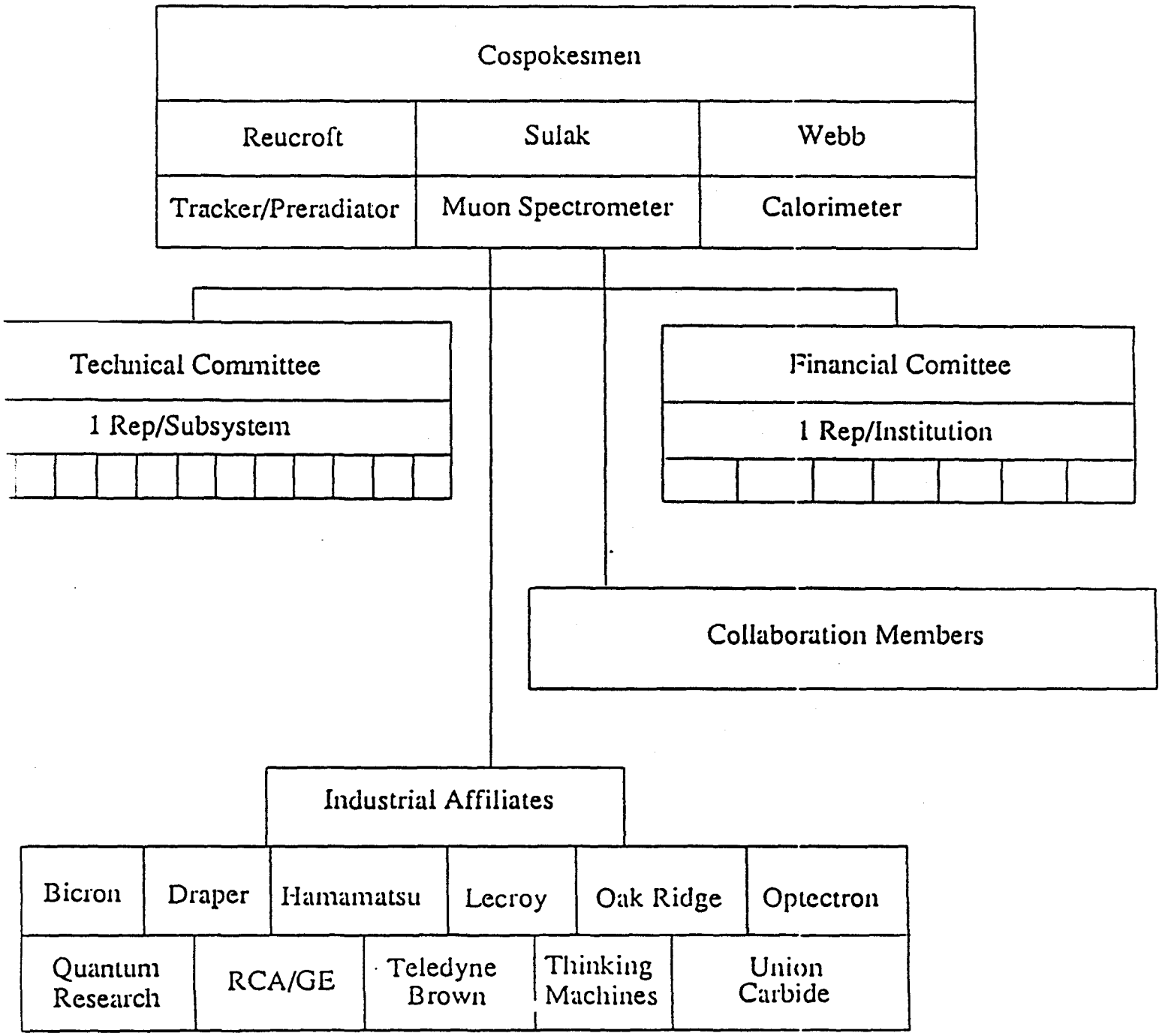

TEXAS Technical Committee

Central Calorimeter

Worstell (Boston)

Forward Liquid Calorimeter

Webb (Texas A&M)

Tracker Pre-Radiator

Reucroft (Northeastern)

Radiation Hard Scintillator Fiber Q.C./Testing

Leedom (Northeastern)

Electro-Optics Q.C./Testing, Power Supplies

Winn (Fairfield)

Muon Trigger Counters

Lane (Drexel)

Muon Tracking Vector Chambers

von Goeler (Northeastern)

Muon TRD's

Sulak (Boston)

Test Beams, Calibration Systems and Detector Data Base

Dye (Boston)

Data Acquisition and Trigger Electronics

Klein (Boston) and Hofteizer (LeCroy)

On-Line Software

Miller (Boston) and Reardon (Thinking Machines)

Systems Integration /Manufacturing/Assembly

Ayer (Draper)

SSCL Facilities/Interaction Hall/Accelerator Liaison

Webb (Texas A&M)

Monte Carlo and Off-Line Software

Kamon (Texas A&M)

Table III: TEXAS Liaison Physicists

And Industrial Affiliates

Task	*Liaison Physicist*	*Industrial Contact Industrial Partner*
Calorimeter Manufacture	Worstell	Hurlbut/Bicron
Scintillating Fiber and Liquid	Leedom/ Jones	Hurlbut/Bicron Jacquet/Optectron
Tracker/Preradiator Support	Reucroft	Gabriel/Oak Ridge
PMT's/Pixel Readout	Winn	Murray/Hamamatsu McIntyre/RCA Woosley/Teledyne Brown
Xenon Gas System	von Goeler	Saupp/Union Carbide
PM/TRD Electronics	Klein/Lane	Hofteizer/LeCroy
On-Line/High Level Triggers	Miller	Dunn/Quantum Research Reardon/Thinking Machines
Mechanical Structure/Integration	Sulak	Ayer/Draper

V3: Why a Muon TRD

Why not use an iron toroid instead of a muon TRD?

The goals of the muon system in our specialized detector are the following:

1. Find and trigger on high energy muons with high efficiency at high luminosity,
2. Measure the muon momentum sufficiently well to extract a high-mass Higgs signal,
3. Allow a missing E_t determination at the level required by the discovery of new physics at $E_t \geq 100$ GeV,
4. Be cost-effective and easily constructed, and
5. Put minimal constraints (thermal, mechanical, magnetic, operational, etc.) on the calorimeter, a precision instrument to be operated with high reliability.

In our opinion, the TRD is an effective way to achieve these goals and to do muon physics with the best possible calorimeter.

The TRD was proposed after careful consideration of the alternatives and the consequences of its use. Alas, some dismiss a muon TRD system out of hand simply as an attempt at novelty. It is not. TRD's and muon TRD's in particular have been around for a long time[1] —operating in outer space, measuring muons underground and under water, and in the innards of collider detectors. TEXAS proposes to use TRD's on the outside of a collider detector, where we believe they have a more natural application than in the highly constrained (in space, L_{RAD}, etc.) environment of the inside of a calorimeter. Unlike those necessary to detect electrons, which must struggle to remain below a few percent of a radiation length, a TRD for muons is rugged. The muon TRD will not have a large background from neutron and neutron-capture X-rays or from the accelerator-associated radiation that is faced by central TRD trackers. The proposal to use the TRD technique to measure muon energy is simply an effective compromise with special benefits.

A "standard" magnetized iron/drift chamber system surrounding the calorimeter with resolution between 15–20% over the kinematic region is a clear possibility which the TEXAS collaboration has considered. It is simply cumbersome and expensive for what it delivers. Using SSC laboratory costing[2] for the fabricated iron, and D0 costs for vector-like chambers, a system of three overlapped superlayers (1 inside, 2 outside) would cost about \$60–75 million. For high luminosity operation improved electronics or extra planes would be needed, as well as fast trigger scintillators. It would take up nearly the same amount of space as a muon TRD, assuming the third drift chamber layer were spaced at least 1 meter from the second layer. Splitting the iron and adding planes to approach 10% resolution would add considerably to the price. We estimate that a high rate iron muon system of this size would cost about \$80–100 million.

The muon TRD, on the other hand, offers considerable advantages. Clearly the ease of access to the calorimeter due to the low mass is important. This directly translates to convenience and lower cost. Beyond these practical issues, the physics advantages are considerable:

1. Muons of all energies can be found and measured using dE/dx with a resolution of about 30% between 5 and 50 GeV, where the TRD threshold turns on. The TRD threshold effectively removes from the muon trigger pion punch-through (See Fig V3-1), decay, muons, and most muons from b and c decay (See Fig V3-2). Nonetheless, the low energy muons remain detected and measured by dE/dx for events triggered otherwise. Contrast this with an iron muon chamber system: there, electromagnetic showers exiting a calorimeter add confusion to the reconstruction and ultimate resolution. The maximum electron energy is about 100 MeV, with the same Lorentz γ a 20-GeV muon: all electrons are invisible in the TRD. Just as a central electron TRD tracker locates all tracks using dE/dx but only finds the high energy (high γ) tracks if the TRD threshold is activated, a muon TRD trigger system would find only muons with energies above 50 GeV (or pions above 70 GeV—a rare punch-through energy). The difference between a central electron TRD and an external muon TRD is that the outside of a calorimeter is a much cleaner and quieter place to detect X-rays. The X-rays produced in neutron capture in the central tracking region are not negligible. The outside of a calorimeter is the optimal place for a TRD system, especially at high luminosity.

2. The TRD energy measurement can be made as fast as the drift time. The trigger is simply the sum of the detected TRD X-rays along a road defined by the projective TRD trigger counters. For isolated muons, this trigger is corroborated by the dE/dx, in the preceeding calorimeter module. SPACAL has shown that the calorimeter information would be an important addition to the muon measurement, see Fig. V3-1.

3. The TRD does not contribute to radiative muon losses, as an iron system does. Catastrophic interactions can cripple a muon chamber system or create a critical fluctuation in the assumed energy of a muon in a given event.

4. The TRD has superior momentum resolution compared with iron in the region between 100 and 400 GeV, crucial to the physics at the SCC.

Figure Captions

V3-1 Punchthrough rate as a function of pion momentum

V3-2 Single lepton p_T distribution from c and b decays in QCD jets

REFERENCES

1. M. Castellano *et al.* NIM **A256** (1987) 38.
2. Workshop on Major SSC Detectors, Tucson, Arizona, Feb, 1990, Page 33

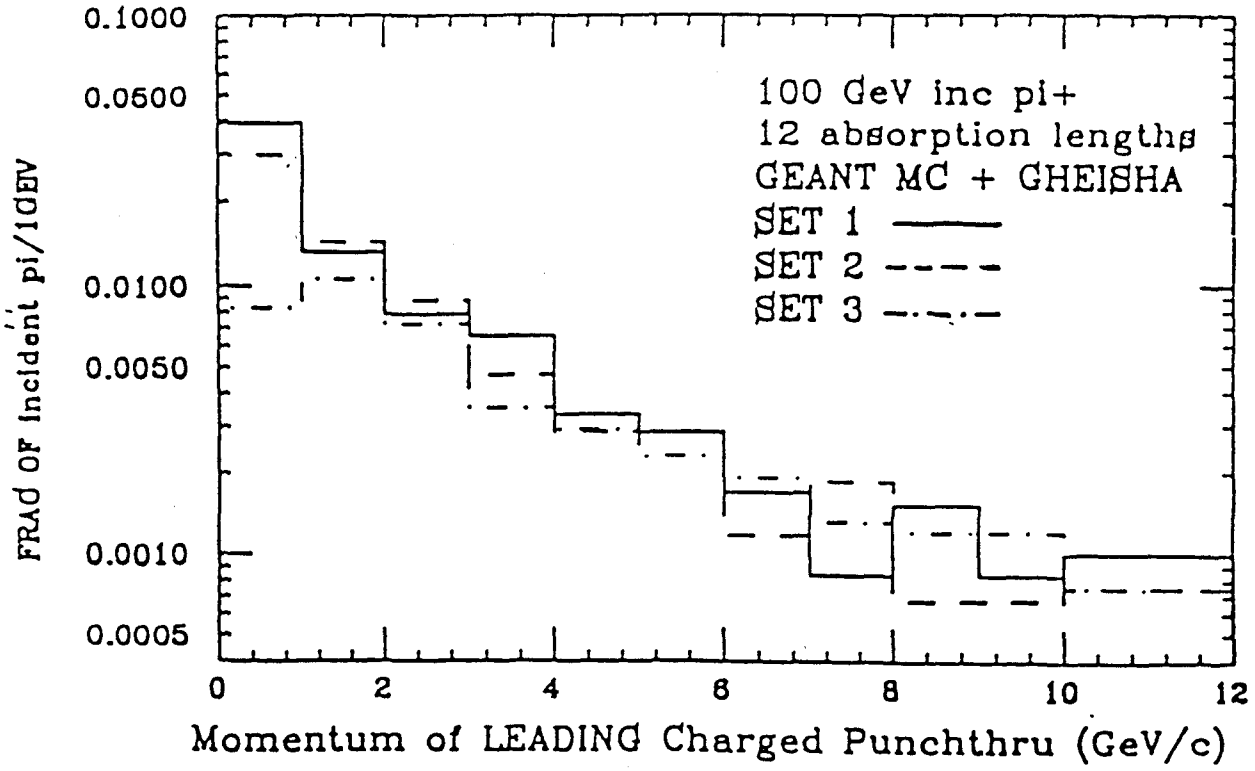
100 GeV inc pi+
12 absorption lengths
GEANT MC + GHEISHA
SET 1
SET 2
SET 3
FRAC OF Incident pi/10EV
0.1000
0.0500
0.0100
0.0050
0.0010
0.0005
0
2
4
6
8
10
12
Momentum of LEADING Charged Punchthru (GeV/c)

Figure V3.1

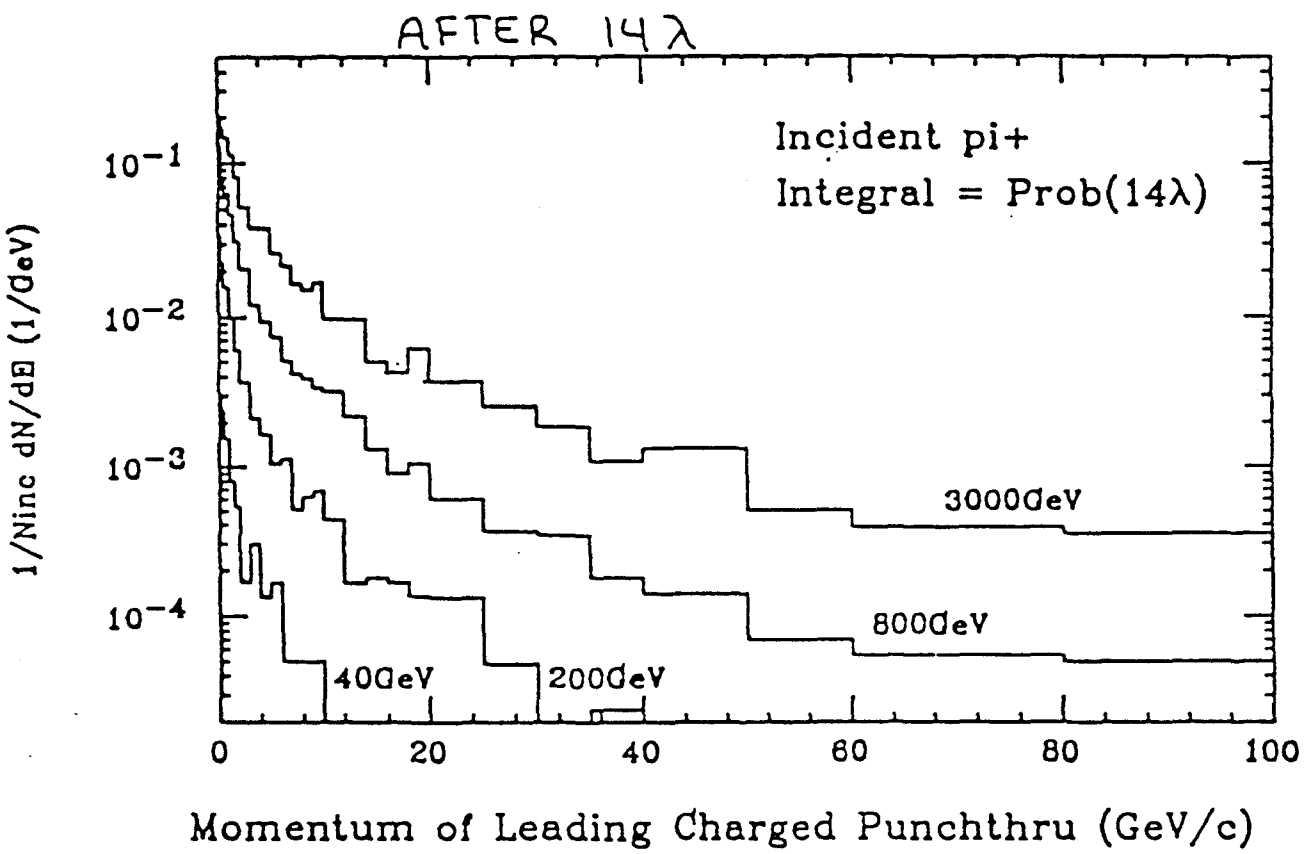
AFTER 14λ
Incident pi+
Integral = Prob(14λ)
1/Ninc dN/dE (1/GeV)
10^{-1}
10^{-2}
10^{-3}
10^{-4}
3000GeV
800GeV
400GeV
200GeV
0
20
40
60
80
100
Momentum of Leading Charged Punchthru (GeV/c)

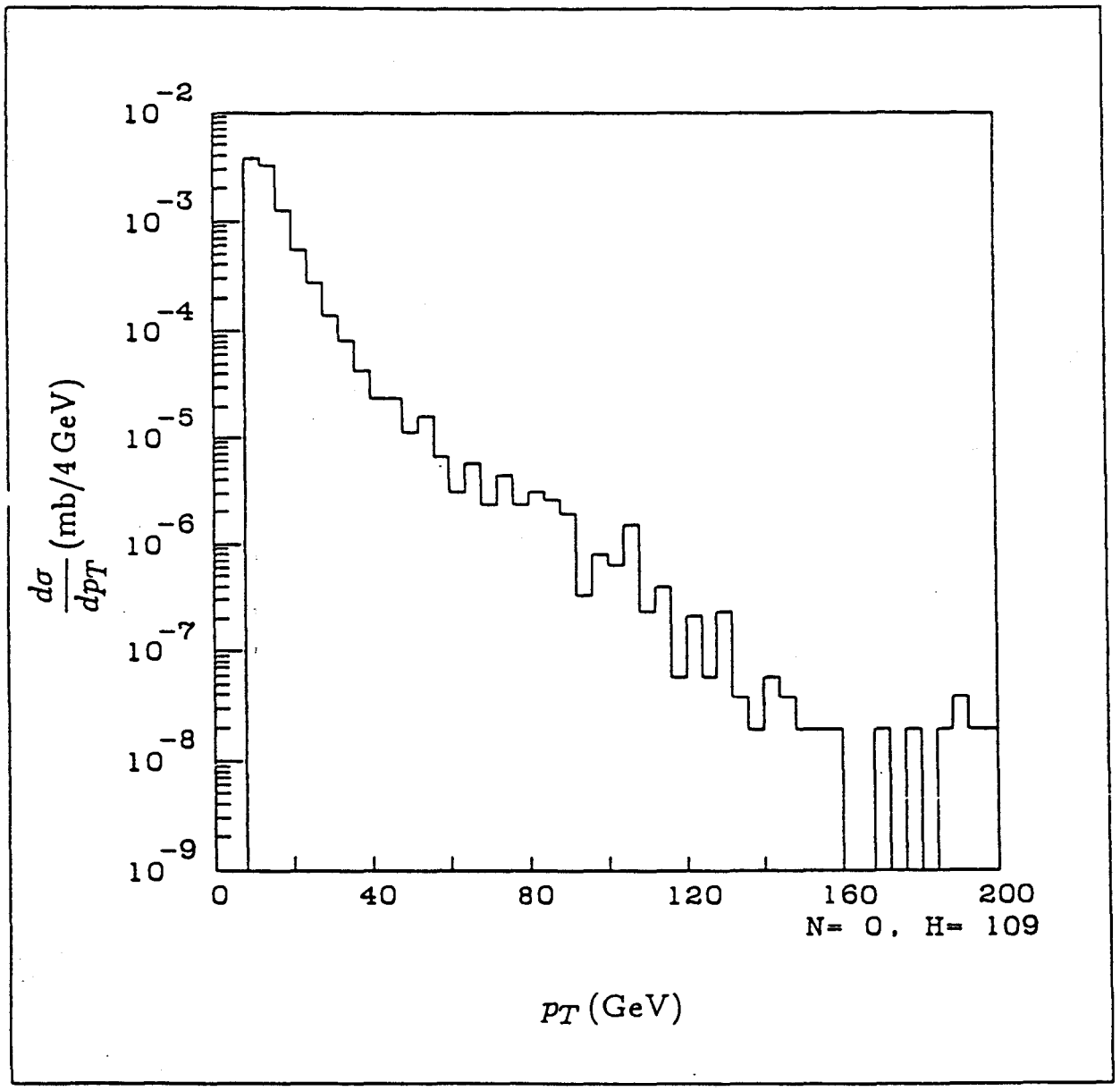

Figure V3.2

Single lepton p_T distribution from c and b decays in QCD jets.

APPENDIX A

Project Management for TEXAS ...
A Draper Lab Report

The Charles Stark Draper Laboratory, Inc.

PROGRAM MANAGEMENT PLAN FOR TEXAS

The TEXAS Collaboration proposes an innovative detector which will provide the maximum scientific return for the resources invested. The basis for this claim is the scientific validity of the experimental approach, the fundamental simplicity of the proposed design, and the relative ease with which the calorimetry based detector can be constructed, installed, and tested on site at SSC. The TEXAS Collaboration will make its detector operational with a management team specifically organized to assure that its scientific goals are achieved on time and within budget. Draper Lab would be the primary contractor for program management.

ENGINEERING PHASE

Currently overall coordination of the Collaboration is in the hands of three Project Spokespersons. The present Spokespersons are: Reucroft (Northeastern U.), Sulak (Boston U.), and Webb (Texas A & M). They are responsible for formal communication with the SSC Laboratory. Two standing committees, one technical and the other financial, manage the operations of the project. The Technical Committee makes all decisions necessary to ensure a fully operational detector upon SSC turn-on. The Financial Committee is responsible for developing the budget and for fiscal oversight of the project.

A Technical Director, currently Sulak, coordinates technical operations. Upon approval, this position would be held by a collaborating physicist dedicated to this tasks. The Technical Committee consists of members elected by the Collaboration, a Chairman who is one of the Spokespersons and the Technical Director. Each member is a liaison physicist responsible for a specific detector subsystem and its integration.

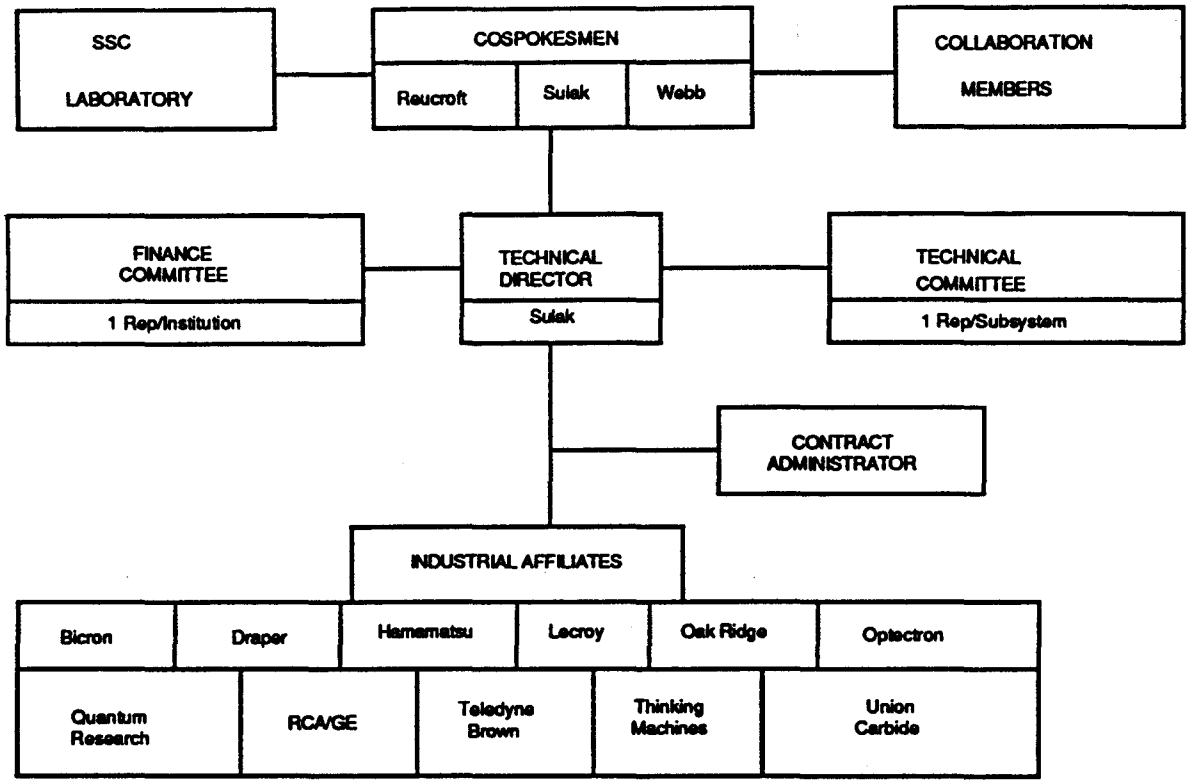

CONSTRUCTION PHASE

Once the formal proposal is approved by the SSCL, the management structure will be expanded to a Program Office and Project Managers at Draper responsible for each of the detector's major subsystems and their integration. They will interface directly with the liaison physicist responsible for each subsystem. The Program Management Team is responsible for meeting the goals of the collaboration on time and within budget. Because of its successful past experience in program management on numerous large system engineering efforts, including the Apollo Lunar Lander Guidance System and the Trident Missile Guidance System, Draper Laboratory would supply the Program Office. Draper brings an appropriate mix of engineering disciplines and experience with scientific endeavors to ensure that schedules and cost goals are met, while not stifling the creative genius required to make this project a success. The Program Management Team will be under the direction of a Program Manager assisted by a Project Support Group, Each of the five major components (Tracker, Calorimeter, Muon Detector, Signal Acquisition

and Processing, and System Integration) will have a Project Manager, reporting to the Program Manager.

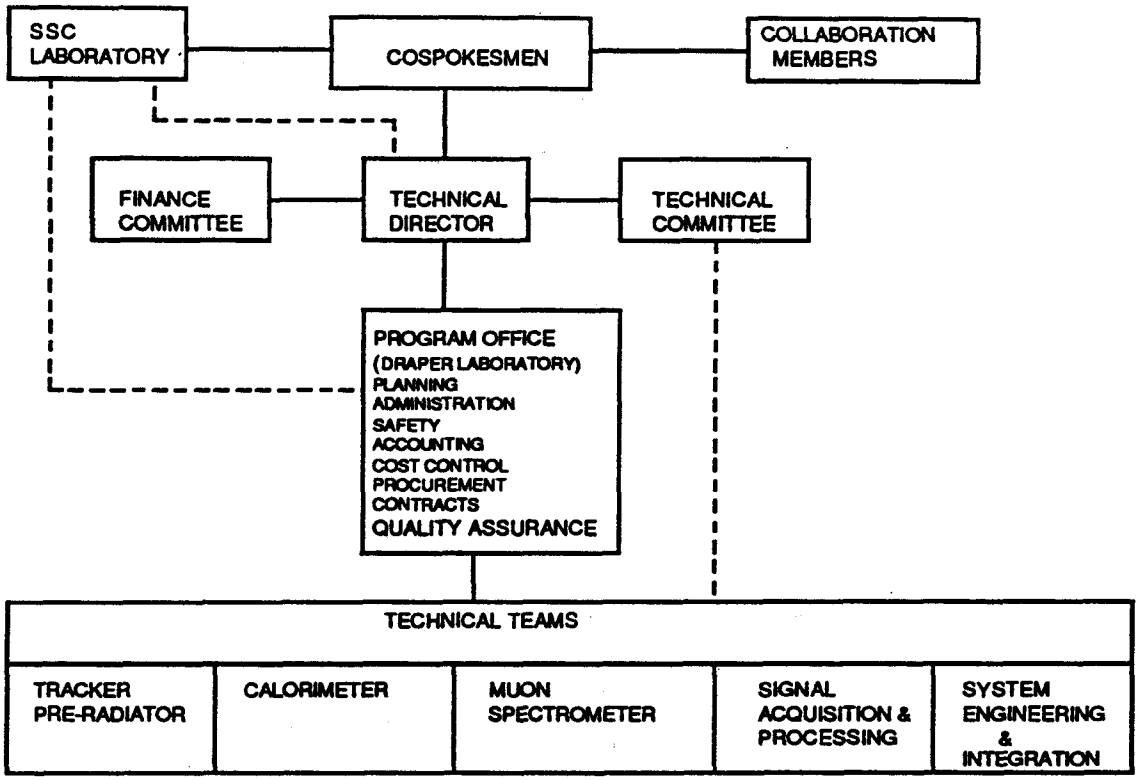

The Program Manager, is responsible to the Technical Director and the Spokespersons, for the execution of the Program (design, fabrication, integration and testing). The Program Manager, who would reside at SSCL during assembly, would preside over monthly program and technical reviews. The Program Office would contain support functions similar to their counterparts at the SSCL --- Planning, Administration, Safety, Accounting, Cost Control, Procurement, Contracts, Configuration Control, and Data Management. The Quality Assurance Manager reports directly to the Program Manager and is responsible for independently verifying that each component is built, tested and assembled in accordance with drawings, specifications and approved procedures. The Quality Assurance Manager also assures that all software is documented and tested to the agreed upon level. Each support function will work closely with their parallels at SSCL to ensure that the Program Office is closely coordinated with SSCLs.

The teams responsible for the components comprising the detector will each be run by a Team Manager who will be responsible for developing and manufacturing that component. This includes

engineering, fabrication and testing. In addition, the System Engineering and Integration Team will be responsible for integrating the components to form the detector, and installing the detector at the SSCL. System engineering and integration techniques, pioneered by the aerospace industry, will be used extensively to ensure the success of the project. The Team will include engineers, physicists, and programmers from each of the component departments to insure the required communication is taking place between the liaison physicist for each component, the component developers, and the system integrators. The system integrators will work closely with SSCL personnel in developing plans, specification documentation, and schedules for installing the detector at SSCL and integrating it with the Collider. The responsibilities of the System Engineering and Integration Team include components and interface requirements definition, the test plan for verifying and validating that requirements are met, interface definition and change control, procurement and fabrication (parts, materials, and fabrication standards), logistics, integration and assembly of the detector, system engineering, management planning, work breakdown structure definition and development of specification trees.

APPENDIX B

Critique of Fiber Calorimeter Cost Estimate of SSCL Note # 728 ...
Draper Lab Memo EEC-90-693

The Charles Stark Draper Laboratory, Inc.
555 Technology Square, Cambridge, Massachusetts 02139 Telephone (617) 258-

EEC-90-683

TO: L. Sulak

FROM: C. Elder

DATE: 11 July 1990

SUBJ: Critique of Cost Estimate of Spaghetti Calorimeter in SSCL-N-728.

DIST: R. Araujo, F. Ayer, J. Deyst, R. Riley, D. Sullivan, E. Womble

The TEXAS 1/ and the SPACAL 2/ Spaghetti Calorimeter for SSC are similar in concept. They both consist of an array of "towers" made up of scintillating fibers encased in lead or lead alloy. The TEXAS calorimeter has 15,360 towers and the SPACAL has 60,510 towers; almost four times as many. The TEXAS calorimeter utilizes only one tower-to-ring mounting scheme and one basic ring design. The SPACAL calorimeter has five different super rings in the central barrel and four super rings in the end caps *((19)). This collection of nine super rings, however, may well reduce to only four actual super ring design concepts ((4)).

The initial TEXAS calorimeter design has 15,360 towers, 15,360 tower mounting brackets and 120 rings. Due to the commonality of construction there will, however, be only one set of three to five tower drawings, one tower bracket drawing and one set of three or four ring drawings. Tables with sixty dimensional entries will account for the variations in these parts. The TEXAS calorimeter drawing inventory will be negligible, the assembly procedure will be uniform and there will be only one learning curve for fabrication of the parts and one for assembly of the unit.

1/ "Scintillator Calorimeter Support Structural Design Evaluation", SSCL-N-727, F. Ayer, and C. Elder, Draper Laboratory, 31 May 1990.

2/ "Final Report for Detector Assembly Cost and Schedule Analysis for Liquid Argon and Scintillator Spaghetti Calorimetry", SSCL-N-728, Martin Marietta, May 30, 1990.

* (( )) Numbers refer to page numbers in reference 2.

The TEXAS and SPACAL Spaghetti calorimeters for SSC are in the conceptual stage of development. Because detail design and fabrication information on the calorimeters has not yet been developed, it is possible to make only broad cost comparisons between the two.

It is intuitive that an assembly with four times as many parts as another will be the more expensive. It is also true that an assembly with a larger number of separate design concepts will also be more costly. "More parts and more designs cost more money" is valid reasoning but complexity has a more far reaching effect on costs than simply parts cost and design time.

Illustrations of the impact of complexity on cost can be seen in the Martin Marietta report. Martin Marietta aptly uses the number of drawing sheets required to estimate engineering design costs ((7)). Clearly the number of drawing sheets will be greater with a more complex design. Martin-Marietta also points out that hours of design analysis (stress, dynamic, thermal and mechanical analysis) is a direct function of design engineering ((8)). They further observe that test engineering and systems engineering costs are directly related to design complexity as well ((8)). Martin Marietta presents the fact that the magnitude of other technical services (OTS) (planning, contracts administration, procurement and management) is a function of on-site engineering fabrication, test and tooling ((9)). For example, in a simple analysis, an assembly with four times the parts would have four times the fabrication effort and therefore around four times the OTS ((19)). In addition, Martin observes that travel is in proportion to the increased OTS ((9)).

There should be little disagreement with Martin's premise that the manufacturing cost for a spaghetti calorimeter would be driven by assembly time ((11)); one would expect that a 60,000 tower calorimeter would take considerably more time to assemble than a 15,000 tower calorimeter. It is also reasonable to assume that if the tower assemblies make up 77% of the calorimeter costs as Martin estimates ((18)), that 60,000 towers are likely to lead to a higher total cost than the 15,000 towers of the TEXAS detector.

A partial list of the overall cost advantages accruing from fewer parts in a calorimeter design is the following:

1. fewer manufactured parts
2. less inspection and testing cost
3. fewer reject parts
4. fewer material review considerations
5. fewer spares required
6. less packaging and shipping costs
7. less handling, warehousing and cataloging
8. less mounting hardware
9. less calorimeter assembly time

A partial list of the cost advantages accruing from fewer basic concepts incorporated in a calorimeter design is the following:

1. less engineering
2. less analysis
3. fewer drawings
4. fewer machine set-ups
5. less tooling for manufacture and handling
6. fewer inspection and test procedures
7. less variety of spares
8. fewer assembly procedures
9. fewer learning curves throughout

It is axiomatic in engineering that "simple is better". Simplicity impacts cost, reliability, maintainability and schedule compliance. Simplicity of concept requires less engineering design and technical support. The goal of simplicity has been a major consideration in the TEXAS calorimeter design effort.

It is fortunate that there is a documented history of engineering, assembly, tooling, testing and material costs for spaghetti calorimeters used in other programs. This history is a major factor in assuring the validity of the cost estimates made for the TEXAS calorimeter. Based on the expression of interest, the SPACAL cost is approximately $118 million ((19)) while the TEXAS calorimeter cost was estimated at $78 million.

C. Elder

C. Elder

CSE/hg

APPENDIX C

MACRO Prototype Muon TRD Costs

Foam (DOW Chemical) Delivered in 2 cm Layers	46ML/SM
Polystyrene Tube, including graphite coating on inner walls, and inserting the wires (Polivar Corp.)	20 ML/SM
Aluminium Enclosure	30 ML/SM
Cables, Connectors, Low and High Voltage Supplies	36ML/SM
Read Out Electronics with Cluster Counting (Frascati Lab)	57ML/SM
ADC's	192ML/SM
Total Price Per Super Module	381ML/SM

1 Super Module = 2 m × 6 m × 10 layers

APPENDIX D

TEXAS Calorimeter Tower Assembly Cost Estimate ...
Bicron Corp.

BICRON

BICRON CORPORATION 12345 Kinsman Road, Newbury, Ohio 44065
(216) 564-2251 Telex 980474

"TEXAS" CALORIMETER TOWER
ASSEMBLY COST ESTIMATE

1. 30,720 TOWERS
   A. Precision fiber arrays cast in die-metal towers
   B. Tower size: 5 cm square tapering to 10 cm square x 2 meters long
   C. 60 different shapes, 512 each
   D. Precision plates or caps on each tower end.
   E. Fibers at the large end bundled and potted to form four polished groups for interfacing to other optics.
   F. QA certification:
      - Scintillation and optical function
      - Mechanical tolerances and form
   G. Crated and shipped to SSC Lab, FOB Newbury, Ohio

2. MAJOR COST ELEMENTS
   Manufacturing Period: 5.5 to 6.5 years, including engineering at the start

   A. Assembly Labor Estimates

Program Management, Eng. Liason	3,000 hours
Precision Array Assembly	102,960 hours
Casting	42,880 hours
Clean-up machining	31,340 hours
Fabricate 122,880 fiber bundles	34,320 hours
Testing	68,640 hours
Shipping & misc. support	34,320 hours
	317,460 hours

   B. First Year On-Site Engineering 2,080 hours

   C. Materials

1600 gallons of epoxy	$ 371,000
Crating materials	951,000
Tower hardware	2,041,000
	$ 3,363,000

D. Factory Expenses

Array equipment and tooling	$ 773,000
120 Casting molds	928,000
Factory infrastructure	773,000
	$ 2,474,000

3. Total Estimated Sale Price of the Above: $ 28,230,000
   This figure includes a 10% contingency factor of $ 2,566,000.

This is not a quotation. The above figures are best estimates at this time. Firm numbers would be available after an extensive engineering study of the anticipated processes.

The labor rates and material costs have been estimated for the averages expected during the anticipated six-year manufacturing period.

The overhead and profit rates included in the calculation are presently accepted by the U.S. Government and are assumed to be applicable during the term of the project

BICRON CORPORATION 12 July 1990

Charles R. Hurlbut
Manager, Organic Scintillators.

APPENDIX E

Cost Risk Analysis for TEXAS Calorimeter Electronics

George Blanar, LeCroy Research Systems

We have reviewed the TEXAS calorimeter electronics budget of $20M ($100 per PMT), and compared it with existing systems in terms of cost. We consider here the application of some existing systems to TEXAS to determine whether the TEXAS budget is realistic.

1. LeCroy Charge ADC

The conversion time of this FASTBUS device is too long, but recent improvements of 100-fold in the conversion times of LeCroy TDC's suggests that new, fast-conversion ADC technology may be available soon. The dynamic range of these devices is 15 bits, which is adequate for TEXAS. The cost is about $55 per channel, including power, interface, and pre-amplifier.

2. Struck Flash ADC

This is a 100MHz flash converter with 6 (8) bit resolution and 8 (10) bit dynamic range. The dynamic range is inadequate; a precision log-amp front end would be required for application to TEXAS. The cost is about $220 ($600) per channel, including packaging and pre-amp.

3. Fermilab D0 Flash ADC System

This is a 100MHz noncommercial flash converter system with 8 bit resolution. It would also require a non-linear front end. This system includes a gate array for zero-suppression. The component cost is about $130 per channel in quantity. A rough estimate of the commercial cost is $500 per channel.

Costs for existing ADC systems range from about $55–$600 per channel, depending upon whether it uses a charge ADC or a flash technique. All of the above systems are rack-mounted. Previous experience shows that the cost of a detector-mounted system is about 1/2 that of an equivalent rack-mounted system. Clearly, TEXAS should pursue an on chamber charge ADC technique. This requires the development of a new ASIC, which is in line with current development programs, at least in TDC's. In summary, it appears that a manufactured cost of $100 per channel in large quantities is realistic for a new, fast-conversion charge ADC system for TEXAS.

APPENDIX F

Intent to Jointly Develop Fiber Calorimetry with TEXAS ...
R. DeSalvo, SPACAL

ORGANISATION EUROPÉENNE POUR LA RECHERCHE NUCLÉAIRE
EUROPEAN ORGANIZATION FOR NUCLEAR RESEARCH

Laboratoire Européen pour la Physique des Particules
European Laboratory for Particle Physics

GENÈVE SUISSE
GENEVA SWITZERLAND

Adresse postale/Mailing address

CERN
CH-1211 GENÈVE 23

Prof. S. Reucroft
Physics dept.
Northeastern University
Boston Mass.

Prof. L. Sulak
Spokesman TEXAS
Physics dept.
Boston University
Boston Mass.

Snowmass Co. 4 July 1990

Dear Steve and Larry, it was a great pleasure to meet you in Snowmass. It was particularly comforting for me to find somebody that, with independent lines of thought, has reached the same logical conclusions as I. From this point of view I am very happy that you were not aware of my Tuscaloosa and Erice reports.

I like TEXAS better than the other SSC EOIs but I will not be able to join it while I am an LAA physicist (LAA is an R&D oriented structure dedicated to detector development and explicitly independent from experiment collaborations) I might accept your invitation in a couple of years when the LAA project will be finished. In the meantime it is a pleasure for me to provide TEXAS with all my personal support and my endorsement.

It is clear that most of your and our R&D aims coincide. While I cannot speak for SPACAL collaboration (a Spaghetti Calorimeter R&D oriented open collaboration started with the LAA-SPACAL group and now including ten different institutions including a US university with members in Empact and SDC) I think that it would be stupid to duplicate such efforts in face of the large challenges and the tight timescales that both our groups face. I then strongly suggest that one or both of you come to one of our collaboration meeting to present us TEXAS and to discuss resource pooling and collaboration options.

Just to give you an idea on what kind of projects on which we can collaborate, I list here our program and our weak points.

Starting in the fall we are going to make a hadronic containing projective prototype, we are confident that we will get the resources to build it but we will not have the strength of building for it a trigger structure and data acquisition system prototype in the guidelines described in my Erice paper or in the TEXAS proposal.

Antonio Ereditato of INFN Napoli has already confirmed that if you could pick up this line of development he would send to Boston one of his graduate students to act as a link.

We need to build a small (2-3 tons) calorimeter prototype with 3HF fibres and test it with electron and pion beams. We think it is important to make this test to measure the effect of slower fibres on the longitudinal sensitivity and e/pi rejection. Even if 3HF will not be used in a final detector this data will allow us to evaluate the performance of different fibre components without building each time a prototype. With our infrastructure we can mount such a small prototype in two or three weeks but we will not have test beam facilities for about an year. If you could provide test beam in Fermilab we could have earlier results and you could start getting familiar with our techniques.

I am certain that our Paris-6 and Nikhef-h engineers studying the detector shape and support structure would like to exchange ideas with your engineers.

The development of the Hybrid Photo Diode into a pixeled detector will require further funding. Some work will be necessary in order to optimize the readout speed and external signal amplification.

The radiation hardening studies badly need a lot of further efforts and in this moment most of the expertise is in the US.

We need to improve our mass fiber quality control procedures.

We need to work on lead metallurgy.

While our know-how is quite advanced compared with some other calorimeter technologies, I could continue this list of unsolved problems for another two or three pages. The point is that we are desperately too few to solve all these problems in the next two years. With all these challenges exceeding our resources, both human and budgetary, and with the EOI engineering support anticipated for TEXAS and for scintillating fibre calorimeters I believe that we could both greatly profit from a tight collaboration.

I will be in vacation from tomorrow to the tenth of August and R. Wigmans will be absent all of August. I hope you will get in touch

with me in the second half of August so that we will schedule your visit to coincide with one of our collaboration meeting in early September when everybody will be back from vacation.

Your Sincerely

Dr. Riccardo DeSalvo

EO1-11

PRACTICAL ISSUES

The Collaboration...
University and Industry
Management

The Cost

The Engineering Studies Program

The Funding Request

Overall Summary

L. Sulak
Presentation to SSC PAC
6/8/90

TEXAS specific...

Engineering and Integration Studies
Funding Request ≤ FY91

Highly focussed program to develop manufacturing/cost confidence:

Rad hard fiber /manufacturing calorimeter modules

low cost, pixel detectors/high dynamic range PMT's

integrated tracker, PMT, TRD electronics

fast simulation/high level triggering

mechanical system design/integration

calorimeter prototype

tracker/pre-radiator prototype

muon TRD spectrometer prototype

Goal: 90% confidence level at proposal submission that

a) detector feasible & manufacturable

b) within 10% of cost estimate

Estimated Total Detector Cost	$ 196M	
Engineering Request	$ 8M	4% of Total

... a new way of doing physics ... not a scale up or extrapolation [illegible]

Presentation of Expression Of Interest

A CALORIMETER-BASED HIGH-RATE DETECTOR FOR THE SSC

S. Dye, G. Jones, C. Oh, S. Klein, J.P. Miller, D. Perlman,
M.A. Rahman, B. Lee Roberts, J. Stone, Larry Sulak**, and Bill Worstell†
Boston University

Chuck Lane
Drexel University

Dave Winn
Fairfield University

George Blanar and J. Hofteizer*
LeCroy Research Corp.

G. Alverson, W. Faissler, M. Glaubman, A. Grimes, Ian Leedom†,
J. Moromisato, E. Pothier, Steve Reucroft**, E. Saletan and E. von Goeler
Northeastern University

Bill Dunn, F. O'Foghludha, S.K. Myers, J.D. Simpkins, and A.M. Yacout
Quantum Research

Teruki Kamon and Bob Webb**
Texas A&M University

and Industrial Partners

Bicron
Chuck Hurlbut*

The Charles Stark Draper Laboratory
R. Araujo and François Ayer*, C. Elder, Dan Sullivan

Hamamatsu Corp.
Joe Murray*

Oak Ridge National Laboratory Detector Center
J.W. Stapleton* and Tony Gabriel

Optectron
Patrick Jacquet*

RCA/General Electric
Henri Dautat, Bob McIntyre*

Teledyne Brown Engineering
Jim Woosley*

Thinking Machines Corp.
G. Bhanot, J. Mucci, David Orr and J. Reardon*

Union Carbide Industrial Gases Inc.
Sharon L. Saupp* and Tom Schulte

SSC Lab Liaison

Marvin Hecht and Tim Thurston

The TEXAS Collaboration
(Totally hermetic EXperiment At the Supercollider)

* Contact person ** Co-spokesman † SSC Fellow

Current

TEXAS Management Structure

FY91

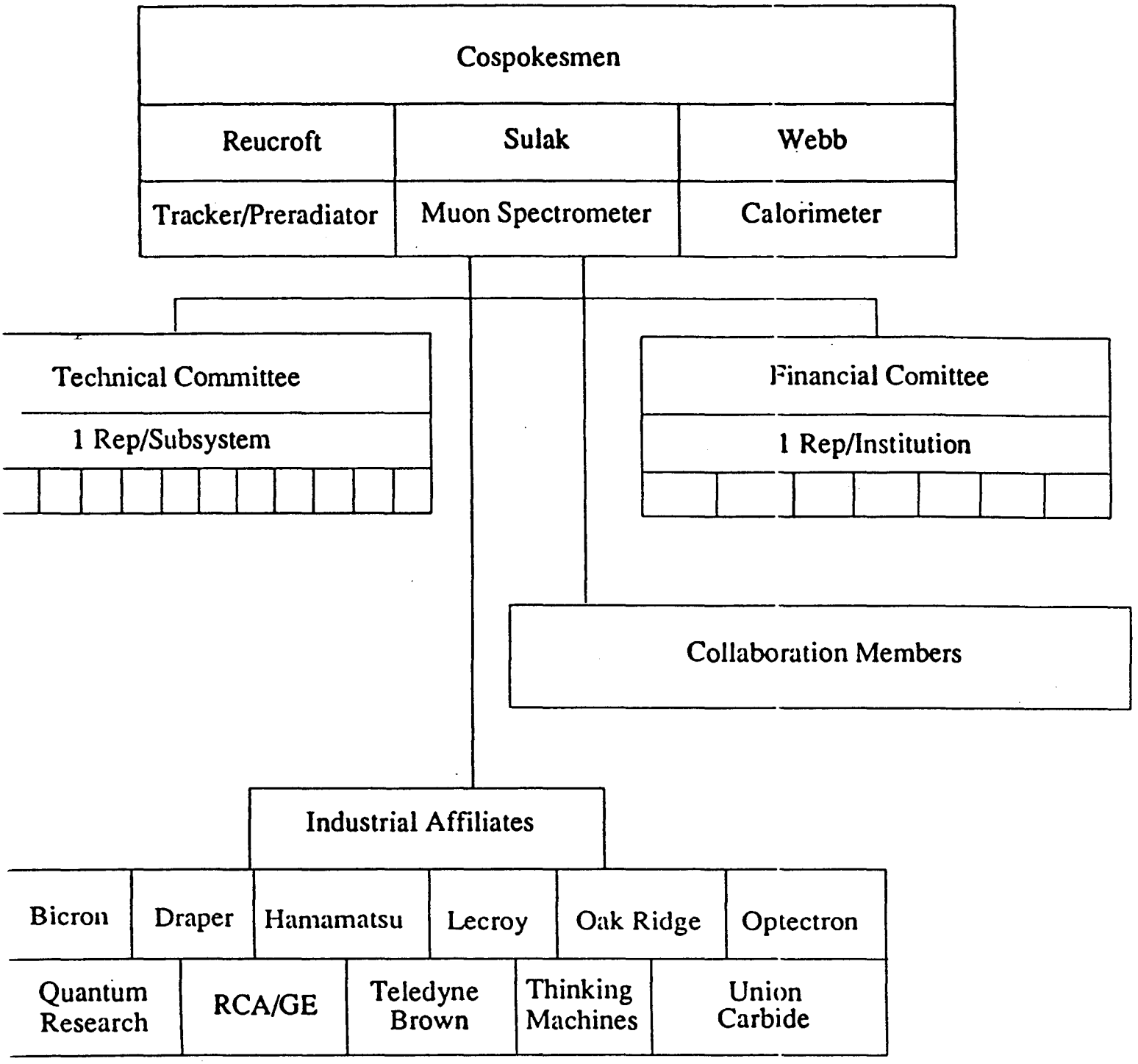

... but we are evolving

Scientific Collision Making ...

TEXAS Technical Committee

Technical Experts for each subsystem

Central Calorimeter
Worstell (Boston)

Forward Liquid Calorimeter
Webb (Texas A&M)

Tracker Pre-Radiator
Reucroft (Northeastern)

Radiation Hard Scintillator Fiber Q.C./Testing
Leedom (Northeastern)

Electro-Optics Q.C./Testing, Power Supplies
Winn (Fairfield)

Muon Trigger Counters
Lane (Drexel)

Muon Tracking Vector Chambers
von Goeler (Northeastern)

Muon TRD's
Sulak (Boston)

Test Beams, Calibration Systems and Detector Data Base
Dye (Boston)

Data Acquisition and Trigger Electronics
Klein (Boston) and Hofteizer (LeCroy) + Hazen (Boston)

On-Line Software
Miller (Boston) and Reardon (Thinking Machines)

Systems Integration /Manufacturing/Assembly
Ayer (Draper) + Cozzi (Boston) & Osborne

SSCL Facilities/Interaction Hall/Accelerator Liaison
Webb (Texas A&M)

Monte Carlo and Off-Line Software
Kamon (Texas A&M)

... a light line between university and industry...

TEXAS LIAISON PHYSICISTS AND INDUSTRIAL AFFILIATES

Task	*Liaison Physicist*	*Industrial Partner*
Calorimeter Manufacture	Worstell	Hurlbut/Bicron
Scintillating Fiber and Liquid	Leedom/ Jones	Hurlbut/Bicron Jacquet/Optectron
Tracker/Preradiator Support	Reucroft	Gabriel/Oak Ridge
PMT's/Pixel Readout	Winn	Murray/Hamamatsu McIntyre/RCA Woosley/Teledyne Brown
Xenon Gas System	von Goeler	Saupp/Union Carbide
PM/TRD Electronics	Klein/Lane	Hofteizer/LeCroy
On-Line/High Level Triggers	Miller	Dunn/Quantum Research Reardon/Thinking Machines
Mechanical Structure/Integration	Sulak	Ayer/Draper

... asking specific questions

our best estimate ... with much external input ...

TEXAS Detector

PRELIMINARY COST ESTIMATE

Central Tracker/Preradiator

Reucroft, Cushman (Yale), Rusack (Rockefeller), and Winn

SSC Subsystem R&D

900K Tracking channels

		($M)
Mechanics		
1mm fibers 900K @ $15	3 layers (Tracker)	14
	9 layers (Pre-Radiator)	3
Construction + leadsheet		1
Electronics		
Channels 300K @ $20 (Tracker)		6
Channels 600K @ $20 (Pre-Radiator)		12
Cables		1
		$37

Calorimeter Mechanics

Barnes (Purdue), Hertzog (Illinois)/PS202 JET SET, Hurlbut (Bicron), Webb, Winn and Worstell/SSC Generic and Substystem R&D

200K Calorimeter channels

1mm Scintillating fiber @ $200/km, 150,000km	30
Lead @ ($2k/T × 5kT)	10
Bonding, weaving	3
Construction and labor	6
Photo multipliers and lightguides (200K @ $100)	20
Calibration system	1
Forward Calorimeter	8
	$78

Calorimeter Electronics

LeCroy, Foster (FNAL) and Hazen (Boston)/ SSC Subsystem R&D

200K Electronics channels

Analog "exponent" digitizer 20 bit @ $10	2
100MHz FADC 8 bit @ $25/chip Sony	5
Trigger gate array @ $25	5
PC Boards, cables, connectors @ $15	3
High voltage @ $50/multiplexed 8PMs + Bases @ $15	4
	$19

Barish (Caltech) and Hazen (Boston)/MACRO Extrapolation

900 Liquid scintillator boxes

PVC Boxes + mirrors	2
Liquid scintillator	1
Labor	2
Photomultipliers + bases (3600 channels)	1
Electronics trigger and ADC + HV (@ $275/channel)	1
	$7

Muon Tracking

Iarocci (Frascati)/MACRO Extrapolation

56K Limited streamer tubes + 56K strips

8-tube chambers (7K)	2
Transverse strips, gas system, HV	1
Digital readout electronics, 100K channels	1
	$4

Muon TRD's Mechanics

Union Carbide, Hubbard (Saclay)/D0 and Iarocci (Frascati)/MACRO Extrapolation

30K extrusions

Foam and extruded tubes (300K channels)	5
Xenon (1600m^3 @ USSR value or USA buyback)	6
Gas System	1
Assembly	1
	$13

Muon TRD Electronics

Hubbard (Saclay)/D0 Extrapolation

30K Multiplexed Channels

Preamps @ $10 and shapers @ $20/pc board components	1
Multihit TDC's @ $10/pc board and $20/pc board components + packaging	2
Labor	2
	$5

All Mechanical Support Structures

Coan (Boston) and Wilk (Draper)

Design, engineering, and analysis	2
Calorimeter support piers	1
Bridges	1
Moving structure	1
Muon C-Tanks	4
Muon End Cap Tanks	2
	$11

Project Cost	$178
Contingency @ 10%	18
Total Project Cost	$196

Data Acquisition

Klein and Wilson (Boston)/SLD Extrapolation

Trigger (level 2 & 3)	3
50 RISC Processors (40 MIPS each)	1
	$4

Why so cheap?

- simple ... only 3 elements
- no precision tracking / no curves
- no magnets

geometry projective ⇒ simple electronics

most technology close to traditional

designed to be cost effective

RESOURCE REQUIREMENTS REPORT
DETECTOR: TEXAS

TABLE 5 CONSTRUCTION SCHEDULE RE: OUTLINE PART 1 g

SUBSYSTEM	START DATE 1/90	1/91	1/92	1/93	1/94	1/95	1/96	1/97	1/98	COMPLETION DATE Date
A. Prototype Design										
conceptual	XXXXXXXXXXX									
preliminary		XXXXXXXXXXXXXXXXXXXX								
final			XXXXXXXXXXXXXXXXXXXX							
Testing				XXXXXXXXXXXXXXXXXXXX						
B. Subsystem Design										
preliminary	XXXXXXXXXXXXXXXXXXX									
final			XXXXXXXXXXXXXXXXXXXX							
Off Site Assembly				XXXXXXXXXXXXXXXXXXXXXXXXXXXXXXXXXXXXX						
On Site Assembly										
1. Sub-surface						XXXXXXXXXXXXXXXXXXXXXXXXXXXXXX				
2. Surface					XXXXXXXXXXXXXXXXXXXXXXXXXXXXXXXXXXXXXX					
Assembly of:										
1. Detector supports						XXXXXXXXXXXXXXXXXXXX				
2. Fixtures							XXXXXXXXXXXXXXXXXXXX			
C. Hall Construction				XXXXXXXXXXXXXXXXXXXX						
D. Utility Building				XXXXXXXXXXXXXXXXXXXX						
E. Cryogenics Facilities										
F. On-site Assembly Facility				XXXXXXXXXXX						

TEXAS Calorimeter Critical Development Issues

- **Radiation Hard Fibers** - Recover from >10 MRad (Corporate Partners) Bicron, Optectron, QRS
  - R&D: (1) red fluors, (2) high fluor concentration, (3) new base, (4) direct shift
  - R&D: Recovery, Role of Oxygen

- **Photodetectors:** High Linear/Dynamic Range, Stable, Low Hysteresis (Corp. Partners) Hamamatsu
  - R&D: improved standard pmt, special bases
  - R&D: solid state diode anode target vacuum photodiode
  - R&D: dual readout - high gain/low gain system
  - R&D: Optical calibration systems

- **Fiber Geometry**
  - parallel fibers vs radial fibers Bicron / Draper
  - R&D: (1) fiber bonding, (2) stepped radius fibers (Corporate Partners) Bicron, Optectron
  - R&D: Monte Carlo: compensation, uniformity and calibration Quantum

- **Electromagnetic Options** Thinking Machines, QRS
  - monolithic with pulse shape discrimination vs separate e-m compartment options
  - enhanced e-m resolution vs fully compensated options
  - R&D: Monte Carlo
  - R&D: Fiber Techniques: bonding, coupling, dichromatic readout

- **Forward Liquid Calorimeter Design**
  - Performance: channel rad-hard optical cladding, light yield, optical coupling
  - Matrix material: hevimet holes and channels GE
  - Liquid containment, circulation
  - Monte Carlo: cell sizes, albedo, compensation, containment, rates

- **Pb Matrix Fiber Insertion/Manufacture** (with Corporate Partners)
  - Grooved lead and insertion
  - Cast Pb-eutectic Bicron, Draper

- **Photodetector Electronics** (Corporate Partners) LeCroy
  - HV/integrated calibration system
  - large dynamic range: preamp/shaper/ADC/analog trigger processor segment
  - digital pipeline trigger processor/readout

fiber progress in last year...

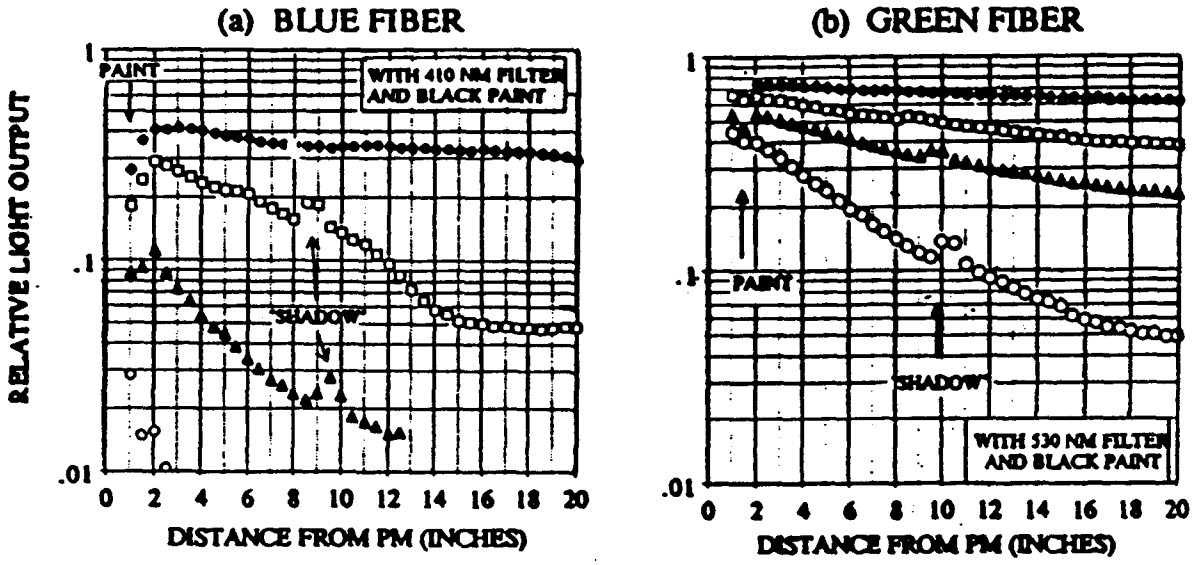

New Rad Hard Blue fiber

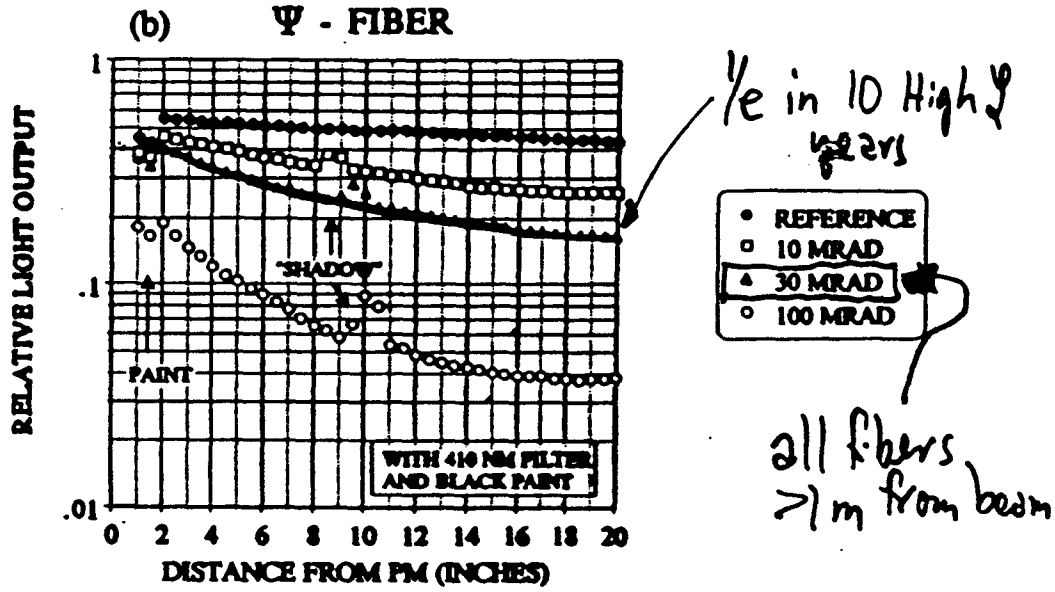

... confirms chemical models

C. Hurlbut, Bicron

A Monolithic Calorimeter with all support on outer surface...

SCINTILLATOR CALORIMETER SUPPORT STRUCTURAL DESIGN

Charles Stark Draper Laboratory

Element	Configuration & Dimension
Shell	Plate 2 cm thick
Circular Rings & Longitudinal Reinforcements	T Section: 22 cm X 1.5 cm web 16 cm X 2 cm flange
Center Ring End Ring	Tubes: 36 X 36 X 4 30 X 30 X 2
Center Frame End Frame	Tubes: 25 X 40 X 4 Vertical 25 X 25 X 3 Diagonal & Horizontal Tubes: 25 X 40 X 3 Vertical & Diagonal 25 X 25 X 3 Horizontal & Diagonal
Longitudinal Frame	Tubes: 20 X 40 X 3 Vertical 20 X 20 X 2 Horizontal & Diagonal

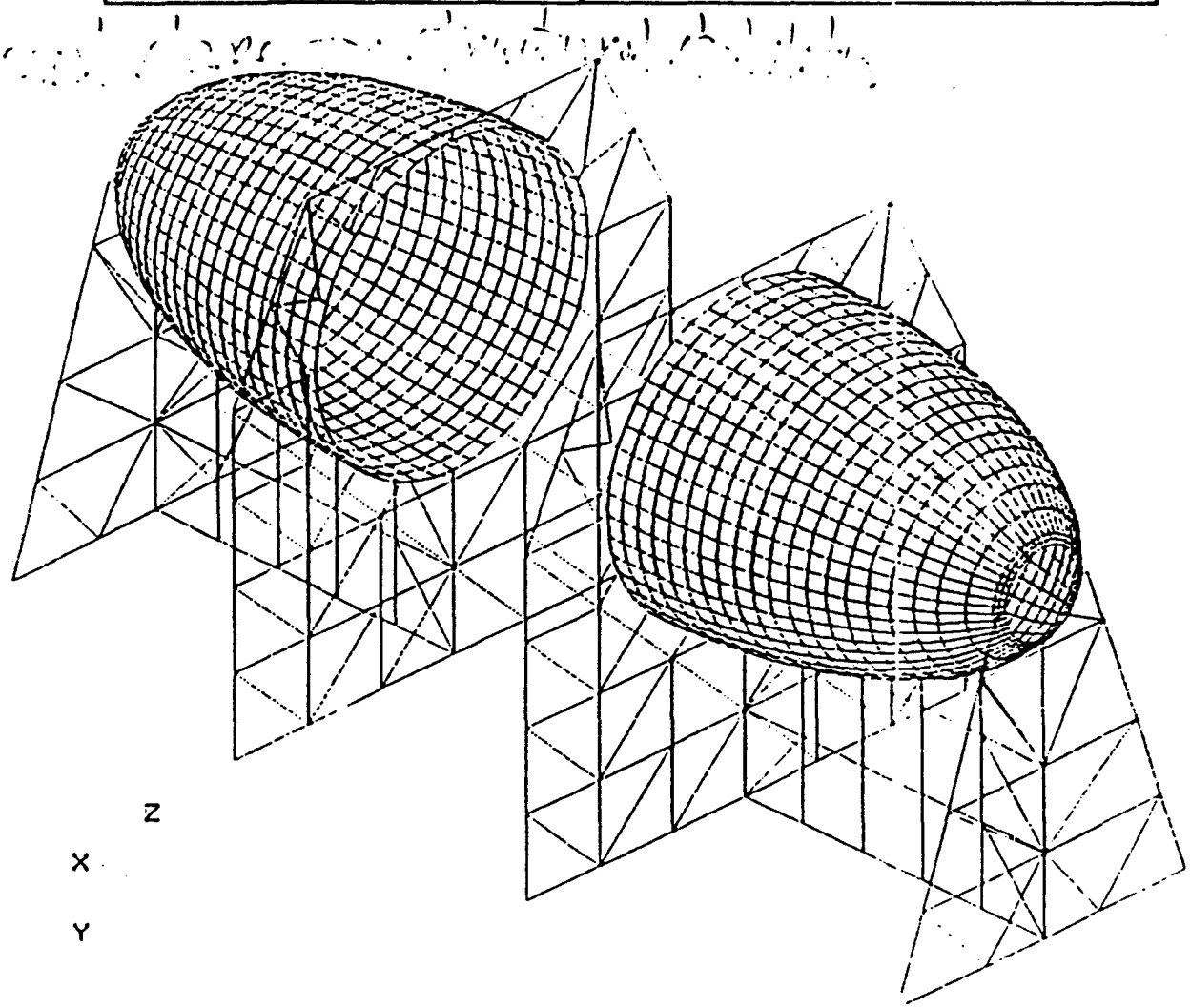

D. Sullivan
Draper

Calorimeter Halves in Open Position Finite Element Model Discretization

Baseline Study ... How to construct Fully Hermetic Calorimeter

MODULAR RING CALORIMETER

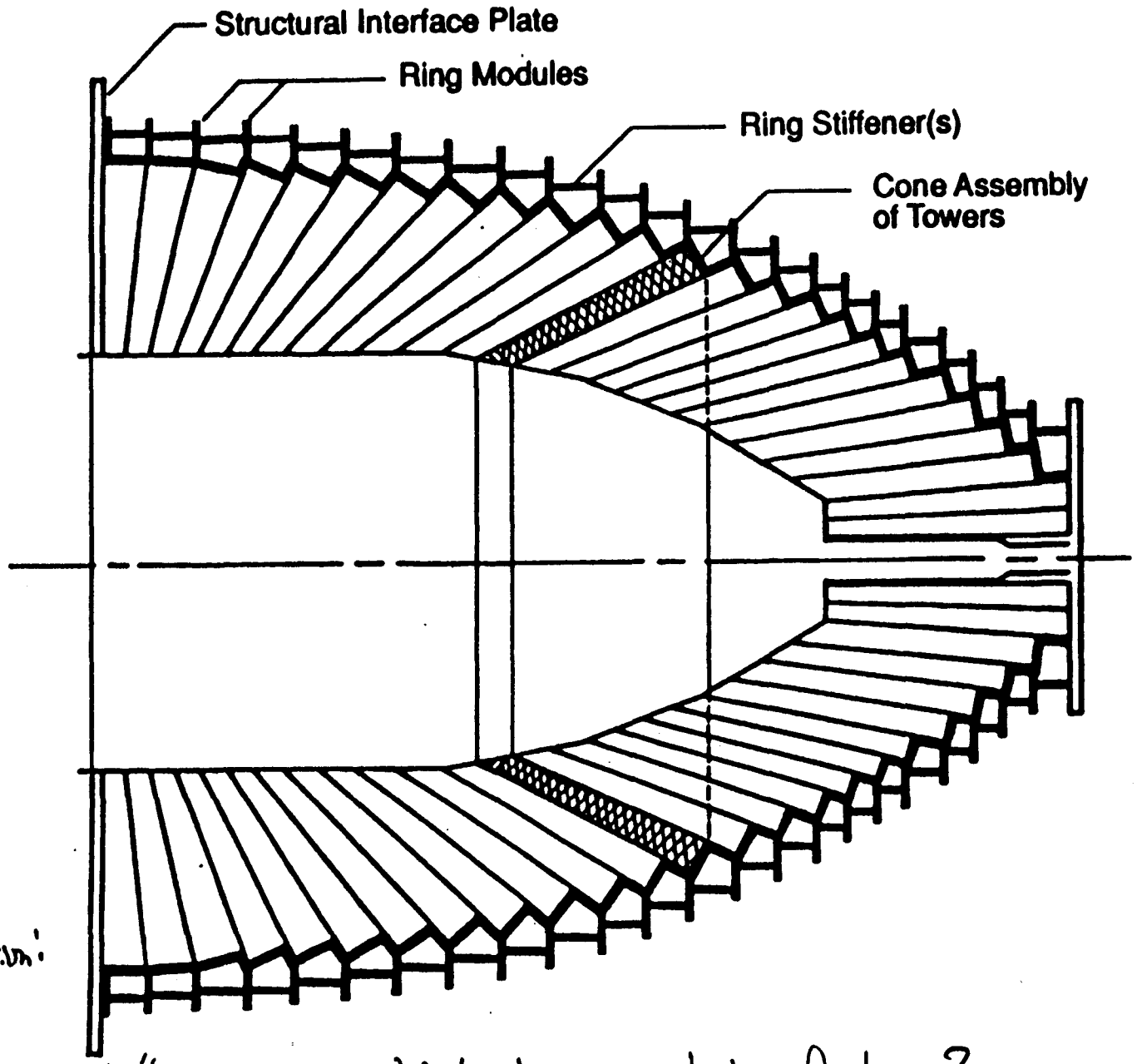

Cost Optimization:

... "Pineapple" rings assembled above or at the factory?

SSL Lab
T. Thurston

Draper Lab
C. Elder

How does one assemble the pineapple slices in the pit?

RAIL LAYOUT

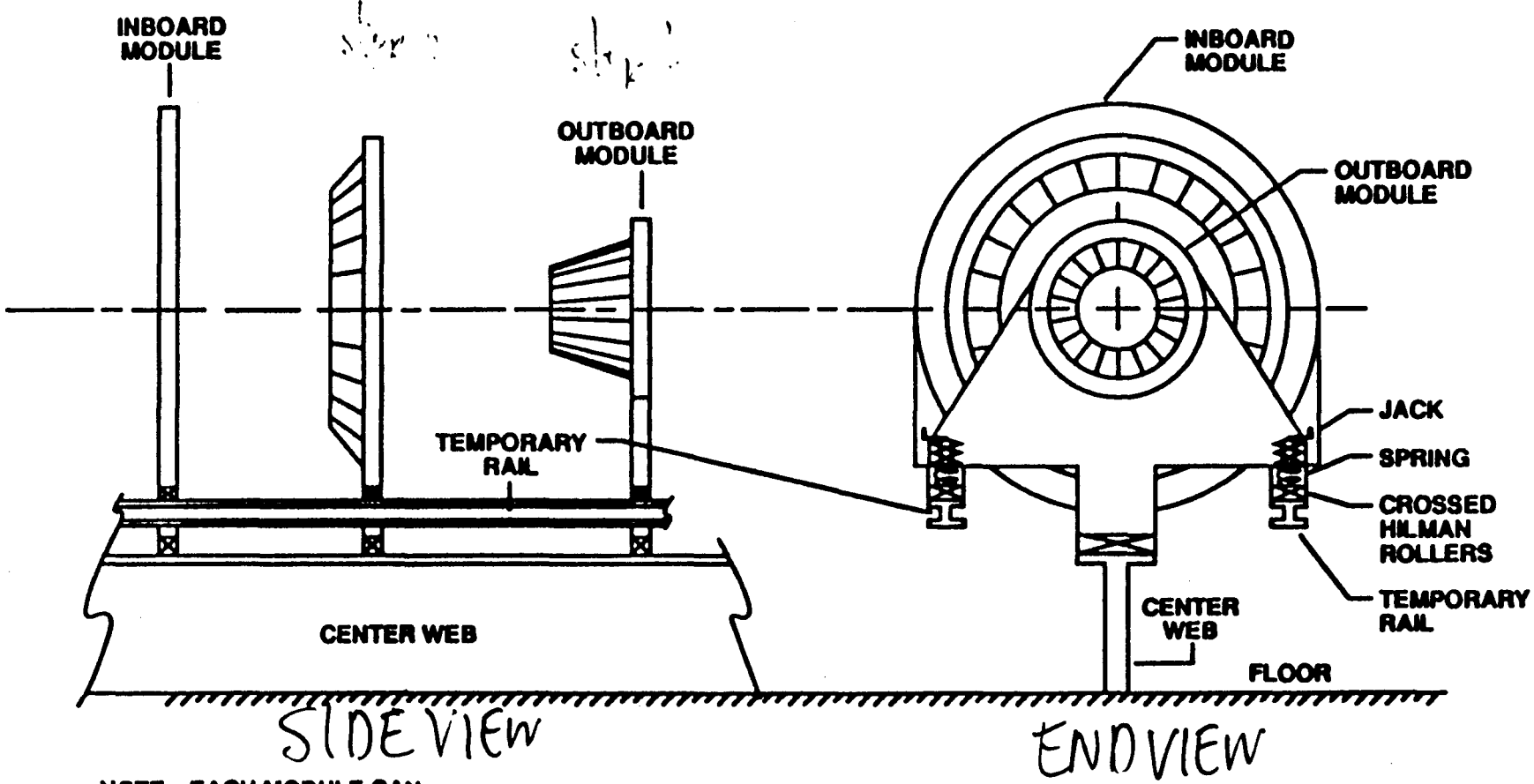

NOTE: EACH MODULE CAN BE ADJUSTED IN SIX DEGREES OF FREEDOM AT ASSEMBLY

... note use of temporary rails, mandrils etc to minimize underground operation

C. Elder
Draper Lab

STRUCTURAL DEFORMATIONS DUE TO GRAVITY

- MOST DISTORTIONS OCCUR IN FRAMES (2 MM)
- SLIGHT OVALIZATION OF CIRCULAR SHELL (1 MM)

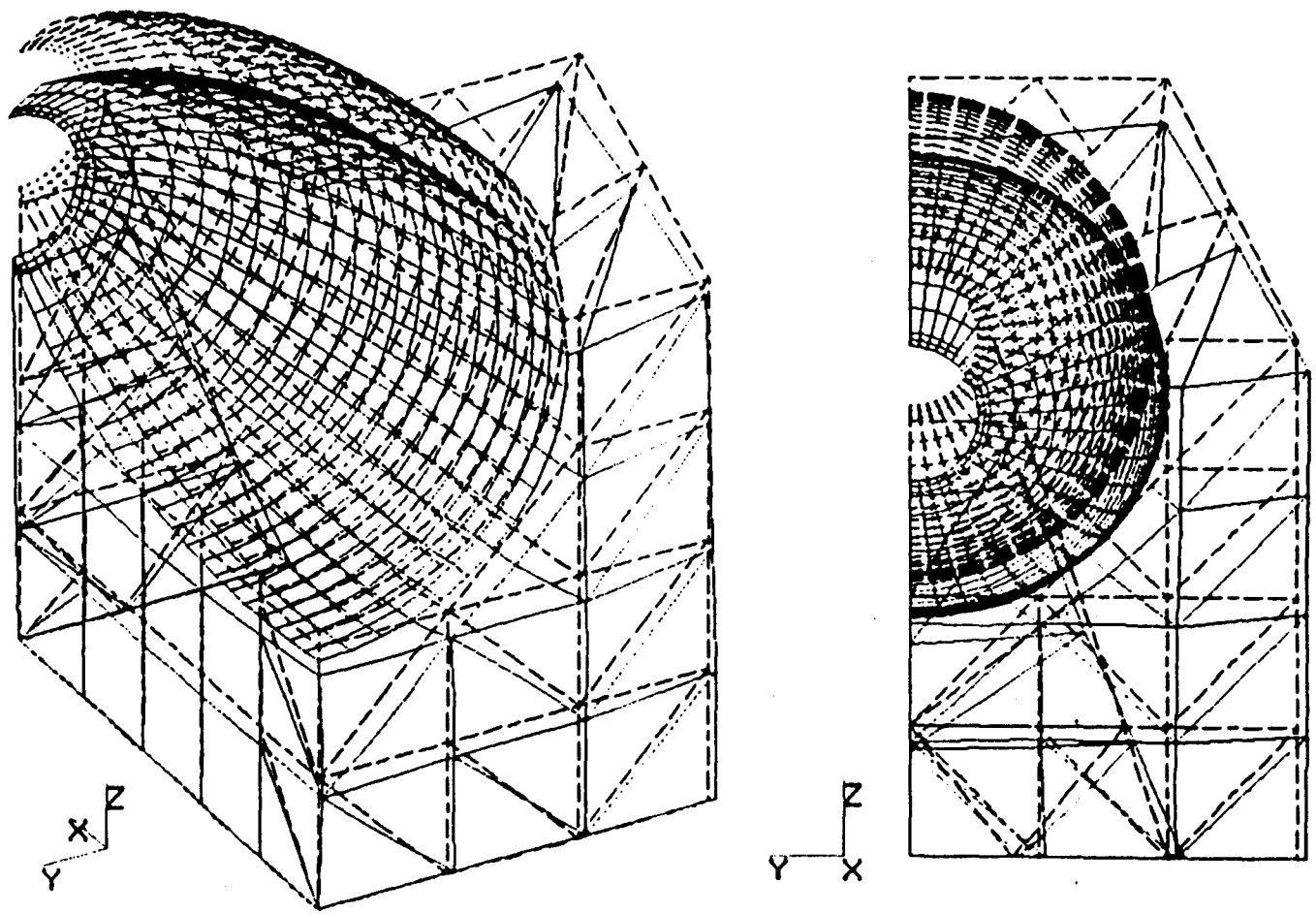

... and all structural elements thin, ~ 20cm

Worst case design ... assume no structural rigidity in lead/fiber composite

SHELL STRESSES UNDER GRAVITY

6.894×10^6 N/M ^{2} = 1 ksi

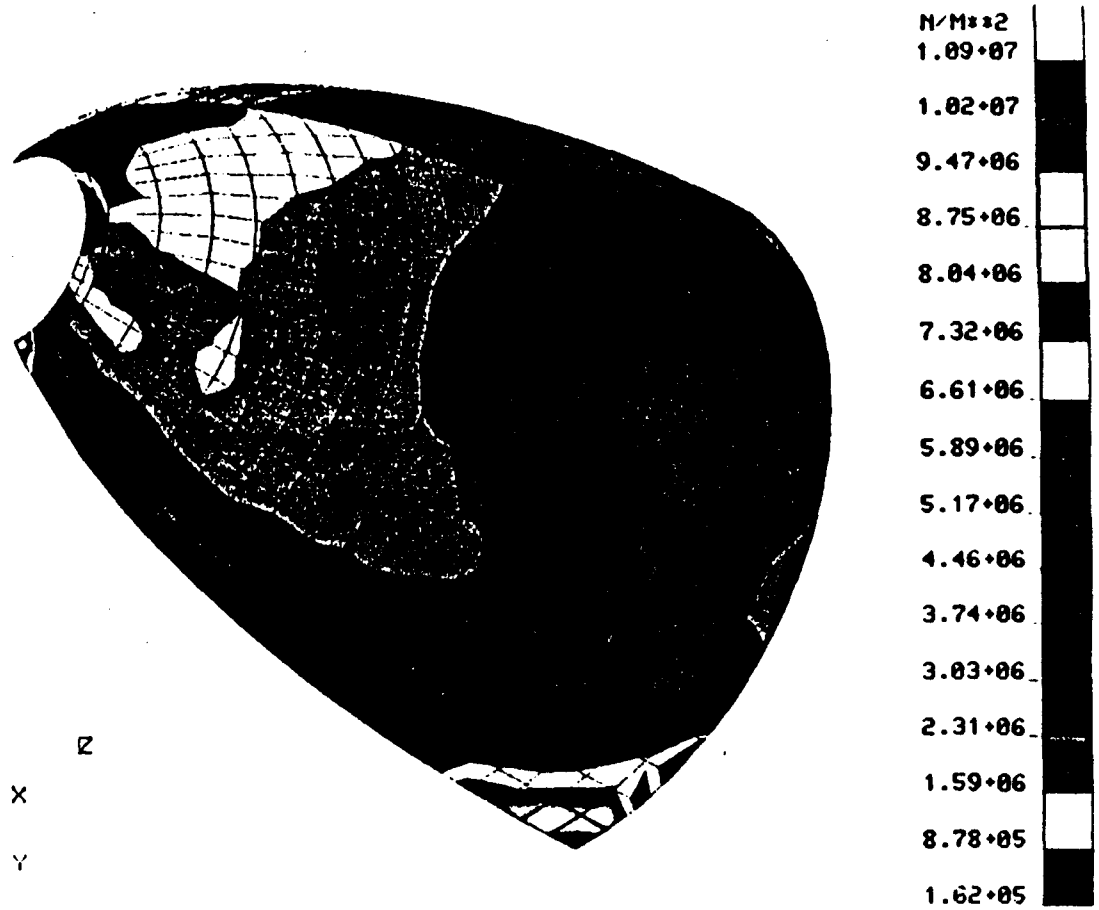

- OVERALL SHELL ACTION PRODUCES VERY LOW (HOOP + LONGITUDINAL) STRESSES < 5 KSI EVEN WITH STRESS CONCENTRATION FACTORS (SCF)
- LOCAL SHELL PLATE BENDING: EXPECT 12 KSI WITH SCF (ALLOWABLE 30 KSI)
- STRESSES IN RINGS REMAIN LOW AT < 6 KSI

... and no manufacturing optimization

The Charles Stark Draper Laboratory, Inc.
555 Technology Square, Cambridge, Massachusetts 02139 Telephone (617) 258-3846

TEXAS DETECTOR ENGINEERING DEVELOPMENT
WORK BREAKDOWN STRUCTURE

	COST
Central Tracker Support Configuration Tradeoffs Structural Analysis Interface/Mounting Definition	$130K
Scintillating Calorimeter Tower Design Studies Support Structure Design and Analysis Tooling Design	$425K
Muon Tracker System Gas Containment Tanks Design X-ray detector and Radiator Foam Module Design Xenon Gas distribution system design Design and Attachment of the Liquid Scintillator Tanks and Limited Streamer Tubes Structural Support Analysis	$375K
System Integration Subsystem Interface Control Build, Test, Transportation, Handling and Facility Requirements Definition System Cost and Assembly Schedule Definition	$190K
Program Management	$115K
Total	$1,235K

Muon TRD•dE/dx Critical Development Issues

- Develop radiator materials for large area and low Xe diffusion — Union Carbide
- Optimize basic TRD geometry with Monte Carlo for a fixed 6 m thickness
  - Radiator type(s)/thickness/spacing/number
  - X-Ray Detector gas/thickness/materials/number — Draper
- Confirm basic Monte Carlo Predictions with Beam Tests — Subsystem, R&D
- X-Ray Detector to maximize TRD signal and speed
  - materials, wire sizes, cell geometry, gasses, gain — Union Carbide
- TRD electronics to maximize TRD signal, using full pulse shapes — LeCroy
- Study punchthrough and low energy muon backgrounds
- Study efficacy of interspersed absorbers to reduce backgrounds

SSC makes TRD's "real" ...

not just novel or cute

... and the easy place to apply them is outside for μ's

How can one retain ~20M of Xenon? ... and keep < 100ppm O_2 etc for gain stability

Xenon Supply System

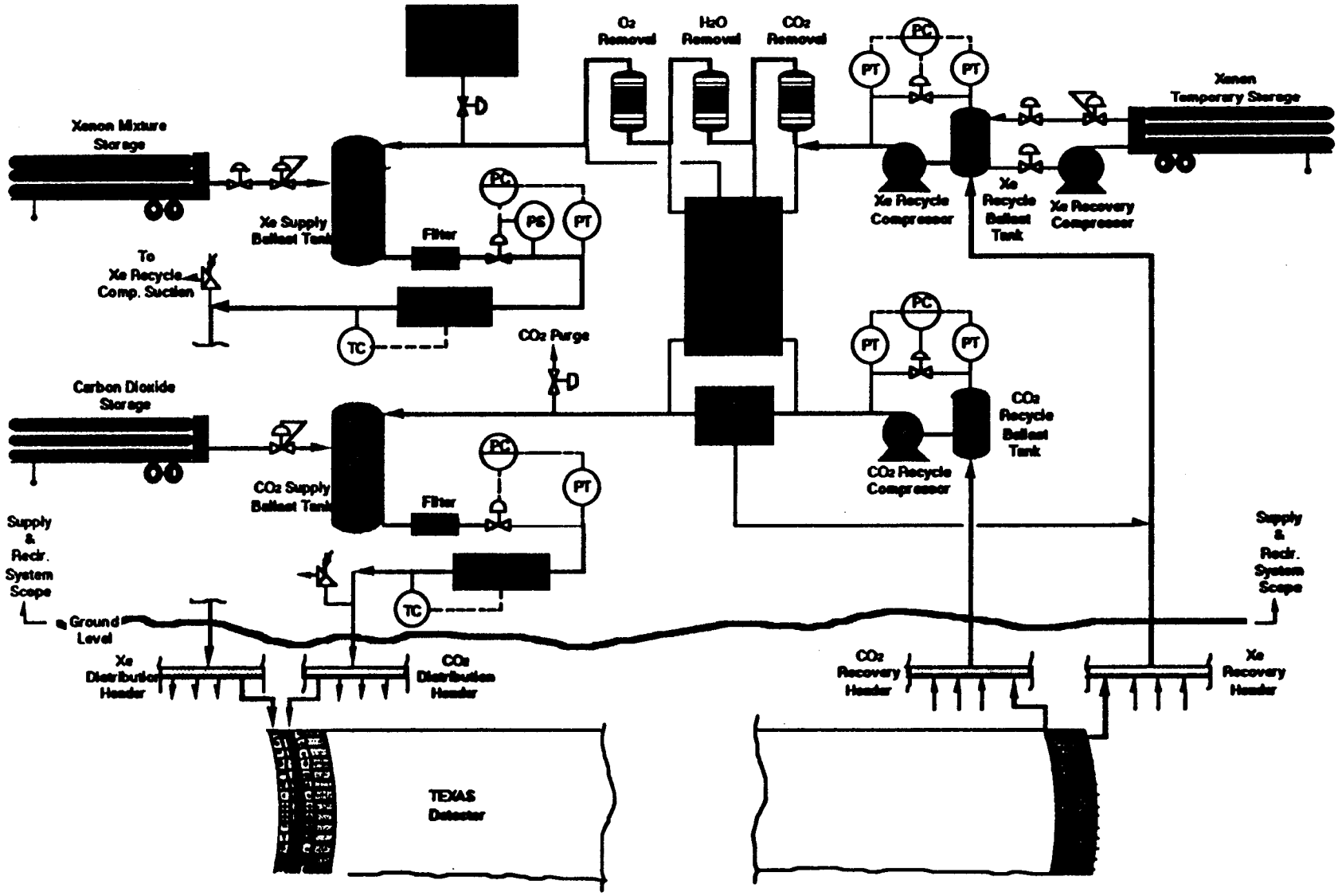

Yes! TiSchulte

Tracker•Imaging Pre-radiator Critical Development Issues

- Pixel Detector RCA, Teledyne Brown, Hamamatsu
  - $[illegible]/pixel
  - gain greater than 1,000
  - radiation hardness

- Pixel Readout LeCroy
  - easily integrated with pixel detector with minimal cabling
  - fast zero-skipping
  - fast analog summed outputs
  - speed ~20 ns/hit
  - radiation hardness

- Radiation-Hard Fibers Bicron, Optectron

- Fiber Bonding ~~spheroidal carbon fiber support~~ Oak Ridge

- Optimal Pre-radiator basic Design (Monte Carlo) Thinking Machines, QRS
  - radiator layer thickness, number
  - fiber diameter, fiber layer number, direction/stereo
  - pixel energy dynamic range
  - contour in calorimeter
  - ambiguity problems

- Optimal Tracker basic Design (Monte Carlo) Thinking Machines, QRS
  - fiber diameter, layers, direction/stereo
  - contour
  - ambiguity
  - pads or cell layers interspersed with fibers

- Forward Region Radiation Dose
  - lifetime
  - replacement
  - alternatives

- Confirm basic Design with Test Data

fast electronics tailored to architecturally projective detectors

	1991		
Detector Element	Task	Manpower	Capital
1. System Integration	• Development Plan • Manage/Liason	1	
2. PMT Data Acquisition	• Evaluate Alternatives • ADC Dynamic Range • Non-linear ADC • Define Concept	1	50K
3. Muon Chambers	• Concept • 4-Bit ADC • 100 ns Drift • Evaluate Alternatives	1	50K
4. HV for PMT & Wires	• System Definition • Generation • Power Distribution ~1W/channel • Monitor & Control • ASICs, pcb • Modeling & Simulation	1	50K
5. Trigger	• Define Concept • Model & Simulate	1	50K
6. Central Tracker	• Explore Scintillating Fiber Option • ~~Explore Straw Tube Option~~ • Define Concepts • Define ASICs	1	50K
Budget ($M)			
Manpower	.750 (6 people at .125)		
Capital Equipment	.250		
Overhead (facility, NRE, technician, support, travel, etc.) 30%	.225		
TOTAL	1.225		

... must process all data between crossings to operate at 10^{34}

LeCroy
Innovators in Instrumentation

+ Hagen Boston

to achieve 90% CL. in manufacturing & costs by 11/91...

Engineering Studies and Integration
Funding Request FY91

	Calorimeter	Tracker	Muon TRD	Integration Management	Total
Boston	750	-	210	200	1160
Drexel	-	-	100	-	100
Fairfield	30	95	-	-	125
Northeastern	-	550	265	150	965
Texas A&M	400	-	-	150	550
Subtotal	1180	645	575	500	2900
LeCroy	450	225	225	325	1225
Quantum Research	-	-	-	120	120
Bicron	495	100	-	-	595
Draper	425	130	375	305	1235
Hamamatsu	-	-	-	-	0*
Oak Ridge	-	535	-	-	535
Optectron	150	150	-	-	300
RCA/GE	150	150	-	-	300
Teledyne	300	300	-	-	600
Thinking Machines	-	-	-	-	0*
Union Carbide	-	-	140	-	140
Subtotal	1970	1590	740	750	5050
Total	3150	2285	1315	1250	7950

Proprietary development

ICHAD SUMMARY

SSC PHYSICS

- **Standard Higgs:**

100 GeV ⟷ **1 TeV**

Calorimeter σ_E ↙ ↘ **$\mathcal{L}$**

2-υ, 2-jet ↙ ↘ **$\mathcal{L}$**

Detector Test Case: <u>Ends of the mass scale, not only the middle</u>

- **SUSY:**
  - **Missing E_T and Multiple Jets (and W -> JetJet)**
  - **High $\mathcal{L}$ for High Mass Spartners**

- **Technicolor/Compositeness: - Large Jet Dynamic Range**

- **New High Mass/Threshold Phenomena:**
  - **W',Z', strong gauge boson interactions, ...**

<u>$\mathcal{L}$uminosity + Jets + Leptons</u>

Most Striking Physics Demands on SSC Detectors:

(1) Operation at 10^{34}

(2) Optimal Calorimetry

- y-coverage: full, uniform and smooth
- fine projective segmentation
- energy resolution at the 1% level
- large linear dynamic range

- Impose Natural Constraints SSC Detector Design -

- **Calorimeter**

speed fast
radius large
size 4π
readout survival
stability

TEXAS Baseline High Luminosity Detector

Energy Flow

- **Large Radius Scintillator Calorimeter Egg**
  - Fiber Scintillator(10-30 MRad)
  - Liquid Scintillator(100's Mrad)

  } 5ns peaking time

  - Outside Readout – no radiation damage, no thermal/power problems
  - Fine Projective Segments (to 0.025 x 0.025) lower singles rates, less jet blurring
  - Uniformly Hermetic and Compensated to η of 5.5

Leptons

- **Tracker/Imaging Preradiator**
  - electron/gamma/jet discrimination in jets and under pile-up
  - Scintillator (10 ns) and Outside Electro-Optic Readout
  - Large Radius ≥ 1m $\Rightarrow$ low rad damage, $\gamma\gamma$ separation π^0/H
  - Level 1 trigger on gammas

- **μTRD**
  - Energetic muons in high rates of punch-through and b,c decay
  - Fast Trigger TRD insensitive to low energy μ's

Summary

TEXAS Detector

Physics Goals:

Wide Mass Reach - $M_{W,Z}$ to 1 TeV and Beyond

ACHIEVED VIA FOCUS ON HIGH LUMINOSITY CALORIMETRY

- **FAST** ... in all 3 systems
- **HIGH RESOLUTION**
- **HERMETIC and UNIFORM**
- **SURVIVABLE**
- **SIMPLE**
- **MODEST COST**
- **READY FOR DATA ON SSC DAY 1**